



# **The effect of photosynthetic gas exchange on $\Delta^{17}\text{O}$ of atmospheric $\text{CO}_2$**

**Getachew Agmuas Adnew**

# **The effect of photosynthetic gas exchange on $\Delta^{17}\text{O}$ of atmospheric $\text{CO}_2$**

**Getachew Agmuas Adnew**

Copyright © 2020 by Getachew Agmuas Adnew

Institute for Marine and Atmospheric research Utrecht (IMAU)  
Department of Physics, Utrecht University  
Princetonplein 5, 3584 CC Utrecht, The Netherlands

ISBN: 978-90-393-7344-6

Printed by GVO drukkers & vormgervers B.V.

# **The effect of photosynthetic gas exchange on $\Delta^{17}\text{O}$ of atmospheric $\text{CO}_2$**

**Het effect van fotosynthetische gasuitwisseling op  $\Delta^{17}\text{O}$  van  
atmosferisch  $\text{CO}_2$**

(met een samenvatting in het Nederlands)

## **Proefschrift**

ter verkrijging van de graad van doctor aan de  
Universiteit Utrecht  
op gezag van de  
rector magnificus, prof.dr. H.R.B.M. Kummeling,  
ingevolge het besluit van het college voor promoties  
in het openbaar te verdedigen op

woensdag 18 november 2020 des middags te 12.45 uur

door

**Getachew Agmuas Adnew**

geboren op 7 november 1985  
te Debrelias, Ethiopië

## **Promoters:**

Prof. Dr. Thomas Röckmann  
Prof. Dr. Wouter Peters

Examining committee:

Prof. Dr. Amaëlle Landaïs  
Prof. Dr. Guus Velders  
Prof. Dr. Harro Meijer  
Prof. Dr. Maarten Krol  
Prof. Dr. Mathew S. Johnson

This work was supported by funding from the European Union's Horizon 2020 ERC for the ASICA under Grant Agreement Number 64908

# Table of Contents

|          |  |           |
|----------|--|-----------|
| <b>1</b> | <b>INTRODUCTION .....</b>  | <b>1</b>  |
| 1.1.     | BACKGROUND .....   | 1         |
| 1.2.     | INTERACTION OF THE ATMOSPHERE WITH TERRESTRIAL VEGETATION .....  | 3         |
| 1.3.     | ISOTOPE MEASUREMENTS OF CO <sub>2</sub> AS A TRACER FOR TERRESTRIAL CARBON CYCLE .....   | 8         |
| 1.3.1.   | KINETIC ISOTOPE FRACTIONATION .....  | 9         |
| 1.3.2.   | Equilibrium isotope fractionation.....   | 11        |
| 1.3.3.   | Triple oxygen isotope composition of CO <sub>2</sub> .....   | 11        |
| 1.4.     | OBJECTIVE AND APPROACH OF THIS THESIS.....   | 15        |
| <b>2</b> | <b>DETERMINATION OF THE TRIPLE OXYGEN AND CARBON ISOTOPIC COMPOSITION OF CO<sub>2</sub> FROM ATOMIC ION FRAGMENTS FORMED IN THE ION SOURCE OF THE 253 ULTRA HIGH-RESOLUTION ISOTOPE RATIO MASS SPECTROMETER.....</b> | <b>17</b> |
| 2.1.     | INTRODUCTION .....   | 18        |
| 2.2.     | EXPERIMENTAL SETUP AND MEASUREMENTS .....  | 20        |
| 2.2.1.   | The 253 Ultra instrument.....  | 20        |
| 2.2.2.   | Characterization of the 253 Ultra for CO <sub>2</sub> measurement.....   | 22        |
| 2.2.3.   | Fragment Method.....   | 23        |
| 2.2.4.   | O <sub>2</sub> -CO <sub>2</sub> exchange method.....   | 27        |
| 2.2.5.   | Samples.....   | 28        |
| 2.3.     | RESULTS.....   | 30        |
| 2.3.1.   | INSTRUMENT CHARACTERIZATION AND SCALE CONTRACTION.....   | 30        |
| 2.3.2.   | Fragment measurement.....  | 32        |
| 2.3.3.   | C-fragment.....  | 37        |
| 2.4.     | DISCUSSION.....  | 39        |
| 2.4.1.   | Scale contraction .....  | 39        |
| 2.4.2.   | Possible interferences .....   | 39        |
| 2.5.     | FUTURE DEVELOPMENTS AND APPLICATIONS .....   | 40        |
| 2.6.     | SUPPLEMENTARY MATERIAL .....   | 43        |
| <b>3</b> | <b>EXPLORING THE USE OF <sup>17</sup>O-EXCESS OF CO<sub>2</sub> FOR ESTIMATING MESOPHYLL CONDUCTANCE OF C<sub>3</sub> AND C<sub>4</sub> PLANTS .....</b>   | <b>57</b> |
| 3.1.     | INTRODUCTION .....   | 58        |
| 3.2.     | THEORY.....  | 60        |
| 3.3.     | RESULTS.....   | 61        |
| 3.3.1.   | CO <sub>2</sub> gradient, and discrimination against <sup>18</sup> O during assimilation.....  | 61        |
| 3.3.2.   | Mesophyll conductance .....  | 63        |
| 3.4.     | DISCUSSION.....  | 68        |
| 3.5.     | CONCLUSIONS .....  | 69        |
| 3.6.     | MATERIALS AND METHODS.....   | 70        |
| 3.6.1.   | Plant material and growing conditions.....   | 70        |
| 3.6.2.   | Gas exchange experiments.....  | 70        |
| 3.6.3.   | Carbon dioxide extraction and isotope analysis.....  | 71        |
| 3.6.4.   | Monte Carlo simulation and leaf cuvette model .....  | 71        |
| 3.7.     | SUPPLEMENTARY MATERIAL.....  | 73        |
| 3.7.1.   | Mesophyll conductance calculation using Δ <sub>A</sub> <sup>13</sup> C.....  | 73        |
| 3.7.2.   | Mesophyll conductance calculation using Δ <sub>A</sub> <sup>18</sup> O.....  | 73        |
| <b>4</b> | <b>LEAF-SCALE QUANTIFICATION OF THE EFFECT OF PHOTOSYNTHETIC GAS EXCHANGE ON Δ<sup>17</sup>O OF ATMOSPHERIC CO<sub>2</sub> .....</b>   | <b>81</b> |
| 4.1.     | INTRODUCTION .....   | 82        |
| 4.2.     | THEORY.....  | 84        |

|         |   |     |
|---------|---|-----|
| 4.2.1.  | Notation and definition of $\delta$ values .....  | 84  |
| 4.2.2.  | Discrimination against $\Delta^{17}\text{O}$ of $\text{CO}_2$ .....   | 85  |
| 4.3.    | MATERIALS AND METHODS .....   | 86  |
| 4.3.1.  | Plant material and growing conditions .....   | 86  |
| 4.3.2.  | Gas exchange experiments .....  | 86  |
| 4.3.3.  | Calibration of the Water Vapor Isotope Analyzer (WVIA) and leaf water analysis .....  | 88  |
| 4.3.4.  | Carbon dioxide extraction and isotope analysis .....  | 88  |
| 4.3.5.  | Leaf cuvette model .....  | 89  |
| 4.4.    | RESULTS .....   | 89  |
| 4.4.1.  | Gas exchange parameters .....   | 89  |
| 4.4.2.  | Discrimination against $^{18}\text{O}$ of $\text{CO}_2$ .....   | 93  |
| 4.4.3.  | Discrimination against $\Delta^{17}\text{O}$ of $\text{CO}_2$ .....   | 93  |
| 4.5.    | DISCUSSION .....  | 97  |
| 4.5.1.  | Discrimination against $^{18}\text{O}$ of $\text{CO}_2$ .....   | 97  |
| 4.5.2.  | Discrimination against the $\Delta^{17}\text{O}$ of $\text{CO}_2$ .....   | 97  |
| 4.5.3.  | Global average value of $\Delta_A \Delta^{17}\text{O}$ and $\Delta^{17}\text{O}$ isoflux .....  | 98  |
| 4.6.    | CONCLUSIONS .....   | 101 |
| 4.7.    | SUPPLEMENTARY MATERIAL .....  | 104 |
| 4.7.1.  | Gas exchange parameters .....   | 104 |
| 4.7.2.  | Isotopic composition of water at the evaporation site .....   | 104 |
| 4.7.3.  | Mole fraction of $\text{CO}_2$ at the site of $\text{CO}_2$ - $\text{H}_2\text{O}$ exchange .....                                       | 106 |
| 4.7.4.  | Mole fraction of $\text{CO}_2$ at the site of assimilation .....  | 107 |
| 4.7.5.  | Derivation of the $^{18}\text{O}$ - and $^{17}\text{O}$ -photosynthetic discrimination .....  | 108 |
| 4.7.6.  | Comparison of equations used in global models and in this study to calculate $\Delta^{17}\text{O}$ -photosynthetic discrimination ..... | 109 |
| 4.7.7.  | Calibration and characterization of the water vapor isotope analyzer (WVIA) .....   | 110 |
| 4.7.8.  | Water extraction and analysis .....   | 110 |
| 4.7.9.  | Leaf cuvette model .....  | 111 |
| 4.7.10. | $^{13}\text{C}$ -photosynthetic discrimination .....  | 113 |
| 5       | DISCUSSION AND OUTLOOK .....  | 123 |
| 5.1.    | DISCUSSION .....  | 123 |
| 5.1.1.  | Measuring $\Delta^{17}\text{O}$ of atmospheric $\text{CO}_2$ .....  | 123 |
| 5.1.2.  | Mesophyll conductance for $\text{CO}_2$ .....   | 124 |
| 5.1.3.  | Effect of photosynthesis on $\Delta^{17}\text{O}$ atmospheric $\text{CO}_2$ .....   | 125 |
| 5.2.    | PERSPECTIVES AND RECOMMENDATIONS .....  | 126 |
| 5.2.1.  | Consensus in the reference slope .....  | 126 |
| 5.2.2.  | Interlaboratory comparison .....  | 127 |
| 5.2.3.  | $\Delta^{17}\text{O}$ of atmospheric $\text{CO}_2$ .....  | 129 |
| 5.3.    | FUTURE PERSPECTIVES .....   | 130 |
|         | SUMMARY .....   | 133 |
|         | SAMENVATTING .....  | 137 |
|         | REFERENCES .....  | 141 |
|         | LIST OF PUBLICATIONS .....  | 161 |
|         | ACKNOWLEDGMENTS .....   | 163 |
|         | CURRICULUM VITAE .....  | 165 |

# Chapter 1

## Introduction

### 1.1. Background

Climate change is one of the most severe threats facing our planet. Global mean surface temperature has increased by 1.2 °C since 1880 (NASA/GISS, 2020; Lenssen et al., 2019), Arctic ice has shrunk by 40 % since 1979 (Windnagel et al., 2017) and global sea level has risen by 24 cm since 1980 (Cassotta et al., 2019). Climate has always changed by natural perturbations such as changes in the Earth's orbit and rotation, changes in solar radiation or volcanic eruptions. Over the past 800,000 years, the period where measurements of CO<sub>2</sub> concentrations are available from air trapped in polar ice cores, scientists have demonstrated a tight connection between temperature and the mole fraction of CO<sub>2</sub> (Augustin et al., 2004) (Figure 1.1). During this period, temperature changes caused by natural climate perturbations were amplified by CO<sub>2</sub> changes. For example, as the planet cools more CO<sub>2</sub> dissolves in the ocean that leads to further cooling and vice versa.

It is well established by now that over the industrial period the emission of greenhouse gases from anthropogenic activity has become the main driver for climate change (Stocker et al., 2013; Cook et al., 2013). Greenhouse gases absorb radiative energy (heat) emitted by the earth which warms our atmosphere like a greenhouse. This results in a disequilibrium between the energy absorbed by the earth and the energy released back to space, called radiative forcing. Carbon dioxide (CO<sub>2</sub>) is the main greenhouse gas, contributing the largest proportion of the total radiative forcing, 2.044 Wm<sup>-2</sup> out of a total of 3.101 Wm<sup>-2</sup> for 2018 relative to 1970 (James and Stephen, 2019). The global average mole fraction of atmospheric CO<sub>2</sub> has increased by more than 130 μmol mol<sup>-1</sup> (parts per million (ppm)) from approximately 277 ppm in 1750 (Joos and Spahni, 2008), to about 410 ppm today (Figure 1.1; (Keeling et al., 2005; Dlugokencky and Tans, 2020; Stocker et al., 2013)). The CO<sub>2</sub> mole fraction in the northern hemisphere is slightly higher than in the southern hemisphere due to higher anthropogenic emissions in the northern hemisphere. Direct measurements of the atmospheric carbon dioxide mole fraction began in 1958 by Charles Keeling (Keeling, 1958). The mole fractions of atmospheric CO<sub>2</sub> before 1959 are retrieved from ice core records (Lüthi et al., 2008; Meure et al., 2006). Direct temperature measurements are available from 1880 on, and the temperature records before 1880 are retrieved from ice cores (Jouzel et al., 2007; Frank et al., 2010). The clear seasonal cycle of CO<sub>2</sub> observed in the Northern Hemisphere, for example at the monitoring station Mauna Lao in Hawaii (MLO), is due to the annual cycle of photosynthesis and respiration (Ciais et al., 1995; Cuntz et al., 2003a; Graven et al., 2013; Forkel et al., 2016).



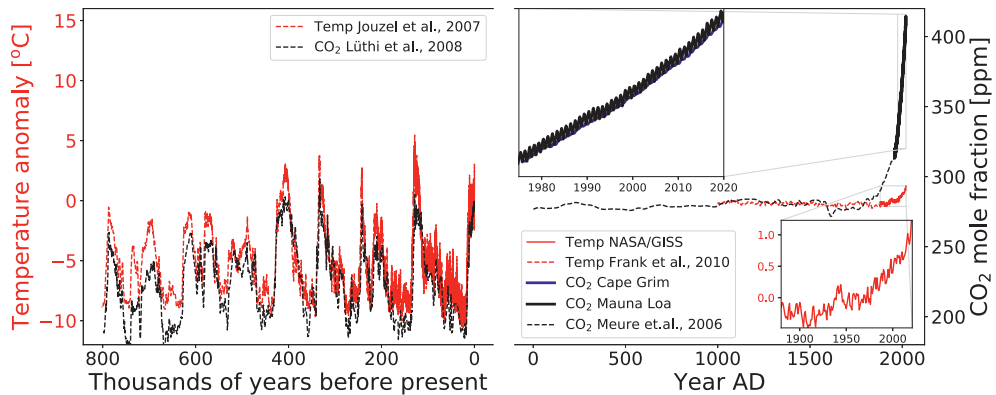


Figure 1.1 Evolution of the atmospheric mole fraction of CO<sub>2</sub> (blue and black lines) and temperature (red lines) over the past 850,000 years. Global mean temperature anomalies from in situ measurements since 1880 are relative to 1951-1980 average temperature (NASA/GISS, 2020; Lenssen et al., 2019) (small bottom right panel). Older average global temperature anomalies are retrieved from ice cores as presented in (Jouzel et al., 2007) and (Frank et al., 2010). Carbon dioxide mole fractions before 1959 are retrieved from ice core records as presented in (Lüthi et al., 2008) for the last 800,000 years, and in (Meure et al., 2006) for the last 1000 years. CO<sub>2</sub> mole fractions since 1959 are from in situ measurements carried out by the Scripps research institute and later by NOAA/ESRL at Mauna Loa (MLO) in the Northern Hemisphere (black) (Dlugokencky and Tans, 2020) and Cape Grim (CGO) station in the Southern Hemisphere (blue) (Steele et al., 2020).

The main cause of the ongoing increase in the mole fraction of atmospheric CO<sub>2</sub> is anthropogenic emissions, mainly from fossil fuel burning (Francey et al., 1999; Kirschbaum et al., 2019; Le Quéré et al., 2018; Stocker et al., 2013), with smaller contributions from cement production and land-use change (Le Quéré et al., 2018; Kirschbaum et al., 2019; Stocker et al., 2013). About 23 % of the CO<sub>2</sub> emitted from anthropogenic sources is sequestered by the terrestrial ecosystems and 23 % is taken up by the ocean; the remaining 54 % stay in the atmosphere, called the airborne fraction (Ballantyne et al., 2012; Canadell et al., 2007; Knorr, 2009; Stocker et al., 2013). The net mass fluxes (in GtC/yr) of CO<sub>2</sub> between the atmosphere and the ocean and the land biosphere, and emissions from the burning of fossil fuels and cement production (Le Quéré et al., 2018; Le Quéré et al., 2015) are shown in Figure 1.2. The interaction of the atmosphere with the lithosphere affects atmospheric CO<sub>2</sub> only on the geological time scale which controls the background level of atmospheric CO<sub>2</sub> through uptake by weathering and carbon burial and release through volcanic degassing and tectonic processes (Berner, 2004). The interaction between the biosphere, ocean and atmosphere can change over short time scales (Archer et al., 2009). As a result, any perturbation in the functioning of oceans and the terrestrial biosphere can affect the airborne fraction of CO<sub>2</sub> within years to decades (Stocker et al., 2013; Cox et al., 2000).

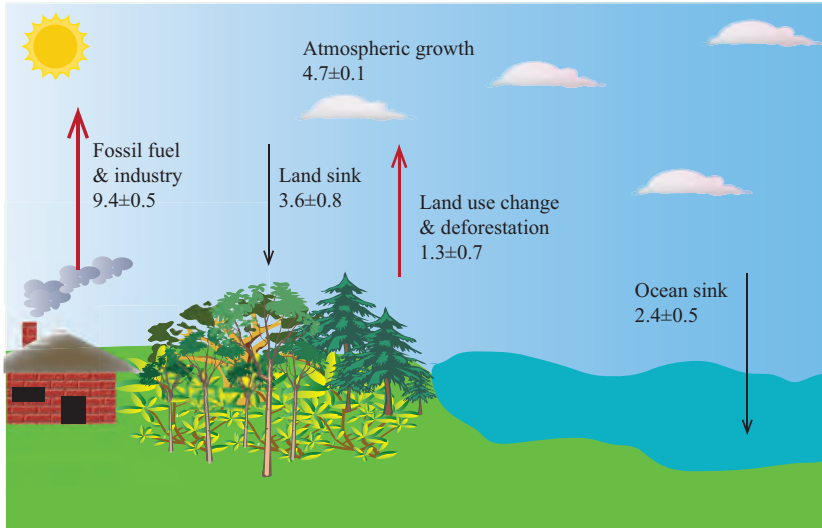
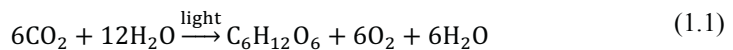


Figure 1.2 Overview of the net mass fluxes (in GtC/yr) of the global carbon cycle controlling the mole fraction of CO<sub>2</sub> in the atmosphere for the decade 2007 to 2016, modified from (Le Quéré et al., 2018). The red arrows show fluxes that increase the mole fraction of atmospheric CO<sub>2</sub> whereas fluxes that decrease the mole fraction of atmospheric CO<sub>2</sub> are shown with black arrows.

Carbon dioxide exchange between the ocean and atmosphere depends on ocean carbonate chemistry (regulated by temperature and pH value) and circulation (Prentice et al., 2007; Zeebe and Wolf-Gladrow, 2001). An increase in the mole fraction of atmospheric CO<sub>2</sub> and temperature might reduce the relative uptake of anthropogenic carbon dioxide by the oceans, as a greater concentration of CO<sub>2</sub> in the atmosphere results in the oceans becoming more acidic (lower pH), thereby reducing the uptake capacity of CO<sub>2</sub> in the ocean (Prentice et al., 2007). Since solubility of CO<sub>2</sub> is higher in cold water compared to warm water, and ice melt will increase the surface area that's exposed to the air, it was believed that the Arctic ocean would be an important sink for CO<sub>2</sub>. But data from three research cruises (1994, 2005, and 2015) recently revealed that the amount of dissolved inorganic carbon is decreased due to a decrease in the CO<sub>2</sub> uptake (Woosley and Millero, 2020). The main reason for the decreasing uptake of CO<sub>2</sub> in the Arctic is due to the lower alkalinity/buffering capacity of fresh water and the rapid temperature increase in the Arctic ocean relative to other oceans (Woosley and Millero, 2020; Thomasy, 2020).

## 1.2. Interaction of the atmosphere with terrestrial vegetation

Plants exchange air with the atmosphere via small pores on the surface of leaves called stomata. During photosynthesis (in the presence of light), plants use light energy to convert CO<sub>2</sub> and H<sub>2</sub>O to sugars (glucose) and as a byproduct oxygen (O<sub>2</sub>) is produced.



Generally, plants are classified into three classes,  $C_3$ ,  $C_4$  and crassulacean acid metabolism (CAM) plants, based on their metabolism.  $C_3$  plants convert the  $CO_2$  entering the leaf to a three-carbon acid called 3-phosphoglyceric acid, while  $C_4$  plants convert the  $CO_2$  to a four-carbon acid called oxaloacetate. CAM plants are intermediate between  $C_3$  and  $C_4$  plants. In the dark, they follow a similar metabolism as  $C_4$  plants while during early and late light they follow a combination of the  $C_3$  and  $C_4$  metabolisms (Ting, 1985). During the day the stomata of CAM plants are closed and there is no net exchange of  $CO_2$  from the leaf (Lee, 2010). For a detailed explanation of the different plant types, the reader is referred to (Cousins et al., 2020; Ubierna et al., 2019; Ubierna et al., 2018b; Ehleringer and Cerling, 2002; Ehleringer and Monson, 1993; Orsenigo et al., 1997; Tipple and Pagani, 2007; Ehleringer, 2005) and references therein.  $C_3$  and  $C_4$  plants not only vary in the type of organic acid they form during assimilation but also in the enzyme involved in the first conversion of  $CO_2$  and where the assimilation takes place (Figure 1.3). In the  $C_3$  metabolism, the first conversion of  $CO_2$  occurs in the chloroplast with the enzyme Ribulose-1,5-bisphosphate carboxylase oxygenase (RuBisCO). In  $C_4$  photosynthesis the conversion of  $CO_2$  to a  $C_4$  carbonic acid occurs in the cytoplasm with the enzyme Phosphoenolpyruvate carboxylase (PEP carboxylase or PEPC).

The net assimilation rate of plants does not only depend on the activity of the enzyme and radiation but it is also strongly limited by the conductance (reciprocal of resistance) of  $CO_2$  as it diffuses from the air surrounding the leaf through the boundary layer ( $g_b$ ), stomata ( $g_s$ ) to the intercellular airspace and from the intercellular airspace to the initial sites of  $CO_2$  fixation ( $g_m$ ). From Fick's first law of diffusion, the net photosynthetic flux at steady state (assimilation rate  $A_n$ , in  $\mu\text{mol m}^{-2}\text{s}^{-1}$ ) can be expressed as:

$$A_n = g_b(c_a - c_s) = g_s(c_s - c_i) = g_m(c_i - c_m) \quad (1.2)$$

where  $c_a$ ,  $c_s$ ,  $c_i$  and  $c_m$  are the  $CO_2$  concentration in the atmosphere, at the leaf surface, in the intercellular air space and in the chloroplast stroma, respectively (Long and Bernacchi, 2003). In gas exchange experiments, the boundary layer conductance is very high and the stomatal conductance can be calculated from leaf transpiration (von Caemmerer and Farquhar, 1981).

As shown in Figure 1.3 (for  $C_3$  plants), the diffusion of  $CO_2$  from the intercellular air space to the carboxylation site is complex and involves various phases, the gas phase (intercellular air space), the liquid phase (cell wall, cytosol and stroma) and lipid protein (plasmalemma and chloroplast envelope). In gas-exchange studies the mesophyll conductance was assumed to be very large (i.e. no concentration gradient between  $c_i$  and  $c_m$ ) (Farquhar et al., 1980). However, advancements in measurement techniques reveal mesophyll conductance is small and limits photosynthesis (Warren, 2006; Evans et al., 1986; Loreto et al., 1992; Harley et al., 1992; Marco et al., 1990). Mesophyll conductance ( $g_m$ ) is an important parameter that limits photosynthesis, but it is impossible to measure  $g_m$  directly (Pons et al., 2009; Cousins et al., 2020). A review of numerous measurement techniques is provided in (Cousins et al., 2020). One of the techniques used to estimate  $g_m$  is measuring the carbon (Evans et al., 1986) and oxygen (Osborn et al., 2017; Barbour et al., 2016; Gillon and Yakir, 2000b, a) isotopic composition of  $CO_2$ . Carbon isotope discrimination is used to determine the conductance in  $C_3$  plants only, from the intercellular airspace to the site of carboxylation. The conductance of  $CO_2$  from the intercellular airspace to the  $CO_2$ - $H_2O$  exchange site is determined using  $\delta^{17}O$ ,  $\delta^{18}O$  and  $\Delta^{17}O$ , for both  $C_3$  and  $C_4$  plants.

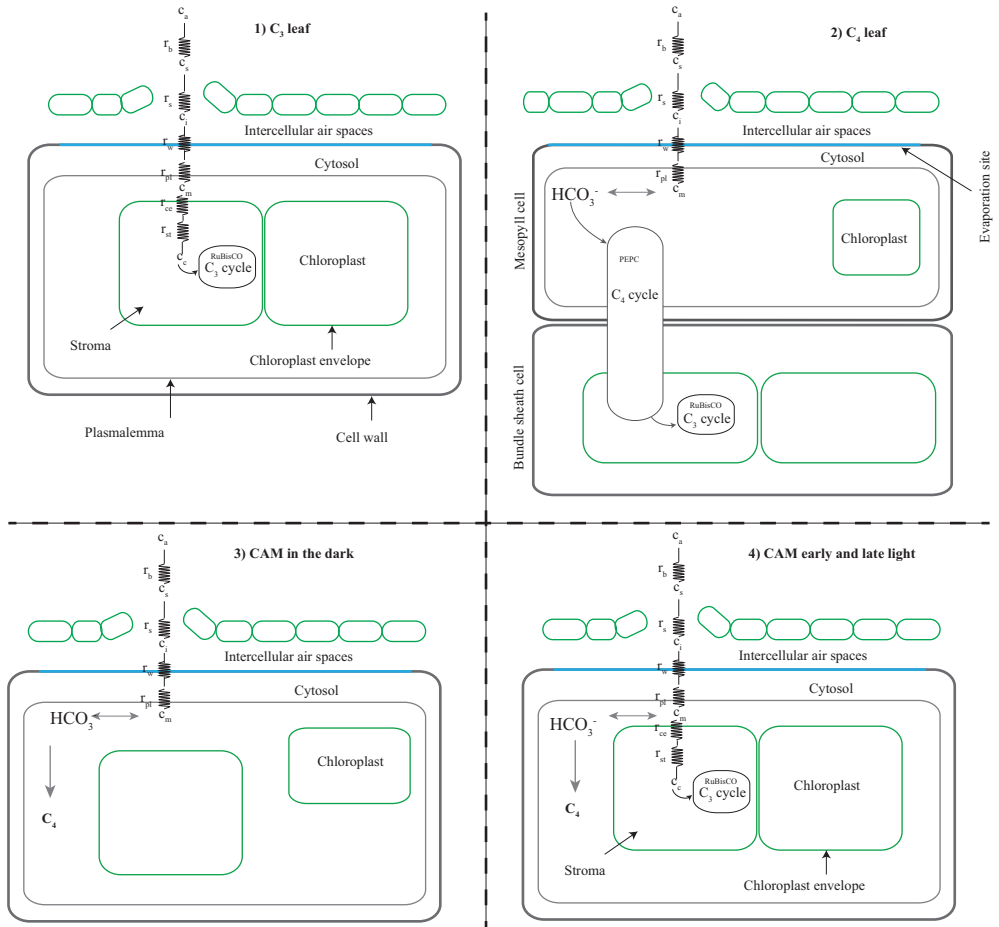
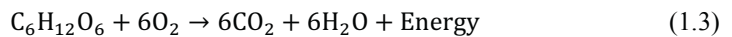


Figure 1.3 Scheme of  $\text{CO}_2$  fluxes in a  $\text{C}_3$ ,  $\text{C}_4$  and CAM leaf, modified from (Cousins et al., 2020). During photosynthesis, ambient  $\text{CO}_2$  (mole fraction  $c_a$ ) diffuses into the leaf intercellular spaces ( $c_i$ ) through the boundary layer ( $r_b$ ) and stomata ( $r_s$ ).  $c_s$  is the mole fraction of  $\text{CO}_2$  in the air surrounding the leaf. In a  $\text{C}_3$  leaf (1) the resistances for  $\text{CO}_2$  diffusion from the intercellular air space to RuBisCO in the chloroplast ( $c_c$ ) includes the cell wall ( $r_w$ ), the plasmalemma ( $r_{pl}$ ), the chloroplast envelope ( $r_{ce}$ ) and the stroma ( $r_{st}$ ) resistance. In a  $\text{C}_4$  leaf (2) the resistances for  $\text{CO}_2$  diffusion to PEPCase in the cytosol ( $c_m$ ) includes the wall ( $r_w$ ) and the plasmalemma ( $r_{pl}$ ) resistances. In a CAM leaf (3 and 4) the primary resistances for  $\text{CO}_2$  diffusion to the initial site of carboxylation will vary depending on the phase. In the dark (3), PEPCase is the primary carboxylase and  $g_m$  will be influenced by resistances similar to what occurs during  $\text{C}_4$  photosynthesis (2). During early and late light (4),  $g_m$  will represent a combination of resistances that will reflect the relative contribution of flux going towards PEPCase and RuBisCO. During the day the stomata are closed and there is no  $\text{CO}_2$  exchange.

Besides taking in  $\text{CO}_2$  during the day in the presence of light, plants also respire  $\text{CO}_2$ . Respiration does not require light and it occurs both during the day and in the night. During respiration, plants use glucose (sugar) to produce energy and a byproduct  $\text{CO}_2$  that is released to the atmosphere.



Respiration by plants is called autotrophic respiration to distinguish it from heterotrophic respiration (microbes and macrofaunal). The overall respiration (both autotrophic and heterotrophic) is called terrestrial ecosystem respiration (TER).

Gross primary production (GPP), the total amount of CO<sub>2</sub> assimilated by land vegetation, and terrestrial ecosystem respiration (TER) are the largest fluxes in the carbon cycle controlling land-atmosphere exchange (Beer et al., 2010). Small changes in GPP and TER can have a large impact on the net uptake of CO<sub>2</sub> by the terrestrial biosphere and to estimate the net effect requires understanding the interaction between GPP and TER (Cuntz, 2011; Raupach, 2011). The precise response of terrestrial CO<sub>2</sub> sources and sinks to changes in climate remains uncertain (Friedlingstein et al., 2006; Friedlingstein et al., 2014), but it can encompass a number of important feedbacks. Due to warming and an increase in the mole fraction of atmospheric CO<sub>2</sub>, net carbon exchange of the terrestrial ecosystem is changing (Baldocchi et al., 2016). Changes in the environmental conditions and ecological factors can thus change the turnover time, the size of different reservoirs and the responses of the carbon pools (Bloom et al., 2016; Baldocchi et al., 2016).

It is believed that an increase in the mole fraction of atmospheric CO<sub>2</sub> increases photosynthesis, especially for plants with C<sub>3</sub> metabolism, a phenomenon called CO<sub>2</sub> fertilization. Unlike C<sub>3</sub> plants, C<sub>4</sub> plants have a CO<sub>2</sub>-concentrating mechanism (Chollet and Ogren, 1975; Sage, 2004; Sage and Monson, 1998), consequently C<sub>4</sub> plants respond less to an increase in the mole fraction of atmospheric CO<sub>2</sub> than C<sub>3</sub> plants (Leakey, 2009; Wand et al., 1999; Ainsworth and Long, 2005). An increase in the mole fraction of CO<sub>2</sub> in the air surrounding the leaf decreases the stomatal conductance which results in an increase in water use efficiency (water loss due to the transpiration to the carbon gain) (Körner, 2000; Farquhar, 1997; Wong et al., 1979; Drake et al., 1997; Degener, 2015). Long-term monitoring studies at ecosystem level give a contradicting results about CO<sub>2</sub> fertilization (Sleen et al., 2015; Lewis et al., 2009). Recent studies predict an increase in the growth rate of vegetation due to an increase in the mole fraction of atmospheric CO<sub>2</sub> (Haverd et al., 2020; Zhu et al., 2016; Campbell et al., 2017). Most of the global carbon models used the biochemical model of Farquhar, von Caemmerer, and Berry for modeling photosynthesis (Farquhar et al., 1980). This model excludes mesophyll conductance, thus assumes that the mole fraction of CO<sub>2</sub> in the intercellular air space is the same as in the chloroplast available for the RuBisCO (Sun et al., 2014). This results in an underestimation of CO<sub>2</sub> fertilization since mesophyll conductance is one of the important mechanisms controlling photosynthesis (Knauer et al., 2019a; 2019b; Sun et al., 2014). The increase in photosynthesis with the mole fraction of atmospheric CO<sub>2</sub> is non-linear, decreasing towards higher mole fractions, and there is an upper limit above which it is expected not to increase further. For C<sub>3</sub> plants the upper limit is estimated to be 1000 ppm (Prentice et al., 2007; Degener, 2015), but other studies have shown lower limits for a decline in CO<sub>2</sub> fertilization below 1000 ppm (Körner, 2000; Ainsworth and Rogers, 2007). The concept of CO<sub>2</sub>-fertilization is controversial at extreme climate conditions that perturb the fluxes of carbon dioxide to and from plants (Reichstein et al., 2013; Frank et al., 2015; Obermeier et al., 2017). The carbon dioxide uptake of plants is variable depending on temperature variations, precipitation anomalies and land use change (Baldocchi et al., 2016; Zhu et al., 2016; Still, 2018; Peters et al., 2018).

There is no single direct sensor or method to measure GPP perfectly, as a result GPP can only be determined indirectly and remains poorly constrained (Canadell et al., 2000; Cuntz, 2011; Bloom et al., 2016; Ma et al., 2015), ranging from 100 to 175 PgCyr<sup>-1</sup> (Wang et al., 2012). Currently, we have more than a 60-year record for the direct measurement of the mole fraction

of atmospheric CO<sub>2</sub> (Le Quéré et al., 2015; Keeling, 1958) contributing to our understanding of terrestrial carbon cycle variability. In addition to the ground-based measurement of the mole fraction of atmospheric CO<sub>2</sub>, there is a multi-year record of satellite data including spatial and temporal variability of leaf area index as a tracer for greening of the terrestrial biosphere (Zhu et al., 2016). Even though we have such a long record of the mole fraction of atmospheric CO<sub>2</sub> and leaf area index, the terrestrial carbon cycle remains the least constrained component of the global carbon budget (Le Quéré et al., 2013; Anav et al., 2015). This is because of the complex response of terrestrial ecosystem CO<sub>2</sub> exchange to short- and long-term changes in temperature, water availability, nutrient availability, and rising atmospheric CO<sub>2</sub> mole fraction (Schimel et al., 2015; Gatti et al., 2014; Dieleman et al., 2012). For example, an increase in temperature enhances the microbial activity and kinetics of mitochondrial enzyme activity resulting in an increased respiration flux (Baldocchi et al., 2016).

It is critical that we understand how large-scale, climate-driven changes will affect the carbon sequestration of the terrestrial biosphere for predicting future climate changes and atmospheric CO<sub>2</sub> mole fraction. This requires untangling the biosphere uptake flux and respiration flux, thus, GPP and TER from net ecosystem exchange (NEE). One way to estimate GPP indirectly on the ecosystem scale is from a combined measurement of the net ecosystem-atmosphere CO<sub>2</sub> exchange (NEE) and terrestrial ecosystem respiration (TER, heterotrophic and autotrophic respiration) (Zscheischler et al., 2017; Kirschbaum et al., 2019; Reichstein et al., 2012; Jung et al., 2011; Beer et al., 2010) as:

$$NEE = GPP - TER \quad (1.4)$$

NEE can be determined with the eddy covariance (EC) method where trace gas fluxes are determined from fast fluctuations of vertical wind speed and gas mole fractions above an ecosystem (Reichstein et al., 2012). There is no direct method to partition NEE into GPP and TER, flux partitioning algorithms are developed with their limitations (Reichstein et al., 2012; Baldocchi, 2003; Wehr et al., 2016). Flux partitioning methods use either only night-time NEE data or both daytime and night-time data (Raj et al., 2016). One of the limitations is that nighttime TER measurements are prone to methodological error, as turbulence dies down and eddies become too small to properly apply the EC-theories. Further uncertainties arise from extrapolating nighttime temperature-TER relationships to daytime, assuming a similar TER response to temperature both during day and night (Reichstein et al., 2005; Papale et al., 2006; Aubinet et al., 2012). GPP estimates at the ecosystem scale using networks of carbon flux measurements and meteorological stations are extended to the global scale to produce spatially resolved flux maps of CO<sub>2</sub> with a monthly time resolution (Beer et al., 2010; Jung et al., 2011; Jung et al., 2019; Jung et al., 2009). Such studies estimated GPP ranging from 113 to 125 PgCyr<sup>-1</sup> (Beer et al., 2010; Jung et al., 2011; Jung et al., 2019; Jung et al., 2009). A different approach of estimating GPP uses remote sensing proxies such as photosynthetically active radiation (PAR) or sun-induced fluorescence (SIF) in combination with networks of carbon flux measurements, yielding GPP estimates from 91 to 169 PgCyr<sup>-1</sup> (Zhao et al., 2005; Yu et al., 2018; Joiner et al., 2018; Anav et al., 2015; Piao et al., 2013; Bloom et al., 2016; Badgley et al., 2019).

In addition to the mole fraction of atmospheric CO<sub>2</sub>, scientists use measurements of carbonyl sulfide (OCS) to quantify GPP. OCS is the most abundant and longest-lived sulfur-containing

gas in the atmosphere with a half-life of two to four years, and uptake by plants is the dominant OCS sink (Campbell et al., 2008; Asaf et al., 2013; Stimler et al., 2010). Using the relationship of the OCS and CO<sub>2</sub> uptake mechanism by plants during photosynthesis, measurements of OCS can be used as a tracer to estimate GPP (Campbell et al., 2008; Asaf et al., 2013). This is because it follows a similar diffusion pathway through the stomata that involves a similar hydration mechanism catalyzed by CA, where OCS is hydrolyzed to H<sub>2</sub>S and CO<sub>2</sub> (Seibt et al., 2010; Stimler et al., 2010). Unlike CO<sub>2</sub>, the OCS taken up by plants is not re-emitted back to the atmosphere (Stimler et al., 2010). The use of OCS as a tracer for GPP is based on the assumption that there is no interaction between CO<sub>2</sub> and OCS, there is only a one way OCS flux, fluxes to/from the soil are negligible and the mesophyll conductance is similar for OCS and CO<sub>2</sub> (Asaf et al., 2013; Blonquist et al., 2011). The limitation of using OCS as a tracer for GPP are: 1) the assumption of a similar mesophyll conductance between OCS and CO<sub>2</sub> (Asaf et al., 2013); 2) similar ratio of mole fraction of CO<sub>2</sub> in the intercellular airspace to the mole fraction of the CO<sub>2</sub> in the leaf surrounding ( $c_i/c_a$ ) for both C<sub>3</sub> and C<sub>4</sub> plants (Asaf et al., 2013); 3) assuming a constant OCS/CO<sub>2</sub> uptake and the limited amount of COS data due to more challenging measurements and the presence of other sources and sinks for OCS besides uptake by plants (Whelan et al., 2018; Seibt et al., 2010; Stimler et al., 2010; Kooijmans et al., 2019). OCS as a tracer for GPP remains a hot topic of research due to recent advancements in measurement techniques allowing online measurement of OCS, CO<sub>2</sub> and other trace gases simultaneously that can be deployed in the field (Berkelhammer et al., 2014; McManus et al., 2010; Kooijmans et al., 2016).

In the next section we will discuss the ongoing effort to determine fluxes in the terrestrial carbon cycle using measurements of the isotopic composition of CO<sub>2</sub>.

### 1.3. Isotope measurements of CO<sub>2</sub> as a tracer for terrestrial carbon cycle

When CO<sub>2</sub> diffuses to the site of carboxylation, it passes through different compartments as shown in Figure 1.3. The heavier isotopologues (e.g. <sup>13</sup>C<sup>16</sup>O<sup>16</sup>O, <sup>12</sup>C<sup>18</sup>O<sup>16</sup>O) have lower diffusivity, as a consequence a larger proportion of the light isotopologue (<sup>12</sup>C<sup>16</sup>O<sup>16</sup>O) enters the leaf via the stomata. During fixation, the enzyme RuBisCO preferentially binds to the light isotopologue <sup>12</sup>C<sup>16</sup>O<sup>16</sup>O relative to <sup>13</sup>C<sup>16</sup>O<sup>16</sup>O. RuBisCO has only a minor or no effect on the <sup>12</sup>C<sup>18</sup>O<sup>16</sup>O (Gillon and Yakir, 2000a; Cernusak et al., 2004). The oxygen isotope composition of CO<sub>2</sub> will be modified during the exchange of isotopes between CO<sub>2</sub> and leaf water, and as a result the CO<sub>2</sub> after exchange with leaf water will retain the isotopic composition of leaf water with a temperature dependent fractionation (Brenninkmeijer et al., 1983; Barkan and Luz, 2012). In C<sub>3</sub> plants, approximately 1/3 of the CO<sub>2</sub> entering the stomata is assimilated, the remaining 2/3 undergo isotope exchange with leaf water and diffuses back to the atmosphere, which modifies the isotopic composition of atmospheric CO<sub>2</sub> (Cuntz et al., 2003b; Affek and Yakir, 2014). Combining measurements of the mole fraction and isotopic composition of carbon dioxide is an additional method to identify different gross fluxes of CO<sub>2</sub> since isotope effects associated with different physical and chemical processes result in characteristic isotope signatures for CO<sub>2</sub> produced or removed by different processes. Most of these processes in nature depend on the mass of the molecules, leading to a so-called mass dependent fractionation signatures (Hulston and Thode, 1965), i.e. for oxygen, the isotope effect (or fractionation) is about two time larger when <sup>16</sup>O in a molecule is substituted by <sup>18</sup>O compared to <sup>17</sup>O (Craig, 1957; Dauphas and Schauble, 2016; Hulston and Thode, 1965). Fractionation



processes can be expressed quantitatively in terms of a fractionation factor  $\alpha$  or the related quantity fractionation  $\varepsilon$ . The fractionation factor is the ratio of a heavy to light isotope R (e.g.  $^{18}\text{R} = ^{18}\text{O}/^{16}\text{O}$  in two compounds, or two reservoirs or phases of the same compound).

$$\alpha_{a-b} = \frac{R_a}{R_b} \quad (1.5)$$

The fractionation factor  $\alpha$  is related to the fractionation ( $\varepsilon$ ) as:

$$\varepsilon_{a-b} = \alpha_{a-b} - 1 \quad (1.6)$$

In the plant sciences community, the fractionation factor is generally calculated as the isotope ratio in the reactant relative to the one in the product, i.e., the isotope ratio of air entering the leaf relative to the isotope ratio of the assimilated  $\text{CO}_2$  (Farquhar et al., 1989a; Farquhar and Lloyd, 1993; Farquhar and Richards, 1984), and the associated fractionation is called discrimination. Both fractionation and discrimination are independent of the reference material used.

The isotopic composition of a certain compound is expressed in  $\delta$  notation (McKinney et al., 1950) and since the signal is very small, it is expressed in per mill (‰).

$$\delta = \frac{R_{\text{sample}}}{R_{\text{ref}}} - 1 \quad (1.7)$$

The fractionation factor can be expressed in  $\delta$  notation as:

$$\alpha_{a-b} = \frac{\delta_a + 1}{\delta_b + 1} \quad (1.8)$$

Fractionation processes are generally classified as either kinetic or equilibrium (thermodynamic) fractionation (Dauphas and Schauble, 2016; Cao and Liu, 2011; Young et al., 2002; Matsuhisa et al., 1978) and the characteristics of these two processes are described in the following section.

### 1.3.1. Kinetic isotope fractionation

Assuming that there is no interaction between the gas molecules apart from collision (i.e. ideal gases), their kinetic energy will be the same at the same temperature. In this case, the kinetic mass-dependent fractionation can be calculated from the mass of the isotopologues (Dauphas and Schauble, 2016; Cao and Liu, 2011; Young et al., 2002; Matsuhisa et al., 1978; Craig, 1957). For instance, for oxygen with three stable isotopes, the kinetic fractionation factors can be calculated as:

$$^{17/16}\alpha_{a-b} = \frac{(m_{17}/m_{16})_a}{(m_{17}/m_{16})_b} \quad (1.9)$$



$$^{18/16}\alpha_{a-b} = \frac{(m_{18}/m_{16})_a}{(m_{18}/m_{16})_b} \quad (1.10)$$

where  $m$  stands for the mass of the isotopologue and the subscripts 16, 17, 18 designate  $^{16}\text{O}$ ,  $^{17}\text{O}$  and  $^{18}\text{O}$ , respectively. The triple isotope relationship ( $\theta$ ) between two compounds  $a$  and  $b$  during kinetic fractionation can be calculated as:

$$\theta = \frac{\ln(^{17/16}\alpha_{a-b})}{\ln(^{18/16}\alpha_{a-b})} = \frac{\ln(m_{16}/m_{17})}{\ln(m_{16}/m_{18})} \quad (1.11)$$

The logarithms can be ignored in many cases and for small enrichments because  $\ln X \cong X-1$  for  $X$  close to 1, i.e.  $(R/R_{\text{ref}}-1) = \ln(R/R_{\text{ref}})$  (Dauphas and Schauble, 2016). However, for very precise determinations this approximation does results in significant errors. The symbol  $\theta$  describes the triple oxygen isotope relationship between two compounds in a specific process whereas  $\lambda$  (see below) represents a slope of the  $\ln(\delta^{17}\text{O}+1)$  vs  $\ln(\delta^{18}\text{O}+1)$  for a sample which depends on the cumulative effect of different fractionation process (Cao and Liu, 2011; Miller et al., 2020).

An example of a kinetic fractionation process that strongly depends on the mass of the molecule is diffusional fractionations. The diffusion constant of a gas ( $D$ ) is proportional to the inverse square root of the mass. Under the assumption that all the molecules are at equal temperature (similar kinetic energy), the diffusional fractionation will be solely dependent on the mass of the molecule. If the diffusion process of interest involves the movement of gas  $A$  through gas  $B$ , the relevant mass is the reduced mass of the two molecules ( $\mu$ ).

$$\mu_{16} = \frac{m^B m^A_{16}}{m^B + m^A_{16}} \text{ and } \mu_{17} = \frac{m^B m^A_{17}}{m^B + m^A_{17}} \quad (1.12)$$

For a three-isotope system like oxygen, the fractionation factor during the diffusion of the gas  $A$  through gas  $B$  is calculated as:

$$^{17/16}\alpha_{a-b} = \frac{^{17}D}{^{16}D} = \sqrt{\frac{\mu_{16}}{\mu_{17}}} = \sqrt{\frac{m^B + m^A_{17}}{m^B m^A_{17}} \frac{m^B m^A_{16}}{m^B + m^A_{16}}} \quad (1.13)$$

$$^{18/16}\alpha_{a-b} = \frac{^{18}D}{^{16}D} = \sqrt{\frac{\mu_{16}}{\mu_{18}}} = \sqrt{\frac{m^B + m^A_{18}}{m^B m^A_{18}} \frac{m^B m^A_{16}}{m^B + m^A_{16}}} \quad (1.14)$$

where the indices 16,17 and 18 represent the isotopologues with  $^{16}\text{O}$ ,  $^{17}\text{O}$  and  $^{18}\text{O}$ , respectively. For example, water vapor will be depleted by 16.4 ‰ and 31.3 ‰ in  $^{17}\text{O}$  and  $^{18}\text{O}$ , respectively as it diffuses through air compared to the reservoir. Similarly,  $\text{CO}_2$  in air will be depleted by 4.4 ‰, 4.4 ‰, 8.7 ‰ in  $^{13}\text{C}^{16}\text{O}^{16}\text{O}$ ,  $^{12}\text{C}^{17}\text{O}^{16}\text{O}$  and  $^{12}\text{C}^{18}\text{O}^{16}\text{O}$ , respectively as it diffuses through air relative to the reservoir. The triple isotope relationship ( $\theta$ ) associated with diffusion of molecule  $A$  through  $B$  can be calculated as:

$$\theta = \frac{\ln\left(\sqrt{\mu_{16}/\mu_{17}}\right)}{\ln\left(\sqrt{\mu_{16}/\mu_{18}}\right)} = \frac{\ln\left(\sqrt{\frac{m^B m^A_{16}}{m^B + m^A_{16}} \frac{m^B m^A_{17}}{m^B + m^A_{17}}}\right)}{\ln\left(\sqrt{\frac{m^B m^A_{16}}{m^B + m^A_{16}} \frac{m^B m^A_{18}}{m^B + m^A_{18}}}\right)} \quad (1.15)$$

### 1.3.2. Equilibrium isotope fractionation

For equilibrium (thermodynamic) fractionation, the fractionation depends on the partition function of the oxygen bearing isotopologues (Urey, 1947; Bigeleisen and Mayer, 1947). The partition function describes the translational, rotational and vibrational energy of a molecule assuming all molecular vibrations are harmonic, quanta of molecular rotations are closely spaced relative to thermal kinetic energy, and isotopic substitution does not affect the electronic energy levels (Dauphas and Schauble, 2016; Urey, 1947; Bigeleisen and Mayer, 1947).  $\theta$  for equilibrium fractionation at high temperature (temperature exceeding 500 °C) can be calculated from the mass of the isotopologues of the molecules (Young et al., 2002; Matsuhisa et al., 1978; Weston, 1999; Dauphas and Schauble, 2016; Cao and Liu, 2011) as:

$$\theta = \frac{\ln(^{17/16}\alpha_{a-b})}{\ln(^{18/16}\alpha_{a-b})} \approx \frac{1/m_{16} - 1/m_{17}}{1/m_{16} - 1/m_{18}} \quad (1.16)$$

Equation 1.16 holds true also at low- temperatures for atoms in a molecule with light bonding partners such as hydrogen (Dauphas and Schauble, 2016). For example, for oxygen isotope fractionation,  $\theta$  will be 0.5305 for both low and high temperature extremes when the bonding partner is a light atom such as hydrogen (Young et al., 2002; Weston, 1999; Dauphas and Schauble, 2016; Matsuhisa et al., 1978). When the bonding partner is heavier than the isotopic masses, at low temperature,  $\theta$  can be calculated as:

$$\theta = \frac{\ln(^{17/16}\alpha_{a-b})}{\ln(^{18/16}\alpha_{a-b})} \approx \frac{\sqrt{1/m_{16}} - \sqrt{1/m_{17}}}{\sqrt{1/m_{16}} - \sqrt{1/m_{18}}} \quad (1.17)$$

For instance, for oxygen with a heavier bonding partner  $\theta$  is approx. 0.5232 (Dauphas and Schauble, 2016). Sharp et al. (2016) determined the  $\theta$  value for SiO<sub>2</sub>-H<sub>2</sub>O equilibrium fractionation at low temperature (0 to 50 °C) to be approx. 0.523 to 0.524.

### 1.3.3. Triple oxygen isotope composition of CO<sub>2</sub>

For purely mass dependent fractionation processes, the triple oxygen isotope fractionation is calculated as (Young et al., 2002; Miller, 2002; Dauphas and Schauble, 2016; Cao and Liu, 2011).

$$\alpha^{17} = (\alpha^{18})^\lambda \quad (1.18)$$

where  $\lambda$  is the three-isotope exponent pertaining to the process in question. It ranges from 0.5 to 0.5305 for equilibrium and kinetic processes (Young et al., 2002; Cao and Liu, 2011; Matsuhisa et al., 1978; Thiemens, 1999). Equation 1.18 can be rewritten using the  $\delta$  notation as:

$$(\delta^{17} + 1) = (\delta^{18} + 1)^\lambda \quad (1.19)$$

or

$$\ln(\delta^{17} + 1) = \lambda \times \ln(\delta^{18} + 1) \quad (1.20)$$

Deviations from equation 1.20 are called mass independent fractionation and the  $^{17}\text{O}$ -excess relative to mass dependent fractionation is quantified as:

$$\Delta^{17}\text{O} = \ln(\delta^{17} + 1) - \lambda \times \ln(\delta^{18} + 1) \quad (1.21)$$

The choice of  $\lambda$  in equation 1.21 is arbitrary. For scientific studies that investigate individual reactions, the exponent pertaining to the respective reaction is often used. In these cases, the symbol  $\theta$  is often used. However, when several processes overlap it is difficult to decide on a suitable exponent.

Triple oxygen isotope measurement of terrestrial rocks and minerals when plotted in a three-isotope diagram ( $\ln(\delta^{18}\text{O}+1)$  vs  $\ln(\delta^{17}\text{O}+1)$ ), they fall on a line with a single slope of  $\sim 0.52$ , which is commonly called the terrestrial fractionation line (TFL) (Matsuhisa et al., 1978; Rumble et al., 2007; Clayton et al., 1973). The first deviation of the  $^{17}\text{O}$  abundance from terrestrial fractionation line (TFL) was discovered in 1973 in meteorites and ascribed to nucleosynthesis (Clayton et al., 1973; Clayton et al., 1976). The discovery of mass-independent fractionation in ozone formation (Thiemens, 1983; Heidenreich and Thiemens, 1983, 1986) suggested that mass independent fractionation can occur in chemical reactions, which is in contrast to the classical isotope theory. The  $^{17}\text{O}$ -excess of ozone can be transferred to other oxygen bearing molecules via direct chemical reaction with ozone or via  $\text{O}(^1\text{D})$ . As a result, most of oxygen bearing molecules in the atmosphere possess anomalous oxygen isotope composition (Thiemens and Shaheen, 2014; Thiemens, 2006; Brenninkmeijer, 2009). For instance, the  $^{17}\text{O}$ -excess of ozone is transferred to  $\text{CO}_2$  via  $\text{O}(^1\text{D})$  as shown in equations 1.22 and 23 (Thiemens et al., 1995; Thiemens et al., 1991; Yung et al., 1997; Lyons, 2001; Yung et al., 1991).  $^{17}\text{O}$ -excess of ozone can also be transferred to other molecules, for example  $\text{NO}_2$  (Röckmann et al., 2001),  $\text{SO}_4^{2-}$  (Savarino et al., 2000),  $\text{H}_2\text{O}_2$  (Lyons, 2001) and  $\text{NO}_3$  (Savarino et al., 2008; Berhanu et al., 2012) via direct reaction of  $\text{O}_3$  with  $\text{NO}$ ,  $\text{SO}_2$ , via reaction of  $\text{O}_3$  and  $\text{OH}$ , and  $\text{NO}_2$ , respectively. The isotopic composition for different oxygen bearing compounds in the atmosphere is shown in Figure 1.4. In the stratosphere, the  $\delta^{17}\text{O}$  of  $\text{CO}_2$  is 1.7 to 2.2 times  $\delta^{18}\text{O}$  of  $\text{CO}_2$  (Wiegel et al., 2013). The only sink for the anomalous stratospheric  $\text{CO}_2$  is when it re-enters into the troposphere and undergoes isotope exchange with water bodies such as leaf water, soil water and ocean water. The isotope exchange in the atmosphere is negligible due to lower liquid water content, lower residence time and the absence of hydration catalyst enzyme called carbonic anhydrase (Mills and Urey, 1940; Johnson, 1982; Miller et al., 1971; Silverman, 1982).  $\Delta^{17}\text{O}$  has become a useful tracer for chemical reaction systems (Thiemens et al., 2001; Thiemens and Shaheen, 2014; Thiemens, 1999).

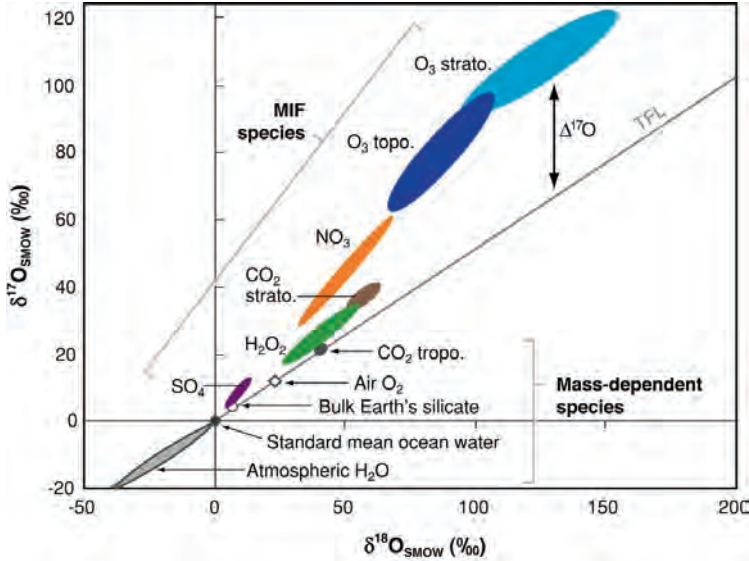
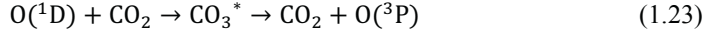
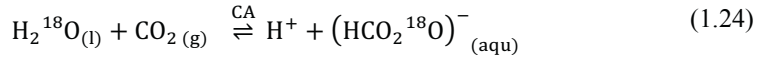


Figure 1.4 The triple oxygen isotope composition of atmospheric species relative to the terrestrial fractionation line (TFL), adopted from (Thiemens, 2006). It shows that the isotopic composition of most oxygen bearing molecules in the atmosphere does not fall on the TFL. Ozone has a very high  $^{17}\text{O}$ -excess both in the troposphere and stratosphere. However, the  $^{17}\text{O}$  anomaly is much smaller in tropospheric  $\text{CO}_2$  compared to stratospheric  $\text{CO}_2$  due to isotope exchange with water at the Earth's surface.

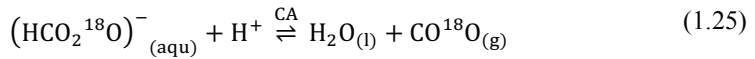
Combining the mixing ratio and isotopic composition of  $\text{CO}_2$  is useful to study the interaction between biosphere-atmosphere and ocean-atmosphere (Yakir and Sternberg, 2000). Charles Keeling was the first to use  $^{13}\text{C}$  measurements combined with mole fractions of  $\text{CO}_2$  to describe seasonal variations in the  $\text{CO}_2$  mole fraction and  $\delta^{13}\text{C}$  to seasonal variations in plant activity (Keeling, 1958, 1960, 1961). Ciais et al. (1995) used  $^{13}\text{C}$  measurements to partition the global net  $\text{CO}_2$  uptake between the terrestrial biosphere and the ocean. As discussed above, the underlying principle of using  $\delta^{13}\text{C}$  to separate the uptake of  $\text{CO}_2$  between ocean and terrestrial biosphere is that plants take up preferentially  $^{12}\text{CO}_2$  over  $^{13}\text{CO}_2$  resulting in  $^{13}\text{C}$ -enriched  $\text{CO}_2$  in the atmosphere whereas exchange with the ocean has a negligible effect on the  $\delta^{13}\text{C}$  of atmospheric  $\text{CO}_2$  (O'Leary, 1984).  $^{13}\text{C}$  and mole fraction measurements of  $\text{CO}_2$  alone do not allow to quantitatively separate gross fluxes between the atmospheric and the terrestrial biosphere on the one hand and the ocean on the other hand (Keeling et al., 2005, 2001).

Measurements of  $^{18}\text{O}$  isotope composition of  $\text{CO}_2$  have been used to separate gross fluxes between the terrestrial biosphere and soil respiration that provide the opportunity to estimate GPP (Ciais et al., 1997a; Ciais et al., 1997b; Cuntz et al., 2003b; Cuntz et al., 2003a; Peylin et al., 1999; Francey and Tans, 1987; Farquhar et al., 1993). The concept behind using  $\delta^{18}\text{O}$  as a

tracer to separate fluxes from the terrestrial biosphere from soil respiration is that CO<sub>2</sub> entering the leaf exchanges oxygen isotopes with leaf and soil water (Yakir, 2002). The exchange between CO<sub>2</sub> and water in the leaf and soil is fast due to the presence of the enzyme carbonic anhydrase (CA). Carbonic anhydrases are a group of metalloenzymes that catalyze the conversion of CO<sub>2</sub> and H<sub>2</sub>O to HCO<sub>3</sub><sup>-</sup> and vice versa rapidly (Gillon and Yakir, 2001; Friedli et al., 1987; Francey and Tans, 1987; Badger and Price, 1994; Mills and Urey, 1940; Yakir, 2002). Some of the isotopically exchanged CO<sub>2</sub> is assimilated via photosynthesis and the remainder diffuses back to the atmosphere.



where *l*, *g* and *aqu* represents liquid, gas and aqueous solution.



Leaf and soil water pools have different oxygen isotope composition due to the differences in pool size and evaporation rate. The H<sub>2</sub><sup>16</sup>O isotopologue has higher vapor pressure relative to H<sub>2</sub><sup>18</sup>O, thus during evapotranspiration H<sub>2</sub><sup>16</sup>O evaporates preferentially and leaf water becomes enriched in the H<sub>2</sub><sup>18</sup>O relative to soil water due to its small pool size (Dongmann et al., 1974; Prentice et al., 2007; Cernusak et al., 2016; Farquhar et al., 2007). As a result, the CO<sub>2</sub> which entered the leaf, exchanged isotopes with leaf water and diffused back to the atmosphere is enriched in δ<sup>18</sup>O relative to the CO<sub>2</sub> which undergoes an exchange with soil water. These differences in the <sup>18</sup>O isotopic signature of CO<sub>2</sub> interacting with leaves and soil can be used to distinguish the contributions of photosynthesis and soil respiration (Yakir and Wang, 1996; Ogée et al., 2004). Recently, Welp et al. (2011) estimated global GPP to be 150-175 PgCyr<sup>-1</sup> using variations in δ<sup>18</sup>O of atmospheric CO<sub>2</sub> after El Nino events. The limitation of using δ<sup>18</sup>O of atmospheric CO<sub>2</sub> as a tracer is its dependency on the δ<sup>18</sup>O value of different water reservoirs and fractionation processes in the hydrological cycle which are difficult to ascertain (Hoag et al., 2005). It has been suggested that the Δ<sup>17</sup>O of CO<sub>2</sub> could be an additional independent tracer for global GPP (Hoag et al., 2005; Koren et al., 2019; Hofmann et al., 2017) since it is less affected by isotope effects associated with the hydrological cycle such diffusion, condensation and evaporation (Hoag et al., 2005).

Recently, Liang et al. (2017b) estimated a global GPP value of 120 ± 30 PgCyr<sup>-1</sup>, from measurements of Δ<sup>17</sup>O. Figure 1.5 shows the assumed Δ<sup>17</sup>O signatures of the different CO<sub>2</sub> fluxes to and from the atmosphere. The stratospheric Δ<sup>17</sup>O signal is well defined (Hofmann et al., 2017; Koren et al., 2019; Hoag et al., 2005), Δ<sup>17</sup>O of fossil fuel combusted CO<sub>2</sub> will retain the triple oxygen isotope signal of atmospheric O<sub>2</sub> (Affek and Yakir, 2014; Laskar et al., 2016; Horváth et al., 2012; Liang et al., 2017b) unless the CO<sub>2</sub> undergoes exchange with water after combustion and the Δ<sup>17</sup>O of CO<sub>2</sub> in exchanged with the ocean is assumed to be relatively constant since the Δ<sup>17</sup>O value of ocean is constant (Affek and Yakir, 2014; Luz and Barkan, 2010; Koren et al., 2019). The contribution of photochemical oxidation of CO to CO<sub>2</sub> has a minor effect on the Δ<sup>17</sup>O of the atmospheric CO<sub>2</sub> since the CO pool is much smaller (Koren et al., 2019). The Δ<sup>17</sup>O value of CO<sub>2</sub> entering the leaf during photosynthesis and back-diffusion to the atmosphere is affected by the diffusional fractionation, exchange with water and in particular on the fraction of CO<sub>2</sub> that diffuses back to the atmosphere after isotope exchange

with leaf water. Similarly, the  $\Delta^{17}\text{O}$  signature of the soil invasion flux is very uncertain (Wingate et al., 2009) and its contribution to  $\Delta^{17}\text{O}$  of atmospheric  $\text{CO}_2$  is unknown, because it depends on the extent which  $\text{CO}_2$  has undergone isotope exchange with soil water. Also, the contribution of terrestrial respiration (autotrophic and heterotrophic respiration) to the  $\Delta^{17}\text{O}$  of atmospheric  $\text{CO}_2$  is unknown. Interpretation of  $\Delta^{17}\text{O}$  measurements of atmospheric  $\text{CO}_2$  depends on the ability to understand and untangle the effect of different process on  $\Delta^{17}\text{O}$  of atmospheric  $\text{CO}_2$ , especially respiration (autotrophic and heterotrophic), soil invasion and photosynthesis since these are the largest components of the global carbon cycle and affect  $\Delta^{17}\text{O}$ .

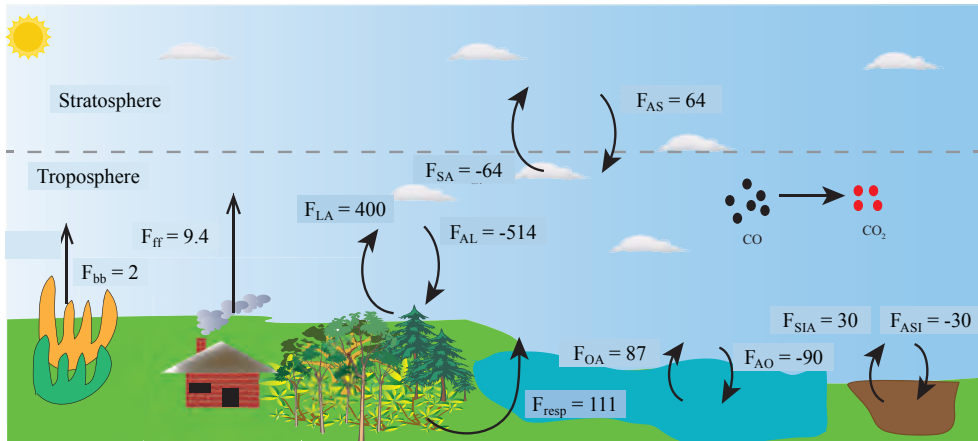


Figure 1.5 Sketch showing the fluxes of the terrestrial carbon cycle that modify the triple oxygen isotope composition of atmospheric  $\text{CO}_2$ , modified from (Koren et al., 2019). The  $\text{CO}_2$  mass fluxes, indicated with symbol  $F$ , are given in units of  $\text{GtC/year}$ . The reported values for  $\text{CO}_2$  mass fluxes are integrated over the global domain, averaged over the years 2012/2013. As a sign convention, the  $\text{CO}_2$  mass fluxes that tend to increase the tropospheric  $\text{CO}_2$  mass are expressed as positive numbers. The subscripts  $ff$ ,  $bb$ ,  $S$ ,  $A$ ,  $L$ ,  $SI$ , and  $resp$  stand for fossil fuel, biomass burning, stratosphere, atmosphere, leaf, soil invasion and respiration, respectively.

## 1.4. Objective and approach of this thesis

$\Delta^{17}\text{O}$  of  $\text{CO}_2$  has been proposed as a promising new tracer to estimate GPP. Measuring  $\Delta^{17}\text{O}$  of  $\text{CO}_2$  is challenging due to the interference of  $^{13}\text{C}^{16}\text{O}^{16}\text{O}$  (exact mass 44.9932) on the  $^{12}\text{C}^{17}\text{O}^{16}\text{O}$  (exact mass 44.9940) isotopologue and the low abundance of  $^{12}\text{C}^{17}\text{O}^{16}\text{O}$ . Partitioning the contribution of  $\Delta^{17}\text{O}$  fluxes from different sources and sinks from the atmospheric samples is difficult. **The goal of this PhD research is to develop a precise method to measure  $\Delta^{17}\text{O}$  of  $\text{CO}_2$  and to quantify the effect of photosynthesis on the  $\Delta^{17}\text{O}$  of atmospheric  $\text{CO}_2$ .**

One of the challenges to use the  $\Delta^{17}\text{O}$  as a tracer is the difficulty to measure  $\delta^{17}\text{O}$  of  $\text{CO}_2$  with standard mass spectrometric methods due to the interference of  $^{13}\text{C}^{16}\text{O}^{16}\text{O}$  isotopologue on the  $^{12}\text{C}^{17}\text{O}^{16}\text{O}$  isotopologue. Recently, different techniques have been developed involving either isotope exchange or conversion of  $\text{CO}_2$  to  $\text{O}_2$ , and directly using laser spectroscopic techniques (Mahata et al., 2013; Barkan et al., 2015; Hofmann and Pack, 2010; McManus et al., 2015, and references therein). The variability in  $\Delta^{17}\text{O}$  of atmospheric  $\text{CO}_2$  is relatively small (Koren et

al., 2019), so it requires precise measurement techniques. In this thesis, two different techniques to measure  $\Delta^{17}\text{O}$  of atmospheric  $\text{CO}_2$  are developed. The first technique is based on the  $\text{CO}_2$ - $\text{O}_2$  isotope exchange where the  $\text{CO}_2$  samples are exchanged with isotopically known oxygen and the  $\Delta^{17}\text{O}$  of  $\text{CO}_2$  is inferred by measuring the isotope composition of oxygen (Mahata et al., 2013; Barkan et al., 2015). The second method is to determine the  $\Delta^{17}\text{O}$  of the  $\text{CO}_2$  from the  $^{17}\text{O}^+$  and  $^{18}\text{O}^+$  ion fragments formed in the ion source of a high-resolution isotope ratio mass spectrometer. Both techniques require pure  $\text{CO}_2$ , the  $\text{CO}_2$  is purified cryogenically from the air samples for  $\Delta^{17}\text{O}$  measurement. The methods are tested for  $\text{CO}_2$  samples with different  $\Delta^{17}\text{O}$  values. This work is presented in **Chapter 2** of this thesis.

As discussed in the previous section, photosynthesis (the gross assimilation flux) is limited by the conductance of  $\text{CO}_2$  from the leaf surrounding to the site of carboxylation. Parameters that limit the net assimilation influences the extent photosynthesis effect on the  $\Delta^{17}\text{O}$  of atmospheric  $\text{CO}_2$ . Stomatal conductance ( $g_s$ ) can be calculated easily from measurements of water loss from a leaf, the air humidity surrounding the leaf, and the leaf temperature with the assumption water vapor in the intercellular airspace is fully saturated (Gaastra, 1959; Caemmerer and Farquhar, 1981). The conductance of  $\text{CO}_2$  from the intercellular air space to the site of carboxylation cannot be measured directly and it varies depending on the type of metabolism, environmental and growing conditions. To address this, we used three plant species that are representative of three different biomes and different photosynthetic pathways. Sunflower ( $\text{C}_3$  plant), a representative for temperate and tropical crops, ivy ( $\text{C}_3$  plant), representative of forests and other woody vegetation and stress subjected habitats and maize ( $\text{C}_4$  plant), typical for savanna type vegetation. To characterize the variation of  $g_m$  depending on the irradiance, we estimated the  $g_m$  using  $\delta^{13}\text{C}$ ,  $\delta^{17}\text{O}$ ,  $\delta^{18}\text{O}$  and  $\Delta^{17}\text{O}$  at two different light intensities. Estimating  $g_m$  using  $\Delta^{17}\text{O}$  is introduced for the first time. This work is presented in **Chapter 3** of this thesis.

To be able to accurately determine the effect of photosynthesis on the  $\Delta^{17}\text{O}$  of  $\text{CO}_2$  and to use  $\Delta^{17}\text{O}$  as a tracer it is important to separate the photosynthesis flux from other fluxes as discussed in the previous section. To quantify the effect of photosynthesis using  $\Delta^{17}\text{O}$  we used a leaf cuvette setup where a single leaf is enclosed in the cuvette and the mole fraction and triple oxygen isotope composition of  $\text{CO}_2$  and water vapor entering and leaving the leaf are measured. From the triple oxygen isotope composition and mixing ratio of the  $\text{CO}_2$  entering and leaving the cuvette, the effect of photosynthesis on  $\Delta^{17}\text{O}$  of  $\text{CO}_2$  is quantified. To investigate the dependency of the effect of photosynthesis on  $\Delta^{17}\text{O}$  of  $\text{CO}_2$  we used the  $\text{CO}_2$  entering the cuvette with two different  $^{17}\text{O}$  anomalies. This work is presented in **Chapter 4** of this thesis.

Finally, the findings of this thesis and future research objectives to use  $\Delta^{17}\text{O}$  both as a tracer for gross primary production and mesophyll conductance are summarized in **Chapter 5** of this thesis.



## Chapter 2

# Determination of the triple oxygen and carbon isotopic composition of CO<sub>2</sub> from atomic ion fragments formed in the ion source of the 253 Ultra High-Resolution Isotope Ratio Mass Spectrometer

### Abstract

**Rationale:** Determination of  $\delta^{17}\text{O}$  directly from CO<sub>2</sub> with traditional gas source isotope ratio mass spectrometry is not possible due to isobaric interference of  $^{13}\text{C}^{16}\text{O}^{16}\text{O}$  on  $^{12}\text{C}^{17}\text{O}^{16}\text{O}$ . The methods developed so far use either chemical conversion or isotope equilibration to determine  $\delta^{17}\text{O}$  of CO<sub>2</sub>. In addition,  $\delta^{13}\text{C}$  measurements require correction for the interference from  $^{12}\text{C}^{17}\text{O}^{16}\text{O}$  on  $^{13}\text{C}^{16}\text{O}^{16}\text{O}$  since it is not possible to resolve the two isotopologues.

**Methods:** We present a technique to determine  $\delta^{17}\text{O}$ ,  $\delta^{18}\text{O}$  and  $\delta^{13}\text{C}$  of CO<sub>2</sub> from the fragment ions that are formed upon electron ionization in the ion source of the Thermo Scientific 253 Ultra High-Resolution Isotope Ratio Mass Spectrometer (hereafter 253 Ultra). The new technique is compared with the CO<sub>2</sub>-O<sub>2</sub> exchange method and the  $^{17}\text{O}$ -correction algorithm for  $\delta^{17}\text{O}$  and  $\delta^{13}\text{C}$  respectively.

**Results:** Scale contractions for  $\delta^{13}\text{C}$  and  $\delta^{18}\text{O}$  are slightly larger for fragment ion measurements compared to molecular ion measurements.  $\delta^{17}\text{O}$  and  $\Delta^{17}\text{O}$  of CO<sub>2</sub> can be measured on the  $^{17}\text{O}^+$  fragment with an internal error that is a factor 1 - 2 above the counting statistics limit. The ultimate precision depends on the signal intensity and on the total time that the  $^{17}\text{O}^+$  beam is monitored; a precision of 14 ppm (parts per million) (standard error of the mean) was achieved in 20 hours at the University of Göttingen. The  $\Delta^{17}\text{O}$  measurements with the O-fragment method agree with the CO<sub>2</sub>-O<sub>2</sub> exchange method over a range of  $\Delta^{17}\text{O}$  values of -0.3 to + 0.7 ‰.

**Conclusions:** Isotope measurements on atom fragment ions of CO<sub>2</sub> can be used as alternative method to determine the carbon and oxygen isotopic composition of CO<sub>2</sub> without chemical processing or corrections for mass interferences.

**Key words:**  $\Delta^{17}\text{O}$ , CO<sub>2</sub> isotopes, fragmentation, isotope ratio, 253 Ultra

---

This chapter is published as: Adnew, G.A., Hofmann, M.E.G., Paul, D., Laskar, A., Surma, J., Albrecht, N., Pack, A., Schwieters, J., Koren, G., Peters, W. and Röckmann, T., 2019. Determination of the triple oxygen and carbon isotopic composition of CO<sub>2</sub> from atomic ion fragments formed in the ion source of the 253 Ultra high-resolution isotope ratio mass spectrometer. *Rapid Commun Mass Spectrom.*, 33, 17, 2019, DOI:10.1002/rcm.8478.



## 2.1. Introduction

Oxygen has three stable isotopes,  $^{16}\text{O}$ ,  $^{17}\text{O}$  and  $^{18}\text{O}$ , with average terrestrial abundances of 99.76 %, 0.04 % and 0.21 %, respectively. These abundances can be changed by kinetic and equilibrium fractionation processes and other physicochemical effects. Variations in isotopic abundance are reported as deviations of a heavy-to-light isotope ratio in a sample relative to a reference material. In the case of oxygen isotopes, the two isotope ratios are  $^{18}\text{R} = [^{18}\text{O}]/[^{16}\text{O}]$  and  $^{17}\text{R} = [^{17}\text{O}]/[^{16}\text{O}]$  and the international standard is Vienna Standard Mean Ocean Water (VSMOW).

$$\delta^{18}\text{O} = \frac{^{18}\text{R}_{\text{sample}}}{^{18}\text{R}_{\text{VSMOW}}} - 1 \quad (2.1)$$

$$\delta^{17}\text{O} = \frac{^{17}\text{R}_{\text{sample}}}{^{17}\text{R}_{\text{VSMOW}}} - 1 \quad (2.2)$$

Since isotope variations are small, they are usually reported in per mill (‰). Most isotope fractionation processes depend on mass. For oxygen isotopes, this results in fractionation patterns where the fractionation in  $^{17}\text{O}$  is approximately half of the fractionation in  $^{18}\text{O}$  (equation 2.3).

$$\ln(\delta^{17}\text{O} + 1) = \lambda \ln(\delta^{18}\text{O} + 1) \quad (2.3)$$

The factor  $\lambda$  (i.e.  $\frac{^{17}\text{R}}{^{17}\text{R}_{\text{ref}}} = (\frac{^{18}\text{R}}{^{18}\text{R}_{\text{ref}}})^\lambda$ ) ranges from 0.5 to 0.53 for such mass dependent isotope fractionation processes (Matsuhisa et al., 1978; Miller, 2002; Thiemens, 1999). Ozone photochemistry is a well-known exception to this rule, and  $\text{O}_3$  and related gases have a large oxygen isotope anomaly, expressed as  $\Delta^{17}\text{O}$  and referred to as mass independent isotope fractionation. We use the logarithmic definition to calculate  $\Delta^{17}\text{O}$  of  $\text{CO}_2$  (equation 2.4) (Miller, 2002; Clayton and Mayeda, 1996; Kaiser et al., 2004). Note that the choice of  $\lambda$  is arbitrary since a variety of sources contribute to the isotopic composition of tropospheric  $\text{CO}_2$  with different fractionations and different three-isotope slopes. In this study we used  $\lambda$  value of 0.528 to calculate  $\Delta^{17}\text{O}$  of  $\text{CO}_2$  following (Barkan and Luz, 2012; Barkan et al., 2015) and the  $^{17}\text{O}$ -correction algorithm by Brand et al. (2010).

$$\Delta^{17}\text{O} = \ln(\delta^{17}\text{O} + 1) - \lambda \ln(\delta^{18}\text{O} + 1) \quad (2.4)$$

Since the discovery of mass independent fractionation (Thiemens, 1983), the  $\Delta^{17}\text{O}$  has been used to study sources/sinks of atmospheric trace gases and chemical reaction pathways. Several studies have shown that  $\text{CO}_2$  acquires  $\Delta^{17}\text{O}$  from  $\text{O}_3$  via photochemical isotope exchange in the stratosphere (Lämmerzahl et al., 2002; Wiegel et al., 2013; Yung et al., 1991; Liang et al., 2006; Kawagucci et al., 2008; Lyons, 2001; Thiemens, 2006; Thiemens et al., 1991). When this  $\text{CO}_2$  re-enters the troposphere (Boering et al., 2004; Liang and Mahata, 2015; Thiemens et al., 2014) the  $\Delta^{17}\text{O}$  is successively diminished ( $\Delta^{17}\text{O}$  is lowered) by oxygen isotope exchange with leaf, soil and ocean water. Isotopic exchange of  $\text{CO}_2$  with leaf water is more efficient than with ocean water due to the presence of carbonic anhydrase in the leaves, and as a result the

main sink for the  $\Delta^{17}\text{O}$  of  $\text{CO}_2$  is exchange with leaf water. Precise measurements of the  $\Delta^{17}\text{O}$  of  $\text{CO}_2$  may therefore help to better constrain the exchange of  $\text{CO}_2$  between the atmosphere and the biosphere/hydrosphere. For several processes it has been shown that  $\Delta^{17}\text{O}$  is a more suitable tracer than  $\delta^{18}\text{O}$  alone (Hoag et al., 2005; Laskar et al., 2016; Liang et al., 2017b; Hofmann et al., 2017).

Determination of  $\Delta^{17}\text{O}$  in  $\text{CO}_2$  with traditional isotope ratio mass spectrometer techniques remains challenging due to the isobaric interference of  $^{13}\text{C}^{16}\text{O}^{16}\text{O}$  (exact mass 44.9932) and  $^{12}\text{C}^{17}\text{O}^{16}\text{O}$  (exact mass 44.9940). Resolving these two isotopologues requires a mass resolving power ( $m/\Delta m$ ) of  $\sim 56000$ , far beyond the resolving power of traditional mass spectrometer systems. Different alternative techniques have been developed to measure  $\delta^{17}\text{O}$  of  $\text{CO}_2$ : (1)  $\text{CO}_2$  fluorination and isotopic measurement of the released  $\text{O}_2$  (Thiemens, 1989); (2) Conversion of  $\text{CO}_2$  to  $\text{H}_2\text{O}$  and  $\text{CH}_4$  followed by  $\text{H}_2\text{O}$  fluorination and isotopic measurement of the released  $\text{O}_2$  (Brenninkmeijer and Rockmann, 1998); (3) Isotope exchange between  $\text{CO}_2$  and  $\text{CeO}_2$  (Assonov and Brenninkmeijer, 2001; Mrozek et al., 2016; Mahata et al., 2012) or  $\text{CuO}$  (Kawagucci et al., 2005) with known oxygen isotopic composition and measurement of the  $\delta^{45}\text{CO}_2$  value before and after exchange to calculate the  $\delta^{17}\text{O}$  value of  $\text{CO}_2$ ; (4) Isotope exchange between  $\text{CO}_2$  and  $\text{CeO}_2$  followed by isotope analysis of the equilibrated  $\text{CeO}_2$  by laser fluorination (Pack, 2010). (5) Equilibrium exchange of  $\text{CO}_2$  with  $\text{H}_2\text{O}$  followed by fluorination of  $\text{H}_2\text{O}$  and measurement of the isotopic composition of released  $\text{O}_2$  (Barkan and Luz, 2012; Passey et al., 2014); (6) Isotope exchange between  $\text{CO}_2$  and  $\text{O}_2$  over hot platinum and measurement of the isotopic composition of oxygen before and after exchange to calculate the  $\delta^{17}\text{O}$  value of  $\text{CO}_2$  (Mahata et al., 2013; Barkan et al., 2015). All these methods require either chemical conversion or isotope exchange, which can introduce procedural errors. In recent years, laser-based absorption spectroscopy techniques to determine  $\delta^{17}\text{O}$  value and other isotope signatures of  $\text{CO}_2$  from air samples have been developed (McManus et al., 2005; McManus et al., 2015; Stoltmann et al., 2017).

Very small variations in the  $\delta^{13}\text{C}$  value are used to quantify fluxes between atmosphere and hydrosphere and/or ocean (Keeling et al., 1979; Mook et al., 1983; Francey, 1999; Allison and Francey, 1995; White, 2002). Due to the mass interference of  $^{12}\text{C}^{17}\text{O}^{16}\text{O}$  and  $^{13}\text{C}^{16}\text{O}^{16}\text{O}$  (Brand et al., 2010; Assonov and Brenninkmeijer, 2003; Kaiser, 2008; Miller et al., 2007; Allison and Francey, 1995; Santrock J., 1985; Craig, 1957), the value of  $\delta^{13}\text{C}$  measurements require an appropriate correction for  $^{17}\text{O}$ -interference. Different “ $^{17}\text{O}$  correction” algorithms are in use to correct for the interference of  $^{12}\text{C}^{17}\text{O}^{16}\text{O}$  on the value of  $\delta^{13}\text{C}$ , causing discrepancies between different correction algorithms used. The discrepancies in the  $\delta^{13}\text{C}$  value introduced by different  $^{17}\text{O}$  correction algorithms (i.e. different  $\lambda$ ,  $^{17}\text{R}$ ,  $^{13}\text{R}$ ) are explored by Assonov and Assonov and Brenninkmeijer (2003) in detail. They reported a discrepancy of 0.058 ‰ for tropospheric  $\text{CO}_2$  with  $\delta^{45}(\text{CO}_2)$  and  $\delta^{46}(\text{CO}_2)$  values of -9.2 ‰ and +2.180 ‰ vs. NBS19- $\text{CO}_2$  between the algorithm by Allison et al. (1993) and Santrock J. (1985) due to differences in the values of  $^{17}\text{R}$  and  $\lambda$ . The discrepancies introduced by  $^{17}\text{O}$  correction algorithms depend on the  $\delta^{46}(\text{CO}_2)$  values (Miller et al., 2007) resulting in a different  $^{17}\text{O}$  correction for  $\text{CO}_2$  having the same  $\delta^{45}(\text{CO}_2)$  value but a different  $\delta^{46}(\text{CO}_2)$  values. By design, most of the  $^{17}\text{O}$  correction algorithms does not consider the  $\Delta^{17}\text{O}$  of the  $\text{CO}_2$  and the ones that include  $\Delta^{17}\text{O}$  requires precise measurement of the  $\delta^{17}\text{O}$  value of  $\text{CO}_2$ . For instance, the Allison et al. (1993) algorithm introduces an error ranging from -0.13 to -0.78 ‰ for stratospheric  $\text{CO}_2$  (Miller et al., 2007). Nevertheless, the error introduced to the  $\delta^{13}\text{C}$  value because of using different  $\lambda$  is different for  $\text{CO}_2$  with different  $\Delta^{17}\text{O}$  even if the same algorithm is used. It is desirable to use an alternative technique that enables the determination of the  $\delta^{13}\text{C}$  value without a bias introduced due to the

$^{17}\text{O}$  correction algorithm for better use of the  $\delta^{13}\text{C}$  values as a tracer to quantify fluxes between atmosphere and hydrosphere and ocean.

Recently developed high resolution isotope ratio mass spectrometers (Eiler et al., 2013; Young et al., 2016b) are designed to overcome limitations of traditional isotope ratio mass spectrometer systems in terms of mass resolution and sensitivity. In this study, we present a technique to determine the isotope composition of  $\text{CO}_2$  from the C and O fragment ions, which are produced from  $\text{CO}_2$  in the ion source of two 253 Ultra (Thermo Fisher Scientific, Bremen, Germany) instruments installed at Utrecht University and the University of Göttingen.

Isotope measurement of fragment ions is not a new concept. The method has been deployed, for example, to study the intramolecular distribution of  $^{15}\text{N}^+$  in  $\text{N}_2\text{O}$  (Röckmann et al., 2003; Brenninkmeijer and Röckmann, 1999; Toyoda and Yoshida, 1999; Yoshida and Toyoda, 2000; Westley et al., 2007), to determine the site specific carbon isotopic composition of propane (Piasecki et al., 2016) and to measure sulfur isotopes in COS (Hattori et al., 2015). Here we establish an analytical method to determine the  $\delta^{17}\text{O}$ ,  $\delta^{18}\text{O}$  and  $\delta^{13}\text{C}$  values of  $\text{CO}_2$  directly on C and O fragment ions of  $\text{CO}_2$  without any chemical manipulation of the  $\text{CO}_2$  molecule. Notably, this method provides an independent technique to measure  $\Delta^{17}\text{O}$  of  $\text{CO}_2$  and the results are validated by comparison with the existing  $\text{CO}_2\text{-O}_2$  exchange method and by measuring  $\text{CO}_2$  with known  $\Delta^{17}\text{O}$ .

## 2.2. Experimental setup and measurements

### 2.2.1. The 253 Ultra instrument

The 253 Ultra is the commercial version of a high mass resolution gas source multi-collector mass spectrometer, which was pioneered with the MAT 253 Ultra prototype in 2012 (Eiler et al., 2013; Stolper et al., 2014). The high mass resolution of the 253 Ultra enables the investigation of the abundance of isotopologues that suffer from isobaric interferences. The mass resolving power of the instrument can be tuned to  $m/\Delta m > 35000$  and the peak stability over time is  $< 5$  ppm in mass.  $m/\Delta m$  is the width of a peak flank between 5 % and 95 % of the maximum peak signal. The instrument is controlled by the Qtegra<sup>TM</sup> software package (Thermo Fisher Scientific, Bremen, Germany).

The ion source of the 253 Ultra is connected to a sample introduction system of four variable volume reservoirs that can be filled with sample or reference gases. The control of ion source chemistry (adduct formation, fragmentation, formation of metastable ions, linearity and exchange reactions of the sample gas with adsorbed species at the inner ion source surfaces) are critical for accurate isotope ratio measurements. The differentially pumped ion source can be baked to high temperature and is fitted with a variable ion source conductance (VISC) window to adjust the source pumping conductance and to control the residence time of the sample gas in the ionization volume, which is one critical parameter for ion source chemistry. The source slit can be switched to three different slit sizes for low, medium and high-resolution settings. For the instruments at Utrecht University and University of Göttingen the slit widths are 250  $\mu\text{m}$ , 16  $\mu\text{m}$  and 5  $\mu\text{m}$ . The intermediate aperture at the entrance of the magnetic sector

allows to select an extra high-resolution mode to achieve  $m/\Delta m > 35000$  mass resolving power. It should be noted that higher resolution comes at the cost of lower ion beam intensities.

The basic setup of the instrument follows a double focusing Nier Johnson geometry with a  $90^\circ$  deflection angle of the electrostatic sector ( $r=22.4$  cm) and the magnetic sector ( $r=23$  cm) as shown in Figure 2.1. Double focusing means that there is stigmatic focusing of the ions passing the source slit regardless of the angular and energy distribution in the ion beam. Usually low-resolution sector mass analyzers are of single focusing type, i.e. just a magnetic sector. The mass resolving power of a single focusing system is limited by the chromatic aberration that is caused by the energy spread of the ions generated in the ion source. Double focusing can overcome this limitation. In a properly designed double focusing system the electrostatic sector optics match the chromatic aberrations of the magnetic sector optics such that the combined system eliminates both, the angular and chromatic aberrations up to the second order (Wollnik, 1987).

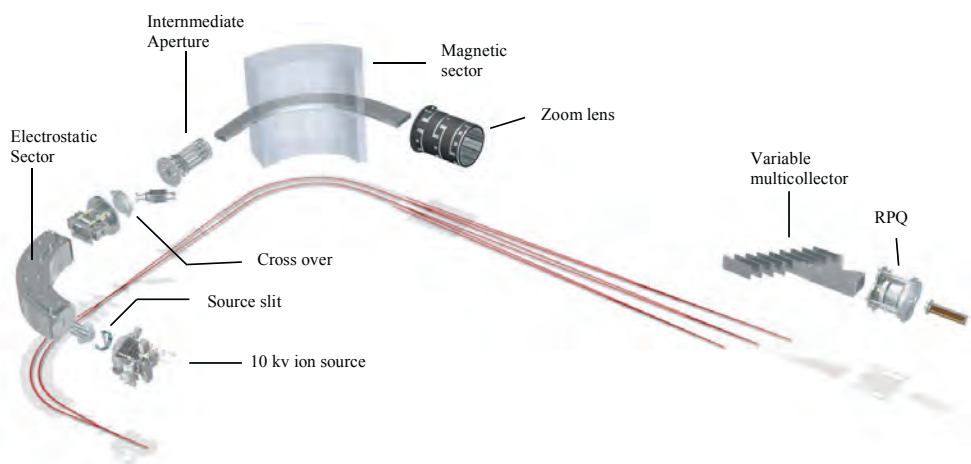


Figure 2.1 Ion optical layout of the Thermo Scientific 253 Ultra high-resolution isotope ratio mass spectrometer. In the ion source, the ions are accelerated to 5 keV onto the source slit. After the electrostatic analyzer the ions are accelerated to 10 keV just before passing the crossover. The switchable intermediate aperture behind the magnetic sector is used for extra high mass resolution settings and the zoom lens allows for fine adjustments of peak overlap. The variable multicollector assembly is mounted on the focal detector plane of the mass spectrometer system. The RPQ filter lens discriminates for scattered ions and reduces abundance sensitivity. It is located behind the focal plane right in front of the ion counter.

In the 253 Ultra the ions are generated at a potential of 10 keV. The ions are accelerated to the source slit of the double focusing mass analyzer to a kinetic energy of 5 keV. After passing through the electrostatic analyzer the ions are further accelerated to 10 keV kinetic energy before they pass through the magnetic sector where the ion trajectories are split up according to their mass. Finally, the ions are focused along the focal detector plane of the mass analyzer. The two-stage acceleration of the ion beam allows a very compact design of the electrostatic sector geometry, which otherwise would have required the radius of the electrostatic sector to be about twice as large as the radius of the magnetic sector. Due to the compact geometry, the ion optical setup of the 253 Ultra fits onto just one monolithic base plate. The resonance frequency of this rigid mechanical construction is very high and precise, which makes the

system robust against low frequency vibrations that usually occur in buildings. In order to achieve ultimate stability, the complete mass analyzer and the electronics are housed in a shielded temperature stabilized cabinet to be robust against temperature fluctuations in the lab (2 °C).

The variable detector array supports eight moveable detector platforms, which are equipped with Faraday detectors that can be read out with selectable resistors with resistances between  $3 \times 10^8 \Omega$  and  $10^{13} \Omega$ . The three collector platforms at the high mass end are additionally equipped with compact discrete dynode ion counting detectors (Tuttas, 2008) next to the Faraday detectors. The axial detector channel is fixed in position and supports a dual detector arrangement, where the ion beam can be switched between a Faraday cup and an ion counting channel. The axial ion counting detector is equipped with a retardation lens (RPQ-lens) to reject scattered background ions originating from scattering events along the ion optical flight path (apertures, residual gas particles) which leads to an abundance sensitivity in the ppb range (Eiler et al., 2013).

### 2.2.2. Characterization of the 253 Ultra for CO<sub>2</sub> measurement

We investigated the effect of equilibration time, emission current, source conductance and signal intensity on the ionization of CO<sub>2</sub> as suggested by Verkouteren et al. (2003a; 2003b) and Meijer et al. (2000). We characterized scale contraction effect of the ion source of the 253 Ultra at Utrecht University using two CO<sub>2</sub> gases (G1 and SCOTT see Table 2.1 for details). The characterization of the instrument is performed at low resolution (250  $\mu\text{m}$  entrance slit width,  $m/\Delta m \sim 2000$ ) with five Faraday collectors that are read out with resistors of  $3 \times 10^8 \Omega$ ,  $1 \times 10^9 \Omega$ ,  $3 \times 10^{10} \Omega$ ,  $1 \times 10^{11} \Omega$ ,  $1 \times 10^{11} \Omega$  for  $m/z$  44, 45, 46, 47 and 48. The corresponding collectors used for this measurement are L2, L1, Center, H1, H2 for  $m/z$  44, 45, 46, 47 and 48, respectively. Here, only data corresponding to  $m/z$  44 to 46 are presented. The ion signal of the high intensity ion beam ( $m/z$  44) is adjusted before each acquisition to  $3.2 \times 10^{11}$  cps (counts per second) with an allowed difference of  $1 \times 10^{10}$  cps between the two bellows that are used for the measurement. Under these conditions the ion source pressure is  $2.5 \times 10^{-7}$  mbar. The reference measurement is performed with 9.9 kV accelerating voltage, filament emission current of 1.8 mA, equilibration time of 60 s, integration time of 67.1 s and with the VISC window closed.

To study the effect of equilibration time and source conductance, we measure the two gases with equilibration time of 10, 20, 30, 40, 50, 60 and 90 s with the VISC window open and closed. The effect of the emission current is quantified by setting the emission current to 1 mA, 1.5 mA and 1.95 mA. To investigate the effect of signal intensity (cps for  $m/z$  44), three experiments with  $2.5 \times 10^{11}$  cps,  $1.5 \times 10^{11}$  cps and  $9 \times 10^{10}$  cps for  $m/z$  44 are performed. Note that measurements to characterize the effect of emission control current and signal intensity are performed with equilibration time of 30 s, so they cannot be directly compared to the reference measurement with equilibration time of 60 s. The effect of cross contamination is calculated according to Meijer et al.(2000) using equation 2.5. To calculate the change in scale contraction with changes in equilibration time, we compare the relative difference of the two gases (in  $\delta^{13}\text{C}$  and  $\delta^{18}\text{O}$  values) measured at different equilibration times with the value obtained at 90 second equilibration time. Similarly, the scale contraction due to emission current is calculated with respect to the results obtained at an emission current of 1 mA. The cross contamination ( $\eta$ ) is calculated as

$$\eta_y = \frac{[\delta_a^y - \delta_m^y]}{[2\delta_a^y + \delta_a^y \times \delta_m^y]} \quad (2.5)$$

Where  $y$  is 13 (for  $\delta^{13}\text{C}$ ) or 18 (for  $\delta^{18}\text{O}$ ), the index  $a$  indicates the respective  $\delta$  value under reference conditions (90 seconds equilibration time and 1 mA emission current), and index  $m$  indicates the  $\delta$  value at a different equilibration time or different emission current.

To link our results to international isotope scales, we use a set of isotopically different pure  $\text{O}_2$  and  $\text{CO}_2$  reference gases. Multiple aliquots of each gas were sent to Eugeni Barkan from the Hebrew University of Jerusalem for analysis. This research group also provides high precision  $\delta^{17}\text{O}$  values and has established a direct link between the oxygen isotope scales of  $\text{O}_2$  and  $\text{CO}_2$ . The reported results were assigned to our reference gas cylinders, which were also measured extensively on the Thermo Scientific Delta<sup>Plus</sup> XL<sup>TM</sup> instrument in our laboratory (Thermo Fisher Scientific, Bremen, Germany) and on the 253 Ultra. The appropriate scale contraction factors (see section 3) are used to convert the raw data to the scale of the Hebrew University of Jerusalem (Luz and Barkan, 2005; Barkan and Luz, 2012; Barkan and Luz., 2004).

### 2.2.3. Fragment Method

The  $^{17}\text{O}^+$  fragment measurements at Utrecht University are performed at medium resolution (16  $\mu\text{m}$  entrance slit width,  $m/\Delta m > 7500$ ) with the “reference” source settings mentioned above, i.e., emission current of 1.80 mA, accelerating voltage 9.9 kV, VISC window closed. The ion signals are registered in three Faraday collectors (L3, Center, H3) that are read out with resistors of  $1 \times 10^{11} \Omega$ ,  $1 \times 10^{13} \Omega$ ,  $1 \times 10^{13} \Omega$  for  $m/z$  16, 17 and 18, respectively. The ion signal intensity is adjusted before each acquisition to  $9.2 \times 10^8$  cps on  $m/z$  16, which corresponds to a source pressure of  $\sim 2.5 \times 10^{-7}$  mbar, with a tolerance of  $3 \times 10^6$  cps between the bellows. Reasonable source pressures for fragment ion measurement are determined to fall between 2.0 and  $4.5 \times 10^{-7}$  mbar (resulting in major ion beam signals of 0.75 to  $1.25 \times 10^9$  cps at medium resolution), corresponding to the linear portion of the source pressure vs. signal intensity relation for  $m/z$  16 (supplementary Figure S2.1). Integration and equilibration times are 67.1 and 60 s, respectively, which implies that in a measurement cycle both sample and reference are measured for 67.1 s out of 254.2 s i.e., 26 % of the time. Figure 2.2 shows the mass spectrum for  $m/z$  16, 17 and 18. The main interference for the  $^{17}\text{O}^+$  ion (mass 16.9991 u) is  $\text{OH}^+$  (mass 17.0027 u). The mass difference between these two ions is only 0.0036 u. With the 253 Ultra, they are sufficiently separated using the medium resolution slit to enable measurement of  $^{17}\text{O}^+$  on a narrow plateau without interference from  $\text{OH}^+$ . In this study the medium resolution slit is chosen since the plateau is sufficiently flat and gives a sufficient signal to allow stable positioning for  $^{17}\text{O}^+$  measurement as shown in Figure 2.2. The width of the plateau can in principle be increased by going to high mass resolution, but this would result in a reduction of the ion current by a factor 3 and a corresponding increase in the required measurement time to reach a certain precision. For  $^{18}\text{O}^+$  (mass 18.9984) the mass difference to its main interference  $\text{H}_2\text{O}^+$  (19.0148 u) is 0.0164 u which results in a broad shoulder even at medium mass resolution. The potential effect of other interferences is discussed below.

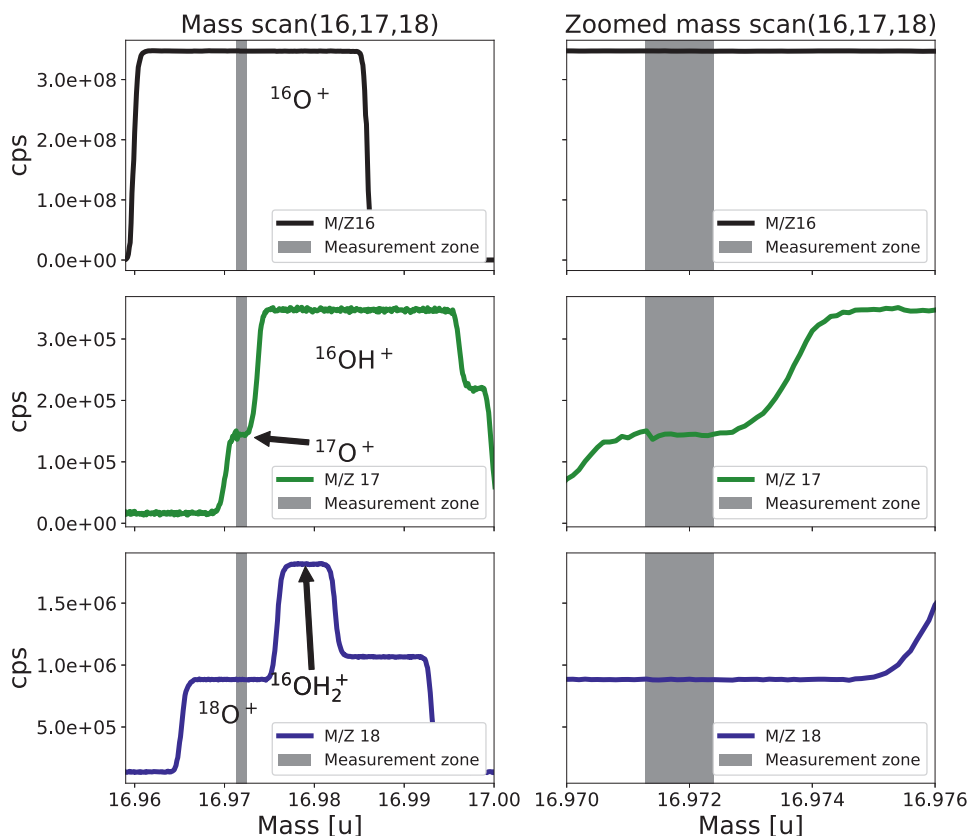


Figure 2.2 Medium resolution mass spectra for measurement of  $^{16}\text{O}^+$ ,  $^{17}\text{O}^+$  and  $^{18}\text{O}^+$  fragment ions of  $\text{CO}_2$ . The shaded area shows the region of the shoulder where  $^{17}\text{O}^+$  is measured interference-free, a magnified view is shown in the right panels. The mass scale (x-axis) applies to the middle panels ( $^{17}\text{O}$ ) for the top and bottom panels, the mass scale is shifted one mass down or up, respectively.

Small shifts in the mass scale regularly lead to a deterioration of measurement precision, when the mass position shifts away from the small  $^{17}\text{O}^+$  shoulder. This can be largely circumvented by resetting the mass scale at regular time intervals during the measurement. The present version of the Qtegra software does not allow automatic positioning on a shoulder of multiple overlapping peaks. Therefore, the collector configuration is carefully arranged such that the center of the  $m/z$  16 peak is precisely located at the shoulder of the  $m/z$  18 and  $m/z$  17 peaks where  $^{17}\text{O}^+$  and  $^{18}\text{O}^+$  can be measured interference-free. A peak center is then performed on  $m/z$  16 before each acquisition which is precise enough to relocate the system on the narrow shoulder of the  $m/z$  17 peak. Nevertheless, instabilities in the mass scale are still considered a main contributor to the remaining error above counting statistics, and an automatic positioning routine that scans the  $^{17}\text{O}^+$  shoulder directly to reposition the peak may improve precision.

All  $^{17}\text{O}^+$  fragment measurements on the 253 Ultra at University of Göttingen are performed at medium resolution (16  $\mu\text{m}$  entrance slit width,  $m/\Delta m \sim 7500$ ) with 9.85 kV accelerating voltage and 1.85 mA emission current, with the VISC window closed. The integration and equilibration times are 67.1 and 12 seconds, respectively, which implies that in a measurement cycle both



sample and reference are measured for 67.1 out of 158.2 s i.e., 42.4 % of the time. Three Faraday collectors (L3, Center, H3), equipped with  $1 \times 10^{10} \Omega$ ,  $1 \times 10^{13} \Omega$ , and  $1 \times 10^{12} \Omega$  resistors, are used to detect the ion signals for  $m/z$  16, 17, and 18 respectively. The signal intensity is adjusted per acquisition on  $m/z$  16, with a target intensity of  $1.2 \times 10^9$  cps (tolerance 0.2 %), corresponding to a source pressure of  $4.12 \times 10^{-7}$  mbar.

The doubly charged ion  $^{16}\text{O}^{18}\text{O}^{++}$  is very close in mass to  $^{17}\text{O}^+$  (Table S2.5) and interferes at the lower mass shoulder of the  $^{17}\text{O}^+$  peak. Figure 2.3 shows mass spectra recorded at medium resolution using the compact discrete dynode (CDD) collector of the H2 collector unit of the Ultra (H2-CDD). The interference of  $^{16}\text{O}^{18}\text{O}^{++}$  can be detected 0.002 mass units before the larger  $^{17}\text{O}^+$  peak starts.  $^{16}\text{O}^{18}\text{O}^{++}$  is formed in the ion source most likely from the recombination of  $^{16}\text{O}$  and  $^{18}\text{O}$  atom fragments. Therefore, the contribution  $^{16}\text{O}^{18}\text{O}^{++}$  to  $^{17}\text{O}^+$  depends on the  $^{18}\text{O}$  content of the gas, and it has to be corrected to avoid a systematic bias in the  $\delta^{17}\text{O}$  determination when the  $\delta^{18}\text{O}$  of sample and working reference gas is different. Figure 2.3 c shows that the  $^{16}\text{O}^{18}\text{O}^{++}$  signal increases relative to the  $^{17}\text{O}^+$  and  $^{18}\text{O}^+$  signal towards lower source pressures but it is quite stable at pressures above  $10^{-7}$  mbar.

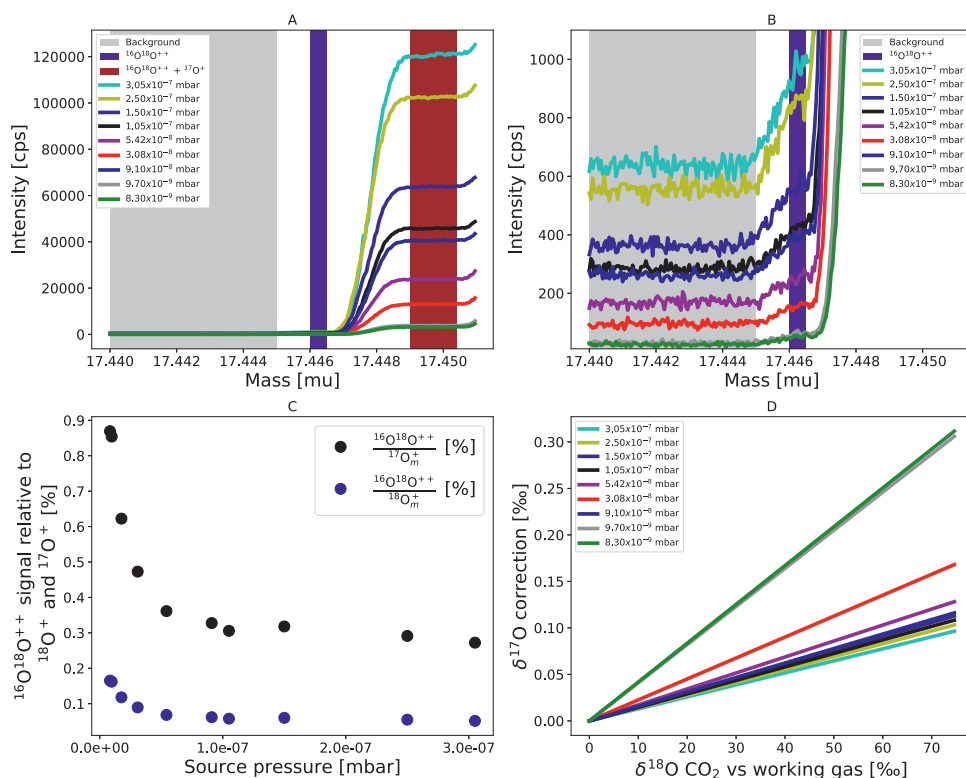


Figure 2.3 Interference of  $^{16}\text{O}^{18}\text{O}^{++}$  on the measurement of the  $^{17}\text{O}^+$  fragment. A) Mass spectra at different source pressure. B) Zoom to the background signal where the interference of  $^{16}\text{O}^{18}\text{O}^{++}$  can be detected starting around mass 17.445, 0.002 mass units before the larger  $^{17}\text{O}^+$  peak. The CDD background signals determined in the grey shaded area were subtracted from the signals in the dark shaded area to quantify the contribution from  $^{16}\text{O}^{18}\text{O}^{++}$ . C) Abundance of the  $^{16}\text{O}^{18}\text{O}^{++}$  signal relative to the measured signals  $^{17}\text{O}_m^+$  and  $^{18}\text{O}_m^+$  (in %). For source pressures above  $10^{-7}$  mbar, where our measurements were carried out, the  $^{16}\text{O}^{18}\text{O}^{++}$  signal is 0.06 % of the  $^{18}\text{O}^+$  signal, which results in a contribution of 0.3 % to the  $^{17}\text{O}^+$  ion beam D) Bias in  $\delta^{17}\text{O}$  introduced by  $^{16}\text{O}^{18}\text{O}^{++}$  as a function of the difference in  $\delta^{18}\text{O}$  between sample and working gas for different source pressures.



At  $2.5 \times 10^{-7}$  mbar, where our measurements were carried out, the  $^{16}\text{O}^{18}\text{O}^{++}$  signal is 0.055 % of the  $^{18}\text{O}^+$  signal, which results in a  $^{16}\text{O}^{18}\text{O}^{++}$  contribution of about 0.3 % to the  $^{17}\text{O}^+$  ion beam. Based on this correction factor, Figure 2.3 D shows the calculated effect of  $^{16}\text{O}^{18}\text{O}^{++}$  on the measured  $\delta^{17}\text{O}$  values, as a function of the  $\delta^{18}\text{O}$  difference between sample and working reference gas and for different source pressures. The correction is likely instrument and tuning-dependent and should be determined regularly. We applied a corresponding correction to the data where we compare the results from the O-fragment method and  $\text{CO}_2$ - $\text{O}_2$  exchange method.

The  $^{13}\text{C}^+$  fragment is measured at Utrecht University at medium resolution (16  $\mu\text{m}$  entrance slit width) with the same emission current, acceleration voltage, integration time and equilibration time as used for the  $^{17}\text{O}^+$  fragment method, again with the VISC window closed. The ion signals are registered in two Faraday collectors (L4 and Center) that are read out with resistors of  $1.0 \times 10^{11} \Omega$  and  $1.0 \times 10^{13} \Omega$  for  $^{12}\text{C}^+$  and  $^{13}\text{C}^+$  respectively. The mass spectra for  $^{12}\text{C}^+$  and  $^{13}\text{C}^+$  are shown in Figure 2.4. The main interference for  $^{13}\text{C}^+$  (mass 13.0034 u) is  $^{12}\text{CH}^+$  (mass 13.0078 u), which requires a mass resolving power of 2900. This is well resolved with medium resolution slit of the 253 Ultra ( $m/\Delta m > 7500$ ).

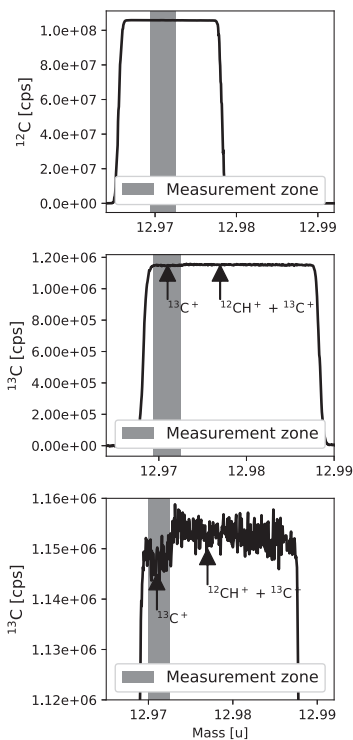


Figure 2.4 Medium resolution mass spectra for measurement of  $^{12}\text{C}^+$  and  $^{13}\text{C}^+$  fragment ions of  $\text{CO}_2$ . The shaded area shows the region where the isotope measurements were performed. Measurement of the C fragment is performed at medium resolution. The mass scale (x-axis) applies to the middle and bottom panels ( $^{13}\text{C}$ ) for the top panel, the mass scale is shifted one mass down.

To establish the scale contraction correction for fragment ion measurements, isotopically well-characterized pure CO<sub>2</sub> gases (see section 2.2) were analyzed both with the molecular ion method and with the fragment ion method. The CO<sub>2</sub> and O<sub>2</sub> working reference gases used in this study are summarized in Table 2.1. The two CO<sub>2</sub> samples G3 and G4 are prepared from G2 by adding isotopically anomalous CO<sub>2</sub> generated by UV-induced isotope exchange between CO<sub>2</sub> and O<sub>3</sub>.

Table 2.1 Overview of name, supplier and isotopic composition of the CO<sub>2</sub> and O<sub>2</sub> working standards used in this study. All the CO<sub>2</sub> gases used have a purity of 99.995 % and O<sub>2</sub> gases have a purity of 99.9998 %.

| CO <sub>2</sub> working reference gases |                               |                                |                                 |
|---|-------------------------------|--------------------------------|---------------------------------|
| Name                                    | Supplier                      | δ <sup>13</sup> C vs. VPDB [‰] | δ <sup>18</sup> O vs. VSMOW [‰] |
| G1                                      | Air products, Germany         | -39.47±0.012                   | 4.843±0.013                     |
| G2                                      | Linde Gas, the Netherlands    | -31.733±0.008                  | 34.998±0.023                    |
| G5                                      | Air products, Germany         | -10.445±0.010                  | 30.404±0.020                    |
| SCOTT                                   | Air products, Germany         | -2.900±0.011                   | 25.803 ±0.015                   |
| O <sub>2</sub> working reference gases  |                               |                                |                                 |
| Name                                    | Supplier                      | δ <sup>17</sup> O vs VSMOW     | δ <sup>18</sup> O vs VSMOW      |
| IMAU-O2                                 | Air products, the Netherlands | 9.254 ±0.007                   | 18.542±0.008                    |
| GU-O <sub>2</sub>                       | Air products, Germany         | 3.849±0.017                    | 8.218±0.007                     |

The reported internal precision of the fragment technique is compared to the expected error (precision) based on counting statistics (EECS), which is calculated as:

$$EECS = \sqrt{\frac{2}{N \times t_{int} \times n}} \quad (2.6)$$

Where N is the average count rate (cps),  $t_{int}$  is the integration time in seconds, n is the number of measurement cycles and the factor  $\sqrt{2}$  accounts for the fact that both reference and the sample introduce the same error to the δ value. Throughout the manuscript the error of a single measurement series is reported as standard error of the mean. When we quantify errors for more than one measurement (series), we report the standard error times student t-factor to cover the 95 % confidence interval.

#### 2.2.4. O<sub>2</sub>-CO<sub>2</sub> exchange method

A schematic diagram of the O<sub>2</sub>-CO<sub>2</sub> exchange experimental setup at Utrecht University is shown in Supplementary Figure S2.2. The central part of the CO<sub>2</sub>-O<sub>2</sub> exchange system is the exchange reactor, which is made of quartz while the other parts are made from borosilicate glass. The general design is similar to the one in Barkan et al. (2015), except for some modifications in the ways of introducing CO<sub>2</sub> and O<sub>2</sub> into the reactor.

Approximately 1.7 mL of pure CO<sub>2</sub> with known (measured) δ<sup>18</sup>O value was expanded to the glass line and trapped cryogenically using liquid nitrogen in the calibrated volume (CV, 2.319 mL). The amount of CO<sub>2</sub> was precisely determined with a pressure sensor (PS9504, Geological

and Nuclear Sciences limited, New Zealand). The CO<sub>2</sub> sample was then transferred cryogenically to the quartz reactor. The trapping in the quartz reactor occurs at the horizontal tube that is continuously cooled using liquid nitrogen provided by a microdosing system (Norhof 900 series LN<sub>2</sub> cooling system, the Netherlands). After introduction of the CO<sub>2</sub> sample, an approximately equal amount of pure O<sub>2</sub> (IMAU-O<sub>2</sub>) with known  $\delta^{17}\text{O}$  and  $\delta^{18}\text{O}$  values is admitted to the small volume above the reactor and then expanded into the reactor. The CO<sub>2</sub> is then released from the cold tube by stopping the LN<sub>2</sub> microdosing system, and the gases are allowed to react for 30 minutes in the quartz reactor that contains 0.18 g of platinum sponge (99.9 % purity, Sigma Aldrich, USA) at the bottom, which is heated to 750 °C with a temperature-controlled oven (CFH VC401A06A-0000R, Kurval, The Netherlands). After 30 minutes, CO<sub>2</sub> is extracted cryogenically in a double U trap, while O<sub>2</sub> is collected behind this trap on 3 pellets of molecular sieve 13X (1.6 mm, Sigma Aldrich, USA) at liquid nitrogen temperature. The isotopic composition of the exchanged O<sub>2</sub> is measured using a dual inlet system on the Delta<sup>Plus</sup>XL isotope ratio mass spectrometer (Thermo Fisher Scientific, Bremen, Germany) using three Faraday collectors equipped with resistors of  $3 \times 10^8 \Omega$ ,  $3 \times 10^{10} \Omega$  and  $3 \times 10^{11} \Omega$  for  $m/z$  32, 33 and 34 respectively. The value of  $\delta^{17}\text{O}$  (CO<sub>2</sub>) is then calculated from the change in  $\delta^{17}\text{O}(\text{O}_2)$  value before (index  $i$  = “initial”) and after (index  $f$  = “final”) isotope exchange with CO<sub>2</sub> based on the following mass balance equation (equation 2.7), after Barkan et al. (2015).

$$\delta^{17}\text{O}_i(\text{CO}_2) = \frac{1}{\beta} [(\delta^{17}\text{O}_f(\text{O}_2) + 1)(\alpha^{17}\beta + 1) - (\delta^{17}\text{O}_i(\text{O}_2) + 1)] - 1 \quad (2.7)$$

where  $\beta$  is the molar ratio of CO<sub>2</sub> to O<sub>2</sub> and  $\alpha^{17}(\text{CO}_2/\text{O}_2) = \frac{\delta^{17}\text{O}_f(\text{CO}_2)+1}{\delta^{17}\text{O}_f(\text{O}_2)+1}$  and  $\alpha^{18}(\text{CO}_2/\text{O}_2) = \frac{\delta^{18}\text{O}_f(\text{CO}_2)+1}{\delta^{18}\text{O}_f(\text{O}_2)+1}$  are the <sup>17</sup>O and <sup>18</sup>O equilibrium fractionation factors between CO<sub>2</sub> and O<sub>2</sub> in presence of the hot platinum catalyst (Barkan et al., 2015). In our CO<sub>2</sub>-O<sub>2</sub> exchange setup the equilibrium fractionation factors are  $\alpha^{17}(\text{CO}_2/\text{O}_2) = 1.0006657$  and  $\alpha^{18}(\text{CO}_2/\text{O}_2) = 1.000998$ , determined by measuring the isotopic composition of CO<sub>2</sub> and O<sub>2</sub> after isotope exchange was fully established.

## 2.2.5. Samples

### 2.2.5.1. Preparation of CO<sub>2</sub> with known $\delta^{17}\text{O}$ and $\delta^{18}\text{O}$ values

At Utrecht University, CO<sub>2</sub> with known isotopic composition is prepared by combusting a pure graphite rod (99.9995 % purity, Alfa Aesar, Part number: 40765) (Thermo Fisher Scientific, Germany) in isotopically known pure IMAU-O<sub>2</sub> (Table 2.1). The graphite rod (3.05 mm x 32mm) is wrapped in a sheet of platinum foil and platinum wire and placed inside a quartz reactor as shown in Supplementary Figure S2.3. The experimental setup is similar to the one presented in Barkan and Luz (1996), except for a modification in the way CO<sub>2</sub> is trapped. The graphite rod is conditioned by heating to 1000 °C in vacuum for 2 days. The combustion experiment is performed at 750 °C and the CO<sub>2</sub> is trapped immediately at liquid nitrogen temperature using a collar trap (Figure S2.3) to avoid fractionation due to possible exchange with the graphite. After O<sub>2</sub> has been fully combusted to CO<sub>2</sub> (as indicated by the pressure), the reactor is cooled to below 200 °C and the collar trap is heated to room temperature (25 °C) to release the CO<sub>2</sub>. The CO<sub>2</sub> is collected in a break seal tube at liquid nitrogen temperature. After

each conversion experiment the graphite rod is re-conditioned by heating at 900 °C for 1 hour to avoid contamination from remaining oxygen.

At the University of Göttingen, isotopically light CO<sub>2</sub> was produced from combustion with isotopically depleted O<sub>2</sub> using a slightly different setup. Instead of using platinum foil and wire as catalyst, the graphite rod was immersed in chloroplatinic acid and dried before being installed in the quartz reactor. Isotopically light oxygen for the reaction was provided by hydrolysis of Antarctic precipitation (Dronning Maud Land,  $\delta D = -341.1$  ‰ vs SMOW and  $\delta^{18}O = -42.4$  ‰ vs SMOW). After full combustion, the produced CO<sub>2</sub> was transferred into a glass vial, which was kept at liquid nitrogen temperature.

#### **2.2.5.2. Preparation of <sup>17</sup>O-enriched CO<sub>2</sub>**

<sup>17</sup>O-enriched CO<sub>2</sub> is prepared by inducing oxygen isotope exchange between CO<sub>2</sub> (G2) and O<sub>2</sub> (IMAU-O2) (via O<sub>3</sub> and O(<sup>1</sup>D)) (Shaheen et al., 2007) using a Hg Ultra Violet (UV) lamp (Oriol instruments, Newport corporation, USA). The 2L borosilicate photolysis reactor is equipped with a UV-transparent Suprasil<sup>TM</sup> finger in the center to place the lamp as shown in Supplementary Figure S2.4. 50 mbar of CO<sub>2</sub> is expanded into the 2L reactor and then O<sub>2</sub> is expanded into the reactor until the pressure reading reaches around 1bar. Then the mixture is allowed to photolyze for 18 hours without regulating the temperature. Due to the heat produced by the UV light the temperature outside the reactor reaches to 30 °C during photolysis, and is much hotter at the Suprasil finger, but this is only a preparative experiment where the exact conditions are not critical. After photolysis-induced isotope exchange, CO<sub>2</sub> is separated cryogenically in a glass spiral trap at liquid nitrogen temperature and O<sub>2</sub> is pumped out. Finally, the CO<sub>2</sub> is collected in a sample vial containing nickel foil (thickness 0.05 mm, 99.98 % purity, Goodfellow, Cambridge Ltd, UK). O<sub>3</sub> that is formed during photolysis is also condensed with CO<sub>2</sub> and is decomposed to O<sub>2</sub> by heating the sample vial with a heat gun at 500 °C for 10 minutes. Ni foil catalyzes the decomposition of O<sub>3</sub> to O<sub>2</sub>. Then the CO<sub>2</sub> is trapped again with liquid nitrogen and the O<sub>2</sub> that has formed from O<sub>3</sub> decomposition is pumped out. Finally, the CO<sub>2</sub> is passed through a glass U-trap at dry ice temperature (-78 °C) to remove remaining traces of water. Heating O<sub>3</sub> and CO<sub>2</sub> mixture above 200 °C might cause isotope exchange between O<sub>3</sub> and CO<sub>2</sub> (Katakis and Taube, 1962), but it does not cause a problem for our purpose which is to prepare <sup>17</sup>O-enriched CO<sub>2</sub>.

The isotopic composition of the <sup>17</sup>O-enriched CO<sub>2</sub> sample is measured with the 253 Ultra for both molecular ions (*m/z* of 44 to 46) to determine  $\delta^{18}O$  and  $\delta^{13}C$  values, and atom fragments to measure  $\delta^{17}O$  and  $\delta^{18}O$  values. By diluting the <sup>17</sup>O-enriched CO<sub>2</sub> with pure non-anomalous CO<sub>2</sub> from the reference CO<sub>2</sub> tank (G2), two gas mixtures are prepared with a target  $\Delta^{17}O$  of approximately 0.25 ‰ and 0.55 ‰. The two mixtures are finally measured both with the CO<sub>2</sub>-O<sub>2</sub> exchange method and the fragment technique.

## 2.3. Results

### 2.3.1. Instrument characterization and scale contraction

Scale contraction decreases with equilibration time and source pressure (signal intensity), when the variable conductance window fully opened and when decreasing the emission current. A detailed investigation of these parameters is presented in the supplementary information (Figure S2.5, S2.6, and S2.7 and Table S2.1 and S2.2). The effect of ion source pressure and emission control current are the major contributors to the scale contraction. Scale contraction can be minimized if the measurement is performed at high source pressure, low emission control current and with the VISC window open. The drawback of having higher source pressure is potentially a reduction in the life time of the filament while having lower emission control current reduces the ionization of the molecules which leads to lower signal. We suggest to follow the recommendations suggested by Verkouteren et al. (2003b) to minimize cross contamination in dual inlet isotope ratio mass spectrometer measurements. In general, the different parameters affect both the  $\delta^{18}\text{O}$  and  $\delta^{13}\text{C}$  values in the same way, but the effects are larger for  $\delta^{18}\text{O}$  than for  $\delta^{13}\text{C}$ . The origin of the qualitatively different behavior for  $\delta^{18}\text{O}$  and  $\delta^{13}\text{C}$  could not be identified and requires further study.

By comparing the results of the molecular ion measurements on the 253 Ultra to the values assigned to our reference gases by the Hebrew University of Jerusalem, a scale contraction factor of 0.981 is established and applied for molecular ion measurements. The scale contraction factor is the ratio of the difference between the two  $\text{CO}_2$  gases (G1 and SCOTT) measured with the 253 Ultra at Utrecht University and the assigned relative difference by the Hebrew University of Jerusalem. Thus, the final values reported below are linked to the isotope scale of the Hebrew University of Jerusalem (Luz and Barkan, 2005; Barkan and Luz, 2012; Barkan and Luz., 2004).

The key parameter relevant for the validation of the fragment method is the scale contraction of a fragment ion measurement relative to a molecular ion measurement. This was determined by analyzing a set of three isotopically distinct pure  $\text{CO}_2$  gases both with the traditional  $\text{CO}_2^+$  method and with the fragment method (both  $\text{O}^+$  and  $\text{C}^+$  fragments). For the traditional molecular ion measurements, the  $^{17}\text{O}$ -correction procedure from Brand et al. (2010) is used. Table 2.2 shows that the scale contraction for fragment ion measurements is slightly larger than the one for molecular ion measurements. The scale contraction seems to be also slightly larger for measurements on the  $\text{C}^+$  fragment than for the  $\text{O}^+$  fragment, but more measurements are required to quantify this more thoroughly.

Table 2.2  $\delta^{13}\text{C}$  and  $\delta^{18}\text{O}$  scale contraction factors for measurements with the fragment method relative to the traditional measurement technique on molecular ions, using the  $^{17}\text{O}$  correction algorithm from Brand et al. (2010). Both measurements are carried out on the 253 Ultra using three  $\text{CO}_2$  gases (G1, SCOTT and G2).

| Measurement                 | Fragment (253 Ultra) vs molecule (253 Ultra) |                       |
|-----------------------------|--|-----------------------|
|                             | $\delta^{13}\text{C}$                        | $\delta^{18}\text{O}$ |
| G1 vs G2                    | 0.996  | 0.997                 |
| G1 vs SCOTT                 | 0.993  | 0.997                 |
| SCOTT vs G2                 | 0.996  | 0.997                 |
| Average $\pm$ SE $\times$ t | $0.995 \pm 0.0016$                           | 0.997                 |

Note that each individual measurement series presented in Table 2.3 and Table 2.4 ( $\text{CO}_2^+$  molecule plus  $\text{O}^+$  fragment plus  $\text{C}^+$  fragment) takes one full day. For the evaluation of the  $\Delta^{17}\text{O}$  measurements below we use the relative scale contraction of 0.997 determined for the value of  $\delta^{18}\text{O}$  measurements between the traditional  $\text{CO}_2^+$  method and the O- fragment method (Table 2.2).

Table 2.3 Oxygen isotope composition of various  $\text{CO}_2$  reference gases measured with the  $^{17}\text{O}^+$  fragment method.  $\delta^{17}\text{O}$  and  $\delta^{18}\text{O}$  values are given relative to VSMOW;  $\Delta^{17}\text{O}$  is calculated according to Equation 2.4 using  $\lambda = 0.528$ . Individual errors are standard errors of the mean of the corresponding measurement series. The error for the mean is the standard error of the mean for the six experiments multiplied by the student t-factor for the 95 % two sided confidence.  $\Gamma$  is the ratio between the measured precision and the precision expected from counting statistics for  $\delta^{17}\text{O}$  and  $n$  is the number of sample-standard cycles. For  $\delta^{18}\text{O}$ ,  $\Gamma \approx 1$  for individual measurement series, but the weighted mean error is similar to the one for  $\delta^{17}\text{O}$ , which indicates additional handling errors in sample introduction at the 0.01 ‰ level. The values in the parentheses are the isotopic composition of oxygen used for combustion.

| Exp.  | n   | $\Gamma$ | $\delta^{17}\text{O}$ [‰] | $\delta^{18}\text{O}$ [‰] | $\Delta^{17}\text{O}$ [‰] |
|---|-----|----------|---------------------------|---------------------------|---------------------------|
| Reference $\text{CO}_2$ [Figure 2.5a]   |     |          |                           |                           |                           |
| 1   | 227 | 1.54     | $15.661 \pm 0.037$        | $30.406 \pm 0.011$        | $-0.276 \pm 0.036$        |
| 2   | 109 | 1.53     | $15.719 \pm 0.048$        | $30.419 \pm 0.14$         | $-0.225 \pm 0.048$        |
| 3   | 47  | 1.73     | $15.672 \pm 0.082$        | $30.444 \pm 0.025$        | $-0.284 \pm 0.081$        |
| 4   | 109 | 1.48     | $15.701 \pm 0.047$        | $30.397 \pm 0.014$        | $-0.231 \pm 0.047$        |
| 5   | 169 | 1.42     | $15.672 \pm 0.038$        | $30.380 \pm 0.011$        | $-0.251 \pm 0.038$        |
| 6   | 68  | 1.47     | $15.668 \pm 0.057$        | $30.379 \pm 0.016$        | $-0.255 \pm 0.057$        |
| Mean $\pm$ SE $\times$ t  |     |          | $15.682 \pm 0.019$        | $30.404 \pm 0.021$        | $-0.254 \pm 0.019$        |
| Reference $\text{O}_2$ to $\text{CO}_2$ [Figure 2.5b] (vs reference $\text{CO}_2$ ) |     |          |                           |                           |                           |
| 1   | 64  | 1.1      | $-10.518 \pm 0.028$       | $-19.266 \pm 0.017$       | $-0.303 \pm 0.026$        |
| 2   | 64  | 0.8      | $-10.586 \pm 0.021$       | $-19.367 \pm 0.009$       | $-0.316 \pm 0.020$        |
| 3   | 64  | 1.2      | $-10.639 \pm 0.035$       | $-19.360 \pm 0.010$       | $-0.373 \pm 0.036$        |
| 4   | 64  | 1.1      | $-10.534 \pm 0.027$       | $-19.184 \pm 0.009$       | $-0.362 \pm 0.028$        |
| 5   | 64  | 1.0      | $-10.516 \pm 0.026$       | $-19.194 \pm 0.011$       | $-0.339 \pm 0.026$        |
| 6   | 64  | 1.2      | $-10.743 \pm 0.030$       | $-19.595 \pm 0.010$       | $-0.352 \pm 0.030$        |
| 7   | 64  | 1.2      | $-10.741 \pm 0.030$       | $-19.610 \pm 0.007$       | $-0.342 \pm 0.030$        |
| 8   | 64  | 1.3      | $-10.611 \pm 0.34$        | $-19.345 \pm 0.009$       | $-0.353 \pm 0.034$        |
|   |     |          | $-10.611 \pm 0.062$       | $-19.365 \pm 0.109$       | $-0.342 \pm 0.016$        |
| Reference $\text{O}_2$ to $\text{CO}_2$ [Figure 2.8a]                               |     |          |                           |                           |                           |
| 1   | 200 | 2.43     | $9.206 \pm 0.071$         | $18.510 \pm 0.018$        | $-0.520 \pm 0.071$        |
| 2   | 300 | 1.99     | $9.220 \pm 0.048$         | $18.539 \pm 0.018$        | $-0.522 \pm 0.048$        |
| 3   | 180 | 1.88     | $9.298 \pm 0.042$         | $18.495 \pm 0.017$        | $-0.423 \pm 0.042$        |

|   |     |      |                                  |                                  |                                |
|---|-----|------|----------------------------------|----------------------------------|--------------------------------|
| 4   | 200 | 2.16 | 9.302±0.048                      | 18.465±0.017                     | -0.403±0.048                   |
| Mean ±SE×t  |     |      | 9.256±0.059<br>(9.254±0.007)     | 18.503±0.035<br>(18.542±0.008)   | -0.467±0.074<br>(-0.489±0.008) |
| Light O <sub>2</sub> to CO <sub>2</sub> [Figure 2.8b] |     |      |                                  |                                  |                                |
| 1   | 216 | 2.13 | -26.934±0.097                    | -50.791±0.024                    | 0.219±0.067                    |
| 2   | 208 | 1.43 | -26.611±0.355                    | -50.075±0.512                    | 0.182±0.059                    |
| 3   | 256 | 1.34 | -26.381±0.231                    | -49.824±0.318                    | 0.311±0.056                    |
| Mean ±SE×t  |     |      | -26.666±0.488<br>(-26.239±0.002) | -50.329±0.817<br>(-49.614±0.002) | 0.237±0.097<br>(0.279±0.011)   |

When the appropriate scale correction parameters are applied, the  $\delta^{13}\text{C}$  and  $\delta^{18}\text{O}$  values obtained from the fragment and molecular ion measurements generally agree at the  $\sim 0.01 - 0.03 \%$  reproducibility level (except for one outlier in  $\delta^{13}\text{C}$ , G1 vs SCOTT =  $-36.665 \pm 0.002 \%$  and  $-36.601 \pm 0.020 \%$  for molecular and fragment ion measurements respectively, Figure S2.10). Isotope ratio measurements on C and O fragment ions could be an independent method to validate/evaluate traditional isotope measurements and ion ( $^{17}\text{O}$ ) correction algorithms at the level of precision similar to the reported differences between different ion correction schemes. Figures S2.8, S2.9 and S2.10 shows that the fragment method returns the same value when two pure CO<sub>2</sub> gases are measured directly, and via a third intermediate gas for  $\delta^{13}\text{C}$ ,  $\delta^{18}\text{O}$  and  $\delta^{17}\text{O}$ . Table 2.3 and 2.4 show that both the  $^{13}\text{C}^+$  and  $^{18}\text{O}^+$  fragment isotope ratios are measured with a precision close to the counting statistics limit.

## 2.3.2. Fragment measurement

### 2.3.2.1. $\delta^{17}\text{O}$ , $\delta^{18}\text{O}$ and $\Delta^{17}\text{O}$ : reproducibility

Figure 2.5A shows  $\Delta^{17}\text{O}$  for a pure CO<sub>2</sub> (G5) sample with six replicates measured using the O-fragment method at Utrecht University. The  $\delta^{17}\text{O}$  and  $\delta^{18}\text{O}$  values of the CO<sub>2</sub> are given in Table 2.3. Measurement times are between 3 and 12 hours.  $\delta^{17}\text{O}$  is measured with an individual measurement error (standard error of the mean) ranging from 37 to 82 ppm, while the  $\delta^{18}\text{O}$  values have an individual measurement error of 11 to 25 ppm (standard error of the mean). The measurement precision for  $\delta^{17}\text{O}$  is worse than that expected from counting statistics by a factor of 1.42 to 1.73. As shown in Figure 2.5A and Table 2.3, from these 6 replicates the  $\Delta^{17}\text{O}$  reproducibility is 19 ppm (standard error times student t factor for 95 % confidence). At University of Göttingen the reproducibility experiment is performed using CO<sub>2</sub> produced by combustion of a graphite rod with pure O<sub>2</sub> (GU-O<sub>2</sub>), Figure 2.5B. The  $\delta^{17}\text{O}$  and  $\delta^{18}\text{O}$  values of the CO<sub>2</sub> are given in Table 2.3 relative to working reference.  $\delta^{17}\text{O}$  is measured with an individual measurement error (standard error of the mean) ranging from 21 to 35 ppm while the  $\delta^{18}\text{O}$  values have an individual measurement error of 7 to 17 ppm (standard error of the mean). As shown in Figure 2.5B and Table 2.3, from these 8 replicates the  $\Delta^{17}\text{O}$  reproducibility is 16 ppm (standard error times student t factor for 95 % confidence). The reproducibility for  $\delta^{17}\text{O}$  and  $\delta^{18}\text{O}$  is lower due to incomplete combustion of the graphite rod.

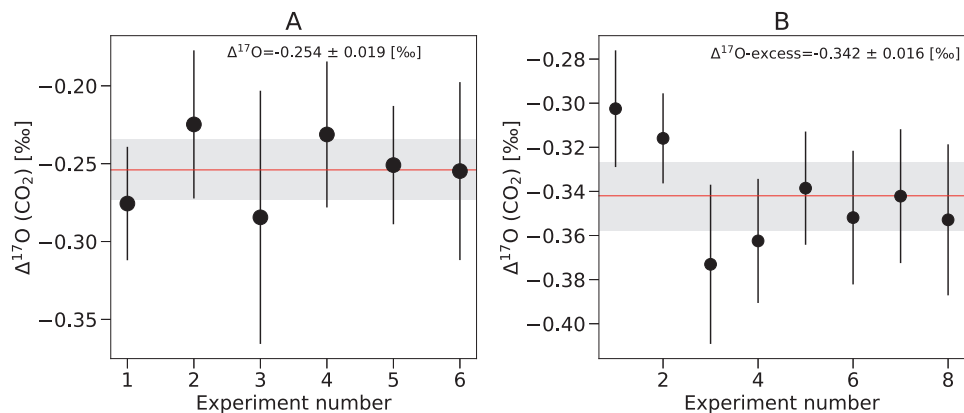


Figure 2.5 A)  $\Delta^{17}\text{O}(\text{CO}_2)$  measured with the O-fragment method for a pure  $\text{CO}_2$  (G5, see Table 2.1), measured at Utrecht University. B)  $\Delta^{17}\text{O}(\text{CO}_2)$  measured with the O-fragment method for  $\text{CO}_2$  prepared by combusting graphite rod with pure  $\text{O}_2$  (GU- $\text{O}_2$ ) ( $\delta^{17}\text{O} = -10.611 \pm 0.062$  ‰ and  $\delta^{18}\text{O} = -19.365 \pm 0.109$  ‰, relative to the working standard) measured at University of Göttingen. Error bars represent  $\pm 1$  standard error of the mean (SE). The red line shows the mean and the shaded area is the standard error of the mean times student t-factor (95 % confidence).

Due to the low ion counts very long measurement times are required to achieve a precision of the order of 10 ppm. A long-term zero enrichment measurement of a cylinder reference gas at University of Göttingen (Tyczka Industrie Gase, Tyczka Industrie-Gase GmbH, Germany) yielded a precision of 14 ppm for  $\Delta^{17}\text{O}$  and  $\delta^{17}\text{O}$  (5 ppm for  $\delta^{18}\text{O}$ ) after a measurement time of 20 hours (Figure 2.6). As mentioned above, a requirement is that the mass scale remains very stable over the entire measurement period.



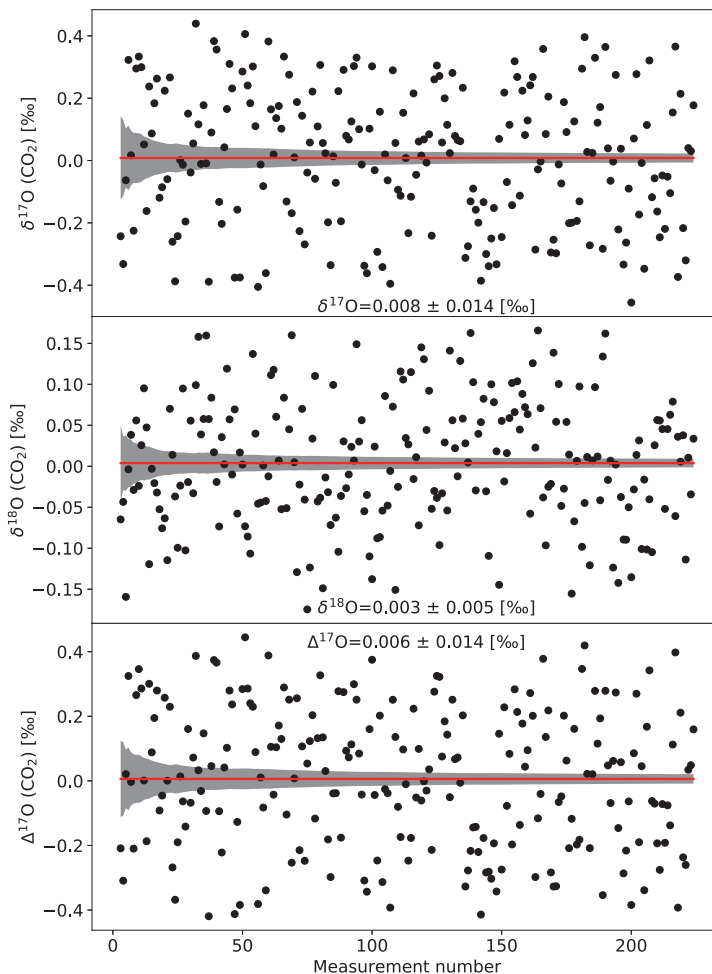


Figure 2.6 A long-term zero enrichment experiment ( $\Delta^{17}\text{O}$ ,  $\delta^{17}\text{O}$  and  $\delta^{18}\text{O}$ ) at the University of Göttingen. After 20 hours of measurement time a precision of 14 ppm for  $\delta^{17}\text{O}$  and  $\Delta^{17}\text{O}$ , and 5 ppm for  $\delta^{18}\text{O}$  is achieved.

At Utrecht University we monitor the stability of the mass scale by recording a medium-resolution mass spectrum at regular intervals during the measurement. Figure 2.7A and B show an example of a long-term fragment measurement during which the mass scale was very stable. However, the mass scale is not always that stable, and mass instabilities are one limitation for measurements that require long measurement times. Instabilities in the mass scale are likely to contribute to the larger errors compared to counting statistics, factor  $\Gamma$  in Table 2.3, in some measurements.

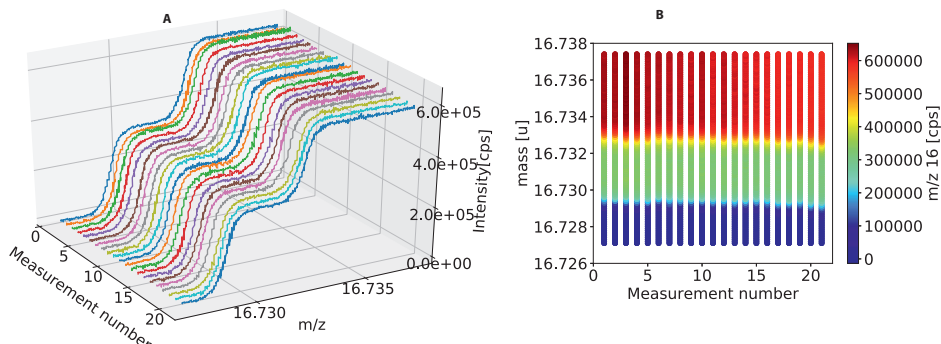


Figure 2.7 A) Medium resolution mass sweep for  $m/z$  17 performed during the isotope measurement to monitor the stability of the mass scale. Each line represents a single mass spectrum that was recorded after each acquisition of 10 cycles of dual inlet isotope measurements. The separation between two mass sweeps is roughly 21 minutes. B) shows the 2 D projection of A, where the ion count rate is presented in color to show the stability of the plateau used for measurement of the  $^{17}\text{O}^+$  fragment (green section).

### 2.3.2.2. $\Delta^{17}\text{O}$ accuracy

The accuracy of  $\Delta^{17}\text{O}$  and  $\delta^{17}\text{O}$  measurements using the O-fragment method is evaluated by measuring  $\text{CO}_2$  with known  $\delta^{17}\text{O}$  and  $\delta^{18}\text{O}$  values, prepared from isotopically known  $\text{O}_2$  (see section 2.2.5.2) The results presented in Figure 2.8A and Table 2.3 show that  $\Delta^{17}\text{O}$  of the  $\text{CO}_2$  obtained by measuring the  $\delta^{17}\text{O}$  and  $\delta^{18}\text{O}$  values from the  $^{17}\text{O}^+$  and  $^{18}\text{O}^+$  fragment ions is indistinguishable within the experimental error from the isotopic composition of  $\text{O}_2$  used for the preparation of the  $\text{CO}_2$ . The assigned  $\Delta^{17}\text{O}$  value of the reference  $\text{O}_2$  used for combustion at Utrecht University is  $-0.489 \pm 0.008 \text{ ‰}$  while the  $\text{CO}_2$  obtained by combustion has  $\Delta^{17}\text{O} = -0.467 \pm 0.074 \text{ ‰}$  when measured with the fragment method (Figure 2.8A and Table 2.3). To enable easy comparison,  $\Delta^{17}\text{O}$  of  $\text{O}_2$  and  $\text{CO}_2$  are both calculated with the same value of  $\lambda=0.528$ . Also, the individual  $\delta^{17}\text{O}$  and  $\delta^{18}\text{O}$  values agree with the source  $\text{O}_2$  within the errors. It should be noted that the discrepancy of  $\Delta^{17}\text{O}$  results within our measurement series is larger than the errors from the individual measurements, which indicates that sample handling errors have contributed to the rather large spread in the fragment measurements. The isotopically light  $\text{O}_2$  in Göttingen has assigned values of  $\delta^{17}\text{O} = -26.239 \pm 0.002 \text{ ‰}$ ,  $\delta^{18}\text{O} = -49.614 \pm 0.002 \text{ ‰}$  relative to VSMOW, which yields  $\Delta^{17}\text{O} = 0.279 \pm 0.006 \text{ ‰}$ . The  $\text{CO}_2$  produced by combustion and measured with the O-fragment method (Figure 2.8B, Table 2.3) shows a rather wide range of  $\delta^{17}\text{O}$  and  $\delta^{18}\text{O}$  values, indicating fractionation (and/or incomplete combustion) in the process of preparing the  $\text{CO}_2$ . The effect on  $\Delta^{17}\text{O}$  is much smaller.

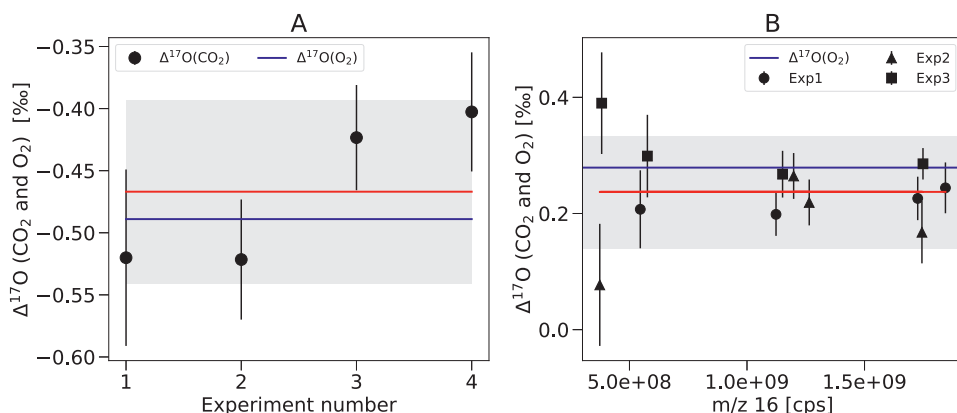


Figure 2.8 A)  $\Delta^{17}\text{O}$  of CO<sub>2</sub> produced by combustion of a graphite rod (black points and red line showing the mean) and  $\Delta^{17}\text{O}$  of the pure O<sub>2</sub> used for combusting the graphite (blue line), measured at Utrecht University. B) Similar results for CO<sub>2</sub> that was prepared from isotopically depleted O<sub>2</sub> at the University of Göttingen, plotted versus the  $m/z$  16 signal intensity.  $\Delta^{17}\text{O}$  values obtained from the fragment method are indistinguishable from the  $\Delta^{17}\text{O}$  values of the combusted O<sub>2</sub>. The  $\Delta^{17}\text{O}$  is calculated using  $\lambda = 0.528$  for both gases. Individual error bars represent  $\pm 1$  standard error of the mean (SE). The shaded area shows the standard error of the mean times student t-factor (95% confidence).

The good agreement between  $\delta^{17}\text{O}$ ,  $\delta^{18}\text{O}$  and  $\Delta^{17}\text{O}$  of oxygen and the CO<sub>2</sub> produced by combusting graphite shows that determination of the triple isotopic composition of CO<sub>2</sub> using the O-fragment method is not only reproducible but also accurate. Furthermore, the agreement in the triple isotopic composition of oxygen between O<sub>2</sub> and CO<sub>2</sub> (produced by combustion) suggests that our isotope scales for CO<sub>2</sub> and O<sub>2</sub> are very compatible.

As shown in supplementary Table S2.3,  $\Delta^{17}\text{O}$  is measured with an average standard error of 39 ppm (standard error of the mean) for four measurements (A<sub>3</sub>, B<sub>2</sub>, B<sub>3</sub>, C<sub>2</sub>) at an intensity for  $m/z$  16 of  $1.18 \times 10^9$  cps. When measurements are done at lower signal intensity than the linear range for source pressure vs. signal intensity relation for  $m/z$  16 (see above), measurement precision decreases. For instance, the precision drops from 39 to 83 ppm (average standard error of the mean for the four measurements shown in supplementary Table S2.3) when the intensity on  $m/z$  16 decreases from  $1.18 \times 10^9$  to  $4.70 \times 10^8$  cps. Measurement at higher signal intensity, outside of the linear window, does not show a significant improvement in the precision of the  $\Delta^{17}\text{O}$  measurement relative to measurements with lower signal intensity in the linear window (supplementary Table S2.3). This might be also due to statistics since we only have four measurements.

### 2.3.2.3. Comparison of O-fragment method with CO<sub>2</sub>-O<sub>2</sub> exchange method

After confirming the accuracy and reproducibility of the O-fragment method, we measured  $\delta^{17}\text{O}$ ,  $\delta^{18}\text{O}$  and  $\Delta^{17}\text{O}$  of four CO<sub>2</sub> gases both with the O-fragment method and with the oxygen exchange method (see above). Two of the gases are commercial CO<sub>2</sub> gases (G1 and G2, Table 2.1) and the other two (G3 and G4) were artificially enriched in <sup>17</sup>O as described in section 2.5.2 (above). As shown in Figure 2.9 and supplementary Table S2.4 the results obtained with the two totally independent techniques are indistinguishable within the error bars. The  $\delta^{18}\text{O}$  values are in the range of 4.8 ‰ to 35.0 ‰ vs. VSMOW and values of  $\Delta^{17}\text{O}$  range from -0.3

‰ to +0.7 ‰ ( $\lambda = 0.528$ ) which covers and extends the  $\Delta^{17}\text{O}$  range expected for tropospheric  $\text{CO}_2$  samples, including international carbonate standards (Passey et al., 2014). The  $\Delta^{17}\text{O}$  is determined on the O-fragment method with a precision of 36 to 79 ppm (standard error times student t-factor for 95 % confidence). The excellent agreement between the two totally independent methods provides an independent validation of the fragment ion technique.

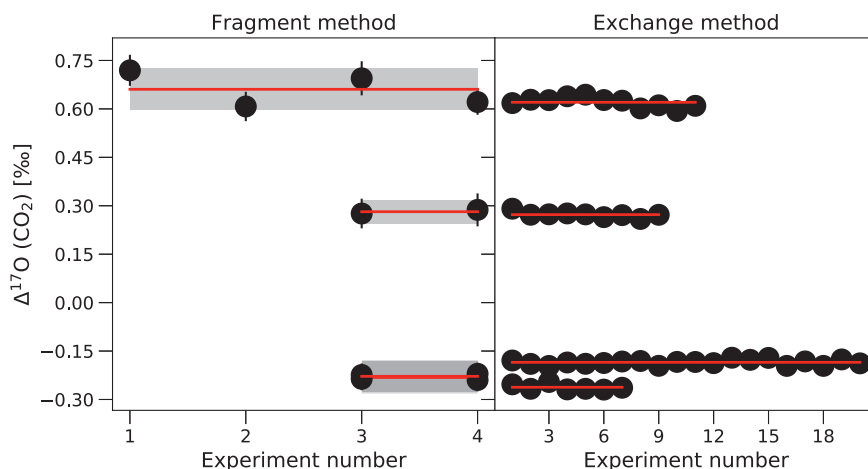


Figure 2.9 Comparison of  $\Delta^{17}\text{O}$  measured with the fragment method and the  $\text{CO}_2\text{-O}_2$  exchange method for four different  $\text{CO}_2$  gases. The  $\delta^{18}\text{O}$  values of the  $\text{CO}_2$  gases range from 4.48 ‰ to 35.00 ‰. The horizontal axis shows the number of experiments. Error bars for the fragment measurement represent  $\pm 1$  standard error of the mean (SE). The red line shows the mean and the shaded area is the standard error of the mean times student t-factor (95 % confidence).

### 2.3.3. C-fragment

The  $\delta^{13}\text{C}$  values of the two  $\text{CO}_2$  gases G1 and SCOTT were measured against G2 with the C-fragment method and with the traditional measurement on the  $\text{CO}_2$  molecule (evaluated with the Brand et al. (2010) procedure). As shown in Table 2.4, the  $\delta^{13}\text{C}$  values obtained from the C-fragment method and molecular measurement are the same within the error (at the  $\approx 0.01$  ‰ reproducibility level). A possible challenge for measuring  $\delta^{13}\text{C}$  with the fragment method, is the interference from the  $^{12}\text{CH}^+$  adduct due to ion source chemistry (e.g. in the presence of water). The  $^{12}\text{CH}^+$  adduct is only 0.004 u separated from  $^{13}\text{C}^+$  as shown in the mass spectra (Figure 2.4). However, the figure also shows that this interference can be resolved at medium resolution.

Table 2.4 Comparison of  $\delta^{13}\text{C}$  and  $\delta^{18}\text{O}$  values obtained using the C-fragment and O-fragment technique with results from the traditional molecular measurements for pure  $\text{CO}_2$  gases. For the measurements on the molecule, the  $^{17}\text{O}$  correction according to Brand et al. (2010) is used.  $\Gamma$  is the ratio between measured precision and the precision estimated from the counting statistics and  $n$  is number of cycles for the fragment measurement.

| $\delta^{13}\text{C}$ |              |     |          |   |   |
|-----------------------|--------------|-----|----------|---|---|
| Sample                | Ex p         | n   | $\Gamma$ | $\delta^{13}\text{C}$ [‰]<br>( $^{13}\text{C}^+$ measurement) | $\delta^{13}\text{C}$ [‰]<br>$^{13}\text{CO}_2^+$ measurement |
| G1 vs G2              | 1            | 45  | 1.0      | -7.968±0.015  | -7.963±0.001  |
|                       | 2            | 20  | 0.73     | -7.967±0.022  | -7.984±0.001  |
|                       | 3            | 38  | 0.74     | -7.991±0.016  | -7.967±0.001  |
|                       | 4            |     |          |   | -7.981±0.001  |
|                       | 5            |     |          |   | -7.972±0.001  |
|                       | 6            |     |          |   | -7.978±0.002  |
| Average±SE×t          |              |     |          | -7.975 ±0.023   | -7.974±0.007  |
| G2 vs SCOTT           | 1            | 49  | 0.84     | -28.933±0.015   | -28.881±0.001   |
|                       | 2            |     |          |   | -28.923±0.001   |
|                       | 3            |     |          |   | -28.916±0.001   |
|                       | 4            |     |          |   | -28.913±0.001   |
|                       | 5            |     |          |   | -28.915±0.001   |
| Average±SE×t          |              |     |          |   | -28.910±0.016   |
| $\delta^{18}\text{O}$ |              |     |          |   |   |
| Sample                | Ex p         | n   | $\Gamma$ | $\delta^{18}\text{O}$ (‰)<br>( $^{18}\text{O}^+$ measurement) | $\delta^{18}\text{O}$ (‰)<br>$\text{CO}_2^+$ measurement      |
| G1 vs G2              | 1            | 145 | 0.9      | -29.106±0.010   | -29.140±0.001   |
|                       | 2            | 146 | 0.9      | -29.138±0.010   | -29.146±0.015   |
|                       | 3            | 107 | 0.7      | -29.125±0.010   | -29.132±0.001   |
|                       | 4            | 81  | 0.8      | -29.128±0.012   | -29.101±0.001   |
|                       | 5            | 143 | 0.9      | -29.086±0.010   | -29.093±0.001   |
|                       | 6            | 89  | 1        | -29.102±0.013   | -29.135±0.002   |
|                       | Average±SE×t |     |          | -29.114±0.016   | -29.124±0.018   |
| SCOTT vs G2           | 1            | 196 | 0.7      | -8.885±0.010  | -8.841±0.001  |
|                       | 2            | 163 | 0.9      | -8.873±0.010  | -8.847±0.001  |
|                       | 3            | 143 | 0.8      | -8.866±0.010  | -8.886±0.002  |
|                       | 4            | 177 | 0.9      | -8.881±0.010  | -8.876±0.002  |
|                       |              | 139 | 0.7      | -8.835±0.010  | -8.876±0.002  |
|                       | Average±SE×t |     |          | -8.868±0.019  | -8.865±0.019  |

## 2.4. Discussion

### 2.4.1. Scale contraction

We observe a higher scale contraction when measuring on the fragment ions compared to the measurements on the molecular ions (Table 2.2). The difference might be due to the fact that fragment ions are more reactive than the molecular ion. High energy collisions between ions and the source material cause sputtering and implantation, which may be more effective for fragment ions. Therefore, fragment ions may remain effectively longer in the ion source causing the observed higher scale contraction. The difference in scale contraction between fragment measurement and molecular measurement requires further study.

### 2.4.2. Possible interferences

Oxygen isotope measurements on O fragment ions with low resolution mass spectrometers are mainly limited by the interference from water and its OH fragment ions. The background level of water in mass spectrometers is always significant, and it also generally varies when switching between bellows in dual inlet measurements. With the 253 Ultra, these interferences can be separated from the O<sup>+</sup> fragments (Figure 2.2, supplementary Table S2.5), even if the shoulder for interference-free <sup>17</sup>O<sup>+</sup> measurements is narrow. H<sub>2</sub><sup>16</sup>O<sup>+</sup> is the main interference for <sup>18</sup>O<sup>+</sup> and <sup>16</sup>OH<sup>+</sup> for <sup>17</sup>O<sup>+</sup>. The two rare isotopologues of OH, <sup>17</sup>OH and <sup>16</sup>OD could also interfere with <sup>18</sup>O, but they are negligible in abundance compared to H<sub>2</sub><sup>16</sup>O and can be resolved at medium mass resolving power. Table S2.5 shows a list of other potential interferences with cardinal masses 17 and 18. The molecules made up of lighter atoms than O have masses that are always higher than the cardinal mass 17 and 18, because O is the lightest element where the exact isotope masses are lighter than the cardinal masses. Therefore, these interferences all fall on the high mass side of the O<sup>+</sup> fragment ion, and they can also be resolved with the 253 Ultra at medium resolution (the mass resolving power required is lower than that for separating OH<sup>+</sup> and H<sub>2</sub>O<sup>+</sup>). Therefore, only interferences from doubly ionized oxygen formed in the ion source (<sup>16</sup>O<sup>18</sup>O<sup>++</sup>) and other doubly ionized molecules with higher masses (e.g. <sup>34</sup>S<sup>++</sup> or <sup>36</sup>Ar<sup>++</sup>, see supplementary Table S2.5) can potentially interfere at the low-mass shoulders where we perform measurements. Formation of doubly ionized ions is usually suppressed by several orders of magnitude compared to the singly charged ions. Nevertheless, they interfere at the low mass shoulder of the O atom fragments. The interference of <sup>16</sup>O<sup>18</sup>O<sup>++</sup> on <sup>17</sup>O<sup>+</sup> depends on  $\delta^{18}\text{O}$  and source pressure as shown in Figure 2.3. At a source pressure of  $2.5 \times 10^{-7}$  mbar, the size of the correction in our instrument is about 0.5 ppm in  $\delta^{17}\text{O}$  (and thus  $\Delta^{17}\text{O}$ ) per 1 ‰ difference in  $\delta^{18}\text{O}$  between sample and working reference gas. Thus, when the working reference gas is close in isotopic composition to the samples that are measured, the correction is negligible.

The other challenge to measure the  $\delta^{17}\text{O}$  and  $\delta^{18}\text{O}$  values of CO<sub>2</sub> using the fragment method is the possible interference of O fragment ions from other oxygen bearing impurities (OBI) such as H<sub>2</sub>O, O<sub>2</sub> or N<sub>2</sub>O. The sample and the mass spectrometer background should be very clean to avoid any oxygen contribution from other molecules. The effect of an OBI on the values of  $\delta^{17}\text{O}$ ,  $\delta^{18}\text{O}$  and  $\Delta^{17}\text{O}$  measurements of CO<sub>2</sub> ( $\delta^{\text{l}_{\text{imp}}}$ ) can be estimated using equation 2.8. The

magnitude of the interference depends on the isotopic composition, the fragmentation pattern (efficiency of producing O fragment ions relative to CO<sub>2</sub>), ionization efficiency and the abundance of the impurity relative to the CO<sub>2</sub> (equation 2.8).

$$\delta_{\text{imp}}^I = \psi \times \Omega \times \rho \times \varphi \times \delta_{(\text{OBI vs CO}_2)}^I \quad (2.8)$$

Where  $I$  is 17 or 18,  $\rho = \frac{[\text{OBI}]}{[\text{CO}_2]}$  is the abundance ratio,  $\Omega$  is ratio of oxygen atoms in OBI to the oxygen atoms of CO<sub>2</sub>,  $\psi$  is the ratio in ionization efficiency of OBI to CO<sub>2</sub> and  $\varphi$  is the ratio of O<sup>+</sup> fragment formation of OBI versus CO<sub>2</sub>. As mentioned above, a water background is always present in mass spectrometer instruments and therefore we estimate the effect of water on  $\delta^{17}\text{O}$ ,  $\delta^{18}\text{O}$  and  $\Delta^{17}\text{O}$  measurements of CO<sub>2</sub> using equation 2.8. For water  $\Omega = 0.5$  and  $\varphi = 0.1$  because the O<sup>+</sup> fragment production is only 1 % for H<sub>2</sub>O, whereas it is 10 % for CO<sub>2</sub> (NIST, 2018b, a). We assume a similar ionization efficiency between CO<sub>2</sub> and H<sub>2</sub>O (i.e.  $\psi = 1$ ) for the calculation. Table S2.6 shows the calculated effect of water impurity on the  $\delta^{17}\text{O}$ ,  $\delta^{18}\text{O}$  and  $\Delta^{17}\text{O}$  values of CO<sub>2</sub> measured with the O-fragment method for different water levels and isotopic composition of the water. For instance, when the isotopic composition of the water impurity relative to the CO<sub>2</sub> is  $\delta^{17}\text{O} = -20 \text{ ‰}$  and  $\delta^{18}\text{O} = -40 \text{ ‰}$ , the effect on the  $\delta^{17}\text{O}$  and  $\delta^{18}\text{O}$  of CO<sub>2</sub> will be significant for  $\rho > 0.3 \text{ ‰}$  and  $\rho > 0.1 \text{ ‰}$ , respectively. Since the isotopic composition of the water is assumed (roughly) mass dependent, the effect on the  $\Delta^{17}\text{O}$  will be only significant when  $\rho > 1 \text{ ‰}$ . When isotopic composition is strongly mass independent ( $\delta^{17}\text{O} = \delta^{18}\text{O} = -40 \text{ ‰}$  relative to CO<sub>2</sub>), the effect on  $\Delta^{17}\text{O}$  will be significant for  $\rho > 0.3 \text{ ‰}$  (supplementary Table S2.6).

## 2.5. Future developments and applications

In the present state of development, the O-fragment method can be used to quantify  $\Delta^{17}\text{O}$  of CO<sub>2</sub> with a precision about of 37 ppm in about 12 hours measurement time (67.1 seconds integration time and 60 seconds equilibration time). Higher precisions can be achieved by i) increasing signal intensity; ii) increasing observation/integration time of the  $^{17}\text{O}^+$  fragment ions (Figure 2.6) and iii) achieving measurement precisions at the counting statistics limits. The signal intensity can be increased by increasing source pressure, but the present measurements are already at the upper end of the range where signal intensity increases linearly with source pressure (supplementary Figure S2.1). Increasing the ion current will also shorten the filament lifetime. Observation time can be increased by simply extending the integration time, by reducing the time that is used for peak centering, pressure adjust, etc., and by reducing the equilibration time. Reducing equilibration time introduces additional error due to cross contamination/mixing between sample and reference. Ideally, a LIDI (Long Integration Dual Inlet) technique where the sample-reference switching is not performed at all would enable longer observation times of the sample (Hu et al., 2014). LIDI measurements were attempted with the 253 Ultra but not continued because of instability issues. An increase in stability may also enable measurements at the counting statistics limit, which would improve precision by a factor of 1.5.

Compared to traditional  $\delta^{13}\text{C}$  measurements that require a  $^{17}\text{O}$ -correction, the C-fragment is not subject to the following uncertainties related to the  $^{17}\text{O}$ -correction:

- The use of different  $^{17}\text{R}$ ,  $^{13}\text{R}$  and  $\lambda$  values in different algorithms induces discrepancies that are larger than the precision of current isotope ratio mass spectrometry techniques (Assonov and Brenninkmeijer, 2003)
- Most of the correction algorithms used do not include the impact of  $\Delta^{17}\text{O}$  of  $\text{CO}_2$
- The accepted values for  $^{17}\text{R}$  and  $^{13}\text{R}$  may require revision to meet the current measurement precision (Miller et al., 2007)
- There is no single  $\lambda$  value that can be assigned to  $\text{CO}_2$  since different processes that contribute to the formation or removal of  $\text{CO}_2$  follow different three-isotope slopes.

The fragment technique is simple and unlike other techniques does not require any additional chemical conversion or exchange steps to measure the  $\delta^{17}\text{O}$  value of  $\text{CO}_2$ . Therefore, it can be used to independently assess discrepancies in  $\delta^{17}\text{O}$  values measured by different laboratories, such as the difference in  $\delta^{17}\text{O}$  of IAEA (International Atomic Energy Agency) carbonate standard (NBS-18) measured by Passey et al. (2014) and Barkan et al. (2015). However, the signal intensities for rare isotopes of fragment ions are relatively small, especially when they have to be separated from near-by mass interferences and require higher mass resolution, which reduces ion transmission in the 253 Ultra. Therefore, long measurement times are required to reach a precision of the order of 0.01 ‰. When this precision is reached, the fragment technique can also be useful to evaluate discrepancies introduced in  $\delta^{13}\text{C}$  measurements due to the use of different algorithms for  $^{17}\text{O}$ -correction.

Isotope measurements of atomic ion fragments may have many applications for other molecules. A straightforward extension of the application presented here is the mass-interference-free measurement of  $^{17}\text{O}^+$  and  $^{18}\text{O}^+$  in other oxygen-containing compounds, for example  $\text{CO}$ , or  $\text{N}_2\text{O}$ . Current isotope techniques of these gases rely in many cases on an assumed relation of mass dependent fractionation between  $\delta^{17}\text{O}$  and  $\delta^{18}\text{O}$ , and (e.g. in the case of the  $\text{CO}$ ) chemical conversion to  $\text{CO}_2$  (Pathirana et al., 2015; Brenninkmeijer et al., 1999; Bergamaschi et al., 1998). Direct isotope ratio measurements on the  $\text{O}^+$  fragment can overcome these limitations and provide quantification of  $\Delta^{17}\text{O}$ . Similar to the case of  $\text{CO}_2$  presented here, the  $^{13}\text{C}^+$  content of  $\text{CH}_4$  and  $\text{CO}$  can be measured directly on the  $\text{C}^+$  fragment of these gases, without chemical conversion steps that are known to cause artifacts in traditional isotope techniques (Pathirana et al., 2015; Brenninkmeijer et al., 1999; Lowe et al., 1991; Bergamaschi et al., 1998). Furthermore, isotope measurement on atomic fragment ions may be combined with measurements of larger fragments of hydrocarbons to determine the position specific carbon isotope composition of hydrocarbons (Piasecki et al., 2016).

The position specific  $^{15}\text{N}^+$  content of  $\text{N}_2\text{O}$  is presently determined by measurement of the parent  $\text{N}_2\text{O}$  molecule and the  $\text{NO}$  fragment, which allow to quantify the average  $\delta^{15}\text{N}$  value and the  $^{15}\text{N}$  content at the central nitrogen position, and the  $\delta^{15}\text{N}$  value of the terminal N atom is derived by mass balance, which induces large errors (Brenninkmeijer and Röckmann, 1999; Toyoda and Yoshida, 1999). In principle, the  $^{15}\text{N}^+$  content of the terminal N atom could be derived from the  $\text{N}^+$  fragment, which originates primarily from the terminal N atom in  $\text{N}_2\text{O}$ . Similar to the case of O atoms shown here, this requires a very good vacuum system to avoid contamination from the main atmospheric gas  $\text{N}_2$ .

In addition to these environmental applications, the analysis of atomic fragment ions of different compounds may be a useful tool to study fractionation processes in the ion source of an isotope ratio mass spectrometer. As discussed earlier, the scale contractions for isotopic measurements are different for the fragment ions and molecular ions of  $\text{CO}_2$ . Examining these



effects further may help to understand the chemistry and surface effects in the ion source of isotope ratio mass spectrometers by studying different fragments. In addition, analysis of fragment ions facilitates measuring the isotopic composition of two different chemical compounds versus each other (e.g.  $\delta^{13}\text{C}$  in  $\text{CH}_4$  versus  $\delta^{13}\text{C}$  in  $\text{CO}_2$ ). This can on the one hand provide information on ion source effects associated with fragmentation, but may also help to directly compare isotope scales between different compounds.

## **Acknowledgment**

The authors thank Eugeni Barkan from the Hebrew University of Jerusalem for calibration of our  $\text{O}_2$  and  $\text{CO}_2$  reference gases. This work is funded by the EU ERC project ASICA. The Thermo Scientific 253 Ultra instrument was funded by the Ministry of Education, Culture and Science (OCW) as part of Netherlands Earth System Science Centre (NESSC), and Utrecht University. Helpful comments and suggestions from the three anonymous reviewers are appreciated.

## **Conflict of interest**

There is no conflict of interest.

## **Author contributions**

The project was designed by MH and TR. GAA, MH, TR and DP developed the fragment method and carried out the measurements on the 253 Ultra at Utrecht University, supported by AL. JS, NA and AP carried out fragment measurements on the 253 Ultra at the University of Göttingen. GAA and TR developed the isotope exchange method at Utrecht University. GK provided useful discussion. WP enabled the work within the ASICA project. JS provided the description of the 253 Ultra. All authors provided comments on the manuscript, which was mainly written by GAA and TR.

## 2.6. Supplementary Material

Effect of emission control current, source pressure, equilibration time and source conductance on the scale contraction

In order to characterize the 253 Ultra instrument, we performed an extensive investigation of factors that are known to affect the scale contraction in isotope ratio mass spectrometers (Verkouteren et al., 2003a; Verkouteren et al., 2003b), in particular the ion source pressure (quantified by signal intensity), the filament current and the equilibration time after switching the changeover valve. The experimental results are provided in Tables S2.1 - S2.2 and Figures S2.5 - S2.7, and discussed below. The  $\delta^{18}\text{O}$  and  $\delta^{13}\text{C}$  values obtained from the molecular ion measurements are calculated using the algorithm presented in Brand et al. (2010).

When the VISC window is closed, the source pressure of  $2.5 \times 10^{-7}$  mbar corresponds to an ion count rate of  $3 \times 10^{11}$  cps for  $m/z$  44, which reduces to  $8.0 \times 10^9$  cps when the VISC window is fully open (the signal reduces to about 3 %). As shown in Figure S2.5 A and 2.5 B, with the VISC window open, the measurement with equilibration time of 10 seconds results in a scale contraction of -36 ppm for  $\delta^{13}\text{C}$  values and -33 ppm for  $\delta^{18}\text{O}$  values compared with measurements at 90-seconds equilibration time. The scale contractions are smaller at 20-seconds equilibration time, and for equilibration times  $\geq 30$  seconds we do not find a significant scale contraction compared with measurements with 90-seconds equilibration time for both  $\delta^{13}\text{C}$  and  $\delta^{18}\text{O}$  values. When the VISC window is closed, the effect of equilibration time is much higher: at an equilibration time of 10 seconds, the scale is contracted by -79 ppm and -71 ppm for  $\delta^{13}\text{C}$  and  $\delta^{18}\text{O}$  values, respectively, relative to a measurement at 90-seconds equilibration time. Again, the scale contraction reduces with longer equilibration times, but only at an equilibration time of  $\geq 50$  seconds; the scale contraction does not change significantly any more with longer equilibration times. In general, the cross-contamination coefficient is higher for  $\delta^{18}\text{O}$  measurements than for  $\delta^{13}\text{C}$  measurements as shown in Figure S2.5 A and 2.5 B (VISC closed) and 2.5 C and 2.5 D (VISC fully open) for different equilibration time, and 2.5 E and 2.5 F for different emission current.

The relative difference between  $\delta^{13}\text{C}$  measurements with VISC open and VISC closed decreases from 0.110 ‰ to 0.066 ‰ when the equilibration time increases from 10 seconds to 90 seconds (Figure S2.6 A). The corresponding relative difference for  $\delta^{18}\text{O}$  measurements changes from 0.125 ‰ to 0.088 ‰ (Figure S2.6 B).

Measurements at a filament emission current of 1.95 mA cause a scale contraction of -21 ppm in  $\delta^{13}\text{C}$  values and -39 ppm in  $\delta^{18}\text{O}$  values relative to measurements at an emission current of 1 mA (Figures S2.5 C and 2.5 D). At 1.5 mA emission current, the scale contraction relative to the measurement at 1 mA emission current is -8 ppm for  $\delta^{13}\text{C}$  values while the difference between measurements at 1.5 mA and 1 mA emission current is insignificant for  $\delta^{18}\text{O}$  values.

The source pressure (quantified using the signal intensity under otherwise constant conditions) can also influence the scale contraction. A decrease in the intensity of  $m/z$  44 from  $2.5 \times 10^{11}$  cps to  $9 \times 10^{10}$  cps causes a scale contraction of -39 ppm and -35 ppm for  $\delta^{13}\text{C}$  and  $\delta^{18}\text{O}$  respectively (Figure S2.5 E and 2.5 F).

One factor that can be responsible for a scale contraction is that a fraction of the previous gas remains in the ion source when the changeover valve is switched. This effect is often called cross contamination. To obtain an indication of gas exchange rates when switching between different gases, we monitored the pressure drop when the changeover valve was closed. The percentage of the gas remaining in the ion source with time depends on the initial source pressure or signal intensity (at  $m/z$  44) in the ion source as shown in Figure S2.7. As expected, the source is evacuated much more quickly when the VISC window is open. The loss rate of  $\text{CO}_2$  from the ion source can be approximated mathematically by a double exponential function (Figure S2.7). The first exponential term is interpreted as a time scale for the pumping of gas out of the ion source, while the second exponential may reflect timescales of surface interactions in the ion source. At lower source pressure (lower count  $m/z$  44) the absolute amount of gas remaining in the source with time is lower than at higher ion source pressure (higher count  $m/z$  44). However, the relative amount of the gas in the source with respect to the initial source pressure is higher when the ion source pressure is lower which explains partly why we have larger scale contraction /memory effect when the ion source pressure, or signal intensity, is lower (Figures S2.5 E and 2.5 F). At higher ion source pressure, the relative effect of the remaining gas is smaller than at lower source pressure.

As shown in Figures S2.5 C and 2.5 D, when the emission control current increases the absolute relative difference in  $\delta^{18}\text{O}$  and  $\delta^{13}\text{C}$  values between the two gases decreases (scale contraction). Verkouteren et al (2003a; 2003b) showed that a higher emission current results in higher sputtering and implantation of ions in the source slit material. This causes adsorption and desorption of molecules from the surface and to the surface resulting in considerable memory effect (cross contamination (Assonov and Brenninkmeijer, 2001) or mixing of reference and sample) (Verkouteren et al., 2003a; Verkouteren et al., 2003b). These scale contraction effects depend on the material of the source slit and are lowest for a tantalum slit. Although the source slit in the 253 Ultra is made from tantalum we still observe a scale contraction at equilibration times of 15 second unlike the observation reported by Verkouteren et al (2003a; 2003b). This might partly be due to the difference in measurement conditions (source pressure, accelerating voltage, emission current, etc.), differences in the source housing and differences in tuning parameters between the MAT 253 and 253 Ultra instruments.

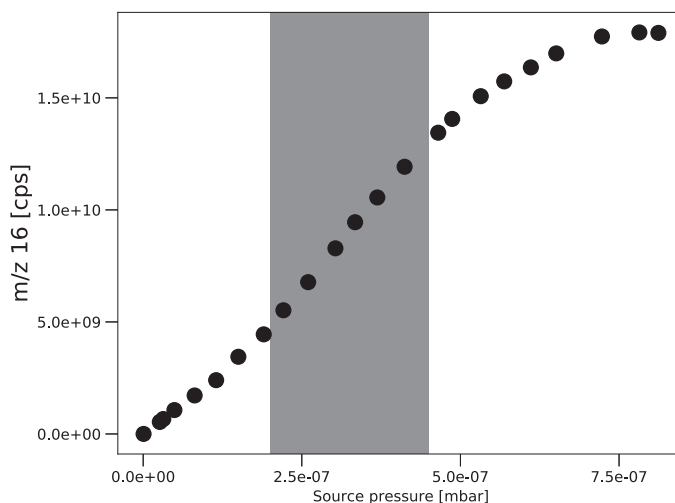


Figure S2.1 Relationship between source pressure and signal intensity at  $m/z$  16 (Faraday collector L3, equipped with a  $1 \times 10^{10} \Omega$  resistor). The linear range (shaded area) ends at a source pressure of  $4.5 \times 10^{-7}$  mbar (corresponding to a signal intensity of approx.  $1.3 \times 10^9$  cps).

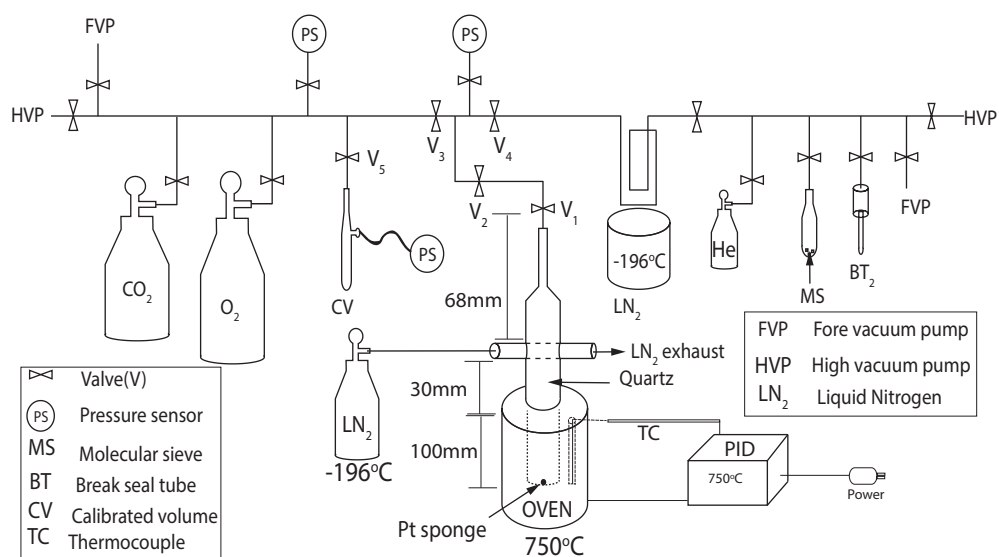


Figure S2.2 Schematic diagram of the  $O_2$ - $CO_2$  exchange experimental setup. The quartz reactor has an outer diameter of 21 mm. PID stands for proportional-integral-derivative temperature controller.

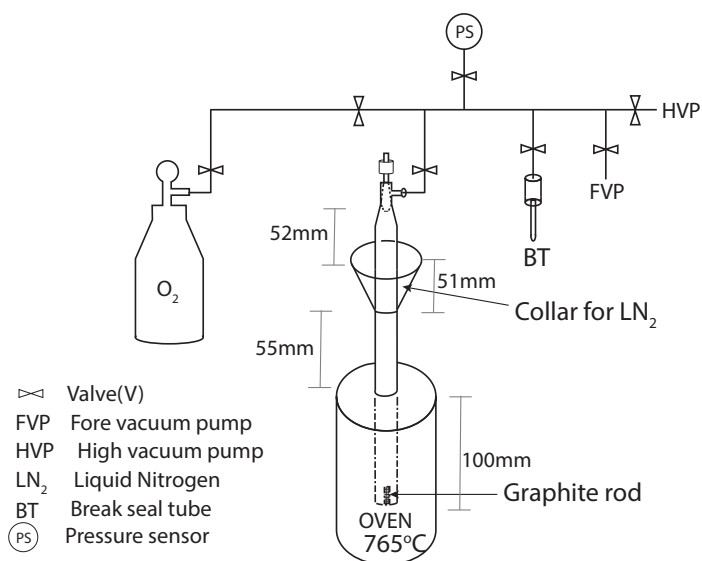


Figure S2.3 Schematic diagram of the setup used for conversion of  $O_2$  to  $CO_2$  by combusting a graphite rod. The reactor is made out of quartz with 21 mm outer diameter.

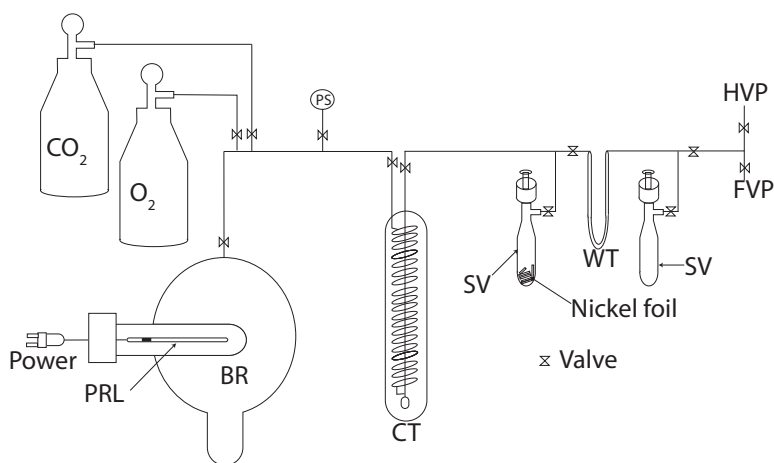


Figure S2.4 Schematic diagram of the setup used for preparing  $CO_2$  with a positive  $\Delta^{17}O$  by photolysing a mixture of  $O_2$  and  $CO_2$  with UV light. BR: Borosilicate reactor (2 L), PRL: pen ray Hg vapor lamp, CT:  $CO_2$  trap (liquid nitrogen temperature), SV: sample vial, WT: water trap (operated at dry ice temperature), PS: pressure sensor, HVP: high vacuum pump, FVP: fore vacuum pump.

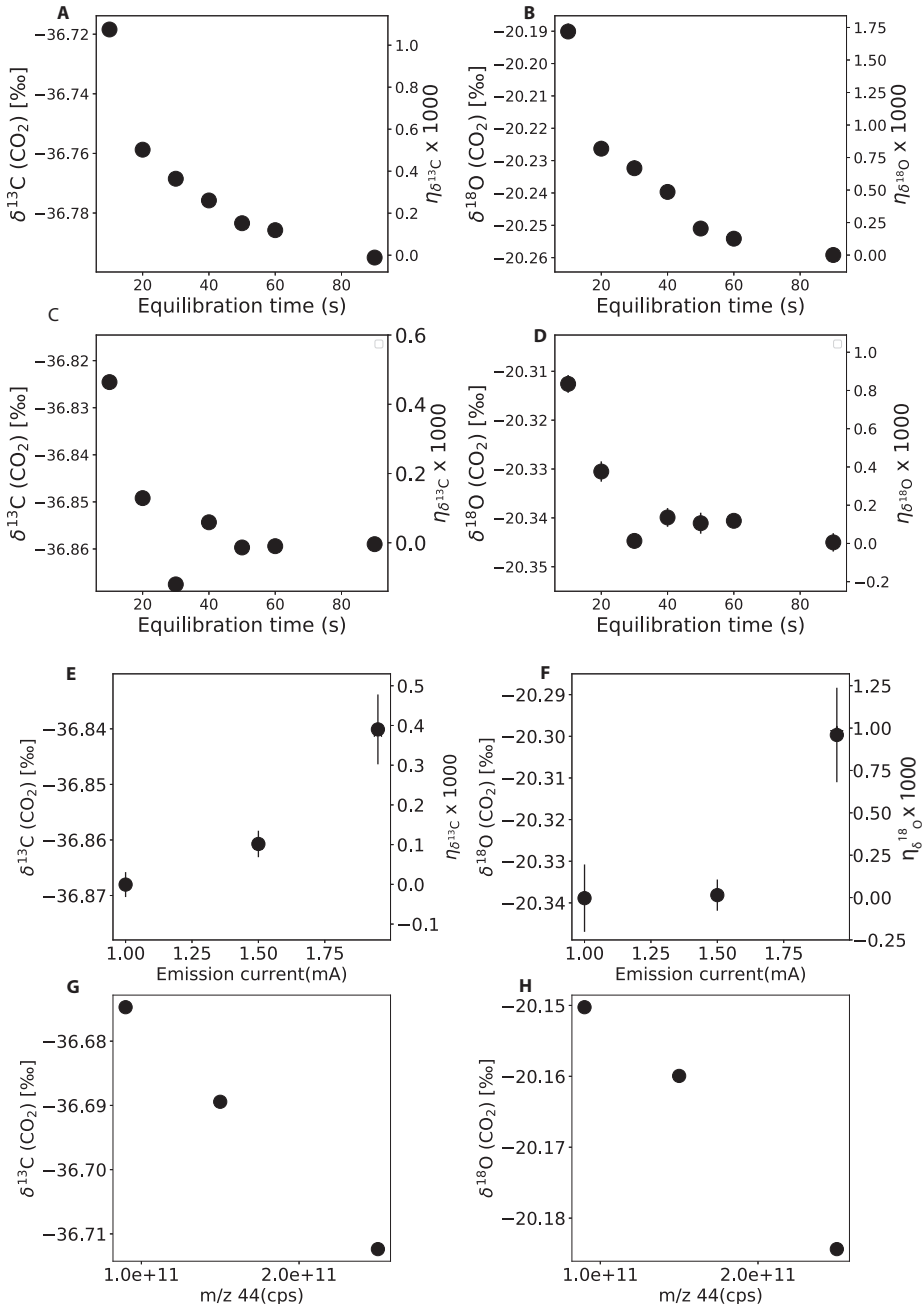


Figure S2.5  $\delta^{13}\text{C}$  and  $\delta^{18}\text{O}$  values of SCOTT measured against G2. A and B) Effect of equilibration time with VISC window closed. C and D) Effect of equilibration time with VISC window fully opened; E and F) Effect of filament emission current on the relative difference between the two gases in  $\delta^{13}\text{C}$  and  $\delta^{18}\text{O}$  values. G and H) Effect of amount of gas in the ion source quantified by the signal intensity in cps for  $m/z$  44. The emission current experiments are performed at 60-seconds equilibration time and the sensitivity to the amount of gas was determined with 30-seconds equilibration time. The VISC window was kept closed.

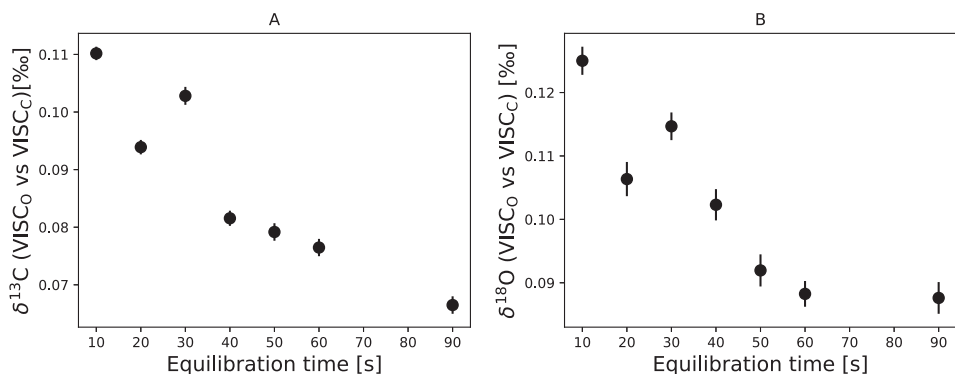


Figure S2.6 Effect of the equilibration time on the  $\delta^{13}\text{C}$  (A) and  $\delta^{18}\text{O}$  (B) differences between measurement with open VISC window (VISC<sub>0</sub>) and closed VISC window (VISC<sub>C</sub>).

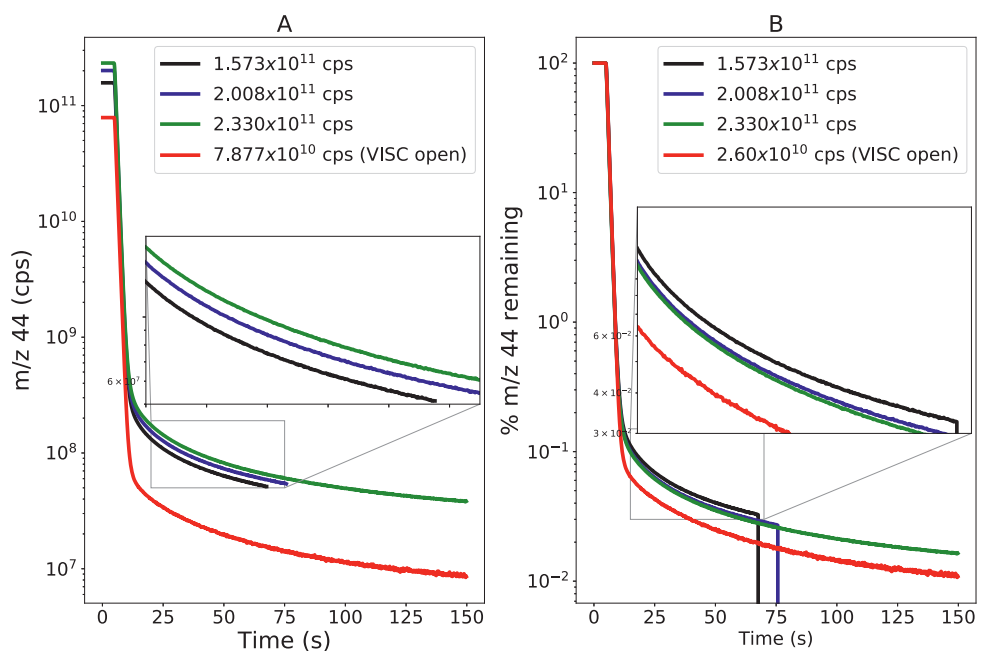


Figure S2.7 Drop in signal intensity for at  $m/z$  44 (corresponding to the source pressure) when the dual inlet valve was closed for different initial source pressures. A) decrease of the main ion signal of  $\text{CO}_2$  as a function of time. B) fraction of  $\text{CO}_2$  remaining as a function of time for the main ion signal of  $\text{CO}_2$ . The emission current and accelerating voltage were 1.95 mA and 9.9 kV, respectively.

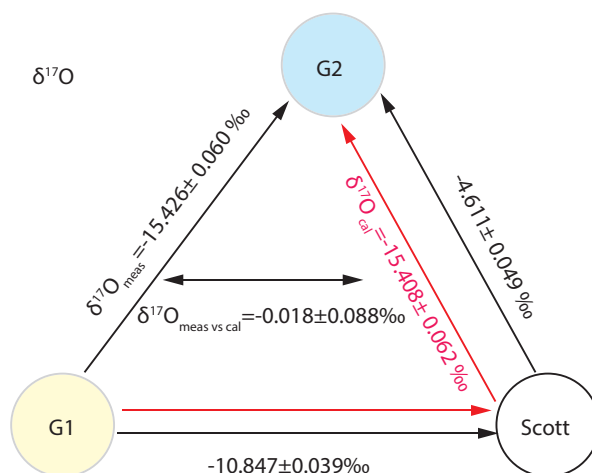


Figure S2.8 Comparison of  $\delta^{17}\text{O}$  differences between three different  $\text{CO}_2$  gases with the fragment technique using the 253 Ultra at Utrecht University. The red arrows indicate that the respective measured  $\delta$  values are combined for comparison with the directly measured third  $\delta$  value.

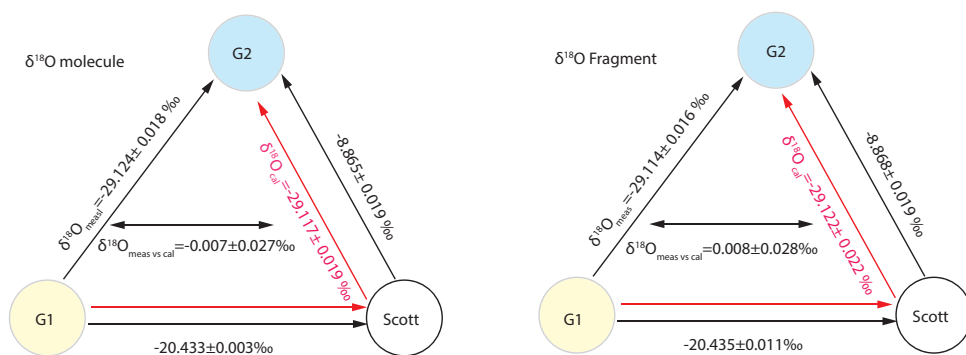


Figure S2.9 Comparison of  $\delta^{18}\text{O}$  differences between three different  $\text{CO}_2$  gases using either the molecular  $\text{CO}_2$  ion technique (left) or the atom fragment technique (right) with the 253 Ultra at Utrecht University. The red arrows indicate that the respective measured  $\delta$  values are combined for comparison with the directly measured third  $\delta$  value.



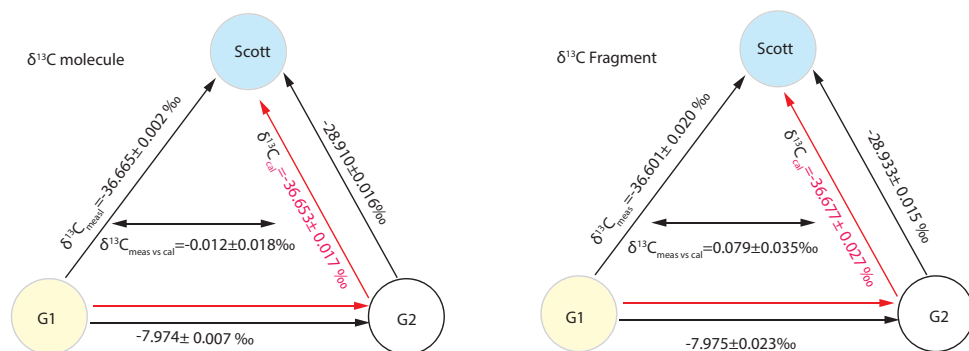


Figure S2.10 Comparison of  $\delta^{13}\text{C}$  differences between three different  $\text{CO}_2$  gases using either the molecular  $\text{CO}_2$  ion technique (left) or the atom fragment technique (right) with the 253 Ultra mass spectrometer at Utrecht University. The red arrows indicate that the respective measured  $\delta$  values are combined for comparison with the directly measured third  $\delta$  value.

Table S2.1 Effect of equilibration time on the absolute isotopic difference of two gases measured on the 253 Ultra with VISC window open and closed. The errors given are standard errors of the mean. The  $\delta$  values are in ‰.

| Equilibration time (s) | VISC window closed           |                              | VISC window open             |                              |
|------------------------|------------------------------|------------------------------|------------------------------|------------------------------|
|                        | $\delta^{13}\text{C}$ values | $\delta^{18}\text{O}$ values | $\delta^{13}\text{C}$ values | $\delta^{18}\text{O}$ values |
| 10                     | $-36.7184 \pm 0.001$         | $-20.1901 \pm 0.001$         | $-36.8246 \pm 0.001$         | $-20.3126 \pm 0.002$         |
| 20                     | $-36.7587 \pm 0.001$         | $-20.2263 \pm 0.002$         | $-36.8492 \pm 0.001$         | $-20.3305 \pm 0.002$         |
| 30                     | $-36.7685 \pm 0.001$         | $-20.2324 \pm 0.002$         | $-36.8675 \pm 0.001$         | $-20.3447 \pm 0.002$         |
| 40                     | $-36.7758 \pm 0.001$         | $-20.2397 \pm 0.002$         | $-36.8543 \pm 0.001$         | $-20.3399 \pm 0.002$         |
| 50                     | $-36.7834 \pm 0.001$         | $-20.2510 \pm 0.001$         | $-36.8597 \pm 0.001$         | $-20.3411 \pm 0.0022$        |
| 60                     | $-36.7858 \pm 0.001$         | $-20.2541 \pm 0.002$         | $-36.8594 \pm 0.001$         | $-20.3406 \pm 0.0012$        |
| 90                     | $-36.7949 \pm 0.001$         | $-20.2592 \pm 0.002$         | $-36.8590 \pm 0.0012$        | $-20.3450 \pm 0.002$         |

Table S2.2 Effect of emission control current and source pressure on the absolute isotopic difference of two gases measured on the 253 Ultra (G1 and SCOTT). The errors given are standard errors of the mean. The integration time of individual measurements is 61.7 seconds. The effects of source pressure (intensity of  $m/z$  44) are determined at an equilibration time of 30 seconds and an emission current of 1.8 mA.

| Effect of emission current on $\text{CO}_2$ isotopic composition      |                               |                                  |                                  |
|---|-------------------------------|----------------------------------|----------------------------------|
| Equilibration time (s)  | Emission control current (mA) | $\delta^{13}\text{C}$ values [‰] | $\delta^{18}\text{O}$ values [‰] |
| 60  | 1.00                          | $-36.8679 \pm 0.0013$            | $-20.3443 \pm 0.0023$            |
| 60  | 1.00                          | $-36.8694 \pm 0.0013$            | $-20.3351 \pm 0.0029$            |
| 60  | 1.00                          | $-36.8668 \pm 0.0014$            | $-20.3372 \pm 0.0029$            |
| 60  | 1.50                          | $-36.8589 \pm 0.0010$            | $-20.3399 \pm 0.0019$            |
| 60  | 1.50                          | $-36.8608 \pm 0.0011$            | $-20.3340 \pm 0.0015$            |
| 60  | 1.50                          | $-36.8596 \pm 0.0009$            | $-20.3373 \pm 0.0016$            |
| 60  | 1.50                          | $-36.8635 \pm 0.0009$            | $-20.3413 \pm 0.0018$            |
| 60  | 1.95                          | $-36.8371 \pm 0.0011$            | $-20.2943 \pm 0.0018$            |
| 60  | 1.95                          | $-36.8389 \pm 0.0008$            | $-20.2975 \pm 0.0016$            |
| 60  | 1.95                          | $-36.8443 \pm 0.0010$            | $-20.3072 \pm 0.0016$            |
| Effect of intensity of $m/z$ 44 on $\text{CO}_2$ isotopic composition |                               |                                  |                                  |

| Equilibration time (s) | $m/z$ 44(cps) | $\delta^{13}\text{C}$ values [‰] | $\delta^{18}\text{O}$ values [‰] |
|------------------------|---------------|----------------------------------|----------------------------------|
| 30                     | 2.5E+11       | -36.712±0.001                    | -20.184±0.001                    |
| 30                     | 1.5E+11       | -36.689±0.001                    | -20.160±0.001                    |
| 30                     | 9E+10         | -36.675±0.001                    | -20.150±0.002                    |

Table S2.3 Isotopic composition of CO<sub>2</sub> produced by combustion with isotopically light O<sub>2</sub> at the University of Göttingen. Each CO<sub>2</sub> sample is analyzed four times at different intensity to investigate the effect of signal intensity on the precision of  $\Delta^{17}\text{O}$  measurement based on the relationship between source pressure and signal intensity at  $m/z$  16.

| Experiment   | $\delta^{17}\text{O}$ values [‰] | $\delta^{18}\text{O}$ values [‰] | $\Delta^{17}\text{O}$ [‰] | $m/z$ 16 [cps] |
|--|----------------------------------|----------------------------------|---------------------------|----------------|
| Measurement in the linear range of signal ( $m/z$ 16) vs source pressure               |                                  |                                  |                           |                |
| A3   | -26.940±0.037                    | -50.764±0.038                    | 0.199±0.037               | 1.12E+09       |
| B2   | -26.465±0.038                    | -50.005±0.022                    | 0.265±0.039               | 1.20E+09       |
| B3   | -26.278±0.052                    | -49.579±0.054                    | 0.219±0.039               | 1.26E+09       |
| C2   | -26.453±0.040                    | -49.989±0.014                    | 0.268±0.040               | 1.15E+09       |
| Average standard error   |                                  |                                  | ±0.039                    | 1.18E+09       |
| Measurement outside the linear range, at higher signal intensity than the linear range |                                  |                                  |                           |                |
| A1   | -27.103±0.069                    | -51.148±0.013                    | 0.244±0.044               | 1.84E+09       |
| A2   | -27.094±0.03                     | -51.099±0.014                    | 0.226±0.037               | 1.73E+09       |
| B1   | -26.676±0.053                    | -50.222±0.016                    | 0.168±0.054               | 1.74E+09       |
| B1   | -26.484±0.027                    | -50.078±0.014                    | 0.286±0.027               | 1.75E+09       |
| Average standard error   |                                  |                                  | ±0.041                    | 1.77E+09       |
| Measurement outside the linear range, at lower signal intensity than the linear range  |                                  |                                  |                           |                |
| A4   | -26.977±0.066                    | -50.848±0.041                    | 0.207±0.067               | 5.46E+08       |
| B4   | -26.981±0.104                    | -50.623±0.072                    | 0.077±0.105               | 3.74E+08       |
| C3   | -26.469±0.067                    | -50.074±0.030                    | 0.299±0.071               | 5.76E+08       |
| C4   | -26.0766±0.083                   | -49.514±0.031                    | 0.390±0.088               | 3.82E+08       |
| Average standard error   |                                  |                                  | ±0.083                    | 4.70E+08       |
| error  |                                  |                                  |                           |                |

Table S2.4: Comparison of the results obtained with the O<sub>2</sub>-CO<sub>2</sub> exchange method and O<sub>2</sub>-fragment technique.  $\delta^{17}\text{O}$ ,  $\delta^{18}\text{O}$  and  $\Delta^{17}\text{O}$  values are in per mill (‰) with respect to VSMOW. The error of the mean is the standard error multiplied by the student t-factor for the 95 % two-sided confidence interval while for the individual measurements it is the standard error.  $\Gamma$  is the ratio between measured precision and the precision calculated according to counting statistics,  $n$  is number of cycles,  $i$  stand for initial (before exchange) and  $f$  stands for final (after exchange). For  $\delta^{18}\text{O}$  values the measurement error is similar to the error calculated based on counting statistics.

| Sample code           | n            | Γ   | Fragment technique |                   |                   | CO <sub>2</sub> -O <sub>2</sub> exchange method |                                |                                |                                |                                |                                |                                |  |             |
|-----------------------|--------------|-----|--------------------|-------------------|-------------------|---|--------------------------------|--------------------------------|--------------------------------|--------------------------------|--------------------------------|--------------------------------|--|-------------|
|                       |              |     | δ <sup>17</sup> O  | δ <sup>18</sup> O | Δ <sup>17</sup> O | O <sub>2</sub>                                  |                                | CO <sub>2</sub>                |                                |                                |                                |                                |  |             |
|                       |              |     |                    |                   |                   | δ <sup>17</sup> O <sub>i</sub>                  | δ <sup>18</sup> O <sub>i</sub> | δ <sup>17</sup> O <sub>f</sub> | δ <sup>18</sup> O <sub>f</sub> | δ <sup>17</sup> O <sub>i</sub> | δ <sup>18</sup> O <sub>i</sub> | Δ <sup>17</sup> O <sub>i</sub> |  |             |
| G4                    | 119          | 1.6 | 19.987±0.049       | 36.778±0.013      | 0.719±0.048       | 9.254   | 18.542                         | 14.409                         | 27.456                         | 19.891                         | 36.793                         | 0.618                          |  |             |
|                       | 110          | 1.5 | 19.882±0.046       | 36.796±0.012      | 0.608±0.046       | 9.254   | 18.542                         | 14.111                         | 26.933                         | 19.902                         | 36.793                         | 0.628                          |  |             |
|                       | 110          | 1.7 | 19.974±0.053       | 36.803±0.013      | 0.695±0.053       | 9.254   | 18.542                         | 14.156                         | 27.011                         | 19.900                         | 36.793                         | 0.627                          |  |             |
|                       | 128          | 1.4 | 19.895±0.040       | 36.795±0.012      | 0.621±0.040       | 9.254   | 18.542                         | 14.187                         | 27.054                         | 19.913                         | 36.793                         | 0.639                          |  |             |
|                       |              |     |                    |                   |                   | 9.254   | 18.542                         | 14.047                         | 26.808                         | 19.918                         | 26.808                         | 0.644                          |  |             |
| Mean<br>±SE* <i>t</i> | 19.935±0.069 |     | 36.793±0.012       |                   |                   | 0.661±0.064                                     |                                |                                | 19.894±0.009                   |                                |                                |                                |  | 0.620±0.008 |
|                       |              |     |                    |                   |                   |   |                                |                                |                                |                                |                                |                                |  |             |
|                       |              |     |                    |                   |                   |   |                                |                                |                                |                                |                                |                                |  |             |
|                       |              |     |                    |                   |                   |   |                                |                                |                                |                                |                                |                                |  |             |
|                       |              |     |                    |                   |                   |   |                                |                                |                                |                                |                                |                                |  |             |
|                       |              |     |                    |                   |                   |   |                                |                                |                                |                                |                                |                                |  |             |
|                       |              |     |                    |                   |                   |   |                                |                                |                                |                                |                                |                                |  |             |
|                       |              |     |                    |                   |                   |   |                                |                                |                                |                                |                                |                                |  |             |
| G3                    | 96           | 1.4 | 19.161±0.046       | 36.058±0.013      | 0.277±0.046       | 9.254   | 18.542                         | 13.751                         | 26.562                         | 19.181                         | 36.067                         | 0.291                          |  |             |
|                       | 95           | 1.6 | 19.182±0.052       | 36.076±0.014      | 0.288±0.051       | 9.254   | 18.542                         | 13.788                         | 26.646                         | 19.161                         | 36.067                         | 0.272                          |  |             |
|                       |              |     |                    |                   |                   | 9.254   | 18.542                         | 13.719                         | 26.521                         | 19.163                         | 36.067                         | 0.273                          |  |             |
|                       |              |     |                    |                   |                   | 9.254   | 18.542                         | 13.729                         | 26.537                         | 19.166                         | 36.067                         | 0.276                          |  |             |
|                       |              |     |                    |                   |                   | 9.254   | 18.542                         | 13.867                         | 26.785                         | 19.163                         | 36.067                         | 0.273                          |  |             |
| Mean<br>±SE* <i>t</i> | 0.282±0.036  |     |                    |                   |                   | 9.254   | 18.542                         | 13.683                         | 26.464                         | 19.154                         | 36.067                         | 0.265                          |  |             |
|                       |              |     |                    |                   |                   | 9.254   | 18.542                         | 13.594                         | 26.300                         | 19.160                         | 36.067                         | 0.271                          |  |             |



|               |     |              |              |              |  |       |        |        |        |              |        |              |
|---------------|-----|--------------|--------------|--------------|--|-------|--------|--------|--------|--------------|--------|--------------|
| G2            |     |              |              |              |  | 9.254 | 18.542 | 13.253 | 26.134 | 18.057       | 34.998 | -0.267       |
|               | 143 |              |              |              |  | 9.254 | 18.542 | 13.281 | 26.167 | 18.079       | 34.998 | -0.246       |
|               | 1.1 | 18.068±0.04  | 34.929±0.013 | -0.220±0.034 |  | 9.254 | 18.542 | 13.349 | 26.318 | 18.055       | 34.998 | -0.269       |
|               |     |              |              |              |  | 9.254 | 18.542 | 13.234 | 26.098 | 18.057       | 34.998 | -0.267       |
|               |     |              |              |              |  | 9.254 | 18.542 | 13.247 | 26.125 | 18.055       | 34.998 | -0.269       |
|               |     |              |              |              |  | 9.254 | 18.542 | 13.233 | 26.093 | 18.060       | 34.998 | -0.264       |
| Mean±<br>SE*t |     | 18.061±0.047 | 34.930±0.007 | -0.228±0.049 |  |       |        |        |        | 18.062±0.007 |        | -0.262±0.007 |

Table S2.5 List of potentially interfering ions with masses close to  $^{17}\text{O}^+$  and  $^{18}\text{O}^+$ , and the required resolution to avoid the interference. The interfering ions are ordered based on the resolving power requirement.

| Interfering ion                     | Exact mass [u] | Mass difference [mu] | Required resolution [m/ $\Delta$ m] |
|-------------------------------------|----------------|----------------------|-------------------------------------|
| <b><math>^{17}\text{O}^+</math></b> | <b>16.9991</b> |                      |                                     |
| $^{16}\text{O}^{18}\text{O}^{++}$   | 16.9970        | 2.1                  | 8118                                |
| $^{16}\text{OH}^+$                  | 17.0027        | 3.6                  | 4712                                |
| $^{34}\text{S}^{++}$                | 16.9839        | 15.2                 | 1118                                |
| $^{15}\text{NH}_2^+$                | 17.0158        | 16.6                 | 1023                                |
| $^{14}\text{NHD}^+$                 | 17.0250        | 25.9                 | 658                                 |
| $^{13}\text{CH}_2\text{D}^+$        | 17.0331        | 34.0                 | 501                                 |
| $^{13}\text{CH}_4^+$                | 17.0347        | 35.5                 | 479                                 |
| $^{13}\text{CD}_2\text{H}^+$        | 17.0360        | 36.9                 | 461                                 |
| $^{12}\text{CH}_3\text{D}^+$        | 17.0376        | 38.4                 | 443                                 |
| $^{12}\text{CH}_5^+$                | 17.0391        | 40.0                 | 426                                 |
| <b><math>^{18}\text{O}^+</math></b> | <b>17.9992</b> |                      |                                     |
| $^{17}\text{OH}^+$                  | 18.0070        | 7.8                  | 2309                                |
| $^{16}\text{OD}^+$                  | 18.0090        | 9.9                  | 1827                                |
| $^{16}\text{OH}_2^+$                | 18.0106        | 11.4                 | 1579                                |
| $^{36}\text{Ar}^{++}$               | 17.9838        | 15.4                 | 1169                                |
| $^{15}\text{NH}_3^+$                | 18.0236        | 24.4                 | 737                                 |
| $^{14}\text{NH}_4^+$                | 18.0344        | 35.2                 | 512                                 |
| $^{14}\text{CH}_4^+$                | 18.0345        | 35.4                 | 509                                 |
| $^{13}\text{CDH}_3^+$               | 18.0409        | 41.8                 | 431                                 |
| $^{13}\text{CH}_5^+$                | 18.0425        | 43.3                 | 416                                 |
| $^{12}\text{CD}_2\text{H}_2^+$      | 18.0439        | 44.7                 | 403                                 |
| $^{12}\text{CDH}_4^+$               | 18.0454        | 46.2                 | 390                                 |

Table S2.6 Simulated effect of a H<sub>2</sub>O impurity (contamination level quantified by  $\gamma = [\text{H}_2\text{O}]/[\text{CO}_2]$  as source of oxygen during  $\Delta^{17}\text{O}$  measurement using the O-fragment method for an intensity for  $m/z$  16 of  $4.05 \times 10^7$  cps. The signal of O atom fragments relative to molecular ions is 10 % for CO<sub>2</sub> and 1 % for H<sub>2</sub>O (NIST, 2018b, a). For these conceptual calculations we assumed the same ionization efficiency for H<sub>2</sub>O and CO<sub>2</sub>.

| $\rho$  | O fragment from water |                   | O fragment of the mixture |                   |                   | Isotopic composition |                       |                       |
|---|-----------------------|-------------------|---------------------------|-------------------|-------------------|----------------------|-----------------------|-----------------------|
|   | $^{16}\text{O}^+$     | $^{17}\text{O}^+$ | $^{18}\text{O}^+$         | $^{16}\text{O}^+$ | $^{17}\text{O}^+$ | $^{18}\text{O}^+$    | $\delta^{17}\text{O}$ | $\delta^{18}\text{O}$ |
| $\delta^{17}\text{O}$ and $\delta^{18}\text{O}$ values of water vs CO <sub>2</sub> are -20 and -40 ‰, respectively [mass dependent]   |                       |                   |                           |                   |                   |                      |                       |                       |
| 1.00E-04  | 2.00E+05              | 7.47E+01          | 3.95E+02                  | 4.05E+09          | 1.54E+06          | 8.33E+06             | -0.001                | -0.002                |
| 3.00E-04  | 6.00E+05              | 2.24E+02          | 1.18E+03                  | 4.05E+09          | 1.54E+06          | 8.33E+06             | -0.003                | -0.006                |
| 1.00E-03  | 2.00E+06              | 7.47E+02          | 3.95E+03                  | 4.06E+09          | 1.54E+06          | 8.33E+06             | -0.010                | -0.020                |
| 3.00E-03  | 6.00E+06              | 2.24E+03          | 1.18E+04                  | 4.06E+09          | 1.55E+06          | 8.34E+06             | -0.030                | -0.059                |
| 1.00E-02  | 2.00E+07              | 7.47E+03          | 3.95E+04                  | 4.07E+09          | 1.55E+06          | 8.37E+06             | -0.098                | -0.196                |
| 3.00E-02  | 6.00E+07              | 2.19E+04          | 1.18E+05                  | 4.11E+09          | 1.57E+06          | 8.45E+06             | -0.584                | -0.584                |
| $\delta^{17}\text{O}$ and $\delta^{18}\text{O}$ values of water vs CO <sub>2</sub> are -40 and -40 ‰, respectively [mass independent] |                       |                   |                           |                   |                   |                      |                       |                       |
| 1.00E-04  | 2.00E+05              | 7.32E+01          | 3.95E+02                  | 4.05E+09          | 1.54E+06          | 8.33E+06             | -0.002                | -0.002                |
| 3.00E-04  | 6.00E+05              | 2.19E+02          | 1.18E+03                  | 4.05E+09          | 1.54E+06          | 8.33E+06             | -0.006                | -0.006                |
| 1.00E-03  | 2.00E+06              | 7.32E+02          | 3.95E+03                  | 4.06E+09          | 1.54E+06          | 8.33E+06             | -0.020                | -0.020                |
| 3.00E-03  | 6.00E+06              | 2.19E+03          | 1.18E+04                  | 4.06E+09          | 1.55E+06          | 8.34E+06             | -0.059                | -0.059                |
| 1.00E-02  | 2.00E+07              | 7.32E+03          | 3.95E+04                  | 4.07E+09          | 1.55E+06          | 8.37E+06             | -0.196                | -0.196                |

## Chapter 3

# Exploring the use of $^{17}\text{O}$ -excess of $\text{CO}_2$ for estimating mesophyll conductance of $\text{C}_3$ and $\text{C}_4$ plants

### Abstract

Mesophyll conductance of  $\text{CO}_2$  ( $g_m$ ) is an important parameter controlling photosynthesis and water use efficiency, and vegetation-atmosphere  $\text{CO}_2$  exchange. Here we demonstrate the potential to estimate  $g_m$  from measurements of  $\Delta^{17}\text{O}$  of  $\text{CO}_2$ , where  $\Delta^{17}\text{O} = \delta^{17}\text{O} - 0.528 \times \delta^{18}\text{O}$  quantifies the  $^{17}\text{O}$ -excess compared to what is expected from the  $^{18}\text{O}$  content of  $\text{CO}_2$  according to mass-dependent isotope fractionation. The main limitation to the use of  $g_{m\Delta 17}$  is the uncertainty in the measurement of the very small signals in  $\Delta^{17}\text{O}$  in experiments where normal atmospheric  $\text{CO}_2$  is used. The calculations are supported by measurements of  $\delta^{18}\text{O}$  and  $\Delta^{17}\text{O}$  in leaf cuvette gas exchange measurement with sunflower, ivy, and maize, using normal and slightly  $^{17}\text{O}$ -enriched  $\text{CO}_2$ . In general, the precision of a  $g_m$  determination with oxygen isotope techniques decreases when the isotopic difference between  $\text{CO}_2$  in the intercellular airspace and at the  $\text{CO}_2\text{-H}_2\text{O}$  oxygen exchange site becomes very small. In leaf cuvette experiments this limitation can partially be overcome by using  $^{17}\text{O}$ - or  $^{18}\text{O}$ -enriched  $\text{CO}_2$ .  $\Delta^{17}\text{O}$  (i.e.  $g_{m\Delta 17}$ ) is in principle less sensitive to the unknown isotope fractionation during evapotranspiration of leaf water than  $\delta^{18}\text{O}$  (i.e.  $g_{m18}$ ) because the isotope fractionation processes involved are all mass-dependent.



### 3.1. Introduction

During photosynthesis  $\text{CO}_2$  diffuses from the air surrounding the leaf through the leaf boundary layer and stomata to the intercellular airspace and from there to the carboxylation site (Figure 3.1). The conductance from the intercellular air space to the carboxylation site is called mesophyll conductance. For  $\text{C}_3$  plants, this transport path crosses different media, gas phase (intercellular air space), liquid phase (cell wall, cytosol, and stroma) and lipid-protein (plasmalemma and chloroplast envelope) (Farquhar et al., 1982; Evans et al., 2009; Gillon and Yakir, 2000b). For  $\text{C}_4$  plants, the carbon fixation step already occurs in the mesophyll, by the enzyme Phosphoenolpyruvate carboxylase (PEPC) (von Caemmerer et al., 2014) (Figure 3.1).

Estimating mesophyll conductance ( $g_m$ ) and understanding its variability in response to environmental change is essential to improve the scientific understanding of water use efficiency (Flexas et al., 2013; Peters et al., 2018) and plant-atmosphere  $\text{CO}_2$  exchange and gross primary productivity (GPP) of terrestrial plants (Knauer et al., 2019a; Koren et al., 2019) across a range of spatial and temporal scales.  $g_m$  cannot be measured directly and its indirect determination is challenging (Pons et al., 2009). Several techniques are used to estimate  $g_m$  indirectly, including the variable J method (Fabre et al., 2007; Flexas et al., 2007), the leaf anatomical method (Tomás et al., 2013), the curve-fitting method (Ubierna et al., 2007), the  $^{13}\text{C}$ -photosynthetic discrimination ( $\Delta_A^{13}\text{C}$ ) method (Evans et al., 1986) and the  $^{18}\text{O}$ -photosynthetic discrimination ( $\Delta_A^{18}\text{O}$ ) method (Gillon and Yakir, 2000b; Barbour et al., 2016). Details on these  $g_m$  measurement techniques can be found in (Pons et al., 2009; Cousins et al., 2020) and references therein.

Among the isotope discrimination techniques,  $\Delta_A^{13}\text{C}$  can only be applied to estimate mesophyll conductance ( $g_{m13}$ ) of  $\text{C}_3$  plants, whereas  $\Delta_A^{18}\text{O}$  is suitable to measure the mesophyll conductance ( $g_{m18}$ ) for both  $\text{C}_3$  and  $\text{C}_4$  plants. It is important to note that  $g_{m13}$  and  $g_{m18}$  in  $\text{C}_3$  plants might not be the same because the carbon and oxygen isotopes are modified by different processes. The fractionation against  $^{13}\text{C}$  occurs primarily during the assimilation step in the chloroplast. In  $\text{C}_3$  plants,  $g_{m13}$  is therefore the conductance from the intercellular air space to the site of carboxylation (Cousins et al., 2020). In contrast, there is no or little enzymatic fractionation associated with assimilation of  $^{12}\text{C}^{17}\text{O}^{16}\text{O}$  and  $^{12}\text{C}^{18}\text{O}^{16}\text{O}$ , but the oxygen isotope effect during photosynthesis is caused by oxygen isotope exchange between  $\text{CO}_2$  and leaf water (Farquhar and Lloyd, 1993). The isotope exchange between  $\text{CO}_2$  and  $\text{H}_2\text{O}$  involves interconversion with bicarbonate and is catalyzed by carbonic anhydrase (CA) (Gillon and Yakir, 2001). In  $\text{C}_3$  plants, CA is found in the chloroplast, cytosol, mitochondria, and the plasma membrane (Fabre et al., 2007; DiMario et al., 2016), and the  $\text{CO}_2$ - $\text{H}_2\text{O}$  exchange can occur anywhere between the plasma membrane and chloroplast. For  $\text{C}_4$  plants, CA is mainly found in the cytosol where  $\text{CO}_2$ - $\text{H}_2\text{O}$  exchange occurs (Badger and Price, 1994).  $g_{m18}$  is thus the conductance of  $\text{CO}_2$  as it diffuses from the intercellular air space to the site of  $\text{CO}_2$ - $\text{H}_2\text{O}$  exchange for both  $\text{C}_3$  and  $\text{C}_4$  plants (Gillon and Yakir, 2000b, a; Barbour et al., 2016).

The oxygen isotope composition of leaf water at the point where the  $\text{CO}_2$ - $\text{H}_2\text{O}$  exchange takes place is a key source of uncertainty in the estimation of  $g_{m18}$  using oxygen isotopes because a considerable and strong oxygen isotope variation can develop within the leaf due to the discrimination associated with evaporation, transport, and diffusion of  $\text{H}_2\text{O}$  (Gan et al., 2002; Song et al., 2015; Cernusak et al., 2016). Recently, Holloway-Phillips et al. (2019) explored the consistency in the calculated  $g_{m18}$  using  $^{18}\text{O}$ -enriched  $\text{CO}_2$  and  $^{18}\text{O}$ -enriched water vapor entering the cuvette and provided guidelines to minimize the sensitivity of  $g_{m18}$  estimates to

measurement errors.  $g_{m18}$  estimates are relatively more precise when the difference in  $\delta^{18}\text{O}$  of the  $\text{CO}_2$  between the intercellular air space and  $\text{CO}_2\text{-H}_2\text{O}$  exchange site is large (Holloway-Phillips et al., 2019). A higher  $\delta^{18}\text{O}$  difference can be achieved by manipulating the  $\delta^{18}\text{O}$  of the  $\text{CO}_2$ , the water vapor entering the leaf cuvette and/or the irrigation water (Holloway-Phillips et al., 2019).

Oxygen has two heavy isotopes  $^{17}\text{O}$  and  $^{18}\text{O}$ , with a respective natural abundance of 0.038 % and 0.2 %. Since most isotope fractionations depend on mass, the variations in  $\delta^{17}\text{O}$  and  $\delta^{18}\text{O}$  are closely related as:

$$\frac{{}^{17}R_{\text{sample}}}{{}^{17}R_{\text{reference}}} = \left( \frac{{}^{18}R_{\text{sample}}}{{}^{18}R_{\text{reference}}} \right)^{\lambda} \quad (3.1)$$

where  ${}^nR = {}^n\text{O}/{}^{16}\text{O}$ , where  $n$  is 17 or 18. The mass dependent isotope fractionation equation 3.1 can be written in  $\delta$  notation as:

$$(\delta^{17}\text{O} + 1) = (\delta^{18}\text{O} + 1)^{\lambda} \quad (3.2)$$

$$\ln(\delta^{17}\text{O} + 1) = \lambda \times \ln(\delta^{18}\text{O} + 1) \quad (3.3)$$

where  $\delta^n\text{O} = ({}^nR_{\text{sample}} - {}^nR_{\text{reference}})/{}^nR_{\text{reference}}$  and  $\lambda$  varies from 0.5 to 0.5305 for different mass-dependent isotope fractionation processes (Thiemens, 1999). Deviations from equation 3.3 are quantified as  $^{17}\text{O}$ -excess,  $\Delta^{17}\text{O}$ , and in this study we used the linearized definition for  $\Delta^{17}\text{O}$ .

$$\Delta^{17}\text{O} = \delta^{17}\text{O} - \lambda \times \delta^{18}\text{O} \quad (3.4)$$

Note that the  $\Delta$  symbol is also commonly used for isotopic discrimination in biological processes, but we use it here to quantify  $^{17}\text{O}$ -excess. The choice of  $\lambda$  is arbitrary, in this study we use  $\lambda = 0.528$ , the value associated with meteoric water (Luz and Barkan, 2010; Meijer and Li, 1998). For discrimination associated with assimilation we used  $\Delta_A$  (equation 3.11).

Our objective was to investigate whether  $\Delta^{17}\text{O}$  can be used for the estimation of  $g_m$ . We hypothesized that  $\Delta^{17}\text{O}$  is less sensitive to the isotope fractionation due to evapotranspiration of leaf water compared to  $\delta^{18}\text{O}$  because the processes involved follow mass-dependent isotope fractionation (Hoag et al., 2005). We performed gas exchange measurements for the estimation of  $g_{m18}$  and  $g_{m\Delta17}$  with two  $\text{C}_3$  and one  $\text{C}_4$  species at two photon flux densities (PFD), generating a wide variation in  $c_m/c_a$  ratios ( $c_m$  and  $c_a$  are the mole fraction of  $\text{CO}_2$  at  $\text{CO}_2\text{-H}_2\text{O}$  exchange site and the leaf surrounding, respectively). The data were previously used to estimate the effect of photosynthetic gas exchange on the  $\Delta^{17}\text{O}$  of atmospheric  $\text{CO}_2$  (Adnew et al., 2020). To quantify the sensitivity of the  $g_{m18}$  and  $g_{m\Delta17}$  estimates to various parameters, we used Monte Carlo simulations and a leaf cuvette model (Adnew et al., 2020). The leaf cuvette model and analytical equations of gas exchange (Farquhar and Cernusak, 2012) were used to quantify the uncertainty due to potential errors in the assumption of the oxygen isotope composition of leaf water at the  $\text{CO}_2\text{-H}_2\text{O}$  exchange site similar to Holloway-Phillips et al. (2019).

### 3.2. Theory

$g_{m\Delta 17}$  (mol m<sup>-2</sup>s<sup>-1</sup>bar<sup>-1</sup>) can be derived from measurements of  $\Delta^{17}\text{O}$  using equation 3.9 under the assumption that the degree of equilibration between CO<sub>2</sub> and H<sub>2</sub>O is 100 % and that the oxygen isotopic composition of leaf water at the CO<sub>2</sub>-H<sub>2</sub>O exchange site is the same as at the evaporation site (Farquhar et al., 1993; Barbour et al., 2016; Holloway-Phillips et al., 2019).

$$g_{m\Delta 17} = \frac{A_n/P}{c_i - c_{m,\Delta 17}} \quad (3.5)$$

$A_n$  (μmol m<sup>-2</sup>s<sup>-1</sup>) is the assimilation rate,  $P$  (bar) is the total atmospheric pressure,  $c_i$  (μmol mol<sup>-1</sup>) is the CO<sub>2</sub> mole fraction in the intercellular air space.  $c_{m,\Delta 17}$  is the mole fraction at the CO<sub>2</sub>-H<sub>2</sub>O exchange site, calculated using  $\Delta^{17}\text{O}$  measurements as:

$$c_{m,\Delta 17} = c_i \left[ \frac{\Delta^{17}O_i - \Delta^{*17}O_A - \Delta^{*17}O_w}{\Delta^{17}O_m - \Delta^{*17}O_A - \Delta^{*17}O_w} \right] \quad (3.6)$$

where  $\Delta^{17}O_i$  and  $\Delta^{17}O_m$  are the <sup>17</sup>O-excess of CO<sub>2</sub> in the intercellular air space and at the CO<sub>2</sub>-H<sub>2</sub>O exchange site, respectively.  $\Delta^{*17}O_w$  is the <sup>17</sup>O-excess of the discriminations against <sup>12</sup>C<sup>17</sup>O<sup>16</sup>O and <sup>12</sup>C<sup>18</sup>O<sup>16</sup>O during diffusion and dissolution in water.

$$\Delta^{*17}O_w = a_{17w} - \lambda a_{18w} \quad (3.7)$$

$\alpha_{18w}$  is the fractionation factor for <sup>12</sup>C<sup>18</sup>O<sup>16</sup>O during diffusion and dissolution in water,  $a_{18w} = \alpha_{18w} - 1$  is the associated discrimination (Farquhar and Cernusak, 2012).  $a_{17w}$  and  $\alpha_{17w}$  are the corresponding values for <sup>12</sup>C<sup>17</sup>O<sup>16</sup>O.  $\Delta^{*17}O_A$  is a modified definition of  $\Delta^{17}\text{O}$  of the assimilated CO<sub>2</sub> where the individual  $\delta$  values are multiplied by  $\alpha_{17w}$  and  $\alpha_{18w}$ , respectively.

$$\Delta^{*17}O_A = \delta^{17}O_A \alpha_{17w} - \lambda \delta^{18}O_A \alpha_{18w} \quad (3.8)$$

Substituting equation 3.6 for  $c_{m,\Delta 17}$  in equation 3.5 and rearranging terms,  $g_{m\Delta 17}$  can be expressed as:

$$g_{m\Delta 17} = \frac{A_n/P}{c_i} \frac{\Delta^{*17}O_A + \Delta^{*17}O_w - \Delta^{17}O_m}{\Delta^{17}O_i - \Delta^{17}O_m} \quad (3.9)$$

The detailed derivation of equation 3.9 is provided in the supplementary material.

In addition to estimating  $g_m$  using the oxygen isotope composition, we also calculated  $g_m$  using  $\delta^{13}\text{C}$  of CO<sub>2</sub> ( $g_{m13}$ ). The derivation and explanation for determining  $g_{m13}$  is provided in Evans et al. (1986). More detailed information on  $\Delta^{18}\text{O}$  can be found in (Gillon and Yakir, 2000b, a; Barbour et al., 2016; Holloway-Phillips et al., 2019) (see Table S3.1 for equations and list of variables and detailed derivations in the supplementary material).

To estimate the precision with which  $g_{m18}$  and  $g_{m\Delta17}$  can be derived from measurements in gas exchange experiments, we used Monte Carlo simulations of  $g_m$  similar to Holloway-Phillips et al. (2019). Using a leaf cuvette model (Adnew et al., 2020) and assuming constant assimilation rate, stomatal and mesophyll conductance, we simulated the mole fraction and isotopic composition of  $\text{CO}_2$  in the air surrounding the leaf, in the intercellular airspace and at the  $\text{CO}_2$ - $\text{H}_2\text{O}$  exchange site under steady-state conditions, varying the isotopic composition of the incoming  $\text{CO}_2$  over a wide range. We then used the model results, including realistic measurement error estimates based on experiments and uncertainties in assumptions, to calculate the apparent discrimination and the oxygen isotope composition of the assimilated  $\text{CO}_2$  (Evans et al., 1986; Barbour et al., 2016), and their uncertainties:

$$\delta^{18}\text{O}_A = \frac{\delta^{18}\text{O}_a - \Delta_A^{18}\text{O}}{\Delta_A^{18}\text{O} + 1} = \delta^{18}\text{O}_a - \zeta(\delta^{18}\text{O}_a - \delta^{18}\text{O}_e) \quad (3.10)$$

$$\Delta_A^{18}\text{O} = \frac{\zeta(\delta^{18}\text{O}_a - \delta^{18}\text{O}_e)}{1 + \delta^{18}\text{O}_a - \zeta(\delta^{18}\text{O}_a - \delta^{18}\text{O}_e)} \quad (3.11)$$

$\zeta = c_e/(c_e - c_a)$ ,  $c_e$  and  $c_a$  are the mole fractions of  $\text{CO}_2$  entering and leaving the cuvette respectively. Details of the model setup are provided in the supplementary material.

### 3.3. Results

#### 3.3.1. $\text{CO}_2$ gradient, and discrimination against $^{18}\text{O}$ during assimilation

The  $\text{CO}_2$  mole fraction successively decreased from the cuvette air (set to about  $400 \mu\text{mol mol}^{-1}$  by adjusting the airflow with  $500 \mu\text{mol mol}^{-1}$  of  $\text{CO}_2$ ) to the site of carboxylation during photosynthetic activity (Table 3.1, Figure 3.1).

Table 3.1: Summary of gas exchange parameters determined in experiments with sunflower, ivy and maize. The mole fraction of  $\text{CO}_2$  at the  $\text{H}_2\text{O}$ - $\text{CO}_2$  exchange site ( $c_m$ ) is calculated assuming that the isotopic composition of leaf water at the site of  $\text{CO}_2$ - $\text{H}_2\text{O}$  exchange is the same as at the site of evaporation. Numbers in parenthesis are the standard deviation of the mean ( $1\sigma$ ). PFD is a photon flux density of photosynthetically active radiation.

| Parameter       | unit  | PFD ( $\mu\text{mol m}^{-2} \text{s}^{-1}$ )                   | Sunflower     | Ivy         | Maize       |
|-----------------|---|--|---------------|-------------|-------------|
| $A_n$           | $\mu\text{mol m}^{-2} \text{s}^{-1}$              | 300  | 18 (0.7)      | 12 (0.8)    | 17 (2)      |
|                 |   | 1200   | 26 (6)        | 15 (2)      | 32 (2)      |
| $g_s$           | $\text{mol m}^{-2} \text{s}^{-1}$                 | 300  | 0.45 (0.14)   | 0.11 (0.02) | 0.08 (0.01) |
|                 |   | 1200   | 0.35 (0.01)   | 0.15 (0.03) | 0.16 (0.02) |
| $g_{m18}$       | $\text{mol m}^{-2} \text{s}^{-1} \text{bar}^{-1}$ | 300  | 0.50 (0.15)   | 0.20 (0.05) | 0.30 (0.07) |
|                 |   | 1200   | 0.46 (0.13)   | 0.17 (0.03) | 0.31 (0.02) |
| $g_{m\Delta17}$ | $\text{mol m}^{-2} \text{s}^{-1} \text{bar}^{-1}$ | 300 (Normal $\text{CO}_2$ )                                    | 0.32 (single) | 0.27 (0.15) | 0.38 (0.19) |
|                 |   | 300 ( $^{17}\text{O}$ -enriched $\text{CO}_2$ )                | 0.32 (0.08)   | 0.13 (0.04) | 0.20 (0.07) |
|                 |   | 300 (both Normal and $^{17}\text{O}$ -enriched $\text{CO}_2$ ) | 0.32 (0.06)   | 0.20 (0.12) | 0.29 (0.16) |
|                 |   | 1200 (Normal $\text{CO}_2$ )                                   | 0.47 (0.11)   | 0.18 (0.05) | 0.31 (0.19) |

|                  |   |   |             |             |             |
|------------------|---|---|-------------|-------------|-------------|
|                  |   | 1200 ( $^{17}\text{O}$ -enriched $\text{CO}_2$ )                | 0.27 (0.04) | 0.15 (0.01) | 0.20 (0.03) |
|                  |   | 1200 (both Normal and $^{17}\text{O}$ -enriched $\text{CO}_2$ ) | 0.39 (0.14) | 0.16 (0.03) | 0.31 (0.16) |
| $g_{m13}$        | $\text{mol m}^{-2}\text{s}^{-1}\text{bar}^{-1}$ | 300   | 0.23 (0.05) | 0.13 (0.04) | -           |
|                  |   | 1200  | 0.25 (0.08) | 0.11 (0.02) | -           |
| $c_a$            | $\mu\text{mol mol}^{-1}$                        | all   | 402 (3)     | 403 (3)     | 403 (3)     |
| $c_i$            | $\mu\text{mol mol}^{-1}$                        | 300   | 377 (8)     | 284 (12)    | 194 (20)    |
|                  |   | 1200  | 319 (12)    | 301 (13)    | 194 (15)    |
| $c_c$            | $\mu\text{mol mol}^{-1}$                        | 300   | 277 (15)    | 188 (30)    | -           |
|                  |   | 1200  | 208 (39)    | 163 (21)    | -           |
| $c_m, \Delta 17$ | $\mu\text{mol mol}^{-1}$                        | 300 (both Normal and $^{17}\text{O}$ -enriched $\text{CO}_2$ )  | 300 (6)     | 207 (36)    | 120 (41)    |
|                  |   | 1200 (both Normal and $^{17}\text{O}$ -enriched $\text{CO}_2$ ) | 241 (37)    | 207 (12)    | 71 (46)     |
| $c_m, 18$        | $\mu\text{mol mol}^{-1}$                        | 300 (both Normal and $^{17}\text{O}$ -enriched $\text{CO}_2$ )  | 319 (10)    | 219 (10)    | 134 (15)    |
|                  |   | 1200 (both Normal and $^{17}\text{O}$ -enriched $\text{CO}_2$ ) | 256 (26)    | 213 (12)    | 89 (17)     |

For sunflower, typical values for highlight (hereafter HL) calculated from the gas exchange experiments are: cuvette air:  $c_a = 402 \mu\text{mol mol}^{-1}$ ; intercellular air space:  $c_i = 319 \mu\text{mol mol}^{-1}$ ;  $\text{CO}_2$ - $\text{H}_2\text{O}$  exchange site:  $c_m, \Delta 17 = 241 \mu\text{mol mol}^{-1}$  and chloroplast:  $c_c = 208 \mu\text{mol mol}^{-1}$ . The average fraction of  $\text{CO}_2$  entering the leaf that is actually assimilated, calculated as  $(c_a - c_c)/c_a$ , is only 50 % and 60 % for sunflower and ivy, respectively. For maize, the  $\text{CO}_2$  gradient was even stronger, as expected for a  $\text{C}_4$  plant (Figure 3.1, Table 3.1).

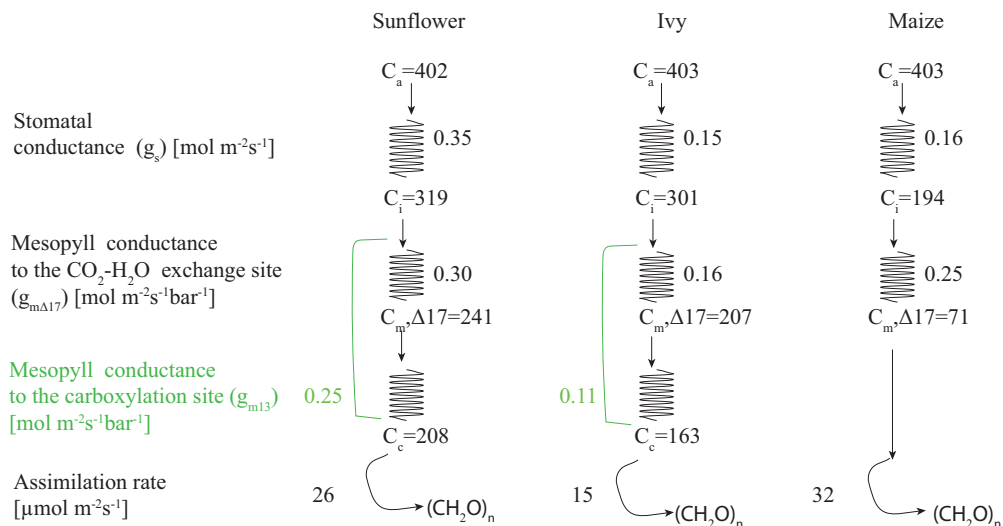


Figure 3.1 A schematic representation of the resistance path to diffusion of  $\text{CO}_2$  in  $\text{C}_3$  (sunflower and ivy) and  $\text{C}_4$  (Maize) leaves. The values of the  $\text{CO}_2$  mole fraction for the corresponding compartments and the conductance are typical values for the high light experiments in this study, where  $c$  is the mole fraction of  $\text{CO}_2$  in  $\mu\text{mol mol}^{-1}$  and the subscript  $a$ ,  $i$ ,  $m$  and  $c$  stand for leaf surrounding, intercellular air space,  $\text{CO}_2$ - $\text{H}_2\text{O}$  exchange site and chloroplast, respectively. Typical assimilation rates are also indicated.

Figure 3.2a shows discrimination against  $^{18}\text{O}$  associated with assimilation ( $\Delta_A^{18}\text{O}$ ) for sunflower, ivy, and maize as a function of the  $c_m/c_a$  ratio.  $\Delta_A^{18}\text{O}$  varied with  $c_m/c_a$ , in agreement with previous studies (Gillon and Yakir, 2000b; Barbour et al., 2016). For sunflower, we observe  $\Delta_A^{18}\text{O}$  values between 29 ‰ and 64 ‰ for  $c_m/c_a$  between 0.54 and 0.86. Ivy showed relatively little variation of  $\Delta_A^{18}\text{O}$  around a mean of 22 ‰ for  $c_m/c_a$  between 0.48 and 0.58. For maize,  $\Delta_A^{18}\text{O}$  was lower than for the  $\text{C}_3$  plants measured in this study, with values between 10 ‰ and 20 ‰ for  $c_m/c_a$  between 0.15 and 0.37. Figure 3.2b, shows a comparison between observed discrimination against  $^{18}\text{O}$  with the Farquhar model (Farquhar et al., 1993) for sunflower, ivy, and maize. The discrimination calculated with the Farquhar model agrees well (root mean square error of 0.93 ‰ and  $r^2$  of 0.9998, sample size=33) with the observed discrimination with a slight underestimation at a higher  $c_m/c_a$  ratio.

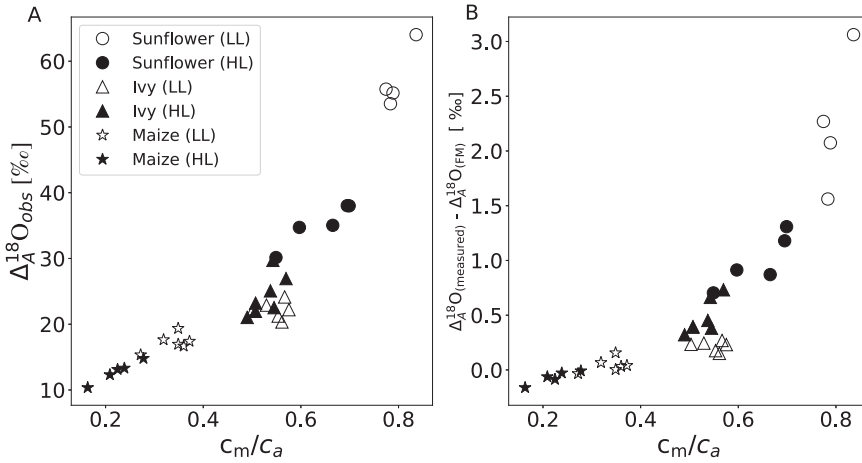


Figure 3.2 A)  $\Delta_A^{18}\text{O}_{\text{obs}}$  during photosynthesis for two  $\text{C}_3$  plants, sunflower and ivy and the  $\text{C}_4$  plant maize as a function of  $c_m/c_a$  for low light (LL) and high light (HL) experiments, adopted from Adnew et al. (2020). B) comparison of the observed  $\Delta_A^{18}\text{O}$  with the Farquhar model (FM) (see table S3.1 in the supplementary material as a function of  $c_m/c_a$ ).

### 3.3.2. Mesophyll conductance

The results presented in Table 3.1 and Figure 3.3 show that  $g_{m17}$  and  $g_{m18}$  agree within the errors, but  $g_{m17}$  values are systematically lower than  $g_{m18}$  (Figure S3.1, Table 3.1). Figure 3.3 shows the  $g_{m18}$  and  $g_{m17}$  and results of the individual experiments, as a function of  $\delta^{18}\text{O}_i - \delta^{18}\text{O}_m$  and  $\Delta^{17}\text{O}_i - \Delta^{17}\text{O}_m$ , respectively. For sunflower, at low light (hereafter LL),  $g_{m18} = 0.50 \text{ mol m}^{-2}\text{s}^{-1}\text{bar}^{-1}$  and  $g_{m17} = 0.32 \text{ mol m}^{-2}\text{s}^{-1}\text{bar}^{-1}$  (average for both normal and  $^{17}\text{O}$ -enriched  $\text{CO}_2$ ) (Table 3.1, Figure 3.3). At HL,  $g_{m18}$  is slightly decreased to  $0.46 \text{ mol m}^{-2}\text{s}^{-1}\text{bar}^{-1}$  while  $g_{m17}$  increases to  $0.39 \text{ mol m}^{-2}\text{s}^{-1}\text{bar}^{-1}$  (average for both normal and  $^{17}\text{O}$ -enriched  $\text{CO}_2$ ) (Table 3.1). Equation 3.9 suggests that  $g_{m17}$  values can become very high when  $\Delta^{17}\text{O}$  in the intercellular space and in the mesophyll are very similar. This may lead to large errors in  $g_{m17}$  if the difference  $\Delta^{17}\text{O}_i - \Delta^{17}\text{O}_m$  is of the order of the measurement precision (0.01 ‰). For the  $g_{m17}$  estimate, the experiments are categorized into four groups (HL- $^{17}\text{O}$ -enriched  $\text{CO}_2$ , HL-Normal  $\text{CO}_2$ , LL- $^{17}\text{O}$ -enriched  $\text{CO}_2$  and LL-Normal  $\text{CO}_2$ ). The uncertainty in the  $g_m$  estimate using

$\Delta^{17}\text{O}$  increases when  $^{17}\text{O}$ -enriched  $\text{CO}_2$  is used that result in a higher  $|\Delta^{17}\text{O}_i - \Delta^{17}\text{O}_m|$ . For instance, for sunflower at LL,  $g_{m\Delta 17}$  was  $0.47 \pm 0.11 \text{ mol m}^{-2}\text{s}^{-1}\text{bar}^{-1}$  and  $0.32 \pm 0.08 \text{ mol m}^{-2}\text{s}^{-1}\text{bar}^{-1}$  (Table 3.1, Figure 3.3) for the  $\Delta^{17}\text{O}$  of  $\text{CO}_2$  entering the cuvette ( $\Delta^{17}\text{O}_e$ ) of  $-0.333 \text{ ‰}$  and  $0.223 \text{ ‰}$ , respectively (see material and method). Similar to the sunflower,  $g_{m\Delta 17}$  estimates for ivy and maize are lower when  $^{17}\text{O}$ -enriched  $\text{CO}_2$  is used relative to normal  $\text{CO}_2$  at all light conditions (Table 3.1, Figure 3.3). As shown in Table 3.1, the standard deviation between leaf replicates in the  $g_{m\Delta 17}$  estimate decreased when isotopically enriched  $\text{CO}_2$  was used in the experiments. The same is true for  $g_{m18}$  when the  $\delta^{18}\text{O}$  value of the intercellular space and in the mesophyll are very similar as predicted from equation S3.2. For sunflower, the conductance from the intercellular airspace to the site of equilibration, ( $g_{m18}$  and  $g_{m\Delta 17}$ ), was about 1.8 to 2 times higher than the conductance to the site of carboxylation ( $g_{m13}$ ). For ivy, the  $g_{m18}/g_{m13}$  ratio was about 1.5.

We evaluated the sensitivity of  $g_{m\Delta 17}$  on the  $\Delta^{17}\text{O}$  of  $\text{CO}_2$  entering the cuvette ( $\Delta^{17}\text{O}_e$ ) at  $0.2 \text{ ‰}$ ,  $1 \text{ ‰}$ ,  $5 \text{ ‰}$ ,  $10 \text{ ‰}$ , which resulted in  $\Delta^{17}\text{O}_i - \Delta^{17}\text{O}_m$  differences of  $0.3 \text{ ‰}$ ,  $0.5 \text{ ‰}$ ,  $1.6 \text{ ‰}$ , and  $3 \text{ ‰}$ , respectively (Figure 3.5).

The relative error in  $g_{m\Delta 17}$  due to measurement error increases when the  $|\Delta^{17}\text{O}_i - \Delta^{17}\text{O}_m|$  decreases, similar to  $g_{m18}$  estimates for a similar gas exchange parameter (Holloway-Phillips et al., 2019). When  $|\Delta^{17}\text{O}_i - \Delta^{17}\text{O}_m|$  is close to the values used in the experiments with normal  $\text{CO}_2$ , the errors in  $g_m$  are very large (75 %, standard deviation). Also, for  $|\Delta^{17}\text{O}_i - \Delta^{17}\text{O}_m| = 0.5 \text{ ‰}$ , typical errors are still 50 %. Table 3.1 and Figure 3.4 shows that errors in the  $g_{m\Delta 17}$  method can be strongly limited when  $\text{CO}_2$  with a higher  $\Delta^{17}\text{O}$  value is used in the experiments, the scatter in  $g_{m\Delta 17}$  is larger at lower  $|\Delta^{17}\text{O}_i - \Delta^{17}\text{O}_m|$ .

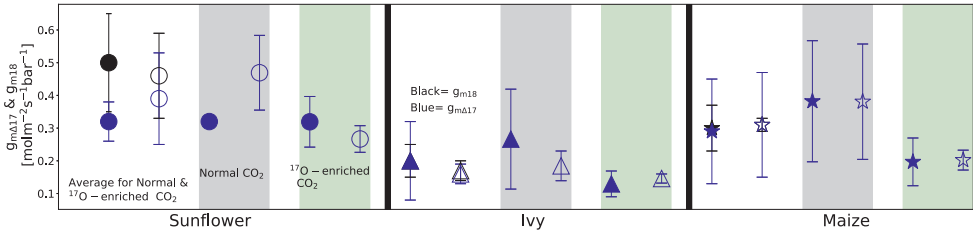


Figure 3.3  $g_{m\Delta 17}$  and  $g_{m18}$  estimates for sunflower, ivy, and maize at low light (solid) and high light (open).

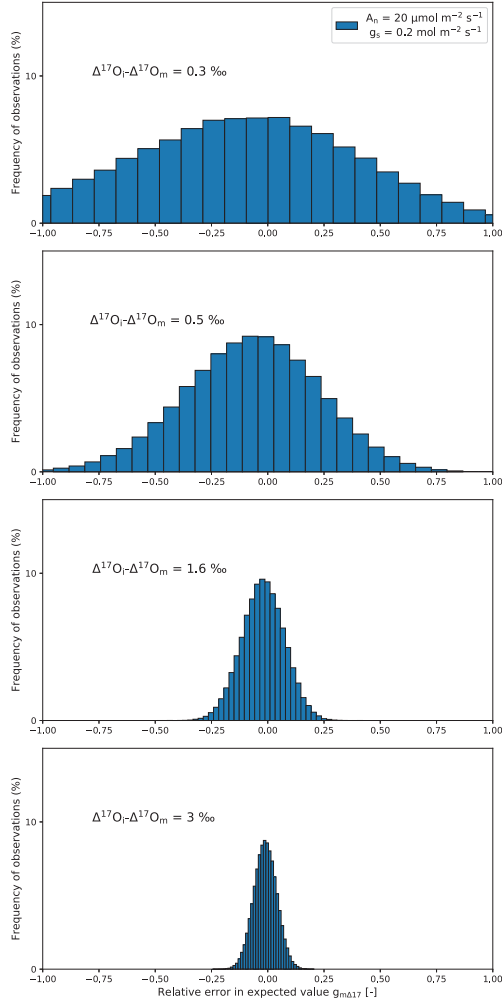


Figure 3.4 Probability distribution of the error in  $g_{m\Delta 17}$  [relative error = (simulated  $g_{m\Delta 17}$  - assigned  $g_{m\Delta 17}$ ) / assigned  $g_{m\Delta 17}$ ] due to measurement error in the  $\Delta^{17}\text{O}$  measurements of  $\text{CO}_2$  and water vapor for four different values of  $\Delta^{17}\text{O}_i - \Delta^{17}\text{O}_m$ , for an “assigned” value of  $g_{m\Delta 17} = 0.5 \text{ mol m}^{-2} \text{s}^{-1} \text{ bar}^{-1}$ . The analysis is performed with a Monte Carlo approach using simulated gas exchange parameters from the leaf cuvette model. We assigned measurement errors of 0.03 ‰ and 0.016 ‰, respectively, to the  $\delta^{17}\text{O}$  and  $\delta^{18}\text{O}$  of  $\text{CO}_2$  in the different compartments (1 sigma standard deviation of the mean). For the water isotopes, the error is assumed to be 0.1 ‰ and 0.05 ‰ for  $\delta^{17}\text{O}$  and  $\delta^{18}\text{O}$ , respectively.



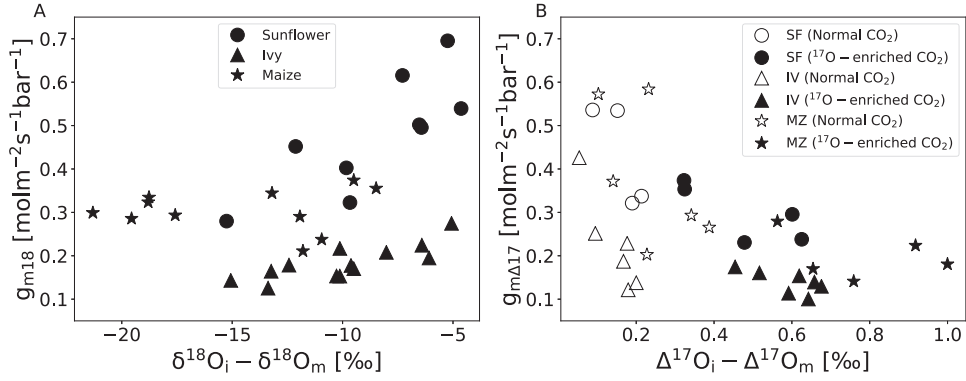


Figure 3.5  $g_m$  estimates using  $\delta^{18}\text{O}$  measurement (A) and  $\Delta^{17}\text{O}$  measurement (B) for sunflower (SF), ivy (IV) and maize (MZ) as a function of the difference in the oxygen isotope composition between the intercellular air space and the  $\text{CO}_2$ - $\text{H}_2\text{O}$  exchange site for Normal and  $^{17}\text{O}$ -enriched  $\text{CO}_2$ .

### 3.3.2.1. Influence of uncertainty in water isotopic composition on $g_m$

There is a large variation in the oxygen isotope composition of water within a leaf and the isotopic composition at the site where  $\text{CO}_2$ - $\text{H}_2\text{O}$  exchange takes place is not well known. This causes an uncertainty in the estimate of the oxygen isotope composition of the  $\text{CO}_2$  in equilibrium with the leaf water. This will result in an error on the oxygen isotope composition of the assimilated  $\text{CO}_2$  (Farquhar et al., 1989b) which in turn causes a bias in the oxygen isotope composition of  $\text{CO}_2$  in the intercellular air space, and thus  $g_m$  (equation 3.9 for  $\Delta^{17}\text{O}$ ). We compared the effect of a potential bias in the oxygen isotope composition of water at the  $\text{CO}_2$ - $\text{H}_2\text{O}$  exchange site of 4.3 ‰ (Song et al., 2015) on  $g_{m18}$ , and how this error caused by evapotranspiration would translate to  $g_{m17}$ . The corresponding bias in  $\Delta^{17}\text{O}$  of the leaf water at the  $\text{CO}_2$ - $\text{H}_2\text{O}$  exchange site is 0.052 ‰ calculated using  $\lambda_{\text{trans}}=0.516$  (Landais et al., 2006), for air humidity surrounding the leaf of 76 %, a typical value in the experiments carried out in this study. Figure 3.6 shows that the error in the  $g_{m18}$  and  $g_{m17}$  estimates are lower when  $|\delta^{18}\text{O}_i - \delta^{18}\text{O}_m|$  and  $|\Delta^{17}\text{O}_i - \Delta^{17}\text{O}_m|$  are larger, respectively which is independent on the assigned  $g_m$  value (Figure 3.6 and Table 3.2).

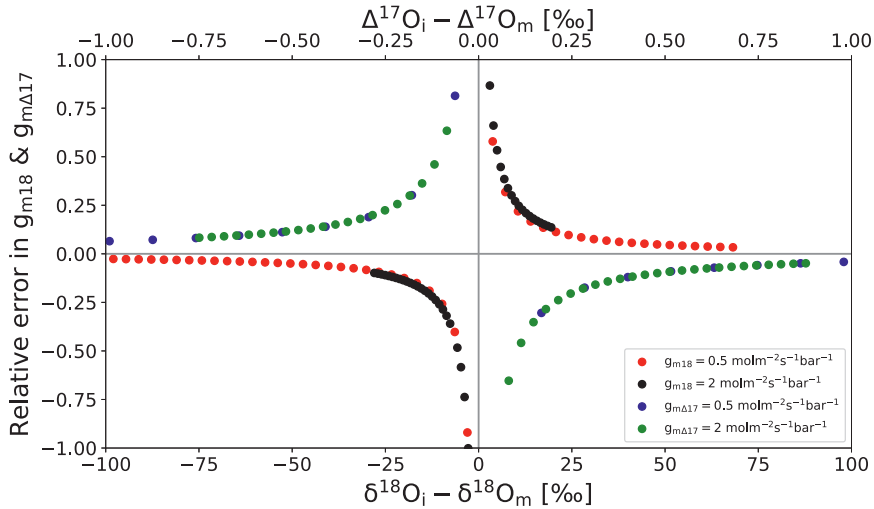


Figure 3.6 Sensitivity analysis showing the relative error ( $\text{relative error} = (\text{simulated value} - \text{assigned value}) / \text{assigned value}$ ) in the simulated  $g_m$  associated with underestimation of  $^{18}\text{O}$  isotope composition of leaf water at the  $\text{CO}_2\text{-H}_2\text{O}$  exchange site by 4.3 ‰.

Table 3.2 shows the required  $\Delta^{17}\text{O}_e$  and  $\delta^{18}\text{O}_e$  of the  $\text{CO}_2$  entering the cuvette to have a  $g_m$  estimated error less than 25 % when there is an underestimation of the  $\delta^{18}\text{O}$  value of leaf water at the  $\text{CO}_2\text{-H}_2\text{O}$  exchange site by 4.3 ‰.  $\Delta^{17}\text{O}_e$  and  $\delta^{18}\text{O}_e$  are different for different  $g_m$  values to get a similar precision. For instance, for a  $g_m$  value of  $2 \text{ mol m}^{-2}\text{s}^{-1}\text{bar}^{-1}$  it requires a higher  $|\Delta^{17}\text{O}_e|$  value compared to a  $g_m$  value of  $0.5 \text{ mol m}^{-2}\text{s}^{-1}\text{bar}^{-1}$  (Table 3.2). The same is true for  $g_{m18}$  estimates. However, the precision of mesophyll conductance estimates as a function of  $\Delta^{17}\text{O}_i - \Delta^{17}\text{O}_m$  is independent of the  $g_m$  value (Table 3.2).

**Table 3.2:** The required  $\Delta^{17}\text{O}_e$  (or  $\Delta^{17}\text{O}_i - \Delta^{17}\text{O}_m$  difference) and  $\delta^{18}\text{O}_e$  ( $\delta^{18}\text{O}_i - \delta^{18}\text{O}_m$  difference) to have an error less 25 % in the  $g_m$  estimate when there is a 4.3 ‰ bias on the  $\delta^{18}\text{O}$  of water at the  $\text{CO}_2\text{-H}_2\text{O}$  exchange site, for  $\delta^{18}\text{O}$  and  $\Delta^{17}\text{O}$  of leaf water 10 ‰ and -0.28 ‰, respectively. The  $\delta^{18}\text{O}$  and  $\Delta^{17}\text{O}$  of  $\text{CO}_2$  at the exchange site is 42 ‰ and -0.33 ‰, respectively.

| $g_m [\text{mol m}^{-2}\text{s}^{-1}\text{bar}^{-1}]$ | $\Delta^{17}\text{O}_e - \Delta^{17}\text{O}_m$ | $\Delta^{17}\text{O}_i - \Delta^{17}\text{O}_m$ | $\delta^{18}\text{O}_e - \delta^{18}\text{O}_m$ | $\delta^{18}\text{O}_i - \delta^{18}\text{O}_m$ |
|---|---|---|---|---|
| 0.5   | $< -1.87$                                       | $< -0.4$  | $< -48$   | $< -17$   |
|   | $> 0.93$  | $> 0.4$   | $> 74$  | $> 17$  |
| 2   | $< -6$  | $< -0.5$  | $< -207$  | $< -17$   |
|   | $> 5.43$  | $> 0.5$   | $> 234$   | $> 18$  |

### 3.4. Discussion

Regarding  $g_{m18}$ , our estimates for sunflower are in good agreement with values from Shrestha et al. (2019). The mesophyll conductance to the site of CO<sub>2</sub>-H<sub>2</sub>O exchange that we found for maize,  $g_{m18} = 0.31 \text{ mol m}^{-2} \text{ s}^{-1} \text{ bar}^{-1}$  is within the wide range of 0.169 to 0.9  $\text{mol m}^{-2} \text{ s}^{-1} \text{ bar}^{-1}$  reported by (Ubierna et al., 2007; Kolbe and Cousins, 2018; Ubierna et al., 2018a). However, Barbour et al. (2016) and Gillon and Yakir (2000b), reported even higher  $g_{m18}$  values for maize, 1.78  $\text{mol m}^{-2} \text{ s}^{-1} \text{ bar}^{-1}$  and 1.0  $\text{mol m}^{-2} \text{ s}^{-1} \text{ bar}^{-1}$ , respectively. Differences in mesophyll conductance between different studies might be due to: 1) difference in  $\delta^{18}\text{O}$  of the CO<sub>2</sub> between the intercellular air space and the CO<sub>2</sub>-H<sub>2</sub>O exchange site. According to the leaf cuvette model and Monte Carlo simulation of this study, high values of  $g_m$  can be produced (erroneously) when  $|\delta^{18}\text{O}_i - \delta^{18}\text{O}_m|$  is very small, a similar result is reported by (Holloway-Phillips et al., 2019). 2) different experimental and growing conditions such as temperature, PFD, CO<sub>2</sub> mixing ratio, and other environmental conditions (Ubierna et al., 2007; Kolbe and Cousins, 2018; Ubierna et al., 2018a; Evans and von Caemmerer, 2013).

The Monte Carlo calculations demonstrate that measurement precision is a limiting factor for determining  $g_{m\Delta 17}$  values (Figure 3.5). This effect likely contributes to our experimental results where we observe more scatter (i.e. a higher standard deviation) for  $g_{m18}$  and  $g_{m\Delta 17}$  estimates at lower  $|\delta^{18}\text{O}_i - \delta^{18}\text{O}_m|$  and  $|\Delta^{17}\text{O}_m - \Delta^{17}\text{O}_i|$ , respectively (Figure 3.4, Table 3.1). Based on the leaf cuvette model and Monte Carlo simulations, the uncertainty in estimates of  $g_{m\Delta 17}$  increases when  $|\Delta^{17}\text{O}_i - \Delta^{17}\text{O}_m|$  values decrease (Table 3.1 and Figure 3.5). For example, at  $\Delta^{17}\text{O}_i - \Delta^{17}\text{O}_m = 3 \text{ ‰}$ ,  $g_{m\Delta 17}$  can be estimated with an error of less than 10 % (Figure 3.5). Bias in the estimate of mesophyll conductance introduced by uncertainty in the  $\delta^{18}\text{O}$  and  $\Delta^{17}\text{O}$  of leaf water at the CO<sub>2</sub>-H<sub>2</sub>O exchange site depends on the  $|\delta^{18}\text{O}_i - \delta^{18}\text{O}_m|$  and  $|\Delta^{17}\text{O}_i - \Delta^{17}\text{O}_m|$  for  $g_{m18}$  and  $g_{m\Delta 17}$  estimates, respectively (Figure 3.5). The higher the relative difference in  $\Delta^{17}\text{O}$  of CO<sub>2</sub> between the intercellular air space and the CO<sub>2</sub>-H<sub>2</sub>O exchange site, the more precise is the  $g_m$  estimate. When normal CO<sub>2</sub> is used,  $|\Delta^{17}\text{O}_i - \Delta^{17}\text{O}_m|$  is small and the scatter of  $g_{m\Delta 17}$  estimates between individual replicates increased strongly, but when <sup>17</sup>O-enriched CO<sub>2</sub> was used the  $g_{m\Delta 17}$  estimates between leaf replicates were much more consistent (Table 3.1).

Our model calculations highlight a potentially important source of uncertainty in the determination of  $g_m$  values between different studies, namely large errors in the derived  $g_m$  values when the difference between the isotopic composition of CO<sub>2</sub> in the intercellular air space and the CO<sub>2</sub> in equilibrium with leaf water ( $|\delta^{18}\text{O}_i - \delta^{18}\text{O}_m|$  or  $|\Delta^{17}\text{O}_i - \Delta^{17}\text{O}_m|$ ) is small. Small differences can occur in an experiment when the isotopic composition of CO<sub>2</sub> is accidentally close to the one in equilibrium with the leaf water, and this should be avoided. Such an overestimation was shown in (Holloway-Phillips et al., 2019) for *Vicia faba* when the  $\Delta^{18}\text{O}$  was close to zero.  $\Delta^{18}\text{O}$  is close to zero when the  $\delta^{18}\text{O}$  of CO<sub>2</sub> entering the leaf is close to  $\delta^{18}\text{O}$  of the CO<sub>2</sub> at the CO<sub>2</sub>-H<sub>2</sub>O exchange site. Thus, smaller differences in  $|\delta^{18}\text{O}_i - \delta^{18}\text{O}_m|$  may cause an overestimation in  $g_{m18}$  estimates especially when the difference is of the order of the measurement precision. There is important feedback between  $g_m$  and  $|\delta^{18}\text{O}_i - \delta^{18}\text{O}_m|$  or  $|\Delta^{17}\text{O}_i - \Delta^{17}\text{O}_m|$ : when  $g_m$  increases, CO<sub>2</sub> exchange between mesophyll and intercellular airspace becomes faster, which decreases  $|\delta^{18}\text{O}_i - \delta^{18}\text{O}_m|$  or  $|\Delta^{17}\text{O}_i - \Delta^{17}\text{O}_m|$ . As such, estimates of  $g_m$  using the oxygen isotope techniques will have larger errors for plants with higher mesophyll conductance. This can be compensated to some degree by choosing CO<sub>2</sub> with an oxygen isotopic composition that is very depleted or enriched compared to the CO<sub>2</sub> at the CO<sub>2</sub>-H<sub>2</sub>O

exchange site. The dependence of the error in  $g_m$  on  $|\delta^{18}\text{O}_i - \delta^{18}\text{O}_m|$  or  $|\Delta^{17}\text{O}_i - \Delta^{17}\text{O}_m|$  complicates comparison of  $g_m$  estimates from different studies.

Estimates of  $g_{m18}$  can be more or less reliably compared to  $g_{m\Delta17}$  depending on  $|\delta^{18}\text{O}_i - \delta^{18}\text{O}_m|$  and  $|\Delta^{17}\text{O}_i - \Delta^{17}\text{O}_m|$ , respectively.  $|\delta^{18}\text{O}_i - \delta^{18}\text{O}_m|$  and  $|\Delta^{17}\text{O}_i - \Delta^{17}\text{O}_m|$  are dependent on the  $^{18}\text{O}$  oxygen isotope composition and  $^{17}\text{O}$ -excess of the  $\text{CO}_2$  gas used for the experiment and the leaf water at the  $\text{CO}_2$ - $\text{H}_2\text{O}$  exchange site, respectively. As shown in Table 3.2, the manipulation required in the  $\Delta^{17}\text{O}$  of the  $\text{CO}_2$  to have a certain precision is smaller than for  $g_m$  estimate using  $\delta^{18}\text{O}$  and at higher  $g_m$  it requires higher manipulation in the  $\Delta^{17}\text{O}$  of the  $\text{CO}_2$  entering the leaf cuvette.

The ratio  $g_{m18}/g_{m13}$  was higher for sunflower than for ivy (2 vs 1.5), a similar behavior reported in previous studies for other  $\text{C}_3$  plant species (Gillon and Yakir, 2000b; Barbour et al., 2016; Holloway-Phillips et al., 2019). This suggests for the two  $\text{C}_3$  plants (sunflower and ivy), that site of carboxylation is different from the  $\text{CO}_2$ - $\text{H}_2\text{O}$  exchange site. In this study, some of the uncertainty in the  $g_{m18}/g_{m13}$  might arise due to the part of the photo-respired  $\text{CO}_2$  flux diffuses out of the leaf via the cytosol, passing through gaps between the chloroplasts rather than through them (Holloway-Phillips et al., 2019; Ubierna et al., 2019) since the measurements were carried out under 21 % (v/v) of oxygen.

One of the limitations of estimating  $g_m$  using  $^{18}\text{O}$  isotope composition is the uncertainty in the  $\delta^{18}\text{O}$  value of water at the  $\text{CO}_2$ - $\text{H}_2\text{O}$  exchange site. Using  $^{17}\text{O}$ -excess measurements, the error in the  $g_m$  estimate due to the uncertainty in the oxygen isotope composition of leaf water at the  $\text{CO}_2$ - $\text{H}_2\text{O}$  exchange site is lower than  $g_{m18}$  estimate as shown in Table 3.1.

### 3.5. Conclusions

The possibility of using  $\Delta^{17}\text{O}$  to estimate  $g_m$  in a gas exchange measurement from  $\Delta^{17}\text{O}$  measurement of the  $\text{CO}_2$  entering and leaving a leaf cuvette, and bulk leaf water is demonstrated in this study. Based on the model developed by Farquhar and co-workers for  $\delta^{18}\text{O}$  (Farquhar and Cernusak, 2012), we derived the mathematical formalism for calculating  $g_m$  from  $\Delta^{17}\text{O}$  value of  $\text{CO}_2$  and leaf water during a gas exchange experiment. We measured for the first-time mesophyll conductance using  $\Delta^{17}\text{O}$  and the values corroborate the results obtained from  $g_{m18}$ . Changing the PFD from LL to HL did not cause a significant change in the mesophyll conductance in our experiments. Our results confirm previous findings that  $g_{m18}$  is higher than  $g_{m13}$ , demonstrating that oxygen isotope equilibration between  $\text{CO}_2$  and  $\text{H}_2\text{O}$  is achieved before the  $\text{CO}_2$  reaches the site of carboxylation for sunflower and ivy.

An important parameter in the determination of  $g_m$  by oxygen isotopes is the difference between the oxygen isotopic composition of  $\text{CO}_2$  in the intercellular air space and the  $\text{CO}_2$ - $\text{H}_2\text{O}$  exchange site. When  $|\Delta^{17}\text{O}_i - \Delta^{17}\text{O}_m|$  is very similar to the measurement error, errors in the  $g_m$  determination become very large. The sensitivity of both oxygen isotope techniques can be enhanced by using  $\text{H}_2\text{O}$  and/or  $\text{CO}_2$  with large differences in  $\delta^{18}\text{O}$  and  $\Delta^{17}\text{O}$  between the intercellular air space and the  $\text{CO}_2$ - $\text{H}_2\text{O}$  exchange site, respectively. Although the uncertainty in the  $\Delta^{17}\text{O}$  of water at the exchange site is much lower than for  $\delta^{18}\text{O}$ , the signal is also much lower and the measurement uncertainty for  $\Delta^{17}\text{O}$  becomes a limiting factor.  $g_{m\Delta17}$  estimates are not necessarily better than  $g_{m18}$  estimates, the precision of  $g_{m\Delta17}$  and  $g_{m18}$  estimates depend on the  $|\Delta^{17}\text{O}_i - \Delta^{17}\text{O}_m|$  and  $|\delta^{18}\text{O}_i - \delta^{18}\text{O}_m|$  differences respectively. When sufficiently higher  $^{17}\text{O}$ -

enriched CO<sub>2</sub> is used,  $g_{m\Delta 17}$  estimates are more precise than  $g_{m18}$  since leaf water isotope fractionations due to evapotranspiration has a minor effect on the  $\Delta^{17}\text{O}$ .

## 3.6. Materials and methods

### 3.6.1. Plant material and growing conditions

Plant growth and experimental conditions have been described in detail in (Adnew et al., 2020) and are briefly summarized here. Plants were grown in a controlled environment growth room at air temperature 20°C, relative humidity 70 %, PFD 300  $\mu\text{mol m}^{-2} \text{s}^{-1}$  and a photoperiod of 16 hrs. A dwarf variety of sunflower (*Helianthus annuus* L. cv “sunny”), an herbaceous C<sub>3</sub> species with the highest  $c_m/c_a$  ratio, was grown from seed in 0.6 L pots. The first leaf pair was used for the experiments, which reached the final size after about 4 weeks of growth. Later appearing leaves above were removed to avoid shading of the target leaves. For Ivy (*Hedera hybernica* L.), a woody C<sub>3</sub> species with an intermediate  $c_m/c_a$  ratio, established juvenile plants were used. They were grown in 6L pots and pruned when placed in the growth room. Leaves that had developed to maturity in the growth room were used for the experiments. Maize (*Zea mays* L. cv “saccharate”), an herbaceous C<sub>4</sub> species with the lowest  $c_m/c_a$  ratio, was grown from seed in 1.6L pots. After at least 7 weeks, the 4<sup>th</sup> or higher leaf number was used for the experiments when fully grown. A section of the leaf at about 1/3 from the tip was used for the experiments.

### 3.6.2. Gas exchange experiments

Gas exchange experiments were performed in an open system with a leaf cuvette that had a window of 7 x 7 cm (Adnew et al., 2020). The air temperature was kept at 20 °C. A fan inside mixed the air thoroughly and kept boundary layer conductance high (19  $\text{mol m}^{-2} \text{s}^{-1}$ ). Leaf temperature was measured with a K type thermocouple. Experiments were performed at two PFD's, the growth PFD of 300  $\mu\text{mol m}^{-2} \text{s}^{-1}$  (LL) and a higher PFD closer to light saturation of 1200  $\mu\text{mol m}^{-2} \text{s}^{-1}$  (HL).

Compressed outside air was passed through soda lime to scrub the CO<sub>2</sub> and pure CO<sub>2</sub> was injected to produce a CO<sub>2</sub> mole fraction of 500  $\mu\text{mol mol}^{-1}$ . Airflow through the cuvette was adjusted to result in a mole fraction in outgoing air of 400  $\mu\text{mol mol}^{-1}$ . The large drawdown of 100  $\mu\text{mol mol}^{-1}$  was necessary to produce a sufficiently large isotope signal. The air was humidified and kept at a specified dewpoint by leading it through a temperature-controlled column. H<sub>2</sub>O partial pressure was adjusted to the transpiration rate of the leaf, which kept the VPD in the cuvette within boundaries (0.4 to 1 kPa). The CO<sub>2</sub> mole fraction of air entering and leaving the cuvette was measured with an infrared gas analyzer in absolute mode (IRGA, model LI-6262, LI-COR Inc., Nebraska, USA). The mole fraction and isotopic composition of water vapor were measured with a triple water vapor isotope analyzer (WVIA, model 911-0034, Los Gatos Research, USA).

Two types of CO<sub>2</sub> were used, “normal” CO<sub>2</sub> (Air Products, Germany) and <sup>17</sup>O-enriched CO<sub>2</sub>. The latter was prepared by photolyzing the mixture of CO<sub>2</sub> and O<sub>2</sub> with UV (Adnew et al.,

2019). The  $\delta^{18}\text{O}$  of the  $\text{CO}_2$  entering the cuvette was 30.485 ‰. The  $\delta^{13}\text{C}$  of the  $\text{CO}_2$  ranged from -10.23 ‰ to -3.27 ‰. For “normal  $\text{CO}_2$ ”,  $\Delta^{17}\text{O}_\text{e} = -0.333$  ‰ for all experiments and plant types. Enriched  $\text{CO}_2$  had  $\Delta^{17}\text{O}_\text{e} = 0.22$  ‰ for the experiments with sunflower and maize and  $\Delta^{17}\text{O}_\text{e} = 0.34$  ‰ for ivy.

Measurements started after the leaf had reached steady state in terms of the rates of  $\text{CO}_2$  uptake and transpiration, and the  $\delta\text{D}$  and  $\delta^{18}\text{O}$  of water vapor leaving the cuvette. Gas exchange variables were recorded and subsequently the air was collected in three 2L glass flask after passing through a  $\text{Mg}(\text{ClO}_4)_2$  dryer. Leaf area was measured with a LI-3100C area meter (LI-COR, Inc. USA) and the leaf was placed in a closed glass vial and kept in a freezer at -20 °C until leaf water extraction. Leaf water was extracted by cryogenic vacuum distillation for 4 h at 60 °C following a well-established procedure (Landais et al., 2006). The  $\delta^{17}\text{O}$  and  $\delta^{18}\text{O}$  of leaf water was determined at the Laboratoire des Sciences du Climat et de l’Environnement using a fluorination technique.

### 3.6.3. Carbon dioxide extraction and isotope analysis

$\text{CO}_2$  was extracted from the air samples cryogenically in a system made from electropolished stainless steel. Our system used four commercial traps (MassTech, Bremen, Germany). The first two traps were operated at dry ice temperature (-78 °C) to remove moisture and some organics. The other two traps were operated at liquid nitrogen temperature (-196 °C) to trap  $\text{CO}_2$ . The extracted  $\text{CO}_2$  was first measured for  $\delta^{13}\text{C}$  and  $\delta^{18}\text{O}$  with a Delta<sup>Plus</sup>XL isotope ratio mass spectrometer (IRMS) (Thermo Finnigan, Germany) in dual inlet mode. After the isotope measurement, the remaining gas in the bellow of the IRMS is frozen back into the break seal tube for the measurement of  $\Delta^{17}\text{O}$ . The  $\Delta^{17}\text{O}$  of  $\text{CO}_2$  is determined using the  $\text{CO}_2$ - $\text{O}_2$  exchange method (Adnew et al., 2019; Barkan et al., 2015). A detailed description of the  $\text{CO}_2$ - $\text{O}_2$  exchange system at Utrecht University is given in (Adnew et al., 2019). Equal amounts of  $\text{CO}_2$  and  $\text{O}_2$  are mixed in a quartz reactor containing a platinum sponge catalyst at the bottom and heated at 750 °C for 2hrs. After isotope equilibration, the  $\text{CO}_2$  is trapped at liquid nitrogen temperature, while the  $\text{O}_2$  is collected with 1 pellet of 5Å molecular sieve (1.6 mm, Sigma Aldrich, USA) at liquid nitrogen temperature. The isotopic composition of the isotopically equilibrated  $\text{O}_2$  is measured with a Delta<sup>Plus</sup>XL isotope ratio mass spectrometer in dual inlet mode with reference to a pure  $\text{O}_2$  working gas that has been assigned values of  $\delta^{17}\text{O} = 9.254$  ‰ and  $\delta^{18}\text{O} = 18.542$  ‰ by measurements of multiple aliquots by E. Barkan at the Hebrew University of Jerusalem.

### 3.6.4. Monte Carlo simulation and leaf cuvette model

In our simple leaf cuvette model, the leaf is partitioned into three different reservoirs: the intercellular air space, the mesophyll cell and the chloroplast (Adnew et al., 2020). For this model we assumed an infinity boundary layer conductance. In the leaf model, we used a 100 ppm drawdown of  $\text{CO}_2$  similar to the photosynthesis experiments. The assimilation rate is set to  $20.0 \mu\text{mol m}^{-2}\text{s}^{-1}$ . The leaf area and flowrate of air are assumed to be  $30 \text{ cm}^2$  and  $0.7 \text{ L min}^{-1}$ , respectively. The isotope composition of leaf water at the site where the  $\text{H}_2\text{O}$ - $\text{CO}_2$  exchange occurs is 5.39 ‰ and 10.648 ‰ in  $\delta^{17}\text{O}$  and  $\delta^{18}\text{O}$ , respectively which is the mean value of  $\delta^{17}\text{O}$  and  $\delta^{18}\text{O}$  value of bulk leaf water measured for sunflower, ivy and maize. The  $\delta^{18}\text{O}$  of the  $\text{CO}_2$

entering the cuvette is 30.47 ‰, similar to the  $\delta^{18}\text{O}$  value of the  $\text{CO}_2$  used in the experiments (normal  $\text{CO}_2$  experiments). The detailed explanation of the leaf cuvette model is reported elsewhere (Adnew et al., 2020) and the model can be found at [https://git.wur.nl/leaf\\_model/D17O](https://git.wur.nl/leaf_model/D17O).

To investigate the dependency of  $g_m$  estimates on the measurement error at different values  $\Delta^{17}\text{O}_i - \Delta^{17}\text{O}_m$ , we first calculated an isotopic steady state (i.e. mole fractions and  $\delta$  values in each of the compartments) for a leaf cuvette experiment using the leaf cuvette model described above.  $\Delta^{17}\text{O}$  of  $\text{CO}_2$  entering the cuvette ( $\Delta^{17}\text{O}_e$ ) was set to 0.2 ‰, 1 ‰, 5 ‰, 10 ‰, which resulted in  $\Delta^{17}\text{O}_i - \Delta^{17}\text{O}_m$  differences of -0.3 ‰, -0.5 ‰, -1.6 ‰ and -3 ‰, respectively (Figure 3.5) to evaluate the sensitivity of  $g_{m\Delta 17}$  on the measurement error depending on  $\Delta^{17}\text{O}_i - \Delta^{17}\text{O}_m$  differences.

After having calculated the isotopic equilibrium state for the different assumptions, we assigned realistic measurement errors of 0.03 ‰ and 0.016 ‰, respectively, to the  $\delta^{17}\text{O}$  and  $\delta^{18}\text{O}$  of  $\text{CO}_2$  in the different compartments (1 sigma standard deviation of the mean). For the water isotopes, the error is assumed to be 0.1 ‰ and 0.05 ‰ for  $\delta^{17}\text{O}$  and  $\delta^{18}\text{O}$  respectively. The errors we used for  $\Delta^{17}\text{O}$  is propagated from the error of  $\delta^{17}\text{O}$  and  $\delta^{18}\text{O}$  measurement errors. For instance, the  $\Delta^{17}\text{O}$  error propagated from  $\delta^{17}\text{O}$  and  $\delta^{18}\text{O}$  of  $\text{CO}_2$  is 0.031 ‰, our measurement precision for  $\Delta^{17}\text{O}$  is better than 0.01 ‰. We then performed a Monte Carlo simulation by sampling  $\delta^{17}\text{O}$  and  $\delta^{18}\text{O}$  values with realistic error distributions 100,000 times and calculated the resulting  $g_m$  according to equation 3.9. These calculations are similar to the ones performed by (Holloway-Phillips et al., 2019) for  $\delta^{18}\text{O}$ .

## Acknowledgments

This work was funded by the EU ERC project ASICA. The authors thank Leonard I. Wassenaar and Stefan Terzer-Wassmuth from the International Atomic and Energy Agency, Vienna for supplying water standards. The authors thank Eugeni Barkan and Rolf Vieten from the Hebrew University of Jerusalem for calibration of our  $\text{O}_2$  and  $\text{CO}_2$  working gases. We are grateful to Amaelle Landais from the Laboratoire des Sciences Du Climat et de l'Environnement Université Paris-Saclay for measuring the  $\Delta^{17}\text{O}$  of leaf water samples for our study.

### 3.7. Supplementary material

#### 3.7.1. Mesophyll conductance calculation using $\Delta_A^{13}\text{C}$

Mesophyll conductance ( $g_{m13}$ ) is the conductance through the intercellular air spaces, the cell wall, the plasmalemma, chloroplast envelope, cytosol, and stroma to the carboxylation site for the  $\text{C}_3$  plants (Flexas et al., 2008; Flexas et al., 2012).  $g_{m13}$  is calculated as a difference between observed discrimination ( $\Delta_A^{13}\text{C}_{\text{obs}}$ ) and the discrimination by assuming infinite mesophyll conductance (no mesophyll resistance) ( $\Delta_A^{13}\text{C}_i$ ).

$$g_{m13} = \left( \frac{1 + t^{13}}{1 - t^{13}} \right) \left( \frac{A(b - a_m - \frac{\alpha_b}{\alpha_e} e \frac{R_d}{R_d + A})}{(\Delta_A^{13}\text{C}_i - \Delta_A^{13}\text{C}_{\text{obs}})Pc_a} \right) \quad (\text{S3.1})$$

where  $t^{13}$  is a ternary correction factor,  $b$  the fractionation due to uptake by Rubisco, and  $a_m$  the sum of the fractionations associated with  $^{13}\text{CO}_2$  dissolution in and diffusion through water, respectively.  $e$ ,  $R_d$ ,  $\alpha_e$ ,  $\alpha_b$  and  $P$  are the fractionations during day respiration (decarboxylation), the day respiration rate, the fractionation factor for day respiration with respect to net assimilation, the fractionation factor for  $\text{C}_3$  carboxylation, and the pressure of the air surrounding the leaf, respectively. A detailed description of the equations, best-fit parameters and definitions of discrimination factors is given in Table S3.1. It is assumed that all respired and photo- respired  $\text{CO}_2$  diffuses into the chloroplasts (i.e., no diffusion of respired and photo-respired  $\text{CO}_2$  directly through the cytosol and plasma membrane without first diffusing through the chloroplasts) (Ubierna et al., 2019).

#### 3.7.2. Mesophyll conductance calculation using $\Delta_A^{18}\text{O}$

$g_{m18}$  ( $\text{mol m}^{-2}\text{s}^{-1}\text{bar}^{-1}$ ), can be derived from measurements of  $\delta^{18}\text{O}$  using equation S3.2 with the assumption that the degree of equilibration between  $\text{CO}_2$  and  $\text{H}_2\text{O}$  is 100 % and that the oxygen isotopic composition of leaf water at the  $\text{CO}_2\text{-H}_2\text{O}$  exchange site is the same as the leaf water at the evaporation site (Farquhar et al., 1993; Barbour et al., 2016; Cernusak et al., 2004), as shown in equation 1 of Holloway-Phillips et al. (2019).

$$g_{m18} = \frac{A_n/P}{c_i - c_{m,18}\text{O}} = \frac{A_n/P}{c_i} \frac{\delta^{18}\text{O}_A \alpha_{18w} + a_{18w} - \delta^{18}\text{O}_m}{\delta^{18}\text{O}_i - \delta^{18}\text{O}_m} \quad (\text{S3.2})$$

where  $A_n$  ( $\text{mol m}^{-2}\text{s}^{-1}$ ) is the assimilation rate,  $c_i$  and  $c_{m,18}\text{O}$  ( $\text{mol mol}^{-1}$ ) are the  $\text{CO}_2$  mole fractions in the intercellular air space and in the mesophyll (derived using  $\delta^{18}\text{O}$ ) and  $P$  (bar) is the total atmospheric pressure.  $\delta^{18}\text{O}_i$  is  $\delta^{18}\text{O}$  of  $\text{CO}_2$  in the intercellular airspace,  $\alpha_{18w}$  is the fractionation factor for  $^{12}\text{C}^{18}\text{O}^{16}\text{O}$  during diffusion and dissolution in water,  $a_{18w}$  is the discrimination in  $^{12}\text{C}^{18}\text{O}^{16}\text{O}$  during diffusion and dissolution in water,  $a_{18w} = \alpha_{18w} + 1$  (Farquhar and Cernusak, 2012),  $\delta^{18}\text{O}_A$  is  $\delta^{18}\text{O}$  of the assimilated  $\text{CO}_2$  and  $\delta^{18}\text{O}_m$  is the  $\delta^{18}\text{O}$  of  $\text{CO}_2$  in equilibrium with leaf water at the  $\text{CO}_2\text{-H}_2\text{O}$  exchange site.  $\delta^{18}\text{O} = (^{18}\text{R}_{\text{sample}} - ^{18}\text{R}_{\text{standard}}) / ^{18}\text{R}_{\text{standard}}$ , where  $^{18}\text{R} = ^{18}\text{O} / ^{16}\text{O}$ .



The CO<sub>2</sub> mole fraction at the site of CO<sub>2</sub>-H<sub>2</sub>O exchange can be calculated from  $\delta^{18}\text{O}$  of CO<sub>2</sub> following (Farquhar and Cernusak, 2012; Osborn et al., 2017; Barbour et al., 2016; Cernusak et al., 2004) as:

$$c_{m18} = c_i \left( \frac{\delta^{18}\text{O}_i - a_{18w} - \delta^{18}\text{O}_A(1 + a_{18w})}{\delta^{18}\text{O}_m - a_{18w} - \delta^{18}\text{O}_A(1 + a_{18w})} \right) \quad (\text{S3.3})$$

Assuming that the isotopic composition of leaf water at the CO<sub>2</sub>-H<sub>2</sub>O exchange site is the same as the  $\delta^{18}\text{O}$  of leaf water at the evaporating site,  $\delta^{18}\text{O}_m$  can be calculated as:

$$\delta^{18}\text{O}_m = (\delta^{18}\text{O}_{\text{wes}} + 1) \times (1 + \epsilon_w^{18}) - 1 \quad (\text{S3.4})$$

where  $\delta^{18}\text{O}_{\text{wes}}$  is the  $\delta^{18}\text{O}$  of H<sub>2</sub>O in at the site of evaporation and  $\epsilon_w^{18}$  is the equilibrium fractionation between CO<sub>2</sub> and water (See Table S3.1). The  $\delta^{18}\text{O}_{\text{wes}}$  is calculated using the modified Craig and Gordon model (Farquhar et al., 1989b; Flanagan et al., 1991; Harwood et al., 1998; Farquhar and Lloyd, 1993) as:

$$\delta^{18}\text{O}_{\text{wes}} = \delta^{18}\text{O}_{\text{trans}} + \epsilon_k^{18} + \epsilon_{\text{equ}}^{18} + \frac{w_a}{w_i} (\delta^{18}\text{O}_{\text{wa}} - \epsilon_k^{18} + \delta^{18}\text{O}_{\text{trans}}) \quad (\text{S3.5})$$

where  $w_i$  and  $w_o$  are the mole fraction of water vapor in the intercellular air spaces and in the air leaving the cuvette, respectively.  $\epsilon_k^{18}$  and  $\epsilon_{\text{equ}}^{18}$  are the kinetic fractionation of for diffusion of water vapor in air and the equilibrium fractionation between liquid and gas-phase water, respectively. See Table S3.1 for a list of symbols.

### 3.7.3. Derivation of $g_m$ from $\Delta^{17}\text{O}$ of CO<sub>2</sub> measurement

The  $\delta^{18}\text{O}$  of CO<sub>2</sub> at the CO<sub>2</sub>-H<sub>2</sub>O exchange site ( $\delta^{18}\text{O}_m$ ) can be calculated as described in (Farquhar and Cernusak, 2012; Cernusak et al., 2004) as:

$$\delta^{18}\text{O}_m = \delta^{18}\text{O}_A \left( 1 - \frac{c_i}{c_m} \right) \alpha^{18}_w + \frac{c_i}{c_m} (\delta^{18}\text{O}_i - a^{18}_w) + a^{18}_w \quad (\text{S3.6})$$

Analogous to  $\delta^{18}\text{O}$ ,  $\delta^{17}\text{O}$  of CO<sub>2</sub> at the CO<sub>2</sub>-H<sub>2</sub>O exchange site can be calculated as:

$$\delta^{17}\text{O}_m = \delta^{17}\text{O}_A \left( 1 - \frac{c_i}{c_m} \right) \alpha^{17}_w + \frac{c_i}{c_m} (\delta^{17}\text{O}_i - a^{17}_w) + a^{17}_w \quad (\text{S3.7})$$

The  $\Delta^{17}\text{O}$  of CO<sub>2</sub> at the CO<sub>2</sub>-H<sub>2</sub>O exchange site can be calculated as:

$$\Delta^{17}\text{O}_m = \delta^{17}\text{O}_m - \lambda \delta^{18}\text{O}_m \quad (\text{S3.8})$$

Substituting equation S3.6 and S3.7 in equation S3.8:

$$\Delta^{17}\text{O}_m = \delta^{17}\text{O}_A \left(1 - \frac{c_i}{c_m}\right) \alpha^{17}_w + \frac{c_i}{c_m} (\delta^{17}\text{O}_i - a^{17}_w) + a^{17}_w \quad (\text{S3.9})$$

$$- \lambda \left[ \delta^{18}\text{O}_A \left(1 - \frac{c_i}{c_m}\right) \alpha^{18}_w + \frac{c_i}{c_m} (\delta^{18}\text{O}_i - a^{18}_w) + a^{18}_w \right]$$

$$\Delta^{17}\text{O}_m = \delta^{17}\text{O}_A \alpha^{17}_w - \frac{c_i}{c_m} \delta^{17}\text{O}_A \alpha^{17}_w + \frac{c_i}{c_m} \delta^{17}\text{O}_i - \frac{c_i}{c_m} a^{17}_w + a^{17}_w \quad (\text{S3.10})$$

$$- \left[ \lambda \delta^{18}\text{O}_A \alpha^{18}_w - \frac{c_i}{c_m} \delta^{18}\text{O}_A \alpha^{18}_w + \frac{c_i}{c_m} \lambda \delta^{18}\text{O}_i - \frac{c_i}{c_m} \lambda a^{18}_w \right. \\ \left. + \lambda a^{18}_w \right]$$

$$\Delta^{17}\text{O}_m = (\delta^{17}\text{O}_A \alpha^{17}_w - \lambda \delta^{18}\text{O}_A \alpha^{18}_w) + \frac{c_i}{c_m} (\delta^{17}\text{O}_i - \lambda \delta^{18}\text{O}_i) \quad (\text{S3.11})$$

$$- \frac{c_i}{c_m} (\delta^{17}\text{O}_A \alpha^{17}_w - \lambda \delta^{18}\text{O}_A \alpha^{18}_w) - \frac{c_i}{c_m} (a^{17}_w - \lambda a^{18}_w) \\ + (a^{17}_w - \lambda a^{18}_w)$$

$$\Delta^{\#17}\text{O}_A = \delta^{17}\text{O}_A \alpha^{17}_w - \lambda \delta^{18}\text{O}_A \alpha^{18}_w \quad (\text{S3.12})$$

$$\Delta^{*17}\text{O}_w = a^{17}_w - \lambda a^{18}_w \quad (\text{S3.13})$$

Substitute equation S3.12 and S3.13 in equation S3.11

$$\Delta^{17}\text{O}_m = \Delta^{\#17}\text{O}_A + \frac{c_i}{c_m} \Delta^{17}\text{O}_i - \frac{c_i}{c_m} \Delta^{\#17}\text{O}_A - \frac{c_i}{c_m} \Delta^{*17}\text{O}_w + \Delta^{*17}\text{O}_w \quad (\text{S3.14})$$

$$c_m (\Delta^{17}\text{O}_m - \Delta^{\#17}\text{O}_A - \Delta^{*17}\text{O}_w) = c_i (\Delta^{17}\text{O}_i - \Delta^{\#17}\text{O}_A - \Delta^{*17}\text{O}_w) \quad (\text{S3.15})$$

Since the  $c_m$  is calculated from  $\Delta^{17}\text{O}$  measurements we used a subscript  $\Delta^{17}$  ( $c_{m\Delta^{17}}$ ) to differentiate the calculations using  $\delta^{18}\text{O}$ .

$$c_{m\Delta^{17}} = c_i \left[ \frac{\Delta^{17}\text{O}_i - \Delta^{\#17}\text{O}_A - \Delta^{*17}\text{O}_w}{\Delta^{17}\text{O}_m - \Delta^{\#17}\text{O}_A - \Delta^{*17}\text{O}_w} \right] \quad (\text{S3.16})$$

Then  $g_{m\Delta^{17}}$  can be calculated based on  $c_{m\Delta^{17}}$  as:

$$g_{m\Delta^{17}} = \frac{A_n/P}{c_i - c_{m\Delta^{17}}} \quad (\text{S3.17})$$

$$g_{m\Delta^{17}} = \frac{A_n/P}{c_i - c_i \left[ \frac{\Delta^{17}\text{O}_i - \Delta^{\#17}\text{O}_A - \Delta^{*17}\text{O}_w}{\Delta^{17}\text{O}_m - \Delta^{\#17}\text{O}_A - \Delta^{*17}\text{O}_w} \right]} \quad (\text{S3.18})$$

Re-arranging equation S3.18:

$$g_{m\Delta 17} = \frac{A_n/P}{c_i} \frac{1}{1 - \frac{\Delta^{17}O_i - \Delta^{17}O_A - \Delta^{17}O_w}{\Delta^{17}O_m - \Delta^{17}O_A - \Delta^{17}O_w}} \quad (S3.19)$$

$$g_{m\Delta 17} = \frac{A_n/P}{c_i} \frac{\Delta^{17}O_A + \Delta^{17}O_w - \Delta^{17}O_m}{\Delta^{17}O_i - \Delta^{17}O_m} \quad (S3.20)$$

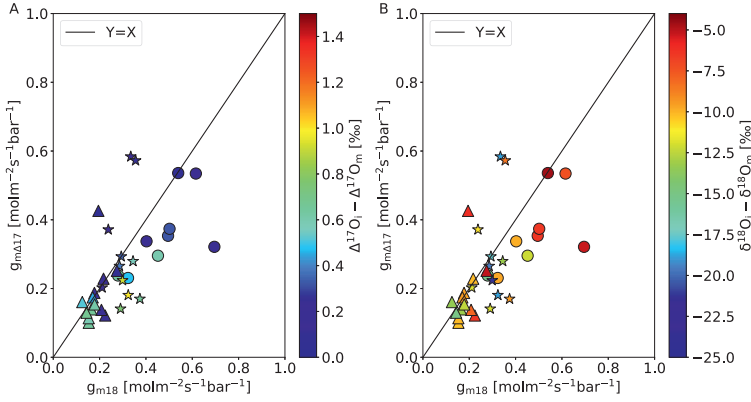


Figure S3.1 Correlation between  $g_m$  estimates using  $\delta^{18}\text{O}$  and  $\Delta^{17}\text{O}$  measurements for sunflower (circles), ivy (triangles) and maize (star). In (A) and (B) the color bar is for  $\Delta^{17}\text{O}_i - \Delta^{17}\text{O}_m$  and  $\delta^{18}\text{O}_i - \delta^{18}\text{O}_m$ , respectively.

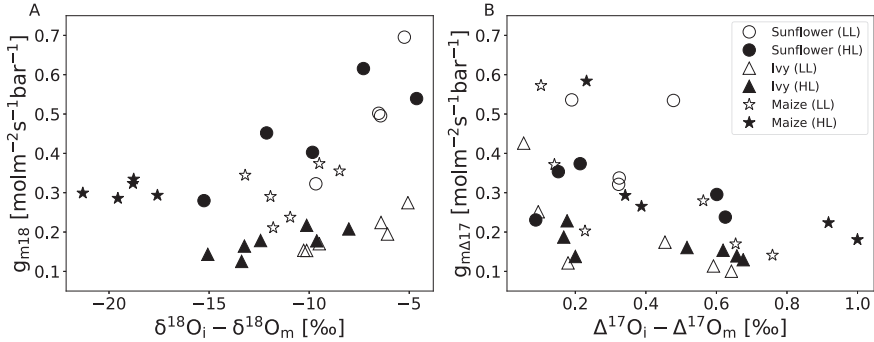


Figure S3.2  $g_m$  estimates using  $\delta^{18}\text{O}$  measurement (A) and  $\Delta^{17}\text{O}$  measurement (B) for sunflower, ivy and maize as a function of the difference in the oxygen isotope composition between the intercellular air space and the  $\text{CO}_2$ - $\text{H}_2\text{O}$  exchange site for low and high PFDs.

Table S3.1 List of variables and equations used in this study to calculate gas exchange parameters and carbon and oxygen three-isotope discriminations.

| Symbol                                   | Description   | Unit/calculation/value   |
|--|---|--|
| <b>Gas exchange</b>                      |   |  |
| $A_n$                                    | Rate of CO <sub>2</sub> assimilation  | $\frac{u_e}{s} \left( c_e - c_a \left( \frac{1-w_e}{1-w_a} \right) \right)$ , mol m <sup>-2</sup> s <sup>-2</sup>                    |
| $E$                                      | Transpiration rate  | $\frac{u_e}{s} \left( \frac{w_a - w_e}{1 - w_a} \right)$ , mol m <sup>-2</sup> s <sup>-2</sup>                                       |
| $w_i$                                    | Mole fraction of water vapour inside a leaf   | $\frac{613.65 \times e^{\left( \frac{17.502 \times T_{leaf}}{240.97 + T_{leaf}} \right)}}{P} \times 10^{-5}$ , mol mol <sup>-1</sup> |
| $w_a$                                    | Mole fraction of water vapour leaving the cuvette /leaf surrounding   | mol mol <sup>-1</sup>  |
| $w_e$                                    | Mole fraction of water vapour entering the cuvette  | mol mol <sup>-1</sup>  |
| $c_e$                                    | Mole fraction of CO <sub>2</sub> entering the cuvette   | mol mol <sup>-1</sup>  |
| $c_a$                                    | Mole fraction of CO <sub>2</sub> in the leaf surrounding/ leaving the cuvette   | mol mol <sup>-1</sup>  |
| $u_e$                                    | Flow rate of air entering the cuvette   | mol s <sup>-1</sup>  |
| $s$                                      | The surface area of the leaf inside the cuvette   | m <sup>2</sup>   |
| $P$                                      | Atmospheric pressure  | bar  |
| $T_{leaf}$                               | Leaf temperature  | °C   |
| $g_{s(H_2O)}$                            | Stomatal conductance for water vapour   | $\frac{g_{H_2O} \times g_b(H_2O)}{g_b(H_2O) + g_{H_2O}}$   |
| $g_{b(H_2O)}$                            | Boundary layer conductance for water vapour   | Calibrated for the cuvette we used   |
| $g_{sH_2O}^*$                            | Conductance for water vapor through the boundary layer and stomata  | $E \left( \frac{1 - \left( \frac{w_i + w_a}{2} \right)}{w_i - w_a} \right)$ , mol m <sup>-2</sup> s <sup>-1</sup>                    |
| $g_s$                                    | Stomatal conductance for CO <sub>2</sub>  | $\frac{g_s(H_2O)}{1.6}$  |
| $g_b$                                    | Boundary conductance for CO <sub>2</sub>  | $\frac{g_b(H_2O)}{1.37}$   |
| $g_{CO_2}^*$                             | Conductance for CO <sub>2</sub> through the boundary layer and stomata  | $\frac{g_s \times g_b}{g_s + g_b}$   |
| $\Gamma^*$                               | CO <sub>2</sub> compensation point  | 45 μmol m <sup>-2</sup> s <sup>-1</sup>  |
| $g_{m13}$                                | CO <sub>2</sub> conductance from intercellular air space to the site of carboxylation calculated using Δ <sub>13</sub> C (for C <sub>3</sub> plants only)     | mol m <sup>-2</sup> s <sup>-1</sup> bar <sup>-1</sup>  |
| $g_{m18}$                                | CO <sub>2</sub> conductance from intercellular air space to CO <sub>2</sub> -H <sub>2</sub> O exchange site calculated using Δ <sub>18</sub> O                | mol m <sup>-2</sup> s <sup>-1</sup> bar <sup>-1</sup>  |
| $g_{m17}$                                | CO <sub>2</sub> conductance from intercellular air space to CO <sub>2</sub> -H <sub>2</sub> O exchange site calculated using Δ <sub>17</sub> O                | mol m <sup>-2</sup> s <sup>-1</sup> bar <sup>-1</sup>  |
| $g_{m\Delta 17}$                         | CO <sub>2</sub> conductance from intercellular air space to CO <sub>2</sub> -H <sub>2</sub> O exchange site calculated using Δ <sub>4</sub> Δ <sub>17</sub> O | mol m <sup>-2</sup> s <sup>-1</sup> bar <sup>-1</sup>  |
| $c_i$                                    | Mole fraction of CO <sub>2</sub> in the intercellular air space   | $\left( \frac{g_{CO_2}^* - \Gamma}{g_{CO_2}^* + \Gamma} \right) c_a - A_n$ , mol mol <sup>-1</sup>                                   |
| $c_s$                                    | Mole fraction of CO <sub>2</sub> at the leaf surface  | $c_a - \frac{A_n}{g_b}$ , mol mol <sup>-1</sup>  |
| $c_m$                                    | Mole fraction of CO <sub>2</sub> at the site of CO <sub>2</sub> -H <sub>2</sub> O exchange  | mol mol <sup>-1</sup>  |
| $c_c$                                    | Mesophyll conductance to the chloroplast (for C <sub>3</sub> plants)  | $c_i - \frac{A_n}{g_{m13}}$ , mol mol <sup>-1</sup>  |
| $l^{13}$                                 | Ternary correction for <sup>13</sup> CO <sub>2</sub>  | $\frac{(1 + a_{13bs})E}{2g_{CO_2}^*}$  |
| $l^{18}$                                 | Ternary correction for <sup>18</sup> CO <sub>2</sub>  | $\frac{(1 + a_{18bs})E}{2g_{CO_2}^*}$  |
| $l^{17}$                                 | Ternary correction for <sup>17</sup> CO <sub>2</sub>  | $\frac{(1 + a_{17bs})E}{2g_{CO_2}^*}$  |
| $R_D$                                    | Dark respiration rate   | 0.8 μmol m <sup>-2</sup> s <sup>-1</sup>   |
| $R_L$                                    | Day respiration rate  | 0.5 × R <sub>D</sub> μmol m <sup>-2</sup> s <sup>-1</sup>  |
| <b>Oxygen and carbon isotope effects</b> |   |  |
| $\epsilon_k^{18}$                        | Kinetic fractionation of water vapour in the air  | $\frac{28g_b + 19g_s}{g_b + g_s}$ , ‰  |
| $\epsilon^{18}_{equ}$                    | Equilibrium fractionation between liquid and gas phase of water vapor   | $2.644 - 3.206 \left( \frac{10^3}{T_{leaf}} \right) + 1.534 \left( \frac{10^6}{T_{leaf}^2} \right)$ , ‰                              |
| $a_{13bs}$                               | Weighted fractionation for <sup>13</sup> CO <sub>2</sub> as CO <sub>2</sub> diffuses through the boundary layer and stomata                                   | $\frac{(c_s - c_i)a_{13s} + (c_a - c_s)a_{13b}}{c_a - c_i}$ , ‰  |
| $a_{17bs}$                               | Weighted fractionation for <sup>17</sup> CO <sub>2</sub> as CO <sub>2</sub> diffuses through the boundary layer and stomata                                   | $\frac{(c_s - c_i)a_{17s} + (c_a - c_s)a_{17b}}{c_a - c_i}$ , ‰  |
| $a_{18bs}$                               | Weighted fractionation for <sup>18</sup> CO <sub>2</sub> as CO <sub>2</sub> diffuses through the boundary layer and stomata                                   | $\frac{(c_s - c_i)a_{18s} + (c_a - c_s)a_{18b}}{c_a - c_i}$ , ‰  |

|                                   |  |  |
|-----------------------------------|--|--|
| $a_{13bs}$                        | Weighted fractionation for $^{13}\text{COO}$ as $\text{CO}_2$ diffuses through the boundary layer and stomata                    | $\frac{(c_a - c_i)a_{13s} + (c_a - c_s)a_{13b}}{c_a - c_i}$ , ‰  |
| $a_{18bs}$                        | Weighted fractionation for $\text{C}^{18}\text{OO}$ as $\text{CO}_2$ diffuses through the boundary layer and stomata             | $\frac{(c_a - c_i)a_{18s} + (c_a - c_s)a_{18b}}{c_a - c_i}$ , ‰  |
| $a_{17bs}$                        | Weighted fractionation for $\text{C}^{17}\text{OO}$ as $\text{CO}_2$ diffuses through the boundary layer and stomata             | $\frac{(c_a - c_i)a_{17s} + (c_a - c_s)a_{17b}}{c_a - c_i}$ , ‰  |
| $\bar{a}_{17}$                    | Weighted fractionation of $\text{C}^{17}\text{OO}$ as it diffuses through the boundary layer, stomata and liquid phase in series | $\frac{(c_i - c_m)a_{17w} + (c_s - c_i)a_{17s} + (c_a - c_s)a_{17b}}{c_a - c_m}$ , ‰   |
| $\bar{a}_{18}$                    | Weighted fractionation of $\text{C}^{18}\text{OO}$ as it diffuses through the boundary layer, stomata and liquid phase in series | $\frac{(c_i - c_m)a_{18w} + (c_s - c_i)a_{18s} + (c_a - c_s)a_{18b}}{c_a - c_m}$ , ‰   |
| $a_{13b}$                         | Fractionation in $^{13}\text{CO}_2$ as $\text{CO}_2$ diffuses through the boundary layer   | 2.9 ‰  |
| $a_{13s}$                         | Fractionation in $^{13}\text{CO}_2$ as $\text{CO}_2$ diffuses through the stomata  | 4.4 ‰  |
| $a_m$                             | Fractionation factor for dissolution and diffusion through water   | 1.8 ‰  |
| $f$                               | Fractionation factor for photorespiration (decarboxylation of glycine)   | 16 ‰   |
| $e$                               | Fractionation factor for day respiration   | $R_p + e^*$ , ‰  |
| $e^*$                             | Apparent fractionation for day respiration   | $\delta^{13}C_a - \Delta_p^{13}C - \delta^{13}C_{\text{substrate}}$ , ‰  |
| $b$                               | Fractionation factor for uptake by RubisCO   | 29 ‰   |
| $\alpha_f$                        | Fractionation due to photorespiration (decarboxylation of glycine)   | $1+f$  |
| $\alpha_e$                        | Fractionation due to day respiration   | $1+e$  |
| $\alpha_b$                        | Fractionation due to uptake by RubisCO   | $1+b$  |
| $a_{17b}$                         | Fractionation of $\text{C}^{17}\text{OO}$ as $\text{CO}_2$ diffuses through the boundary layer                                   | 2.9 ‰  |
| $a_{17s}$                         | Fractionation in $\text{C}^{17}\text{OO}$ as $\text{CO}_2$ diffuses through stomata  | 4.4 ‰  |
| $a_{18b}$                         | Fractionation of $\text{C}^{18}\text{OO}$ as $\text{CO}_2$ diffuses through the boundary layer                                   | 5.8 ‰  |
| $a_{18s}$                         | Fractionation in $\text{C}^{18}\text{OO}$ as $\text{CO}_2$ diffuses through stomata  | 8.8 ‰  |
| $a_{17w}$                         | Fractionation in $\text{C}^{17}\text{OO}$ due to diffusion and dissolution in water  | 0.382 ‰  |
| $a_{18w}$                         | Fractionation in $\text{C}^{18}\text{OO}$ due to diffusion and dissolution in water  | 0.8 ‰  |
| $\varepsilon^{18}W$               | Equilibrium fractionation of $\text{CO}_2$ and water for $\text{C}^{18}\text{OO}$  | $\frac{17604}{T_{\text{leaf}}} - 17.93$ , ‰  |
| $\varepsilon^{18}_k$              | kinetic fractionation of water vapor in air  | $\frac{28 \times g_b + 19 \times g_s}{g_b + g_s}$ , ‰  |
| $\varepsilon^{18}_{\text{equ}}$   | equilibrium fractionation between the liquid and gas phase water   | $2.644 - 3.206 \times (\frac{10^3}{T}) + 1.534 \times (\frac{10^6}{T})$ , ‰  |
| <b>Isotopic composition</b>       |  |  |
| $\delta^{17}O_A$                  | $\delta^{17}\text{O}$ of the assimilated $\text{CO}_2$   | $\frac{\delta^{17}O_a - \Delta_A^{17}O}{\Delta_A^{17}O + 1} = \delta^{17}O_a - \frac{c_e}{c_a - c_a} (\delta^{17}O_a - \delta^{17}O_e)$ , ‰  |
| $\delta^{18}O_A$                  | $\delta^{18}\text{O}$ of the assimilated $\text{CO}_2$   | $\frac{\delta^{18}O_a - \Delta_A^{18}O}{\Delta_A^{18}O + 1} = \delta^{18}O_a - \frac{c_e}{c_a - c_a} (\delta^{18}O_a - \delta^{18}O_e)$ , ‰  |
| $\delta^{17}O_{io}$               | $\delta^{17}\text{O}$ of $\text{CO}_2$ in the intercellular air space ignoring ternary correction                                | $\delta^{17}O_a \left(1 - \frac{c_a}{c_i}\right) (1 + a_{17bs}) + \frac{c_a}{c_i} (\delta^{17}O_a - a_{17bs}) + a_{17bs}$ , ‰  |
| $\delta^{18}O_{io}$               | $\delta^{18}\text{O}$ of $\text{CO}_2$ in the intercellular air space ignoring ternary correction                                | $\delta^{18}O_a \left(1 - \frac{c_a}{c_i}\right) (1 + a_{18bs}) + \frac{c_a}{c_i} (\delta^{18}O_a - a_{18bs}) + a_{18bs}$ , ‰  |
| $\delta^{17}O_i$                  | $\delta^{17}\text{O}$ of $\text{CO}_2$ in the intercellular air space  | $\frac{\delta^{17}O_{io} + t^{17}(\delta^{17}O_A(\frac{c_a}{c_i} + 1) - \delta^{17}O_{eq})}{1 + t^{17}}$ , ‰   |
| $\delta^{18}O_i$                  | $\delta^{18}\text{O}$ of $\text{CO}_2$ in the intercellular air space  | $\frac{\delta^{18}O_{io} + t^{18}(\delta^{18}O_A(\frac{c_a}{c_i} + 1) - \delta^{18}O_{eq})}{1 + t^{18}}$ , ‰   |
| $\delta^{18}O_{\text{trans}}$     | $\delta^{18}\text{O}$ of transpired water vapour   | $\left(\frac{w_a}{w_a - w_e}\right) (\delta^{18}O_{wa} - \delta^{18}O_{we}) + \delta^{18}O_{we}$ , ‰   |
| $\delta^{18}O_{\text{wes}}$       | $\delta^{18}\text{O}$ of water at the evaporation site   | $\delta^{18}O_{\text{wes}} = \delta^{18}O_{\text{trans}} + \varepsilon^{18}_k + \varepsilon^{18}_{\text{equ}} + \frac{w_a}{w_i} \times (\delta^{18}O_{wa} - \varepsilon^{18}_k + \delta^{18}O_{\text{trans}})$ , ‰ |
| $\delta^{17}O_m$                  | $\delta^{17}\text{O}$ of $\text{CO}_2$ at the site of $\text{CO}_2\text{-H}_2\text{O}$ exchange                                  | $(\delta^{17}O_{\text{wes}} + 1) \times (1 + \varepsilon^{17}_w) - 1$ , ‰  |
| $\delta^{18}O_m$                  | $\delta^{18}\text{O}$ of $\text{CO}_2$ at the site of $\text{CO}_2\text{-H}_2\text{O}$ exchange                                  | $(\delta^{18}O_{\text{wes}} + 1) \times (1 + \varepsilon^{18}_w) - 1$ , ‰  |
| $\delta^{13}C_{\text{substrate}}$ | Isotope ( $^{13}\text{C}$ ) ratio of substrate used for dark respiration   | $\frac{\delta^{13}C_a - \Delta_A^{13}C}{\Delta_A^{13}C + 1}$ , ‰   |

|                     |  |  |
|---------------------|--|--|
| $A_A^{13}C$         | $^{13}C$ -photosynthetic discrimination  | $\frac{\zeta(\delta^{13}C_a - \delta^{13}C_e)}{1 + \delta^{13}C_a - \zeta(\delta^{13}C_a - \delta^{13}C_e)}, \text{‰}$   |
| $A_A^{13}C_{obs}$   | $^{13}C$ -photosynthetic discrimination (Farquhar model)   | $\left(\frac{1}{1-t}\right) \left[ a_{13bs} \frac{c_a - c_i}{c_a} \right] + \left(\frac{1+t}{1-t}\right) \left[ a_m \frac{c_i - c_e}{c_a} + b \frac{c_e}{c_a} - \frac{\alpha_b}{\alpha_e} e \frac{R_D}{R_D + A} \frac{c_e - \Gamma^*}{c_a} - \frac{\alpha_b}{\alpha_f} f \frac{\Gamma^*}{c_a} \right], \text{‰}$ |
| $A_A^{13}C_i$       | $^{13}C$ -photosynthetic discrimination (assuming no mesophyll conductance, i.e. $c_i = c_e$ )                               | $\left(\frac{1}{1-t}\right) \left[ a \frac{c_a - c_i}{c_a} \right] + \left(\frac{1+t}{1-t}\right) \left[ b \frac{c_i}{c_a} - \frac{\alpha_b}{\alpha_e} e \frac{R_D}{R_D + A} \frac{c_i - \Gamma^*}{c_a} - \frac{\alpha_b}{\alpha_f} f \frac{\Gamma^*}{c_a} \right], \text{‰}$                                    |
| $A_A^{18}O$         | $^{18}O$ -photosynthetic discrimination  | Equation 3.11, ‰   |
| $A_A^{17}O$         | $^{17}O$ -photosynthetic discrimination  | $\frac{\zeta(\delta^{17}O_a - \delta^{17}O_e)}{1 + \delta^{17}O_a - \zeta(\delta^{17}O_a - \delta^{17}O_e)}, \text{‰}$   |
| $A_A^{17}O_{FM}$    | Farquhar model for $^{17}O$ -photosynthetic discrimination   | $\frac{\bar{a}_{17} + \frac{c_m - \delta^{17}O_{ma}}{a - c_m}}{1 - \frac{c_m}{a} - \delta^{17}O_{ma}}, \text{‰}$   |
| $A_A^{18}O_{FM}$    | Farquhar model for $^{18}O$ -photosynthetic discrimination   | $\frac{\bar{a}_{18} + \frac{c_m - \delta^{18}O_{ma}}{a - c_m}}{1 - \frac{c_m}{a} - \delta^{18}O_{ma}}, \text{‰}$   |
| $\delta^{17}O_e$    | $\delta^{17}O$ of $CO_2$ entering the cuvette  | Measured, ‰  |
| $\delta^{17}O_a$    | $\delta^{17}O$ of $CO_2$ leaving the cuvette   | Measured, ‰  |
| $\delta^{18}O_e$    | $\delta^{18}O$ of $CO_2$ entering the cuvette  | Measured, ‰  |
| $\delta^{18}O_a$    | $\delta^{18}O$ of $CO_2$ leaving the cuvette   | Measured, ‰  |
| $\delta^{17}O_{ma}$ | $\delta^{17}O$ of $CO_2$ equilibrated with the leaf water at the evaporating site relative to the $CO_2$ leaving the cuvette | $\frac{\delta^{17}O_m - \delta^{17}O_a}{1 - \delta^{18}O_a}, \text{‰}$   |
| $\delta^{18}O_{ma}$ | $\delta^{18}O$ of $CO_2$ equilibrated with the leaf water at the evaporating site relative to the $CO_2$ leaving the cuvette | $\frac{\delta^{18}O_m - \delta^{18}O_a}{1 - \delta^{18}O_a}, \text{‰}$   |
| $\delta^{18}O_{ve}$ | $\delta^{18}O$ of water vapour entering the cuvette  | Measured, ‰  |
| $\delta^{18}O_{va}$ | $\delta^{18}O$ of water vapour leaving the cuvette/leaf surrounding  | Measured, ‰  |



## Chapter 4

# Leaf-scale quantification of the effect of photosynthetic gas exchange on $\Delta^{17}\text{O}$ of atmospheric $\text{CO}_2$

### Abstract

Understanding the processes that affect the triple oxygen isotope composition of atmospheric  $\text{CO}_2$  during gas exchange can help constrain the interaction and fluxes between the atmosphere and the biosphere. We conducted leaf cuvette experiments under controlled conditions, using three plant species. The experiments were conducted at two different light intensities and using  $\text{CO}_2$  with different  $\Delta^{17}\text{O}$ . We directly quantify for the first time the effect of photosynthesis on  $\Delta^{17}\text{O}$  of atmospheric  $\text{CO}_2$ . Our results demonstrate the established theory for  $\delta^{18}\text{O}$  is applicable to  $\Delta^{17}\text{O}$ - $\text{CO}_2$  at leaf-level and we confirm the two key factors determine the effect of photosynthetic gas exchange on the  $\Delta^{17}\text{O}$  of atmospheric  $\text{CO}_2$ . The relative difference between  $\Delta^{17}\text{O}$  of the  $\text{CO}_2$  entering the leaf and the  $\text{CO}_2$  in equilibrium with leaf water, and the back-diffusion flux of  $\text{CO}_2$  from the leaf to the atmosphere, which can be quantified by the  $c_m/c_a$  ratio where  $c_a$  is the  $\text{CO}_2$  mole fraction in the surrounding air and  $c_m$  the one at the site of oxygen isotope exchange between  $\text{CO}_2$  and  $\text{H}_2\text{O}$ . At low  $c_m/c_a$  ratio the discrimination is governed mainly by diffusion into the leaf, and at high  $c_m/c_a$  ratio by back-diffusion of  $\text{CO}_2$  that has equilibrated with the leaf water. Plants with a higher  $c_m/c_a$  ratio modify the  $\Delta^{17}\text{O}$  of atmospheric  $\text{CO}_2$  more strongly than plants with a lower  $c_m/c_a$  ratio. Based on the leaf cuvette experiments, the global value for discrimination against  $\Delta^{17}\text{O}$  of atmospheric  $\text{CO}_2$  during photosynthetic gas exchange is estimated to be  $-0.57 \pm 0.14 \text{ ‰}$  using  $c_m/c_a$  values of 0.3 and 0.7 for  $\text{C}_4$  and  $\text{C}_3$  plants, respectively. The main uncertainties in this global estimate arise from variation in  $c_m/c_a$  ratios among plants and growth conditions.



## 4.1. Introduction

Stable isotope measurements of CO<sub>2</sub> provide important information on the magnitude of the CO<sub>2</sub> fluxes between atmosphere and biosphere, which are the largest components of the global carbon cycle (Farquhar et al., 1989a; 1993; Ciais et al., 1997a; 1997b; Flanagan and Ehleringer, 1998; Yakir and Sternberg, 2000; Gillon and Yakir, 2001; Cuntz et al., 2003a; 2003b). A better understanding of the terrestrial carbon cycle is essential for predicting future climate and atmospheric CO<sub>2</sub> mole fractions (Booth et al., 2012). Gross primary productivity (GPP), the total carbon dioxide uptake by vegetation during photosynthesis, can only be determined indirectly and remains poorly constrained (Cuntz, 2011; Welp et al., 2011). For example, Beer et al. (2010) estimated global GPP to be 102-135 PgC yr<sup>-1</sup> (85 % confidence interval, CI) using machine learning techniques by extrapolating from a database of eddy-covariance measurements of CO<sub>2</sub> fluxes. This estimate has since then been widely used as target for terrestrial vegetation models (Sitch et al., 2015), and replicated based on cross-consistency checks with atmospheric inversions, sun-induced fluorescence (SIF) and global vegetation models (Jung et al., 2020). As an alternative, Welp et al. (2011) estimated global GPP to be 150-175 PgC yr<sup>-1</sup> using variations in  $\delta^{18}\text{O}$  of atmospheric CO<sub>2</sub> after the 1997/98 El Nino event; see equation 4.1 for definition of the  $\delta$  value.

The concept behind the latter study was that atmospheric CO<sub>2</sub> exchanges oxygen isotopes with leaf and soil water, and this isotope exchange mostly determines the observed variations in  $\delta^{18}\text{O}$  of CO<sub>2</sub> (Francey and Tans, 1987; Yakir, 1998). Following the 97/98 ENSO event, the anomalous  $\delta^{18}\text{O}$  signature imposed on tropical leaf and soil waters was transferred to atmospheric CO<sub>2</sub>, before slowly disappearing as a function of the lifetime of atmospheric CO<sub>2</sub>. This in turn is governed by the land vegetation uptake of CO<sub>2</sub> during photosynthesis, as well as soil invasion of CO<sub>2</sub> (Miller et al., 1999; Wingate et al., 2009). For the photosynthesis term, the equilibration of CO<sub>2</sub> with water is an uncertain parameter in this calculation, partly because the  $\delta^{18}\text{O}$  of water at the site of isotope exchange in the leaf is not well defined. Importantly, a significant  $\delta^{18}\text{O}$  variation can occur in leaves due to the preferential evaporation of H<sub>2</sub><sup>16</sup>O relative to H<sub>2</sub><sup>18</sup>O (Gan et al., 2002; Farquhar and Gan, 2003; Gan et al., 2003; Cernusak et al., 2016), which induces a considerable uncertainty in estimating  $\delta^{18}\text{O}$  of CO<sub>2</sub>. Similar considerations for the transfer of the  $\delta^{18}\text{O}$  signature of precipitation into the soils, and then up through the roots, stems, and leaves make <sup>18</sup>O of CO<sub>2</sub> a challenging measurement to interpret (Peylin et al., 1999; Cuntz et al., 2003a; 2003b).

Classical isotope theory posits that oxygen isotope distributions are modified in a mass-dependent way. This means that the <sup>17</sup>O/<sup>16</sup>O ratio changes by approximately half of the corresponding change in <sup>18</sup>O/<sup>16</sup>O (equation 4.2), and it applies to the processes involved in gas exchange between atmosphere and plants. However, in 1983 Thiemens and co-workers (Heidenreich and Thiemens, 1983; Thiemens, 1983; Heidenreich and Thiemens, 1986) reported a deviation from mass-dependent isotope fractionation in ozone (O<sub>3</sub>) formation called mass-independent isotope fractionation ( $\Delta^{17}\text{O}$ , equation 4.3). In the stratosphere, the  $\Delta^{17}\text{O}$  of O<sub>3</sub> is transferred to CO<sub>2</sub> via isotope exchange of CO<sub>2</sub> with O(<sup>1</sup>D) produced from O<sub>3</sub> photolysis (Yung et al., 1991; Yung et al., 1997; Shaheen et al., 2007), which results a large  $\Delta^{17}\text{O}$  in stratospheric CO<sub>2</sub> (Thiemens et al., 1991; 1995; Lyons, 2001; Lämmerzahl et al., 2002; Thiemens, 2006; Kawagucci et al., 2008; Wiegel et al., 2013).

Once  $\Delta^{17}\text{O}$  has been created in stratospheric  $\text{CO}_2$ , the only process that modify its signal is isotope exchange with leaf water, soil water and ocean water at the Earth's surface, after  $\text{CO}_2$  has re-entered the troposphere (Boering et al., 2004; Thiemeis et al., 2014; Liang and Mahata, 2015; Hofmann et al., 2017). Isotope exchange with leaf water is more efficient relative to ocean water due to the presence of the enzyme carbonic anhydrase (CA), which effectively catalyzes the conversion of  $\text{CO}_2$  and  $\text{H}_2\text{O}$  to  $\text{HCO}_3^-$  and  $\text{H}^+$  and vice versa (Francey and Tans, 1987; Friedli et al., 1987; Badger and Price, 1994; Gillon and Yakir, 2001). The isotope exchange in the atmosphere is negligible due to lower liquid water content, lower residence time and the absence of carbonic anhydrase (Mills and Urey, 1940; Miller et al., 1971; Johnson, 1982; Silverman, 1982; Francey and Tans, 1987).

$\Delta^{17}\text{O}$  of  $\text{CO}_2$  has been suggested as an additional independent tracer for constraining global GPP (Hoag et al., 2005; Thiemeis et al., 2013; Hofmann et al., 2017; Liang et al., 2017b; Koren et al., 2019), because the processes involved in plant-atmosphere gas exchange are all mass-dependent. Therefore,  $\Delta^{17}\text{O}$  at the  $\text{CO}_2$ - $\text{H}_2\text{O}$  exchange site in the leaf will vary much less than  $\delta^{18}\text{O}$ . Nevertheless, mass-dependent isotope fractionation processes with slightly different three-isotope fractionation slopes are involved, which have been precisely established in the past years. Figure 4.1 shows how the different processes affect  $\Delta^{17}\text{O}$  of the  $\text{H}_2\text{O}$  and  $\text{CO}_2$  reservoirs involved. The triple isotope slope of oxygen in meteoric waters is taken as reference slope,  $\lambda_{\text{Ref}}=0.528$  (Meijer and Li, 1998; Barkan and Luz, 2007; Landais et al., 2008; Luz and Barkan, 2010; Uemura et al., 2010) and we assume that soil water is similar to meteoric water. Due to transpiration and diffusion in the leaf,  $\Delta^{17}\text{O}$  of leaf water gets modified following a humidity dependent three-isotope slope  $\theta_{\text{trans}}=0.522-0.008 \times h$  (Landais et al., 2006). Exchange of oxygen isotopes between leaf water and  $\text{CO}_2$  follows  $\lambda_{\text{CO}_2\text{-H}_2\text{O}}=0.5229$  (Barkan and Luz, 2012) which determines the  $\Delta^{17}\text{O}$  of  $\text{CO}_2$  inside the leaf at the  $\text{CO}_2$ - $\text{H}_2\text{O}$  exchange site. Finally, the  $\Delta^{17}\text{O}$  of the  $\text{CO}_2$  is modified when  $\text{CO}_2$  diffuses into and out of the leaf with  $\lambda_{\text{diff}}=0.509$  (Young et al., 2002).

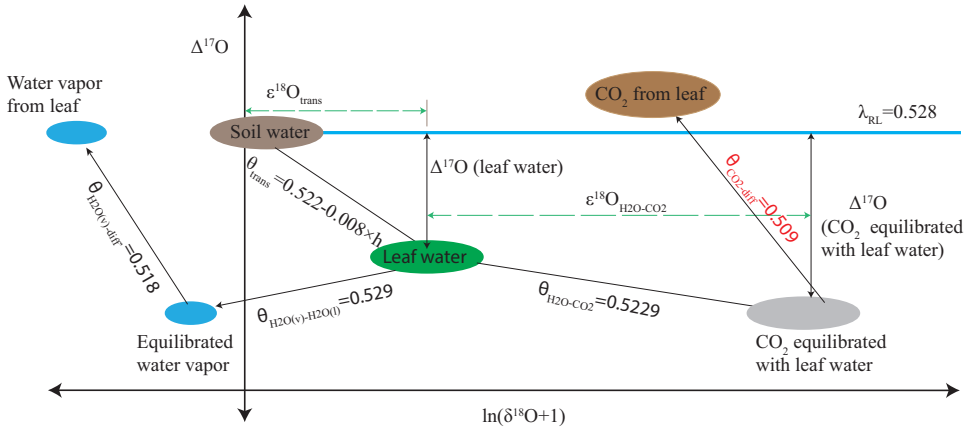


Figure 4.1 Schematic for mass-dependent isotope fractionation process that affects the  $\Delta^{17}\text{O}$  of the  $\text{CO}_2$  and  $\text{H}_2\text{O}$  during the photosynthetic gas exchange (not to scale). The triple oxygen isotope relationship for the individual isotope fractionation processes (both kinetic and equilibrium fractionation) are assigned with  $\theta$ .  $\theta_{\text{trans}}=0.522-0.008 \times h$ , where  $h$  is relative humidity (Landais et al., 2006), in this study the humidity is 75 %,  $\theta_{\text{trans}}=0.516$ .  $\theta_{\text{CO}_2\text{-H}_2\text{O}}$  (Barkan and Luz, 2012),  $\theta_{\text{CO}_2\text{-diff}}$  (Young et al., 2002),  $\theta_{\text{H}_2\text{O(v)-H}_2\text{O(l)}}$  (Barkan and Luz, 2005) and  $\theta_{\text{H}_2\text{O(v)-diff}}$  (Barkan and Luz, 2007). Where  $v$  and  $l$  for vapor and liquid water, respectively;  $\epsilon^{18}\text{O}$  is enrichment or depletion in  $^{18}\text{O}$  isotope composition due to the corresponding isotope fractionation process; *diff* and *trans* stand for diffusion and transpiration, respectively.

In the first box model study of Hoag et al. (2005), the small deviations in  $\Delta^{17}\text{O}$  of  $\text{CO}_2$  due to differences in three-isotope slopes were neglected and exchange with water was assumed to reset  $\Delta^{17}\text{O}$  to 0. Hofmann et al. (2017) included the different isotope effects shown in Figure 4.1 in their box model. Koren et al. (2019) incorporated all the physico-chemical processes affecting  $\Delta^{17}\text{O}$  of  $\text{CO}_2$  in a 3D atmospheric model and investigated the spatiotemporal variability of  $\Delta^{17}\text{O}$  and its use as tracer for GPP. Using these and other similar models, numerous measurements of  $\Delta^{17}\text{O}$  in atmospheric  $\text{CO}_2$  from different locations have been performed and used to estimate GPP (Liang et al., 2006; Barkan and Luz, 2012; Thiemens et al., 2014; Liang and Mahata, 2015; Laskar et al., 2016; Hofmann et al., 2017). The three-isotope slopes of the processes involved in the gas exchange (Figure 4.1) have been precisely determined in idealized experiments. In the advanced models mentioned above it is assumed that when all the pieces are put together they result in a realistic overall modification of  $\Delta^{17}\text{O}$  of  $\text{CO}_2$  in the atmosphere surrounding the leaf. However, this has not been confirmed by measurements previously.

In this study we report the effect of photosynthesis on  $\Delta^{17}\text{O}$  of  $\text{CO}_2$  in the surrounding air at the leaf scale. We measured  $\Delta^{17}\text{O}$  of  $\text{CO}_2$  entering and leaving a leaf cuvette to calculate the isotopic fractionation associated with photosynthesis for three species that are representative for three different biomes. The fast-growing annual herbaceous  $\text{C}_3$  species *Helianthus annuus* (sunflower) has a high photosynthetic capacity ( $A_n$ ) and high stomatal conductance ( $g_s$ ) and is representative for temperate and tropical crops (Fredeen et al., 1991). The slower growing perennial evergreen  $\text{C}_3$  species *Hedera hybernica* (ivy) is representative of forests and other woody vegetation and stress subjected habitats (Pons et al., 2009). The fast-growing, agronomically important crop *Zea mays* (maize) is an herbaceous annual  $\text{C}_4$  species with a high  $A_n$  and a low  $g_s$ , typical for savanna type vegetation (Weijde et al., 2013). The mole fraction of  $\text{CO}_2$  at the  $\text{CO}_2$ - $\text{H}_2\text{O}$  exchange site ( $c_m$ ) is an important parameter to determine the effect of photosynthesis on  $\Delta^{17}\text{O}$  of  $\text{CO}_2$ . In  $\text{C}_3$  plants, the  $\text{CO}_2$ - $\text{H}_2\text{O}$  exchange can occur anywhere between the plasma membrane and the chloroplast since the catalyzing enzyme CA has been found in the chloroplast, cytosol, mitochondria and plasma membrane (Fabre et al., 2007; DiMario et al., 2016). For  $\text{C}_4$  plants, CA is mainly found in the cytosol and the  $\text{CO}_2$ - $\text{H}_2\text{O}$  exchange occurs there (Badger and Price, 1994). In our experiments, sunflower and ivy are used to cover the wide  $c_m/c_a$  ratio range among  $\text{C}_3$  plants and maize represents the  $c_m/c_a$  ratio for the  $\text{C}_4$  plants. Using our results from the leaf scale experiments, we estimated the effect of terrestrial vegetation on  $\Delta^{17}\text{O}$  of  $\text{CO}_2$  in the global atmosphere.

## 4.2. Theory

### 4.2.1. Notation and definition of $\delta$ values

Isotopic composition is expressed as the deviation of the heavy to light isotope ratio in a sample relative to a reference ratio and it is denoted as  $\delta$ , expressed in per mill (‰). In the case of oxygen isotopes, the isotope ratios are  $^{18}\text{R} = [^{18}\text{O}]/[^{16}\text{O}]$  and  $^{17}\text{R} = [^{17}\text{O}]/[^{16}\text{O}]$  and the reference material is Vienna Standard Mean Ocean Water (VSMOW):

$$\delta^n\text{O} = \frac{n_{\text{Rsample}}}{n_{\text{RVSMOW}}} - 1, n \text{ refers to 17 or 18} \quad (4.1)$$

For most processes, isotope fractionation depends on mass, and therefore the fractionation against  $^{17}\text{O}$  is approximately half of the fractionation against  $^{18}\text{O}$  (equation 4.3).

$$\ln(\delta^{17}\text{O} + 1) = \lambda \times \ln(\delta^{18}\text{O} + 1) \quad (4.2)$$

The mass-dependent isotope fractionation factor  $\lambda$  ranges from 0.5 to 0.5305 for different molecules and process (Matsuhisa et al., 1978; Thiemens, 1999; Young et al., 2002; Cao and Liu, 2011).  $\Delta^{17}\text{O}$  is used to quantify the degree of deviation from equation 4.2 (see equation 4.3). Note that  $\Delta^{17}\text{O}$  changes not only by mass-independent isotope fractionation processes, but also by mass-dependent isotope fractionation processes with a different  $\lambda$  value from the one used in the definition of  $\Delta^{17}\text{O}$  (Barkan and Luz, 2005; Landais et al., 2006; 2008; Luz and Barkan, 2010; Barkan and Luz, 2011; Pack and Herwartz, 2014).

$$\Delta^{17}\text{O} = \ln(\delta^{17}\text{O} + 1) - \lambda \times \ln(\delta^{18}\text{O} + 1) \quad (4.3)$$

The choice of  $\lambda$  is in principle arbitrary and in this study, we use  $\lambda = 0.528$ , which was established for meteoric waters (Meijer and Li, 1998; Landais et al., 2008; Brand et al., 2010; Luz and Barkan, 2010; Barkan and Luz, 2012; Sharp et al., 2018). Equation 4.3 can be linearized to (Miller, 2002)  $\Delta^{17}\text{O} = \delta^{17}\text{O} - \lambda \times \delta^{18}\text{O}$ , but this approximation causes an error that increases with  $\delta^{18}\text{O}$  (Miller, 2002; Bao et al., 2016).

#### 4.2.2. Discrimination against $\Delta^{17}\text{O}$ of $\text{CO}_2$

The overall isotope fractionation associated with the photosynthesis of  $\text{CO}_2$  is commonly quantified using the term discrimination as described in (Farquhar and Richards, 1984; Farquhar et al., 1989a; Farquhar and Lloyd, 1993). We use the symbol  $\Delta_A$  for discrimination due to assimilation in this manuscript since the commonly used  $\Delta$  is already used for the definition of  $\Delta^{17}\text{O}$  (see equation 4.3).  $\Delta_A$  quantifies the enrichment or depletion of carbon and oxygen isotopes of  $\text{CO}_2$  in the surrounding atmosphere relative to the  $\text{CO}_2$  that is assimilated (Farquhar and Richards, 1984). It can be calculated from the isotopic composition of the  $\text{CO}_2$  entering and leaving the leaf cuvette (Evans et al., 1986; Gillon and Yakir, 2000b; Barbour et al., 2016) as:

$$\Delta_A^n\text{O}_{\text{obs}} = \frac{n_{\text{Ra}}}{n_{\text{RA}}} - 1 = \frac{\delta^n\text{O}_a - \delta^n\text{O}_A}{1 + \delta^n\text{O}_A} = \frac{\zeta \times (\delta^n\text{O}_a - \delta^n\text{O}_e)}{1 + \delta^n\text{O}_a - \zeta \times (\delta^n\text{O}_a - \delta^n\text{O}_e)} \quad (4.4)$$

where the indices  $e$ ,  $a$  and  $A$  refer to  $\text{CO}_2$  entering and leaving the cuvette and being assimilated, respectively.  $\zeta = \frac{c_e}{c_e - c_a}$ , where  $c_e$  and  $c_a$  are the mole fractions of  $\text{CO}_2$  entering and leaving the cuvette. For quantifying the effect of photosynthesis on  $\Delta^{17}\text{O}$  in our experiments, the  $\Delta_A\Delta^{17}\text{O}$  is calculated from  $\Delta_A^{17}\text{O}$  and  $\Delta_A^{18}\text{O}$  using the three-isotope slope  $\lambda_{\text{RL}} = 0.528$ , similar to equation 4.3. In previous studies slightly, different formulations have been used to define the effect of photosynthesis on  $\Delta^{17}\text{O}$ , and a comparison of the different definitions is provided in the supplementary material (equation S4.37-S4.40).

It is important to note that when the logarithmic definition of  $\Delta^{17}\text{O}$  or  $\Delta_A\Delta^{17}\text{O}$  is used, values are not additive (Kaiser et al., 2004). In linear calculations, the error gets larger when the relative difference in  $\delta^{18}\text{O}$  between the two  $\text{CO}_2$  gases increases regardless of the  $\Delta^{17}\text{O}$  of the individual  $\text{CO}_2$  gases (Figure S4.1). Therefore,  $\Delta_A\Delta^{17}\text{O}$  values have to be calculated from the individual  $\Delta_A^{17}\text{O}$  and  $\Delta_A^{18}\text{O}$  values, and not by linear combinations of the  $\Delta^{17}\text{O}$  of air entering and leaving a plant chamber.

## 4.3. Materials and methods

### 4.3.1. Plant material and growing conditions

Sunflower (*Helianthus annuus* L. cv “sunny”) was grown from seeds in 0.6 L pots with potting soil (Primasta, the Netherlands) for about four weeks. All leaves appearing above the first leaf pair were removed to avoid shading. Established juvenile ivy (*Hedera hybernica* L.) plants were pruned and planted in 6 L pots for 6 weeks. Ivy leaves that had developed and matured were used for the experiments. Maize (*Z. mays* L. cv “saccharate”) was grown from seed in 1.6 L pots for at least 7 weeks. For maize, the 4<sup>th</sup> or higher leaf number was used for the experiments when mature. A section of the leaf at about 1/3 from the tip was inserted in the leaf cuvette. They were placed on a sub-irrigation system that provided water during the growth period in a controlled environment growth chamber, air temperature 20 °C, relative humidity 70 % and  $\text{CO}_2$  mole fraction of about 400 ppm. The photosynthetic photon flux density (PPFD) was about 300  $\mu\text{mol m}^{-2} \text{s}^{-1}$  during a daily photoperiod of 16 hours measured with a PPFD meter (Licor LI-250A, Li-Cor Inc, Nebraska, USA).

### 4.3.2. Gas exchange experiments

Gas exchange experiments were performed in an open system where a controlled flow of air enters and leaves the leaf cuvette similar to the setup used by (Pons and Welschen, 2002). A schematic for the gas exchange experimental setup is shown in Figure 4.2. The leaf cuvette had dimensions of 7 x 7 x 7 cm<sup>3</sup> (lxwxh) and the top part of the cuvette was transparent. The temperature of the leaf was measured with a K type thermocouple. The leaf chamber temperature was controlled by a temperature-controlled water bath kept at 20 °C (Tamson TLC 3, The Netherlands). A halogen lamp (PRADOVIT 253, ERNST LEITZ WETZLAR GMBH, Germany) in a slide projector was used as a light source. Infrared was excluded by reflection from a cold mirror. The light intensity was varied with spectrally neutral filters (PRADOVIT 253, ERNST LEITZ WETZLAR GMBH, Germany).

The  $\text{CO}_2$  mole fraction of the incoming and outgoing air was measured with an infrared gas analyzer (IRGA, model LI-6262, LI-COR Inc., Nebraska, USA). The isotopic composition and mole fraction of the incoming and outgoing water vapor were measured with a triple water vapor isotope analyzer (WVIA, model 911-0034, Los Gatos Research, USA). Compressed air (ambient outside air without drying) was passed through soda lime to scrub the  $\text{CO}_2$ . The  $\text{CO}_2$

free air could be humidified depending on the experiment conditions (see Figure 4.2). The humidity of the inlet air was monitored continuously with a dewpoint meter (HYGRO-M1, General Eastern, Watertown, MA, USA). Pure CO<sub>2</sub> (either normal CO<sub>2</sub> or isotopically enriched CO<sub>2</sub>) was mixed with the incoming air to produce a CO<sub>2</sub> mole fraction of 500 ppm. The isotopically enriched CO<sub>2</sub> was prepared by photochemical isotope exchange between CO<sub>2</sub> and O<sub>2</sub> under UV irradiation (Adnew et al., 2019).

An attached leaf or part of it was inserted into the cuvette, the composition of the inlet air was measured, and both IRGA and WVIA were switched to measure the outlet air. Based on the CO<sub>2</sub> mole fraction of the outgoing air the flow rate of the incoming air to the cuvette was adjusted to establish a drawdown of 100 ppm CO<sub>2</sub> due to photosynthesis in the plant chamber. The water vapor content entering the cuvette was adjusted depending on the transpiration rate relative to CO<sub>2</sub> uptake to avoid condensation (Figure 4.2). The outgoing air was measured continuously until a steady state was reached for CO<sub>2</sub> and H<sub>2</sub>O mole fractions and  $\delta D$  and  $\delta^{18}O$  of the water vapor. After a steady state was established, the air was directed to the sampling flask while the IGRA and WVIA were switched back to measure the inlet air. The air passed through a Mg(ClO<sub>4</sub>)<sub>2</sub> dryer before entering the sampling flask.

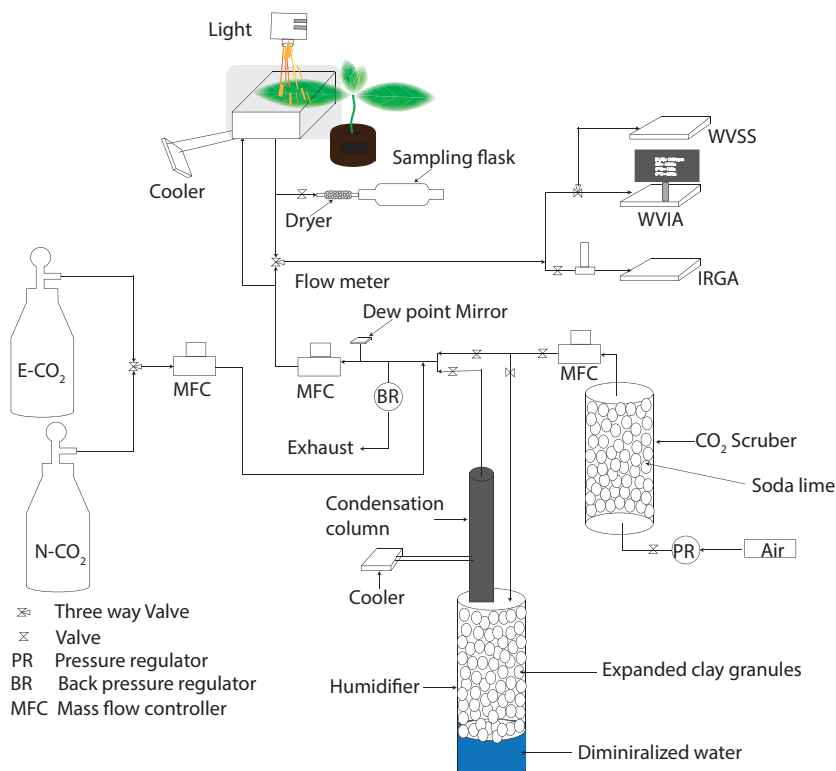


Figure 4.2 Schematic diagram of the leaf cuvette experimental setup. IRGA stands for the infrared gas analyzer, WVSS is the water vapor standard source, WVIA is the water vapor isotope analyzer, N-CO<sub>2</sub> is normal CO<sub>2</sub>, E-CO<sub>2</sub> is <sup>17</sup>O-enriched CO<sub>2</sub>.

After sampling, the leaf area inside the cuvette was measured with a LI-3100C area meter (LI-COR, Inc. USA). Immediately afterward, the leaf was placed in a leak tight 9 mL glass vial and kept in a freezer at -20 °C until leaf water extraction.

#### **4.3.3. Calibration of the Water Vapor Isotope Analyzer (WVIA) and leaf water analysis**

The WVIA was calibrated using five water standards provided by IAEA (Wassenaar et al., 2018) for both  $\delta^{18}\text{O}$  and  $\delta\text{D}$  (Figure S4.2). We did not calibrate the WVIA for  $\delta^{17}\text{O}$ , so the  $\delta^{17}\text{O}$  data are not used in the quantitative evaluation. The isotopic composition of the water standards ranged from -50.93 to 3.64 ‰ and -396.98 ‰ to 25.44 ‰ for  $\delta\text{D}$  and  $\delta^{18}\text{O}$ , respectively. The detailed characterization and calibration of the water WVIA is provided in the supplementary material (Figure S4.2 to S4.4).

Leaf water was extracted by cryogenic vacuum distillation for 4 h at 60 °C following a well-established procedure as shown in Figure S4.5 (Wang and Yakir, 2000; Landais et al., 2006; West et al., 2006). Details are provided in the supplementary material. The  $\delta^{17}\text{O}$  and  $\delta^{18}\text{O}$  of leaf water was determined at the Laboratoire des Sciences du Climat et de l'Environnement laboratory using a fluorination technique as described in (Barkan and Luz, 2005; Landais et al., 2006; 2008).

#### **4.3.4. Carbon dioxide extraction and isotope analysis**

$\text{CO}_2$  was extracted from the air samples in a system made from electropolished stainless steel (Supplementary Figure S4.6). Our system used four commercial traps (MassTech, Bremen, Germany). The first two traps were operated at dry ice temperature (-78 °C) to remove moisture and some organics. The other two traps were operated at liquid nitrogen temperature (-196 °C) to trap  $\text{CO}_2$ . The flow rate during extraction was 55 mL min<sup>-1</sup>, controlled by a mass flow controller (Brooks Instruments, Holland). The reproducibility of the extraction system was 0.030 ‰ for  $\delta^{18}\text{O}$  and 0.007 ‰ for  $\delta^{13}\text{C}$  determined on 14 extractions (1 $\sigma$  standard deviation, Supplementary Table S4.1).

The  $\Delta^{17}\text{O}$  of  $\text{CO}_2$  was determined using the  $\text{CO}_2\text{-O}_2$  exchange method (Mahata et al., 2013; Barkan et al., 2015; Adnew et al., 2019). The  $\text{CO}_2\text{-O}_2$  exchange system used at Utrecht University is described in (Adnew et al., 2019). In short, equal amounts of  $\text{CO}_2$  and  $\text{O}_2$  were mixed in a quartz reactor containing a platinum sponge catalyst and heated at 750 °C for 2hrs. After isotope equilibration, the  $\text{CO}_2$  was trapped at liquid nitrogen temperature, while the  $\text{O}_2$  was collected with 1 pellet of 5Å molecular sieve (1.6 mm, Sigma Aldrich, USA) at liquid nitrogen temperature. The isotopic composition of the isotopically equilibrated  $\text{O}_2$  was measured with a Delta<sup>Plus</sup>XL isotope ratio mass spectrometer in dual inlet mode with reference to a pure  $\text{O}_2$  calibration gas that has been assigned values of  $\delta^{17}\text{O} = 9.254$  ‰ and  $\delta^{18}\text{O} = 18.542$  ‰ by E. Barkan at the Hebrew University of Jerusalem. The reproducibility of the  $\Delta^{17}\text{O}$  measurement was better than 0.01 ‰ (Supplementary Table S4.1).



### 4.3.5. Leaf cuvette model

We used a simple leaf cuvette model to evaluate the dependence of  $\Delta_A \Delta^{17}\text{O}$  on key parameters. In this model, the leaf is partitioned into three different compartments: the intercellular air space, the mesophyll cell, and the chloroplast. In the leaf cuvette model, we used a 100 ppm downdraw of  $\text{CO}_2$ , similar to the leaf exchange experiments, i.e., the  $\text{CO}_2$  mole fraction decreases from 500 ppm in the entering air ( $c_e$ ) to 400 ppm in the outgoing air ( $c_a$ ), which is identical to the air surrounding the leaf ( $c_a$ ) as a result of thorough mixing in the cuvette. The assimilation rate is set to  $20.0 \mu\text{mol m}^{-2}\text{s}^{-1}$ . The leaf area and flowrate of air are set to  $30 \text{ cm}^2$  and  $0.7 \text{ L min}^{-1}$ , respectively. The isotope composition of leaf water at the site where the  $\text{H}_2\text{O}-\text{CO}_2$  exchange occurs is  $\delta^{17}\text{O} = 5.39 \text{ ‰}$  and  $\delta^{18}\text{O} = 10.648 \text{ ‰}$ , which is the mean of the measured  $\delta^{17}\text{O}$  and  $\delta^{18}\text{O}$  values of bulk leaf water in our experiments. The leaf water temperature is set to  $22 \text{ °C}$  (similar to the experiment). In the model, the  $\delta^{18}\text{O}$  of the  $\text{CO}_2$  entering the cuvette is set to  $30.47 \text{ ‰}$  for all the simulations, as in the normal  $\text{CO}_2$  experiments, but the assigned  $\Delta^{17}\text{O}$  values ranges from  $-0.5 \text{ ‰}$  to  $0.5 \text{ ‰}$  which encompasses both the stratospheric intrusion and combustion components. The corresponding  $\delta^{17}\text{O}$  of the  $\text{CO}_2$  entering the cuvette is calculated from the assigned  $\delta^{18}\text{O}$  value ( $30.47 \text{ ‰}$ ) and  $\Delta^{17}\text{O}$  values ( $-0.5 \text{ ‰}$  to  $0.5 \text{ ‰}$ ). For the calculations with this model, we assumed an infinite boundary layer conductance. The leaf cuvette model is illustrated in the supplementary material (Figure S4.7) and the detailed code and description is available at [https://git.wur.nl/leaf\\_model/D17O](https://git.wur.nl/leaf_model/D17O).

## 4.4. Results

### 4.4.1. Gas exchange parameters

Table 4.1 summarizes the isotopic composition and mole fraction of the  $\text{CO}_2$  used in this study for sunflower, ivy and maize. The  $\Delta^{17}\text{O}$  of  $\text{CO}_2$  used in this study varies from  $-0.215 \text{ ‰}$  to  $0.44 \text{ ‰}$  while the  $\delta^{18}\text{O}$  value is close to  $30 \text{ ‰}$  for all the experiments.

Table 4.1 Summary for gas exchange parameters and isotopic composition of maize, sunflower and ivy. Mole fraction at the site of exchange ( $c_m$ ) is calculated assuming complete isotopic equilibrium with the water at the  $\text{CO}_2\text{-H}_2\text{O}$  exchange site. The water at the  $\text{CO}_2\text{-H}_2\text{O}$  exchange site is assumed the same as the isotopic composition at the site of evaporation. Number in the parenthesis are the standard deviation of the mean ( $1\sigma$ ).

| Parameter               |  | Sunflower      | Ivy            | Maize          | Irradiance<br>( $\mu\text{mol m}^{-2} \text{ s}^{-1}$ ) |
|-------------------------|--|----------------|----------------|----------------|---|
| $A_n$                   | $\mu\text{mol mol}^{-1}\text{m}^{-2}\text{s}^{-1}$ | 18 (0.7)       | 12 (0.7)       | 17 (2)         | 300   |
|                         |  | 29 (2)         | 15 (2)         | 32 (2)         | 1200  |
| $g_s$                   | $\text{mol m}^{-2}\text{s}^{-1}$                   | 0.45 (0.14)    | 0.11 (0.02)    | 0.08 (0.01)    | 300   |
|                         |  | 0.40 (0.04)    | 0.15 (0.03)    | 0.16 (0.02)    | 1200  |
| $\delta^{18}\text{O}_e$ | ‰  | 27.26 to 31.80 | 28.28 to 30.48 | 27.26 to 30.48 |   |



|  |     |                 |                 |                 |      |
|--|-----|-----------------|-----------------|-----------------|------|
| $\Delta^{17}\text{O}_e$                    | ‰   | -0.227 to 0.409 | -0.215 to 0.435 | -0.215 to 0.310 |      |
| $\delta^{18}\text{O}_a$                    | ‰   | 33.25 to 43.87  | 32.64 to 35.86  | 34.04 to 29.764 |      |
| $\Delta^{17}\text{O}_a$                    | ‰   | -0.333 to 0.163 | -0.276 to 0.327 | -0.270 to 0.296 |      |
| $\Delta_A^{18}\text{O}_{\text{obs}}$       | ‰   | 57.12 (4.70)    | 22.20 (1.32)    | 17.23 (1.32)    | 300  |
|  |     | 34.48 (3.25)    | 24.35 (3.09)    | 12.78 (0.83)    | 1200 |
| $\Delta_A\Delta^{17}\text{O}_{\text{obs}}$ | ‰   | -2.61 to -0.43  | -1.03 to -0.19  | -0.36 to -0.09  |      |
| $\delta^{18}\text{O}_m$                    | ‰   | 52.02 (1.24)    | 47.17 (1.17)    | 52.62 (0.52)    | 300  |
|  |     | 52.62 (1.42)    | 51.09 (1.76)    | 55.15 (1.55)    | 1200 |
| $\Delta^{17}\text{O}_m$                    | ‰   | -0.41 (0.001)   | -0.35 (0.001)   | -0.40 (0.01)    | 300  |
|  |     | -0.41 (0.01)    | -0.38 (0.02)    | -0.42 (0.02)    | 1200 |
| $c_a$                                      | ppm | 402 (3)         | 403 (3)         | 403 (3)         |      |
| $c_i$                                      | ppm | 357 (10)        | 284 (0.1)       | 194 (20)        | 300  |
|  |     | 323 (10)        | 301 (13)        | 194 (15)        | 1200 |
| $c_c$                                      | ppm | 277 (15)        | 188 (30)        |                 | 300  |
|  |     | 201 (42)        | 163 (21)        |                 | 1200 |
| $c_m$                                      | ppm | 320 (10)        | 220 (10)        | 134 (15)        | 300  |
|  |     | 252 (27)        | 214 (12)        | 88 (17)         | 1200 |

For all the experiments, the mole fraction of  $\text{CO}_2$  entering the leaf ( $c_a$ ) is 400 ppm whereas the mole fraction of the  $\text{CO}_2$  in the intercellular air space ( $c_i$ ), at the  $\text{CO}_2$ - $\text{H}_2\text{O}$  exchange site ( $c_m$ ) and in the chloroplast ( $c_c$ ) varies depending on the assimilation rate and metabolism type of the plants. Estimating the mesophyll conductance is described in the companion paper. A detailed description for estimating  $c_m$  and  $c_c$  is provided in the supplementary material. A list of variables and parameters used in this study are summarized in Table 4.2.

Table 4.2 List of symbols and variables

| Symbol                              | description   | Unit/calculation/value   |
|-------------------------------------|---|--|
| <b>Gas exchange</b>                 |   |  |
| $A_n$                               | Rate of $\text{CO}_2$ assimilation  | $\frac{u_a}{s} \left( c_e - c_a \left( \frac{1-w_a}{1-w_a} \right) \right)$ , $\text{mol m}^{-2}\text{s}^{-2}$   |
| $E$                                 | Transpiration rate  | $\frac{u_a}{s} \left( \frac{w_a-w_e}{1-w_a} \right)$ , $\text{mol m}^{-2}\text{s}^{-2}$  |
| $w_i$                               | Mole fraction of water vapour inside leaf                                   | $\frac{613.65 \times e^{\left( \frac{17.502 \times T_{\text{leaf}}}{240.97 + T_{\text{leaf}}} \right)} \times 10^{-5}}{p}$ , $\text{mol mol}^{-1}$       |
| $w_a$                               | Mole fraction of water vapour leaving the cuvette /leaf surrounding         | WVIA / IRGA, $\text{mol mol}^{-1}$   |
| $w_e$                               | Mole fraction of water vapour entering the cuvette                          | WVIA/IRGA, $\text{mol mol}^{-1}$   |
| $c_e$                               | Mole fraction of $\text{CO}_2$ entering the cuvette                         | IRGA, $\text{mol mol}^{-1}$  |
| $c_a$                               | Mole fraction of $\text{CO}_2$ in the leaf surrounding/ leaving the cuvette | IRGA, $\text{mol mol}^{-1}$  |
| $u_e$                               | Flow rate of air entering the cuvette                                       | $\text{mol s}^{-1}$  |
| $s$                                 | Surface area of the leaf inside the cuvette                                 | $\text{m}^2$   |
| $P$                                 | Atmospheric pressure  | bar  |
| $T_{\text{leaf}}$                   | Leaf temperature  | $^{\circ}\text{C}$   |
| $g_{\text{st}(\text{H}_2\text{O})}$ | Stomatal conductance for water vapour                                       | $\frac{g_{\text{H}_2\text{O}}^{\text{L}} \times R_{\text{b}}(\text{H}_2\text{O})}{R_{\text{b}}(\text{H}_2\text{O}) - R_{\text{H}_2\text{O}}^{\text{L}}}$ |
| $g_{\text{b}(\text{H}_2\text{O})}$  | Boundary layer conductance for water vapour                                 | Calibrated for the cuvette we used   |
| $g_{\text{H}_2\text{O}}^{\text{L}}$ | Conductance for water vapor through the boundary layer and stomata          | $E \left( \frac{1 - \left( \frac{w_i + w_a}{2} \right)}{w_i - w_a} \right)$ , $\text{mol m}^{-2}\text{s}^{-1}$   |

|  |   |  |
|--|---|--|
| $g_s$                                    | Stomatal conductance for CO <sub>2</sub>  | $\frac{g_b(H_{2O})}{1.6}$  |
| $g_b$                                    | Boundary conductance for CO <sub>2</sub>  | $\frac{g_b(H_{2O})}{1.37}$   |
| $g^{CO_2}$                               | Conductance for CO <sub>2</sub> through the boundary layer and stomata  | $\frac{g_s \times g_b}{g_s + g_b}$   |
| $\Gamma^*$                               | CO <sub>2</sub> compensation point  | 45 $\mu\text{mol m}^{-2}\text{s}^{-1}$   |
| $g_{m13}$                                | CO <sub>2</sub> conductance from intercellular air space to the site of carboxylation calculated using $\Delta A^{13}\text{C}$ (for C <sub>3</sub> plants only) | $\text{mol m}^{-2}\text{s}^{-1}\text{bar}^{-1}$  |
| $g_{m18}$                                | CO <sub>2</sub> conductance from intercellular air space to CO <sub>2</sub> -H <sub>2</sub> O exchange site calculated using $\Delta A^{18}\text{O}$            | $\text{mol m}^{-2}\text{s}^{-1}\text{bar}^{-1}$  |
| $g_{m17}$                                | CO <sub>2</sub> conductance from intercellular air space to CO <sub>2</sub> -H <sub>2</sub> O exchange site calculated using $\Delta A^{17}\text{O}$            | $\text{mol m}^{-2}\text{s}^{-1}\text{bar}^{-1}$  |
| $g_{m17}$                                | CO <sub>2</sub> conductance from intercellular air space to CO <sub>2</sub> -H <sub>2</sub> O exchange site calculated using $\Delta A^{17}\text{O}$            | $\text{mol m}^{-2}\text{s}^{-1}\text{bar}^{-1}$  |
| $c_i$                                    | Mole fraction of CO <sub>2</sub> in the intercellular air space   | $\frac{(g_{CO_2} - \frac{e}{r})c_a - A_n}{(g_{CO_2} + \frac{e}{r})}$ , mol mol <sup>-1</sup> |
| $c_s$                                    | Mole fraction of CO <sub>2</sub> at the leaf surface  | $c_a - \frac{A_n}{g_b}$ , mol mol <sup>-1</sup>  |
| $c_m$                                    | Mole fraction of CO <sub>2</sub> at the site of CO <sub>2</sub> -H <sub>2</sub> O exchange  | mol mol <sup>-1</sup>  |
| $c_c$                                    | Mesophyll conductance to the chloroplast (for C <sub>3</sub> plants)  | $c_i - \frac{A_n}{g_{m13}}$ , mol mol <sup>-1</sup>  |
| $f^{13}$                                 | Ternary correction for <sup>13</sup> CO <sub>2</sub>  | $\frac{(1+a_{13bs})E}{2g_{CO_2}}$  |
| $f^{18}$                                 | Ternary correction for C <sup>18</sup> OO   | $\frac{(1+a_{18bs})E}{2g_{CO_2}}$  |
| $f^{17}$                                 | Ternary correction for C <sup>17</sup> OO   | $\frac{(1+a_{17bs})E}{2g_{CO_2}}$  |
| $R_D$                                    | Dark respiration rate   | 0.8 $\mu\text{mol m}^{-2}\text{s}^{-1}$  |
| $R_L$                                    | Day respiration rate  | $0.5 \times R_D$ $\mu\text{mol m}^{-2}\text{s}^{-1}$   |
| <b>Oxygen and carbon isotope effects</b> |   |  |
| $\epsilon^{18}_k$                        | Kinetic fractionation of water vapour in air  | $\frac{28g_b + 19g_s}{g_b + g_s}$ , ‰  |
| $\epsilon^{18}_{equ}$                    | Equilibrium fractionation between liquid and gas phase of water vapor   | $2.644 - 3.206(\frac{10^3}{T_{leaf}}) + 1.534(\frac{10^6}{T_{leaf}^2})$ , ‰                  |
| $a_{13bs}$                               | Weighted fractionation for <sup>13</sup> COO as CO <sub>2</sub> diffuses through the boundary layer and stomata   | $\frac{(c_s - c_i)a_{13s} + (c_a - c_s)a_{13b}}{c_a - c_i}$ , ‰                              |
| $a_{17bs}$                               | Weighted fractionation for C <sup>17</sup> OO as CO <sub>2</sub> diffuses through the boundary layer and stomata  | $\frac{(c_s - c_i)a_{17s} + (c_a - c_s)a_{17b}}{c_a - c_i}$ , ‰                              |
| $a_{18bs}$                               | Weighted fractionation for C <sup>18</sup> OO as CO <sub>2</sub> diffuses through the boundary layer and stomata  | $\frac{(c_s - c_i)a_{18s} + (c_a - c_s)a_{18b}}{c_a - c_i}$ , ‰                              |
| $a_{13bs}$                               | Weighted fractionation for <sup>13</sup> COO as CO <sub>2</sub> diffuses through the boundary layer and stomata   | $\frac{(c_s - c_i)a_{13s} + (c_a - c_s)a_{13b}}{c_a - c_i}$ , ‰                              |
| $a_{18bs}$                               | Weighted fractionation for C <sup>18</sup> OO as CO <sub>2</sub> diffuses through the boundary layer and stomata  | $\frac{(c_s - c_i)a_{18s} + (c_a - c_s)a_{18b}}{c_a - c_i}$ , ‰                              |
| $a_{17bs}$                               | Weighted fractionation for C <sup>17</sup> OO as CO <sub>2</sub> diffuses through the boundary layer and stomata  | $\frac{(c_s - c_i)a_{17s} + (c_a - c_s)a_{17b}}{c_a - c_i}$ , ‰                              |
| $\bar{a}_{17}$                           | Weighted fractionation of C <sup>17</sup> OO as it diffuses through the boundary layer, stomata and liquid phase in series                                      | $\frac{(c_i - c_m)a_{17w} + (c_s - c_i)a_{17s} + (c_a - c_s)a_{17b}}{c_a - c_m}$ , ‰         |
| $\bar{a}_{18}$                           | Weighted fractionation of C <sup>18</sup> OO as it diffuses through the boundary layer, stomata and liquid phase in series                                      | $\frac{(c_i - c_m)a_{18w} + (c_s - c_i)a_{18s} + (c_a - c_s)a_{18b}}{c_a - c_m}$ , ‰         |
| $a_{13b}$                                | Fractionation in <sup>13</sup> CO <sub>2</sub> as CO <sub>2</sub> diffuses through the boundary layer   | 2.9 ‰  |
| $a_{13s}$                                | Fractionation in <sup>13</sup> CO <sub>2</sub> as CO <sub>2</sub> diffuses through the stomata  | 4.4 ‰  |
| $a_m$                                    | Fractionation factor for dissolution and diffusion through water  | 1.8 ‰  |
| $f$                                      | Fractionation factor for photorespiration (decarboxylation of glycine)  | 16 ‰   |
| $e$                                      | Fractionation factor for day respiration  | $R_D + e^*$ , ‰  |
| $e^*$                                    | Apparent fractionation for day respiration  | $\delta^{13}C_p - \Delta A^{13}C - \delta^{13}C_{\text{substrate}}$ , ‰                      |
| $b$                                      | Fractionation factor for uptake by RubisCO  | 29 ‰   |
| $\alpha_f$                               | Fractionation due to photorespiration (decarboxylation of glycine)  | 1+f  |
| $\alpha_e$                               | Fractionation due to day respiration  | 1+e  |
| $\alpha_b$                               | Fractionation due to uptake by RubisCO  | 1+b  |
| $a_{17b}$                                | Fractionation of C <sup>17</sup> OO as CO <sub>2</sub> diffuses through the boundary layer  | 2.9 ‰  |

|                             |  |  |
|-----------------------------|--|--|
| $a_{17s}$                   | Fractionation in $C^{17}O$ as $CO_2$ diffuses through stomata  | 4.4 ‰  |
| $a_{18b}$                   | Fractionation of $C^{18}O$ as $CO_2$ diffuses through the boundary layer   | 5.8 ‰  |
| $a_{18s}$                   | Fractionation in $C^{18}O$ as $CO_2$ diffuses through stomata  | 8.8 ‰  |
| $a_{17w}$                   | Fractionation in $C^{17}O$ due to diffusion and dissolution in water   | 0.382 ‰  |
| $a_{18w}$                   | Fractionation in $C^{18}O$ due to diffusion and dissolution in water   | 0.8 ‰  |
| $\varepsilon^{18}w$         | Equilibrium fractionation of $CO_2$ and water for $C^{18}O$  | $\frac{17604}{T_{leaf}} - 17.93$ , ‰   |
| $\varepsilon^{18}k$         | kinetic fractionation of water vapor in air  | $\frac{28 \times g_b + 19 \times g_s}{g_b + g_s}$  |
| $\varepsilon^{18}equ$       | equilibrium fractionation between liquid and gas phase water   | $2.644 - 3.206 \times \left(\frac{10^3}{T}\right) + 1.534 \times \left(\frac{10^6}{T}\right)$  |
| <b>Isotopic composition</b> |  |  |
| $\delta^{17}O_A$            | $\delta^{17}O$ of the assimilated $CO_2$   | $\frac{\delta^{17}O_A - \Delta_A^{17}O}{\Delta_A^{17}O + 1} = \delta^{17}O_a - \frac{c_e}{c_e - c_a} (\delta^{17}O_a - \delta^{17}O_e)$  |
| $\delta^{18}O_A$            | $\delta^{18}O$ of the assimilated $CO_2$   | $\frac{\delta^{18}O_A - \Delta_A^{18}O}{\Delta_A^{18}O + 1} = \delta^{18}O_a - \frac{c_e}{c_e - c_a} (\delta^{18}O_a - \delta^{18}O_e)$  |
| $\delta^{17}O_{io}$         | $\delta^{17}O$ of $CO_2$ in the intercellular air space ignoring ternary correction  | $\delta^{17}O_A \left(1 - \frac{c_a}{c_i}\right) (1 + a_{17bs}) + \frac{c_a}{c_i} (\delta^{17}O_a - a_{17bs}) + a_{17bs}$ , ‰  |
| $\delta^{18}O_{io}$         | $\delta^{18}O$ of $CO_2$ in the intercellular air space ignoring ternary correction  | $\delta^{18}O_A \left(1 - \frac{c_a}{c_i}\right) (1 + a_{18bs}) + \frac{c_a}{c_i} (\delta^{18}O_a - a_{18bs}) + a_{18bs}$ , ‰  |
| $\delta^{17}O_i$            | $\delta^{17}O$ of $CO_2$ in the intercellular air space  | $\frac{\delta^{17}O_{io} + t^{17}(\delta^{17}O_A(\frac{c_a+1}{c_i}) - \delta^{17}O_e\frac{c_a}{c_i})}{1+t^{17}}$ , ‰   |
| $\delta^{18}O_i$            | $\delta^{18}O$ of $CO_2$ in the intercellular air space  | $\frac{\delta^{18}O_{io} + t^{18}(\delta^{18}O_A(\frac{c_a+1}{c_i}) - \delta^{18}O_e\frac{c_a}{c_i})}{1+t^{18}}$ , ‰   |
| $\delta^{18}O_{trans}$      | $\delta^{18}O$ of transpired water vapour  | $\left(\frac{w_a}{w_a - w_e}\right) (\delta^{18}O_{wa} - \delta^{18}O_{we}) + \delta^{18}O_{we}$ , ‰   |
| $\delta^{18}O_{wes}$        | $\delta^{18}O$ of water at the evaporation site  | $\delta^{18}O_{wes} = \delta^{18}O_{trans} + \varepsilon^{18}k + \varepsilon^{18}equ + \frac{w_a}{w_i} \times (\delta^{18}O_{wa} - \varepsilon^{18}k + \delta^{18}O_{trans})$  |
| $\delta^{17}O_m$            | $\delta^{17}O$ of $CO_2$ at the site of $CO_2$ - $H_2O$ exchange   | $(\delta^{17}O_{wes} + 1) \times (1 + \varepsilon_w^{17}) - 1$ , ‰   |
| $\delta^{18}O_m$            | $\delta^{18}O$ of $CO_2$ at the site of $CO_2$ - $H_2O$ exchange   | $(\delta^{18}O_{wes} + 1) \times (1 + \varepsilon_w^{18}) - 1$ , ‰   |
| $\delta^{13}C_{substrate}$  | Isotope ( $^{13}C$ ) ratio of substrate used for dark respiration  | $\frac{\delta^{13}C_A - \Delta_A^{13}C}{\Delta_A^{13}C + 1}$ , ‰   |
| $\Delta_A^{13}C$            | $^{13}C$ -photosynthetic discrimination  | $\frac{c(\delta^{13}C_a - \delta^{13}C_e)}{1 + \delta^{13}C_a - c(\delta^{13}C_a - \delta^{13}C_e)}$ , ‰   |
| $\Delta_A^{13}C_{obs}$      | $^{13}C$ -photosynthetic discrimination (Farquhar model)   | $\left(\frac{1}{1-t}\right) \left[ a_{13bs} \frac{c_a - c_i}{c_a} + \left(\frac{1+t}{1-t}\right) \left[ a_m \frac{c_i - c_c}{c_a} + b \frac{c_c}{c_a} - \frac{\alpha_b}{\alpha_e} e \frac{R_D}{R_D + A_n} \frac{c_i - \Gamma^*}{c_a} - \frac{\alpha_b}{\alpha_f} f \frac{\Gamma^*}{c_a} \right] \right]$ |
| $\Delta_A^{13}C_i$          | $^{13}C$ -photosynthetic discrimination (assuming no mesophyll conductance, i.e. $c_i = c_c$ )                               | $\left(\frac{1}{1-t}\right) \left[ \frac{c_a - c_i}{c_a} \right] + \left(\frac{1+t}{1-t}\right) \left[ b \frac{c_i}{c_a} - \frac{\alpha_b}{\alpha_e} e \frac{R_D}{R_D + A_n} \frac{c_i - \Gamma^*}{c_a} - \frac{\alpha_b}{\alpha_f} f \frac{\Gamma^*}{c_a} \right]$                                      |
| $\Delta_A^{18}O$            | $^{18}O$ -photosynthetic discrimination  | $\frac{c(\delta^{18}O_a - \delta^{18}O_e)}{1 + \delta^{18}O_a - c(\delta^{18}O_a - \delta^{18}O_e)}$ , ‰   |
| $\Delta_A^{17}O$            | $^{17}O$ -photosynthetic discrimination  | $\frac{c(\delta^{17}O_a - \delta^{17}O_e)}{1 + \delta^{17}O_a - c(\delta^{17}O_a - \delta^{17}O_e)}$ , ‰   |
| $\Delta_A^{17}O_{FM}$       | Farquhar model for $^{17}O$ -photosynthetic discrimination   | $\frac{\bar{\alpha}_{17} + \frac{c_m}{c_a - c_m} \delta^{17}O_{ma}}{1 - \frac{c_m}{c_a - c_m} \delta^{17}O_{ma}}$ , ‰  |
| $\Delta_A^{18}O_{FM}$       | Farquhar model for $^{18}O$ -photosynthetic discrimination   | $\frac{\bar{\alpha}_{18} + \frac{c_m}{c_a - c_m} \delta^{18}O_{ma}}{1 - \frac{c_m}{c_a - c_m} \delta^{18}O_{ma}}$ , ‰  |
| $\delta^{17}O_e$            | $\delta^{17}O$ of $CO_2$ entering the cuvette  | ‰  |
| $\delta^{17}O_a$            | $\delta^{17}O$ of $CO_2$ leaving the cuvette   | ‰  |
| $\delta^{18}O_e$            | $\delta^{18}O$ of $CO_2$ entering the cuvette  | ‰  |
| $\delta^{18}O_a$            | $\delta^{18}O$ of $CO_2$ leaving the cuvette   | ‰  |
| $\delta^{17}O_{ma}$         | $\delta^{17}O$ of $CO_2$ equilibrated with the leaf water at the evaporating site relative to the $CO_2$ leaving the cuvette | $\frac{\delta^{17}O_m - \delta^{17}O_a}{1 - \delta^{18}O_a}$ , ‰   |
| $\delta^{18}O_{ma}$         | $\delta^{18}O$ of $CO_2$ equilibrated with the leaf water at the evaporating site relative to the $CO_2$ leaving the cuvette | $\frac{\delta^{18}O_m - \delta^{18}O_a}{1 - \delta^{18}O_a}$ , ‰   |
| $\delta^{18}O_{we}$         | $\delta^{18}O$ of water vapour entering the cuvette  | WVIA, ‰  |
| $\delta^{18}O_{wa}$         | $\delta^{18}O$ of water vapour leaving the cuvette/leaf surrounding  | WVIA, ‰  |

#### 4.4.2. Discrimination against $^{18}\text{O}$ of $\text{CO}_2$

Figure 4.3a shows discrimination against  $^{18}\text{O}$  associated with photosynthesis ( $\Delta_A^{18}\text{O}$ ) for sunflower, ivy, and maize as a function of the  $c_m/c_a$  ratio.  $\Delta_A^{18}\text{O}$  varies with  $c_m/c_a$ , as found in previous studies (Gillon and Yakir, 2000b; Barbour et al., 2016). For sunflower, we observe  $\Delta_A^{18}\text{O}$  values between 29 ‰ and 64 ‰ for  $c_m/c_a$  between 0.54 and 0.86. Ivy shows a relatively little variation of  $\Delta_A^{18}\text{O}$  around a mean of 22 ‰ for  $c_m/c_a$  between 0.48 and 0.58. For maize,  $\Delta_A^{18}\text{O}$  is lower than for the  $\text{C}_3$  plants measured in this study, with values between 10 ‰ and 20 ‰ for  $c_m/c_a$  between 0.15 and 0.37.

For sunflower changing the irradiance from  $300 \mu\text{mol m}^{-2}\text{s}^{-1}$  (low light, hereafter LL) to  $1200 \mu\text{mol m}^{-2}\text{s}^{-1}$  (high light, hereafter HL) leads to a clear decrease in  $\Delta_A^{18}\text{O}$  (average 22 ‰). For maize, the  $\Delta_A^{18}\text{O}$  change is only 4.4 ‰ on average. For ivy, changing the light intensity does not significantly change the observed  $\Delta_A^{18}\text{O}$ . The solid lines in Figure 4.3a show results of leaf cuvette model calculations, where the dependence of  $\Delta_A^{18}\text{O}$  on  $c_m/c_a$  is explored for a set of calculations with otherwise fixed parameters. The model agrees well with the experimental results except for ivy, where the model overestimates the discrimination.

#### 4.4.3. Discrimination against $\Delta^{17}\text{O}$ of $\text{CO}_2$

The discrimination of photosynthesis against  $\Delta^{17}\text{O}$  of  $\text{CO}_2$  ( $\Delta_A\Delta^{17}\text{O}$ ) is shown in Figure 4.3b.  $\Delta_A\Delta^{17}\text{O}$  is negative for all experiments and it depends strongly on the  $c_m/c_a$  ratio and  $|\Delta_A\Delta^{17}\text{O}|$  increases with  $c_m/c_a$  ratio. For instance, for  $\Delta^{17}\text{O}$  of  $\text{CO}_2$  entering the cuvette of -0.215 ‰,  $\Delta_A\Delta^{17}\text{O}$  is -0.25 ‰ for maize with  $c_m/c_a$  ratio of 0.3, -0.3 ‰ for ivy with  $c_m/c_a$  ratio of 0.5 and -0.5 ‰ for sunflower with  $c_m/c_a$  ratio of 0.7 (Figure 4.3b). For sunflower and ivy,  $\Delta_A\Delta^{17}\text{O}$  is also strongly dependent on the  $\Delta^{17}\text{O}$  of  $\text{CO}_2$  supplied to the cuvette, whereas no significant dependence is found for maize. For an increase in  $\Delta^{17}\text{O}$  of  $\text{CO}_2$  entering the cuvette from -0.215 ‰ to 0.435 ‰,  $\Delta_A\Delta^{17}\text{O}$  increases from -0.3 ‰ to -0.9 ‰ at  $c_m/c_a$  ratio of 0.5 for ivy. For sunflower, an increase in  $\Delta^{17}\text{O}$  of  $\text{CO}_2$  entering the cuvette from -0.215 ‰ to 0.31 ‰ increases  $\Delta_A\Delta^{17}\text{O}$  from -0.8 ‰ to -1.7 ‰ at  $c_m/c_a$  ratio of 0.8. The leaf cuvette model results illustrate the shape of the dependence on the  $c_m/c_a$  ratio and agree well with the experiments. For the leaf cuvette model, the  $\Delta^{17}\text{O}$  value of the water is assigned a constant value of -0.122 ‰ (average  $\Delta^{17}\text{O}$  value for the bulk leaf water).

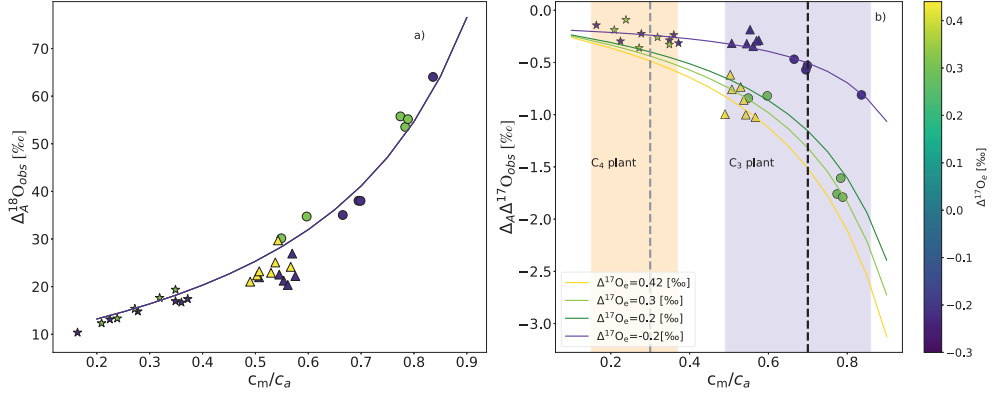


Figure 4.3 a)  $\Delta A^{18}O_{obs}$  during photosynthesis for two C<sub>3</sub> plants, sunflower (circles) and ivy (triangles) and C<sub>4</sub> plant maize (stars) as a function of  $c_m/c_a$ . The solid lines show results from the leaf cuvette model, where  $\delta^{18}O$  of the CO<sub>2</sub> entering the cuvette is 30.47‰. b)  $\Delta A\Delta^{17}O$  of CO<sub>2</sub> as a function of  $c_m/c_a$  for isotopically different CO<sub>2</sub> gases entering the cuvette (color bar shows  $\Delta^{17}O_e$ ) for sunflower (circles), ivy (triangles) and maize (stars).  $\Delta A\Delta^{17}O$  values calculated using the leaf cuvette model are shown as solid lines in corresponding colors ( $\Delta^{17}O_e$  values given in the legend). The shaded areas indicate the  $c_m/c_a$  ranges for C<sub>4</sub> and C<sub>3</sub> plants and the vertical dashed lines indicate the mean  $c_m/c_a$  ratio used for extrapolating from the leaf scale to the global scale. Solid line are leaf cuvette model results for the corresponding  $c_m/c_a$  ratio.

Figure 4.4b shows the same values of  $\Delta A\Delta^{17}O$  as a function of the difference between  $\Delta^{17}O$  of CO<sub>2</sub> entering the leaf and the calculated  $\Delta^{17}O$  of leaf water at the evaporation site where CO<sub>2</sub>-H<sub>2</sub>O exchange takes place ( $\Delta^{17}O_a - \Delta^{17}O_{wes}$ ), for different  $c_m/c_a$  ratios. The leaf cuvette model results (solid lines in Figure 4.4b) suggest a linear dependence between  $\Delta A\Delta^{17}O$  and ( $\Delta^{17}O_a - \Delta^{17}O_{wes}$ ). The experimental results agree with the hypothesis that  $\Delta A\Delta^{17}O$  is linearly dependent on  $\Delta^{17}O_a - \Delta^{17}O_{wes}$  at a certain  $c_m/c_a$  ratio. Figure 4.4a shows the corresponding relation where  $\Delta A\Delta^{17}O$  is divided by  $\Delta^{17}O_a - \Delta^{17}O_m$ .

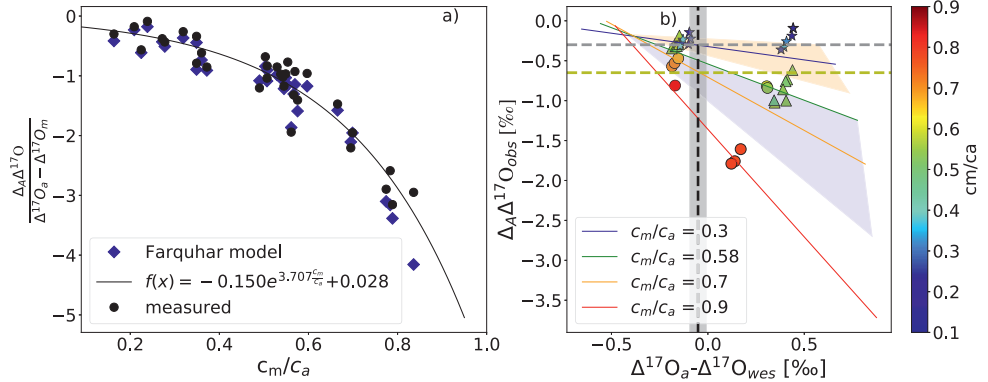


Figure 4.4 a) Dependency of  $\Delta A\Delta^{17}O$  on the relative difference on the  $\Delta^{17}O$  CO<sub>2</sub> entering the leaf and the  $\Delta^{17}O$  of CO<sub>2</sub> in equilibrium with leaf water against  $c_m/c_a$  ratio. b) dependency of  $\Delta A\Delta^{17}O$  on the difference between the  $\Delta^{17}O$  of CO<sub>2</sub> entering the cuvette and the  $\Delta^{17}O$  of leaf water at the evaporation site color coded for different  $c_m/c_a$  ratios. The solid lines are results of the leaf cuvette model for different  $c_m/c_a$  ratios stated in the legend. The dashed vertical black line indicates the difference between the global average  $\Delta^{17}O$  value for CO<sub>2</sub> (-0.168 ‰) and leaf water (-0.067 ‰) (Koren et al., 2019). The gray and yellow horizontal dashed lines indicate  $\Delta A\Delta^{17}O$  of C<sub>4</sub> and C<sub>3</sub> plants for  $c_m/c_a$  ratio of 0.3 and 0.7, respectively globally.

All the values follow the same relationship as function of the  $c_m/c_a$  ratio, which can be approximated quite well by an exponential function (equation 4.5). This function quantifies the dependence of  $\Delta_A \Delta^{17}\text{O}$  on  $c_m/c_a$ , and thus the effect of the diffusion of isotopically exchanged  $\text{CO}_2$  back to the atmosphere, which increases with increasing  $c_m/c_a$  ratio.

$$\frac{\Delta_A \Delta^{17}\text{O}}{\Delta^{17}\text{O}_a - \Delta^{17}\text{O}_m} = -0.150 \times \exp(3.707 \times c_m/c_a) + 0.028 \quad (4.5)$$

Figure 4.5 a and c show results from the leaf cuvette model that illustrates in more detail how  $\Delta^{17}\text{O}_e$  and  $\Delta^{17}\text{O}_{\text{wes}}$  affect  $\Delta^{17}\text{O}_a$  and  $\Delta_A \Delta^{17}\text{O}$  and their dependence on  $c_m/c_a$ . At lower  $c_m/c_a$ , only a very small fraction of  $\text{CO}_2$  that has undergone isotopic equilibration in the mesophyll diffuses back to the atmosphere, and therefore  $\Delta^{17}\text{O}_a$  stays close to the incoming  $\Delta^{17}\text{O}_e$ , modified by the fractionation during  $\text{CO}_2$  diffusion through the stomata (Figure 4.5a). Figure 4.5c confirms that indeed at low  $c_m/c_a$ ,  $\Delta_A \Delta^{17}\text{O}$  approaches the fractionation constant expected for diffusion,  $-0.170 \text{ ‰}$ . This diffusional fractionation is independent of the isotopic composition of the  $\text{CO}_2$  entering the leaf, and therefore at low  $c_m/c_a$ , the  $\Delta_A \Delta^{17}\text{O}$  curves for the different values of the anomaly of the  $\text{CO}_2$  entering the leaf converge. For a high  $c_m/c_a$  ratio, the back-diffusion flux of  $\text{CO}_2$  that has equilibrated with water becomes the dominant factor, and in this case, the isotopic composition of the outgoing  $\text{CO}_2$  converges towards this isotope value, independent of the isotopic composition of the incoming  $\text{CO}_2$  (Figure 4.5a). This can lead to a very wide range of values for the discrimination against  $\Delta^{17}\text{O}$ , because now the effect on  $\Delta^{17}\text{O}$  of the ambient  $\text{CO}_2$  depends strongly on the difference in isotopic composition between incoming  $\text{CO}_2$  and  $\text{CO}_2$  in isotopic equilibrium with the leaf water.

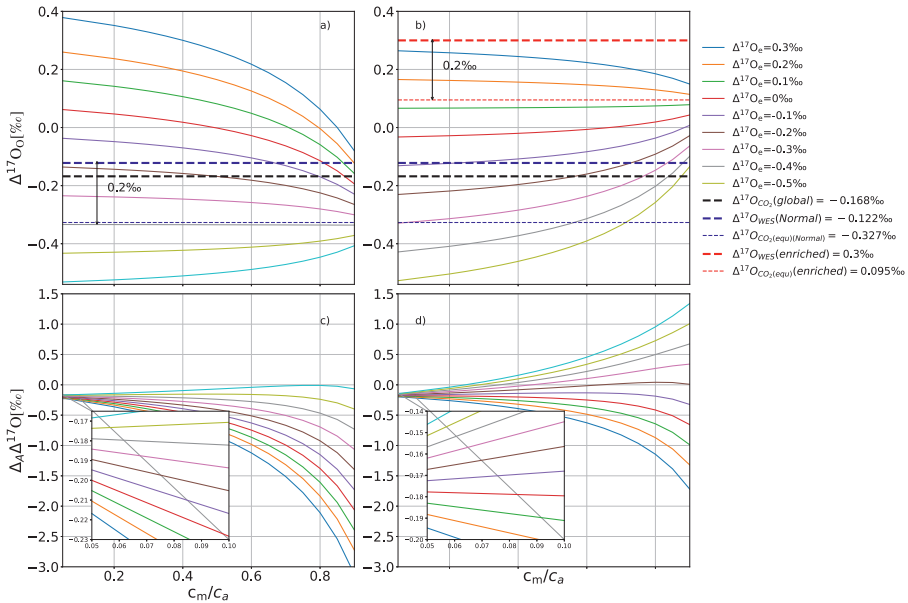


Figure 4.5 a) and b)  $\Delta^{17}\text{O}_a$  as a function of  $c_m/c_a$  for various values of  $\Delta^{17}\text{O}_e$  (see legend) for  $\Delta^{17}\text{O}_{\text{wes}} = -0.122 \text{ ‰}$  in a) and  $\Delta^{17}\text{O}_{\text{wes}} = 0.300 \text{ ‰}$  in b). c) and d) show the corresponding values for  $\Delta_A \Delta^{17}\text{O}$ .  $\Delta^{17}\text{O}_{\text{global}}$  is the global average  $\Delta^{17}\text{O}$  value for atmospheric  $\text{CO}_2$  (Koren et al., 2019). When  $\Delta^{17}\text{O}$  of  $\text{CO}_2$  entering the cuvette is approximately  $0.2 \text{ ‰}$  lower than the  $\Delta^{17}\text{O}$  of leaf water at the  $\text{CO}_2\text{-H}_2\text{O}$  exchange site,  $\Delta^{17}\text{O}$  of the  $\text{CO}_2$  leaving the cuvette does not change when  $c_m/c_a$  vary.

In the model calculations shown in Figure 4.5b and d, the isotopic composition of the water was changed from  $\Delta^{17}\text{O}_{\text{wes}} = -0.122\text{‰}$  to  $0.300\text{‰}$ , whereas all other parameters were kept the same. The value of  $\Delta^{17}\text{O}_e$  for which  $\Delta^{17}\text{O}_a$  does not depend on  $c_m/c_a$  is shifted accordingly, again being similar to  $\Delta^{17}\text{O}_m$ . At low  $c_m/c_a$   $\Delta\Delta^{17}\text{O}$  converges to the same value as in Figure 4.5c, confirming the role of diffusion into the stomata as discussed above.

Figure 4.6 shows how  $\delta^{18}\text{O}$  and  $\Delta^{17}\text{O}$  vary in key compartments of the leaf cuvette system that determine the oxygen isotope effects associated with photosynthesis, based on the previously established three-isotope slopes of the various processes (Figure 4.1). The irrigation water has a  $\Delta^{17}\text{O}$  value of  $0.017$ . The measured bulk leaf water is  $6\text{--}16\text{‰}$  enriched in  $^{18}\text{O}$  and its  $\Delta^{17}\text{O}$  value is lower by  $-0.075$  to  $-0.200\text{‰}$  (mean value  $-0.121\text{‰}$ ) than the irrigation water, calculated using a three-isotope slope of  $\lambda_{\text{trans}} = 0.516$  at  $80\%$  humidity (Landais et al., 2006).  $\Delta^{17}\text{O}$  of leaf water at the evaporation site, calculated from the transpired water, has slightly lower  $\Delta^{17}\text{O}$ , with values between  $-0.119\text{‰}$  and  $-0.237\text{‰}$  (average  $-0.184\text{‰}$ ). Note that the bulk leaf water was not measured for all the experiments. For the experiments where the bulk leaf water is measured,  $\Delta^{17}\text{O}$  of leaf water at the evaporation site ranges from  $-0.160\text{‰}$  to  $-0.231\text{‰}$  with an average value of  $-0.190 \pm 0.020\text{‰}$ . The calculated isotopic composition of water at the exchange site was thus similar, but slightly lower in  $\Delta^{17}\text{O}$  than the values measured for bulk leaf water.  $\text{CO}_2$  exchanges with the water in the leaf with a well-established fractionation constant (see equation S4.17, supplementary material) and a three-isotope slope of  $\lambda_{\text{CO}_2\text{-H}_2\text{O}} = 0.5229$  (Barkan and Luz, 2012), leading to the lower  $\Delta^{17}\text{O}$  values of the equilibrated  $\text{CO}_2$ . In our experiments, the  $\Delta^{17}\text{O}$  value of  $\text{CO}_2$  in equilibrium with leaf water is lower than the  $\Delta^{17}\text{O}$  value of  $\text{CO}_2$  entering the leaf. The  $\Delta^{17}\text{O}$  of the  $\text{CO}_2$  in the intercellular air space is a mixture between two end members, the  $\Delta^{17}\text{O}$  of the  $\text{CO}_2$  entering the leaf and  $\Delta^{17}\text{O}$  of the  $\text{CO}_2$  in equilibrium with leaf water. This explains why the observed values of  $\Delta\Delta^{17}\text{O}$  are negative for the experiments performed in this study.

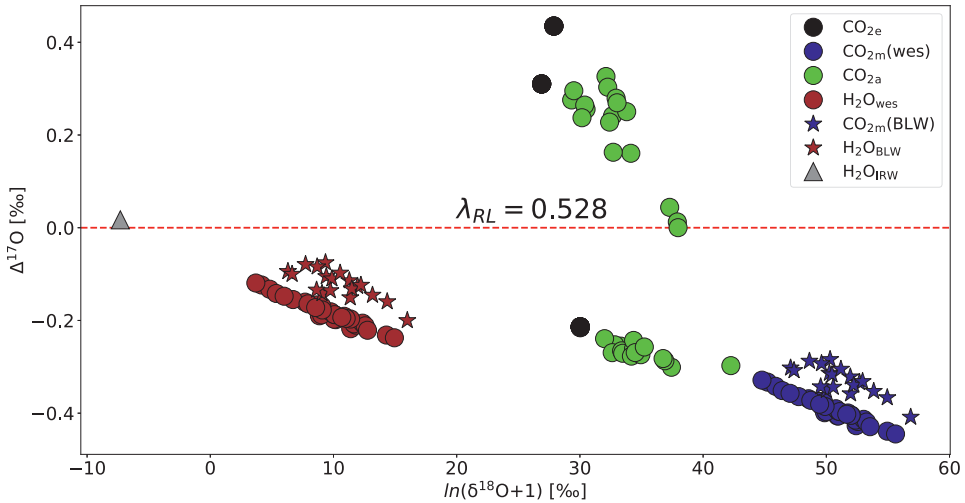


Figure 4.6 Isotopic composition of various relevant oxygen reservoirs that affect the  $\Delta^{17}\text{O}$  of atmospheric  $\text{CO}_2$  during photosynthesis: irrigation water (grey triangle), calculated leaf water at the evaporation site (brown circles), measured bulk leaf water (brown star),  $\text{CO}_2$  entering the cuvette (black circles),  $\text{CO}_2$  leaving the leaf cuvette (green circles),  $\text{CO}_2$  equilibrated with leaf water at the evaporation site (blue circles),  $\text{CO}_2$  equilibrated with bulk leaf water (blue stars).  $\Delta^{17}\text{O}$  is calculated with  $\lambda=0.528$ .

## 4.5. Discussion

### 4.5.1. Discrimination against $^{18}\text{O}$ of $\text{CO}_2$

The higher  $\Delta_A^{18}\text{O}_{\text{obs}}$  values for sunflower compared to maize and ivy (Figure 4.3a) are mainly due to a higher back-diffusion flux ( $c_m/(c_a - c_m)$ ). The back-diffusion flux is higher for the  $\text{C}_3$  plants sunflower and ivy than for the  $\text{C}_4$  plant maize, a consequence of the lower stomatal conductance and higher assimilation rate of  $\text{C}_4$  plants (Gillon and Yakir, 2000b; Barbour et al., 2016). In  $\text{C}_4$  plants most of the  $\text{CO}_2$  entering the stomata is carboxylated by PEPC resulting in a lower  $\text{CO}_2$  mixing ratio in the mesophyll which results in a lower back-diffusion flux. The increase of assimilation rate with higher light intensity decreases the  $c_m/c_a$  ratio and thus leads to a lower back-diffusion flux, which explains the decreases of  $\Delta_A^{18}\text{O}_{\text{obs}}$  for maize and most clearly for sunflower. A similar trend of increase in  $\Delta_A^{18}\text{O}_{\text{obs}}$  with an increase in  $c_m/c_a$  ratio has been reported in previous studies (Gillon and Yakir, 2000a, b; Osborn et al., 2017). For ivy,  $\Delta_A^{18}\text{O}_{\text{obs}}$  and  $\Delta_A^{17}\text{O}_{\text{obs}}$  do not decrease with an increase in irradiance, because the change in assimilation rate with irradiance is small. Thus,  $c_m$  will not decrease strongly and the effect on the back diffusion is smaller than the variability in  $\Delta_A^{18}\text{O}_{\text{obs}}$  of different leaves of the same plant.

In our experiments, photosynthesis causes enrichment in  $\delta^{18}\text{O}$  of atmospheric  $\text{CO}_2$  for both  $\text{C}_3$  and  $\text{C}_4$  plants, i.e. positive values  $\Delta_A^{18}\text{O}$ . In principle,  $\Delta_A^{18}\text{O}$  can also be negative if the  $\delta^{18}\text{O}_m$  are depleted relative to the ambient  $\text{CO}_2$ . This is in contrast to  $\Delta_A^{13}\text{C}$ , which will always be positive since it is determined by the fractionation due to the PEPC and RuBisCO enzyme activity (Figure S4.8 and S4.9, supplementary material). In general, in our experiments, the  $\Delta_A^{18}\text{O}_{\text{obs}}$  values are about five times larger than  $\delta^{18}\text{O}_a - \delta^{18}\text{O}_e$ , the  $\delta^{18}\text{O}$  difference between  $\text{CO}_2$  entering and leaving the cuvette (Figure S4.10 to S4.12 supplementary material). This is easy to understand from the definition of  $\Delta_A$ . Taking  $\Delta_A^{18}\text{O}$  as an example,  $\Delta_A^{18}\text{O}_{\text{obs}} = \frac{\zeta(\delta^{18}\text{O}_a - \delta^{18}\text{O}_e)}{1 + \delta^{18}\text{O}_a - \zeta(\delta^{18}\text{O}_a - \delta^{18}\text{O}_e)} \approx \zeta(\delta^{18}\text{O}_a - \delta^{18}\text{O}_e)$  and in our experiments,  $\zeta = c_e / (c_e - c_a) \approx 500 / (500 - 400) = 5$ .

### 4.5.2. Discrimination against the $\Delta^{17}\text{O}$ of $\text{CO}_2$

The leaf cuvette model includes the isotope fractionations of all the individual processes that have been quantified in dedicated experiments previously (Figure 4.1). The good agreement of the model results with the measurements (Figure 4.3a) demonstrates that when all these processes are combined in the quantitative description of a gas exchange experiment, they actually result in a correct quantification of the isotope effects associated with photosynthesis. This has already been demonstrated before for  $\Delta_A^{18}\text{O}_{\text{obs}}$  but has now been confirmed for  $\Delta_A\Delta^{17}\text{O}$ .

Unlike ivy and sunflower, maize does not show a significant change in  $\Delta_A\Delta^{17}\text{O}$  when  $\text{CO}_2$  gases with different  $\Delta^{17}\text{O}$  are supplied to the plant. The  $\text{C}_4$  plant maize has a small back-diffusion flux due to its high assimilation rate and low stomatal conductance, leading to a low  $c_m/c_a$  ratio. At low  $c_m/c_a$  ratios,  $\Delta_A\Delta^{17}\text{O}$  is expected to be close to the weighted fractionation



due to diffusion through boundary layer and stomata. In general, the effect of diffusion on  $\Delta^{17}\text{O}$  of atmospheric  $\text{CO}_2$  can be expressed as follows:

$$\Delta^{17}\text{O}_{\text{Modified}} = \Delta^{17}\text{O}_a + (\lambda_{\text{RL}} - \lambda_{\text{diffusion}}) \times \ln \alpha_{\text{diffusion}} \quad (4.6)$$

where  $\Delta^{17}\text{O}_a$  is the  $\Delta^{17}\text{O}$  of the  $\text{CO}_2$  surrounding the leaf,  $\Delta^{17}\text{O}_{\text{modified}}$  is the  $\Delta^{17}\text{O}$  of the  $\text{CO}_2$  modified due to diffusional fractionation and  $\lambda_{\text{diffusion}}$ ,  $\lambda_{\text{RL}}$  and  $\alpha_{\text{diffusion}}$  are the oxygen three-isotope relationships during diffusion from the  $\text{CO}_2$ - $\text{H}_2\text{O}$  exchange site to the atmosphere, the reference slope used and the fractionation against  $^{18}\text{O}$  for  $\text{CO}_2$  during diffusion through the stomata. Using the values  $\lambda_{\text{RL}} = 0.528$ ,  $\lambda_{\text{diffusion}} = 0.509$  (Young et al., 2002) and  $\alpha_{\text{diffusion}} = 0.9912$  (Farquhar and Lloyd, 1993), the effect of diffusional fractionation on the  $\Delta^{17}\text{O}$  of atmospheric  $\text{CO}_2$  is  $-0.168 \text{ ‰}$  regardless of the anomaly of the  $\text{CO}_2$  entering the leaf, and the model results confirm this at low  $c_m/c_a$  ratio (Figure 4.5 c and d, inset).

At a high  $c_m/c_a$  ratio,  $\Delta^{17}\text{O}_a$  is dominated by the back-diffusion flux of  $\text{CO}_2$  that has equilibrated with water. As a consequence,  $\Delta^{17}\text{O}_a$  converges to a common value that is independent of the anomaly of the  $\text{CO}_2$  entering the cuvette and is determined by the isotopic composition of leaf water,  $\Delta^{17}\text{O}_m$ . In fact, when  $\Delta^{17}\text{O}_a = \Delta^{17}\text{O}_m$ ,  $\Delta^{17}\text{O}_a$  does not change with  $c_m/c_a$ , indicating that in this case the  $\Delta^{17}\text{O}$  of the  $\text{CO}_2$  diffusing back from the leaf is the same as the  $\Delta^{17}\text{O}(\text{CO}_2)$  entering the leaf.

$\bar{a}_{18}$  is the overall discrimination occurring during the diffusion of  $^{12}\text{C}^{18}\text{O}^{16}\text{O}$  from the ambient air surrounding the leaf to the  $\text{CO}_2$ - $\text{H}_2\text{O}$  exchange site (see Table 4.2 for the list of variables). In our study  $\bar{a}_{18}$  ranges from  $5 \text{ ‰}$  to  $7.2 \text{ ‰}$ , lower than the literature estimate of  $7.4 \text{ ‰}$  (Farquhar et al., 1993).  $\bar{a}_{18}$  depends on the ratio of stomatal conductance, which is associated with a strong fractionation of  $8.8 \text{ ‰}$ , to mesophyll conductance with an associated fractionation of only  $0.8 \text{ ‰}$ . Therefore, the higher the ratio ( $g_s/g_{m18}$ ) the lower the  $\bar{a}_{18}$  (Table S4.2, supplementary material). The difference in  $\bar{a}_{18}$  of  $2.4 \text{ ‰}$  between the literature value of  $7.4 \text{ ‰}$  and the lowest  $\bar{a}_{18}$  estimate in this study will introduce an error of only  $0.046 \text{ ‰}$  in the  $\Delta^{17}\text{O}$  value (see equation 4.6). The uncertainty  $\bar{a}_{18}$  has lower influence on the  $\Delta_A \Delta^{17}\text{O}$  of  $\text{C}_3$  plants compared to  $\text{C}_4$  plants since the diffusional fractionation is less important at the higher  $c_m/c_a$  ratio where  $\text{C}_3$  plants operate.

### 4.5.3. Global average value of $\Delta_A \Delta^{17}\text{O}$ and $\Delta^{17}\text{O}$ isoflux

We can use the established relationship between  $\Delta_A \Delta^{17}\text{O}$  and  $\Delta^{17}\text{O}_a - \Delta^{17}\text{O}_{\text{wes}}$  for a certain  $c_m/c_a$  ratio to provide a bottom-up estimate for the global effect of photosynthesis on  $\Delta^{17}\text{O}$  in atmospheric  $\text{CO}_2$ , based on data obtained in real gas exchange experiments. For this, we use results from a recent modeling study, which provides global average values for  $\text{CO}_2$  and leaf water ( $\Delta^{17}\text{O}(\text{CO}_2) = -0.168 \text{ ‰}$ ,  $\Delta^{17}\text{O}(\text{H}_2\text{O}_{\text{-leaf}}) = -0.067 \text{ ‰}$ ; (Koren et al., 2019); Figure S4.13 and 4.14, supplementary material). The  $\Delta^{17}\text{O}(\text{CO}_2)$  values agree well with the limited amount of available measurements (Table 4.3).

Table 4.3 Summary for the parameters used of the extrapolation of leaf scale experiments to the global scale and the results obtained, and  $\Delta^{17}\text{O}$  value of tropospheric  $\text{CO}_2$  available measurements.

| <b>Parameters and values used for global estimation</b>  |                                 |  |
|--|---------------------------------|--|
| Parameter  | Value                           | ref  |
| GPP  | 120 PgCyr <sup>-1</sup>         | (Beer et al., 2010)                        |
| $f_{C4}$   | 23 %                            | (Still et al., 2003)                       |
| $f_{C3}$   | 77 %                            | (Still et al., 2003)                       |
| $c_m/c_a$ ( $\text{C}_3$ )   | 0.7                             | (Hoag et al., 2005)                        |
| $c_m/c_a$ ( $\text{C}_4$ )   | 0.3                             | (Hoag et al., 2005)                        |
| $\Delta^{17}\text{O}$ leaf water (global mean, modelled)   | -0.067±0.04 ‰                   | (Koren et al., 2019)                       |
| $\Delta^{17}\text{O}$ $\text{CO}_2$ (global mean, modelled)  | -0.168±0.013 ‰                  | (Koren et al., 2019)                       |
| $\Delta_A\Delta^{17}\text{O}$ (global mean for $\text{C}_4$ )  | -0.3±0.18 ‰                     | (Figure 4.5b, for $c_m/c_a$ ratio of 0.3)  |
| $\Delta_A\Delta^{17}\text{O}$ (global mean for $\text{C}_3$ )  | -0.65±0.18 ‰                    | (Figure 4.5b, for $c_m/c_a$ ratio of 0.7)  |
| $\Delta_A\Delta^{17}\text{O}$ (global mean for whole vegetation)   | -0.57±0.14 ‰                    | (Equation 4.13)                            |
| $\Delta_A\Delta^{17}\text{O}$ -isoflux (global mean for $\text{C}_4$ )   | -7.3±4 ‰PgCyr <sup>-1</sup>     | (Equation 4.14, only for $\text{C}_4$ )    |
| $\Delta_A\Delta^{17}\text{O}$ -isoflux (global mean for $\text{C}_3$ )   | -53±15 ‰PgCyr <sup>-1</sup>     | (Equation 4.14, only for $\text{C}_3$ )    |
| $\Delta_A\Delta^{17}\text{O}$ -isoflux (global mean for whole vegetation)  | -60±15 ‰PgCyr <sup>-1</sup>     | (equation 4.14)                            |
| $\Delta_A\Delta^{17}\text{O}$ -isoflux (global mean for whole vegetation)  | -47 ‰PgCyr <sup>-1</sup>        | (Hoag et al., 2005)                        |
| $\Delta_A\Delta^{17}\text{O}$ -isoflux (global mean for whole vegetation)  | -42 to -92 ‰PgCyr <sup>-1</sup> | (Hofmann et al., 2017)                     |
| <b><math>\Delta^{17}\text{O}</math> value of tropospheric <math>\text{CO}_2</math></b>                                   |                                 |  |
| $\Delta^{17}\text{O}(\text{CO}_2)$ for $\text{CO}_2$ samples collected in La Jolla-UCSD (California, USA) (1990 to 2000) | -0.173±0.046 ‰                  | (Thiemens et al., 2014)                    |
| $\Delta^{17}\text{O}(\text{CO}_2)$ for $\text{CO}_2$ samples collected in Israel   | 0.034±0.010 ‰                   | (Barkan and Luz, 2012)                     |
| $\Delta^{17}\text{O}(\text{CO}_2)$ for $\text{CO}_2$ samples collected in South China sea (2013-2014)                    | -0.159±0.084 ‰                  | (Liang et al., 2017a; Liang et al., 2017b) |
| $\Delta^{17}\text{O}(\text{CO}_2)$ for $\text{CO}_2$ samples collected in Taiwan (2012-2015)                             | -0.150±0.080 ‰                  | (Liang et al., 2017a; Liang et al., 2017b) |
| $\Delta^{17}\text{O}(\text{CO}_2)$ for $\text{CO}_2$ samples collected in California (USA) (2015)                        | -0.177±0.029 ‰                  | (Liang et al., 2017a; Liang et al., 2017b) |
| $\Delta^{17}\text{O}(\text{CO}_2)$ for $\text{CO}_2$ samples collected in Göttingen (Germany) (2010-2012)                | -0.122±0.065 ‰                  | (Hofmann et al., 2017)                     |

To extrapolate  $\Delta_A\Delta^{17}\text{O}$  determined in the leaf scale experiments to the global scale, global average  $c_m/c_a$  ratios of 0.7 and 0.3 are used for  $\text{C}_3$  and  $\text{C}_4$  plants, respectively, similar to previous studies (Hoag et al., 2005; Liang et al., 2017b). From SIBCASA model results we obtained an annual variability of  $c_i/c_a$  values with a standard deviation of 0.12 and 0.17 for  $\text{C}_4$  and  $\text{C}_3$  plants respectively (Figure S4.15, supplementary material) (Schaefer et al., 2008; Koren et al., 2019). We use this variability as upper limit of the error estimate for  $c_m/c_a$  as shown in the light orange and light pink shaded areas in Figure 4.4b. This error is converted to an error

in  $\Delta_A \Delta^{17}\text{O}$  using the relation with  $c_m/c_a$ . Based on the linear dependency of  $\Delta_A \Delta^{17}\text{O}$  and  $\Delta^{17}\text{O}_a - \Delta^{17}\text{O}_{\text{wes}}$ , we estimate the  $\Delta_A \Delta^{17}\text{O}$  for tropospheric  $\text{CO}_2$  based on the  $\Delta^{17}\text{O}$  of leaf water and  $c_m/c_a$  ratio. In Figure 4.4b, the dashed black vertical line indicates  $\Delta^{17}\text{O}_a - \Delta^{17}\text{O}_{\text{wes}}$  obtained from the 3D global model (Koren et al., 2019). The results of the global estimate and parameters used for the extrapolation of leaf scale study to the global scale are summarized in Table 4.3.

The  $\delta^{17}\text{O}$  value of atmospheric  $\text{CO}_2$  (21.53 ‰) is calculated from the global  $\delta^{18}\text{O}$  and  $\Delta^{17}\text{O}$  values (41.5 ‰ and -0.168 ‰, respectively) (Koren et al., 2019). The  $\delta^{17}\text{O}$  and  $\delta^{18}\text{O}$  values of global mean leaf water are calculated from the soil water. A global mean  $\delta^{18}\text{O}$  value of soil water is -8.4 ‰ assuming soil water to be similar to precipitation (Bowen and Revenaugh, 2003; Koren et al., 2019). The  $\delta^{17}\text{O}$  value of soil water is -4.4 ‰, calculated using equation 4.7 (Luz and Barkan, 2010).

$$\ln(\delta^{17}\text{O}_{\text{soil}} + 1) = 0.528 \times \ln(\delta^{18}\text{O}_{\text{soil}} + 1) + 0.033 \quad (4.7)$$

$\delta^{17}\text{O}$  and  $\delta^{18}\text{O}$  of leaf water are calculated from  $\delta^{17}\text{O}$  and  $\delta^{18}\text{O}$  of soil water with fractionation factors of 1.0043 and 1.0084, respectively (Hofmann et al., 2017; Koren et al., 2019). The fractionation factor for  $\delta^{17}\text{O}$  is calculated using  $\alpha^{17} = (\alpha^{18})^{\lambda_{\text{trans}}}$  with  $\lambda_{\text{trans}} = 0.516$ , assuming relative humidity to be 75 % (Landais et al., 2006). The  $\delta^{17}\text{O}$  and  $\delta^{18}\text{O}$  values of global mean leaf water are then -0.136 ‰ and -0.131 ‰, respectively. Thus, the difference between global atmospheric  $\text{CO}_2$  and leaf water is  $\delta^{17}\text{O}_{\text{CO}_2 - \text{water}} = 21.666$  ‰ and  $\delta^{18}\text{O}_{\text{CO}_2 - \text{water}} = 41.631$  ‰. This yields  $\Delta^{17}\text{O}_{\text{CO}_2 - \text{water}} = -0.101$  ‰, and this value is indicated as dashed black line in Figure 4.4. The grey shaded area indicates the propagated error using the standard deviation of the relevant parameters in 180 x 360 grid boxes for 12 months of leaf water and 45 x 60 grid boxes for 24 months for  $\text{CO}_2$  (Koren et al., 2019). In Figure 4.4b, the intersection between the dashed black vertical line and the discrimination lines for the representative  $c_m/c_a$  ratios of  $\text{C}_3$  and  $\text{C}_4$  plants corresponds to the  $\Delta_A \Delta^{17}\text{O}$  value of  $\text{C}_3$  and  $\text{C}_4$  plants. For  $\text{C}_4$  plants ( $c_m/c_a = 0.3$ ) this yields  $\Delta_A \Delta^{17}\text{O} = -0.3$  ‰ (gray dashed line in Figure 4.4b) and for  $\text{C}_3$  plants ( $c_m/c_a = 0.7$ ),  $\Delta_A \Delta^{17}\text{O} = -0.65$  ‰ (black dashed line in Figure 4.4b).

Three main factors contribute to the uncertainty of the extrapolated  $\Delta_A \Delta^{17}\text{O}$  value. The first is the measurement error, which contributes 0.25 ‰ (standard error for individual experiments). The second factor is the uncertainty in the difference between  $\Delta^{17}\text{O}$  of atmospheric  $\text{CO}_2$  and leaf water, and we use results from the global model to estimate an error. For  $\Delta^{17}\text{O}$  of atmospheric  $\text{CO}_2$ , statistics for all 45 x 60 grid boxes for 24 months (2012-2013) show a range of -0.218 ‰ to -0.151 ‰, with a mean of -0.168 ‰ and a standard deviation of 0.013 ‰ (Figure S4.13, supplementary material). For  $\Delta^{17}\text{O}$  of the leaf water statistics for all 180 x 360 grid boxes for 12 months show a range of -0.236 ‰ and -0.027 ‰ (Figure S4.14, supplementary material). The mean is -0.067 ‰ with a standard deviation of 0.041 ‰. From the combined errors we estimate the error in  $(\Delta^{17}\text{O}_a - \Delta^{17}\text{O}_{\text{wes}})$  to be 0.043 ‰. The third uncertainty in the extrapolation of  $\Delta^{17}\text{O}$  comes from the uncertainty in the  $c_m/c_a$  ratio. For  $\text{C}_3$  and  $\text{C}_4$  plants, these errors are indicated by the light orange and light blue shadings in Figure 4.4b.

Taking these uncertainties into account leads to a mean value of  $\Delta_A \Delta^{17}\text{O} = -0.3 \pm 0.18$  ‰ for  $\text{C}_4$  plants and  $\Delta_A \Delta^{17}\text{O} = -0.65 \pm 0.18$  ‰ for  $\text{C}_3$  plants. The leaf scale discrimination against  $\Delta^{17}\text{O}$  is then extrapolated to global vegetation using these representative values of  $\Delta_A \Delta^{17}\text{O}$  and the relative fractions of photosynthesis by  $\text{C}_4$  and  $\text{C}_3$  plants, respectively as:

$$\Delta_A \Delta^{17}\text{O}_{\text{global}} = f_{C4} \times \Delta_A \Delta^{17}\text{O}_{C4} + f_{C3} \times \Delta_A \Delta^{17}\text{O}_{C3} \quad (4.8)$$

where  $f_{C4}$  and  $f_{C3}$  are the photosynthesis weighted global coverage of  $C_4$  and  $C_3$  vegetation.  $\Delta_A \Delta^{17}\text{O}_{C4}$  and  $\Delta_A \Delta^{17}\text{O}_{C3}$  quantify the discrimination against  $\Delta^{17}\text{O}$  by  $C_4$  and  $C_3$  plants, which are calculated using estimated values of  $c_m/c_a$  from a model. Using assimilation weighted fractions of 23 % for  $C_4$  and 77 % for  $C_3$  vegetation (Still et al., 2003), the global mean value of  $\Delta_A \Delta^{17}\text{O}$  obtained from equation 4.8 is  $-0.57 \pm 0.14$  ‰.

Isoflux is the product of isotope composition and gross mass flux of the molecule. In the case of assimilation, the net flux  $F_A = F_{AL} - F_{LA}$  is multiplied with the discrimination associated with assimilation (Ciais et al., 1997a).  $F_{LA}$  and  $F_{AL}$  are total  $\text{CO}_2$  fluxes from leaf to the atmosphere and from atmosphere to leaf, respectively. The global scale  $\Delta^{17}\text{O}_A$  isoflux is calculated by multiplying the discrimination with the assimilation flux as:

$$F_A \times \Delta_A \Delta^{17}\text{O} = A \times (f_{C4} \times \Delta_A \Delta^{17}\text{O}_{C4} + f_{C3} \times \Delta_A \Delta^{17}\text{O}_{C3}) \quad (4.9)$$

where,  $A = 0.88 \times \text{GPP}$  is the terrestrial assimilation rate. The factor 0.88 accounts for the fraction of  $\text{CO}_2$  released due to autotrophic respiration (Ciais et al., 1997a). The  $\Delta_A \Delta^{17}\text{O}$  isoflux due to photosynthesis is calculated using a GPP value of  $120 \text{ PgCyr}^{-1}$  (Beer et al., 2010) and  $A = 0.88 \times \text{GPP}$ , resulting in an isoflux of  $-60 \pm 15$  ‰  $\text{PgCyr}^{-1}$  globally. This is the first global estimate of  $\Delta_A \Delta^{17}\text{O}$  based on direct measurements of the discrimination during assimilation. Our value is in good agreement with previous model estimates. Hofmann et al. (2017) estimated an isoflux ranging from  $-42$  to  $-92$  ‰  $\text{PgCyr}^{-1}$  (converted to a reference line with  $\lambda = 0.528$ ) using an average  $c_m/c_a$  ratio of 0.7 for both  $C_4$  and  $C_3$  plants and  $\Delta^{17}\text{O}$  of  $-0.147$  ‰ for atmospheric  $\text{CO}_2$ . A model-estimated value from (Hoag et al., 2005) is  $-47$  ‰  $\text{PgCyr}^{-1}$  (converted to our reference slope of  $\lambda = 0.528$ ), derived with a more simple model and using  $\Delta^{17}\text{O}$  of  $-0.146$  ‰ with  $c_m/c_a$  ratio of 0.33 and 0.66 for  $C_4$  and  $C_3$  plants, respectively.

The main uncertainty in the extrapolation of  $\Delta_A \Delta^{17}\text{O}$  from the leaf experiments to the global scale is the uncertainty in the  $c_m/c_a$  ratio. The error from the uncertainty in  $c_m/c_a$  ratio increases when the relative difference in  $\Delta^{17}\text{O}$  between  $\text{CO}_2$  and leaf water increases (Figure 4.5b). It is difficult to determine a single representative  $c_m$  value for different plants because this value would need to be properly weighted with temperature, irradiance,  $\text{CO}_2$  mole fraction and other environmental factors (Flexas et al., 2008; 2012; Shrestha et al., 2019). Recent developments in laser spectroscopy techniques (McManus et al., 2005; Nelson et al., 2008; Tuzson et al., 2008; Kammer et al., 2011) might enable more and easier measurements of  $c_m/c_a$  both in the laboratory and under field conditions. This could lead to a better understanding of variations in the  $c_m/c_a$  ratio among plant species and, temporally, spatially and environmentally.

## 4.6. Conclusions

In order to directly quantify the effect of photosynthetic gas exchange on the  $\Delta^{17}\text{O}$  of atmospheric  $\text{CO}_2$ , gas exchange experiments were carried out in leaf cuvettes using two  $C_3$  plants (sunflower and ivy) and one  $C_4$  plant (maize) with isotopically normal and slightly anomalous ( $^{17}\text{O}$ -enriched)  $\text{CO}_2$ . Results for  $^{18}\text{O}$  agree with results reported in the literature previously. Our results for  $\Delta^{17}\text{O}$  confirm that the formalism developed by Farquhar and others

for  $\delta^{18}\text{O}$  is also applicable to the evaluation of  $\Delta^{17}\text{O}$ . In particular, our experiments confirm that two parameters determine the effect of photosynthesis on  $\text{CO}_2$ : 1) the  $\Delta^{17}\text{O}$  difference between the incoming  $\text{CO}_2$  and  $\text{CO}_2$  in equilibrium with leaf water and 2) the  $c_m/c_a$  ratio, which determines the degree of back-flux of isotopically exchanged  $\text{CO}_2$  from the mesophyll to the atmosphere. At low  $c_m/c_a$  ratios,  $\Delta_A\Delta^{17}\text{O}$  is mainly influenced by the diffusional fractionation. Under our experimental conditions, the isotopic effect increased with  $c_m/c_a$ , e.g.  $\Delta_A\Delta^{17}\text{O}$  was -0.3 ‰ and -0.65 ‰ for maize and sunflower with  $c_m/c_a$  ratios of 0.3 and 0.7, respectively. However, experiments with mass independently fractionated  $\text{CO}_2$  demonstrate that the results depend strongly on the  $\Delta^{17}\text{O}$  difference between the incoming  $\text{CO}_2$  and  $\text{CO}_2$  in equilibrium with leaf water. This is supported by calculations with a leaf cuvette model.

$\delta^{18}\text{O}$  is largely affected by kinetic and equilibrium processes between  $\text{CO}_2$  and leaf water, and also leaf water isotopic inhomogeneity and dynamics. The  $\Delta^{17}\text{O}$  variation is much smaller compared to  $\delta^{18}\text{O}$  and is better defined since conventional bio-geo-chemical processes that modify  $\delta^{17}\text{O}$  and  $\delta^{18}\text{O}$  follow a well-defined three-isotope fractionation slope. Results from the leaf exchange experiments were upscaled to the global atmosphere using modeled values for  $\Delta^{17}\text{O}$  of leaf water and  $\text{CO}_2$ , which results in  $\Delta_A\Delta^{17}\text{O} = -0.57 \pm 0.14$  ‰ and a value for the  $\Delta^{17}\text{O}$  isoflux of  $-60 \pm 15$  ‰  $\text{PgCyr}^{-1}$ . This is the first study that provides such an estimate based on direct leaf chamber measurements, and the results agree with previous  $\Delta^{17}\text{O}$  calculations. The largest contribution to the uncertainty originates from uncertainty in the  $c_m/c_a$  ratio and the largest contributions to the isoflux come from  $\text{C}_3$  plants, which have both a higher share of the total assimilation and higher discrimination.  $\Delta_A\Delta^{17}\text{O}$  is less sensitive to  $c_m/c_a$  ratios at lower values of  $c_m/c_a$ , for instance for  $\text{C}_4$  plants, maize.

$\Delta^{17}\text{O}$  of tropospheric  $\text{CO}_2$  is controlled by photosynthetic gas exchange, respiration, soil invasion, and stratospheric influx. The stratospheric flux is well established and the effect of photosynthetic gas exchange can now be quantified more precisely. To untangle the contribution of each component to the  $\Delta^{17}\text{O}$  atmospheric  $\text{CO}_2$  we recommend measuring the effects of foliage respiration and soil invasion both in the laboratory and at the ecosystem scale.

#### Code and data availability.

The data used in this study are included in the paper either with figures or tables. The python code for the cuvette model is available at [https://git.wur.nl/leaf\\_model/D17O](https://git.wur.nl/leaf_model/D17O).

#### Author contributions

GAA and TR designed the main idea of the study. GAA and TP designed the leaf cuvette setup. TP monitors plant growth. GAA and TR designed the  $\text{CO}_2$  extraction and  $\text{CO}_2\text{-H}_2\text{O}$  exchange system. GAA conducted all the measurements. GK provided the leaf cuvette model. WP enabled the work within the ASICA project. All authors discussed the results at different steps of the project. GAA and TR prepared the manuscript with contributions from all the co-authors.

#### Competing interests

The authors declare that they have no conflict of interest.

## Acknowledgments

The authors thank Leonard I. Wassenaar and Stefan Terzer-Wassmuth from the International Atomic and Energy Agency, Vienna for supplying water standards. The authors thank Eugeni Barkan and Rolf Vieten from the Hebrew University of Jerusalem for calibration of our O<sub>2</sub> and CO<sub>2</sub> working gases. We are grateful to Amaelle Landais from Laboratoire des Sciences Du Climat et de l'Environnement Université Paris-Saclay for measuring the  $\Delta^{17}\text{O}$  of leaf water samples for our study. The authors thank Amzad Laskar for useful discussion during the design of the experiment. This work is funded by the EU ERC project ASICA.

## 4.7. Supplementary material

### 4.7.1. Gas exchange parameters

Leaf exchange parameters are calculated following von Caemmerer and Farquhar (1981). The transpiration rate ( $E$ ) is calculated from the air flowrate, leaf area and concentration of water vapor entering and leaving the cuvette as:

$$E = \frac{u_e}{s} \times \left( \frac{w_a - w_e}{1 - w_a} \right) \quad (\text{S4.1})$$

where  $w_e$ ,  $w_a$  are the mole fractions of water entering ( $e$ ) and leaving ( $a$ ) the cuvette,  $u_e$  is the flowrate of air entering the cuvette and  $s$  is the leaf surface area. The assimilation rate ( $A_n$ ) is calculated as:

$$A_n = \frac{u_e}{s} \times \left( c_e - c_a \times \left( \frac{1 - w_e}{1 - w_a} \right) \right) \quad (\text{S4.2})$$

where  $c_e$  and  $c_a$  are the mole fractions of  $\text{CO}_2$  leaving and entering the cuvette. The total conductance for water vapor ( $g_{wa}^t$ ) is calculated as:

$$g_{wa}^t = E \times \left( \frac{1 - \left( \frac{w_i + w_a}{2} \right)}{w_i - w_a} \right) \quad (\text{S4.3})$$

where  $w_i$  is the water vapor mole fraction in the intercellular air space (calculated assuming saturation at ambient temperature) and  $w_a$  is the mole fraction of water vapor leaving the cuvette. The mole fraction of  $\text{CO}_2$  in the intercellular air space is calculated as:

$$c_i = \frac{\left( g_{ac}^t - \frac{E}{2} \right) \times c_a - A_n}{\left( g_{ac}^t + \frac{E}{2} \right)} \quad (\text{S4.4})$$

where  $g_{ca}^t$  is the total conductance for  $\text{CO}_2$ . For a detailed derivation of the leaf exchange parameters, the reader is referred to von Caemmerer and Farquhar (1981).

### 4.7.2. Isotopic composition of water at the evaporation site

Using mass balance for the air entering and leaving the cuvette, the  $\delta^{18}\text{O}$  of the transpired ( $\delta^{18}\text{O}_{\text{trans}}$ ) water is calculated according to (Harwood et al., 1998):

$$\delta^{18}\text{O}_{\text{trans}} = \left( \frac{w_a}{w_a - w_e} \right) \times (\delta^{18}\text{O}_{wa} - \delta^{18}\text{O}_{we}) + \delta^{18}\text{O}_{we} \quad (\text{S4.5})$$

where  $\delta^{18}\text{O}_{we}$  and  $\delta^{18}\text{O}_{wa}$  are  $\delta^{18}\text{O}$  values of water vapor entering and leaving the cuvette and  $w_a$  and  $w_e$  are the mole fractions of water vapor entering and leaving the cuvette.  $\delta^{17}\text{O}$  is calculated based on the triple isotope relationship for transpiration,  $\alpha^{17} = (\alpha^{18})^{\lambda_{\text{trans}}}$  where

$\lambda_{trans} = 0.522 - 0.008 \times h$  (Landais et al., 2006).  $h$  is the relative humidity,  $0.3 \leq h \leq 1$ , which is calculated as  $h = \frac{w_a}{w_i}$ ;  $w_i$  is the saturation mole fraction of water vapor in the intercellular air space.

Leaf water at the site of evaporation becomes enriched during evaporation and/or transpiration since the heavier isotopologues diffuse slower than the lighter ones (Flanagan et al., 1991; Flanagan, 1993; Yakir and Sternberg, 2000). The degree isotopic enrichment due to the phase change from water to vapor (evaporation) and diffusion is described by the modified Craig and Gordon model (Craig and Gordon, 1965), including resistance to boundary layer and stomata diffusion as described by (Farquhar et al., 1989b; Flanagan et al., 1991; Flanagan, 1993). Measurement of the isotopic composition of air entering and leaving the cuvette allows determining the isotopic composition of water at the evaporation site even if it is not in steady state as described in (Farquhar et al., 1989b; Flanagan et al., 1991; Harwood et al., 1998). The  $\delta^{18}\text{O}$  of leaf water at the site of evaporation ( $\delta^{18}\text{O}_{\text{wes}}$ ) is:

$$\delta^{18}\text{O}_{\text{wes}} = \delta^{18}\text{O}_{\text{trans}} + \epsilon^{18}_{\text{k}} + \epsilon^{18}_{\text{equ}} + \frac{w_a}{w_i} \times (\delta^{18}\text{O}_{\text{wa}} - \epsilon^{18}_{\text{k}} + \delta^{18}\text{O}_{\text{trans}}) \quad (\text{S4.6})$$

where  $\epsilon^{18}_{\text{k}}$  and  $\epsilon^{18}_{\text{equ}}$  are the kinetic fractionation of water vapor in air and the equilibrium fractionation between liquid and gas phase water, respectively. The equilibrium fractionation is temperature dependent (Bottinga and Craig, 1968) and calculated as:

$$\epsilon^{18}_{\text{equ}} = 2.644 - 3.206 \times \left(\frac{10^3}{T}\right) + 1.534 \times \left(\frac{10^6}{T}\right) \quad (\text{S4.7})$$

where  $T$  is the temperature in Kelvin.  $\text{H}_2^{18}\text{O}$  has a lower vapor pressure and diffuses slower than  $\text{H}_2^{16}\text{O}$  (Farquhar and Lloyd, 1993). The kinetic isotope effect due to diffusion  $\epsilon_{\text{k}}$ , is the weighted sum of the fractionations of water isotopologues during diffusion through the stomata in the air ( $\epsilon_{\text{ks}}$ ) and through the boundary layer ( $\epsilon_{\text{kb}}$ ) (Farquhar and Lloyd, 1993). According to Merlivat (1978) and Barkan and Luz (2007) the fractionation factor for  $\text{H}_2^{18}\text{O}$  as it diffuses through stomata is 28 ‰ ( $\epsilon^{18}_{\text{ks}}$ ). According to Farquhar and Lloyd (1993)  $\epsilon_{\text{kb}} = (\epsilon_{\text{ks}})^{\frac{2}{3}}$ , i.e., the fractionation factor as  $\text{H}_2^{18}\text{O}$  diffuses through the boundary layer is 19 ‰ ( $\epsilon^{18}_{\text{kb}}$ ). The kinetic fractionation of  $\text{H}_2^{18}\text{O}$  as it diffuses through stomata and boundary layer is given by equation S4.8 (Farquhar and Lloyd, 1993).

$$\epsilon^{18}_{\text{k}} = \frac{28 \times g_b + 19 \times g_s}{g_b + g_s} \quad (\text{S4.8})$$

where  $g_b$  and  $g_s$  are boundary layer conductance and stomatal conductance respectively. The fractionation factors for  $\text{H}_2^{17}\text{O}$  for diffusion through stomata and boundary layer are 14.6 ‰ and 9.7 ‰, respectively (Barkan and Luz, 2007).  $\delta^{17}\text{O}_{\text{wes}}$  can be calculated using a similar equation as  $\delta^{18}\text{O}_{\text{wes}}$  if  $\delta^{17}\text{O}_{\text{wa}}$  and  $\delta^{17}\text{O}_{\text{we}}$  are known, for this study we calculated  $\delta^{17}\text{O}_{\text{wes}}$  assuming that the irrigation water (IRW) is the same as soil water.

$$\delta^{17}\text{O}_{\text{wes}} = \left( \frac{\delta^{18}\text{O}_{\text{wes}} + 1}{\delta^{18}\text{O}_{\text{IRW}} + 1} \right)^{\lambda_{trans}} \times (\delta^{17}\text{O}_{\text{IRW}} + 1) - 1 \quad (\text{S4.9})$$



### 4.7.3. Mole fraction of CO<sub>2</sub> at the site of CO<sub>2</sub>-H<sub>2</sub>O exchange

The CO<sub>2</sub> mole fraction at the site of CO<sub>2</sub>-H<sub>2</sub>O exchange is calculated as shown in equation S4.10 following (Farquhar and Cernusak, 2012; Osborn et al., 2017; Barbour et al., 2016).

$$c_m = c_i \left( \frac{\delta^{18}\text{O}_i - a_{18w} - \delta^{18}\text{O}_A \times (1 + a_{18w})}{\delta^{18}\text{O}_m - a_{18w} - \delta^{18}\text{O}_A \times (1 + a_{18w})} \right) \quad (\text{S4.10})$$

where  $\delta^{18}\text{O}_i$  is  $\delta^{18}\text{O}$  of CO<sub>2</sub> in the intercellular airspace (Farquhar and Cernusak, 2012),

$$\delta^{18}\text{O}_i = \frac{\delta^{18}\text{O}_{io} + t^{18} \times \left( \delta^{18}\text{O}_A \times \left( \frac{c_a}{c_i} + 1 \right) - \delta^{18}\text{O}_a \times \frac{c_a}{c_i} \right)}{1 + t^{18}} \quad (\text{S4.11})$$

The ternary correction factor  $t^{18}$  is calculated as:

$$t^{18} = \frac{(1 + a_{18bs}) \times E}{2g_{ac}^t} \quad (\text{S4.12})$$

$g_{ac}^t$  is the conductance as CO<sub>2</sub> diffuses through the boundary layer and stomata,  $a_{18bs}$  is the weighted  $^{18}\text{O}$  fractionation for CO<sub>2</sub> diffusion across the boundary layer and stomata in series.

$$a_{18bs} = \frac{(c_a - c_s) \times a_{18b} + (c_s - c_i) \times a_{18s}}{c_a - c_i} \quad (\text{S4.13})$$

$\delta^{18}\text{O}_{io}$  is the  $\delta^{18}\text{O}$  of CO<sub>2</sub> in the intercellular air spaces ignoring the ternary correction and it is given by (Farquhar and Cernusak, 2012).

$$\delta^{18}\text{O}_{io} = \delta^{18}\text{O}_A \times \left( 1 - \frac{c_a}{c_i} \right) \times (1 + a_{18bs}) + \frac{c_a}{c_i} \times (\delta^{18}\text{O}_a - a_{18bs}) + a_{18bs} \quad (\text{S4.14})$$

where  $a_{18w}$  is the  $^{18}\text{O}$  fractionation of CO<sub>2</sub> for dissolution and diffusion in water (0.8 ‰) and  $a_{18s}$  and  $a_{18b}$  are the  $^{18}\text{O}$  fractionation of CO<sub>2</sub> as it diffuses through stomata (8.8 ‰) and the boundary layer (5.8 ‰), respectively (Farquhar et al., 1982; Farquhar and Lloyd, 1993). The oxygen isotope composition of the assimilated CO<sub>2</sub> is calculated from a mass balance using the mole fraction and isotope composition of CO<sub>2</sub> entering and leaving the cuvette:

$$\delta^{18}\text{O}_A = \frac{\delta^{18}\text{O}_a - \Delta_A^{18}\text{O}}{\Delta_A^{18}\text{O} + 1} \quad (\text{S4.15})$$

$a_{18w}$  is the fractionation of  $\delta^{18}\text{O}$  of CO<sub>2</sub> during diffusion and dissolution in water (0.8 ‰) (Farquhar and Lloyd, 1993),  $\delta^{18}\text{O}_A$  is the  $\delta^{18}\text{O}$  of the assimilated CO<sub>2</sub> and  $\delta^{18}\text{O}_m$  is the  $\delta^{18}\text{O}$  of CO<sub>2</sub> in equilibrium with leaf water at the CO<sub>2</sub>-H<sub>2</sub>O exchange site. Assuming that the isotopic composition of leaf water at the CO<sub>2</sub>-H<sub>2</sub>O exchange site is the same as the  $\delta^{18}\text{O}$  of leaf water at the evaporation site,  $\delta^{18}\text{O}_m$  can be calculated as:

$$\delta^{18}\text{O}_m = (\delta^{18}\text{O}_{\text{wes}} + 1) \times (1 + \epsilon_w^{18}) - 1 \quad (\text{S4.16})$$

The equilibrium fractionation between CO<sub>2</sub> and water ( $\epsilon_w^{18}$ ) is temperature dependent and is calculated after Brenninkmeijer et al. (1983) as:

$$\epsilon_w^{18} = \frac{17604}{T} - 17.93 \quad (\text{S4.17})$$

where  $T$  is leaf temperature. Analogous to  $\delta^{18}\text{O}$ , the mole fraction of CO<sub>2</sub> in the mesophyll cell can be calculated using  $\delta^{17}\text{O}$  values. The  $^{18}\text{O}$  fractionation ( $\alpha^{18}-1$ ) for dissolution is -0.8 ‰ (Vogel J.C. et al., 1970). The corresponding  $^{17}\text{O}$  fractionation is -0.418 ‰, calculated from the  $^{18}\text{O}$  fractionation due to equilibrium dissolution using  $\lambda_{\text{CO}_2\text{-H}_2\text{O}} = 0.5229$  (Barkan and Luz, 2012). We assume that the  $^{17}\text{O}$  fractionation during diffusion in water is the same as the fractionation against  $^{13}\text{CO}_2$  (Farquhar and Lloyd, 1993) and use the average fractionation determined for  $^{13}\text{CO}_2$  of 0.8 ‰ (average of 0.7 ‰ (O'Leary, 1984) and 0.9 ‰ (Jähne et al., 1987)). The  $^{17}\text{O}$  fractionation due to the sum of the equilibrium dissolution and diffusion in water is then  $a_{17w} = 0.382$  ‰. Similar to (Farquhar and Lloyd, 1993), using the principle of binary diffusivities (Mason and Marrero, 1970),  $a_{17s}$  and  $a_{17b}$  are 4.4 ‰ and 2.9 ‰ using the power of 2/3 relationship between the boundary layer and stomatal conductance fractionation ( $\alpha_b = \alpha_s^{2/3}$ ) obtained by Farquhar and Lloyd (1993).

For calculating the isotopic composition at the site of oxygen isotope exchange, we assume that the isotopic composition of CO<sub>2</sub> is fully equilibrated with water at the evaporation site. This includes the implicit assumption that the isotopic composition of the leaf water at the CO<sub>2</sub>-H<sub>2</sub>O exchange site is the same as at the site of evaporation. The  $\delta^{17}\text{O}$  of CO<sub>2</sub> at the CO<sub>2</sub>-H<sub>2</sub>O exchange site ( $\delta^{17}\text{O}_m$ ) is then calculated using the triple oxygen isotope ratio relationship,  $\alpha^{17} = (\alpha^{18})^{\lambda_{\text{CO}_2\text{-H}_2\text{O}}}$ .

$$\delta^{17}\text{O}_m = \left( \frac{\delta^{18}\text{O}_m + 1}{\delta^{18}\text{O}_{\text{wes}} + 1} \right)^{\lambda_{\text{CO}_2\text{-H}_2\text{O}}} \times (\delta^{17}\text{O}_{\text{wes}} + 1) - 1 \quad (\text{S4.18})$$

where  $\lambda_{\text{CO}_2\text{-H}_2\text{O}}$  is 0.5229 (Barkan and Luz, 2012).

#### 4.7.4. Mole fraction of CO<sub>2</sub> at the site of assimilation

For the C<sub>3</sub> plants,  $c_c$  is calculated following (Farquhar and Cernusak, 2012) as:

$$c_c = c_i - \left( \frac{1 - t^{13}}{1 + t^{13}} \right) \left( \frac{(\Delta_A^{13}\text{C}_i - \Delta_A^{13}\text{C}_{\text{obs}})Pc_a}{\left( b - a_m - \frac{\alpha_b}{\alpha_e} e \frac{R_d}{R_d + A} \right)} \right) \quad (\text{S4.19})$$

where  $\Delta_A^{13}\text{C}_{\text{obs}}$  is the observed discrimination against  $^{13}\text{C}$  and  $\Delta_A^{13}\text{C}_i$  is the discrimination that can be calculated for infinite mesophyll conductance (no mesophyll resistance).  $t^{13}$  is a ternary correction factor (considers the collisions between air and CO<sub>2</sub>, air and H<sub>2</sub>O, CO<sub>2</sub> and H<sub>2</sub>O),  $b$  is the fractionation due to uptake by Rubisco, and  $a_m$  is the sum of the fractionations associated with  $^{13}\text{CO}_2$  dissolution in and diffusion through water, respectively.  $e$ ,  $R_d$ ,  $\alpha_e$ ,  $\alpha_b$  and  $P$  are the fractionations during day respiration (decarboxylation), the day respiration rate, the fractionation factor for day respiration with respect to net assimilation, the fractionation factor

for C<sub>3</sub> carboxylation, and the pressure of the air surrounding the leaf, respectively. A detailed description of the equations, best fit parameters and definitions of discrimination factors are given in Table 4.3.

#### 4.7.5. Derivation of the <sup>18</sup>O- and <sup>17</sup>O-photosynthetic discrimination

The assimilation rate for C<sup>16</sup>O<sup>16</sup>O is calculated as:

$$A_n = \frac{c_a - c_m}{r_m} \quad (\text{S4.20})$$

where  $A_n$ ,  $r_m$ ,  $c_a$ ,  $c_m$  are the assimilation rate, the resistance as CO<sub>2</sub> diffuses from the air surrounding the leaf to the CO<sub>2</sub>-H<sub>2</sub>O exchange site, the mole fraction of CO<sub>2</sub> in the air surrounding the leaf and at the CO<sub>2</sub>-H<sub>2</sub>O exchange site, respectively (Farquhar and Lloyd, 1993). The assimilation rate for C<sup>18</sup>O<sup>16</sup>O is calculated as:

$${}^nR_A \times A_n = \frac{{}^nR_a \times c_a - {}^nR_m \times c_m}{\alpha^n_m \times r_m} \quad \text{where } n \text{ is } 17 \text{ or } 18 \quad (\text{S4.21})$$

$\alpha^n_m$  is the fractionation factor as C<sup>18</sup>O<sup>16</sup>O or C<sup>17</sup>O<sup>16</sup>O diffuse from the air surrounding the leaf to the CO<sub>2</sub>-H<sub>2</sub>O exchange site. Dividing equation S4.22 by equation S4.29 leads to:

$${}^nR_A = \frac{{}^nR_a \times c_a - {}^nR_m \times c_m}{\alpha^n_m \times (c_a - c_m)} \quad (\text{S4.22})$$

$$\frac{{}^nR_A}{{}^nR_a} = \frac{c_a - \frac{{}^nR_m}{{}^nR_a} \times c_m}{\alpha^n_m \times (c_a - c_m)} \quad (\text{S4.23})$$

$$\frac{{}^nR_a}{{}^nR_A} = \frac{\alpha^n_m \times (c_a - c_m)}{c_a - \frac{{}^nR_m}{{}^nR_a} \times c_m} \quad (\text{S4.24})$$

$$\frac{{}^nR_a}{{}^nR_A} - 1 = \frac{\alpha^n_m \times (c_a - c_m)}{c_a - \frac{{}^nR_m}{{}^nR_a} \times c_m} - 1 \quad (\text{S4.25})$$

Using the definitions

$$\Delta_A {}^nO_{FM} = \frac{{}^nR_a}{{}^nR_A} - 1 \quad (\text{S4.26})$$

and

$$\delta^n O_{ma} = \frac{{}^nR_m}{{}^nR_a} - 1 \quad (\text{S4.27})$$

this can be written as

$$\Delta_A^{17}O_{FM} = \frac{\alpha_m^n \times (c_a - c_m)}{c_a - c_m \times (\delta^{17}O_{ma} + 1)} - 1 \quad (S4.28)$$

$$\Delta_A^{17}O_{FM} = \frac{\bar{a}_n + \frac{c_m}{c_a - c_m} \times \delta^{17}O_{ma}}{1 - \frac{c_m}{c_a - c_m} \times \delta^{17}O_{ma}} \quad (S4.29)$$

#### 4.7.6. Comparison of equations used in global models and in this study to calculate $\Delta^{17}O$ -photosynthetic discrimination

The discrimination against  $\Delta^{17}O$  associated with assimilation in global models, assuming complete equilibration between  $CO_2$  and  $H_2O$ , is calculated from equation S4.30 (Hofmann et al., 2017; Liang et al., 2017b; Koren et al., 2019).

$$\Delta_A \Delta^{17}O = (\lambda_{diffusion} - \lambda_{RL}) \times \ln(\bar{a}_{18} + 1) + (\Delta^{17}O_m - \Delta^{17}O_a) \frac{c_m}{c_a - c_m} \quad (S4.30)$$

$\bar{a}_{18}$ , is the weighted mean discrimination occurring during the diffusion of  $^{12}C^{18}O^{16}O$  from the ambient air to the  $CO_2$ - $H_2O$  exchange site and it is estimated to be 7.4 ‰ (Farquhar et al., 1993). This value has been adopted in several global studies of  $\delta^{18}O(CO_2)$  (Ciais et al., 1997a; 1997b; Cuntz et al., 2003a; 2003b) and the global  $\Delta^{17}O$  studies (Hofmann et al., 2017; Liang et al., 2017b; Koren et al., 2019).  $\lambda_{diffusion}=0.509$  is the three-isotope coefficient associated with fractionation of  $C^{17}OO$  as it diffuses through air relative to  $C^{18}OO$  (Young et al., 2002) and  $\lambda_{RL}=0.528$  (the reference slope used in this study).  $\Delta^{17}O_m$  and  $c_m$  are the oxygen isotope anomaly and mole fraction of  $CO_2$  at the  $CO_2$ - $H_2O$  exchange site, respectively.

A good approximation for the observed  $^{18}O$ -discrimination can be derived from the leaf exchange parameters (Farquhar and Lloyd, 1993):

$$\Delta_A^{18}O_{FM} = \frac{\bar{a}_{18} + \frac{c_m}{c_a - c_m} \times \delta^{18}O_{ma}}{1 - \frac{c_m}{c_a - c_m} \times \delta^{18}O_{ma}} \approx \bar{a}_{18} + \frac{c_m}{c_a - c_m} \times (\delta^{18}O_m - \delta^{18}O_a) \quad (S4.31)$$

The subscript FM stands for Farquhar model.  $\delta^{18}O_{ma}$  is the enrichment in  $\delta^{18}O$  of  $CO_2$  in full isotopic equilibrium with water at the exchange site relative to the  $CO_2$  in the surrounding air, calculated as:

$$\delta^{18}O_{ma} = \frac{\delta^{18}O_m - \delta^{18}O_a}{1 + \delta^{18}O_a} \quad (S4.32)$$

$\delta^{18}O_m$  is the isotope composition of  $CO_2$  in equilibrium with leaf water at the  $CO_2$ - $H_2O$  exchange site (equation S4.16). In the global models (Hofmann et al., 2017; Liang et al., 2017b; Koren et al., 2019),  $\Delta^{17}O$ -photosynthetic discrimination shown in equation S4.30 is derived from  $\Delta_A^{17}O_{FM}$  and  $\Delta_A^{18}O_{FM}$  as shown from equation S4.33.

$$\begin{aligned}
\Delta_A \Delta^{17}\text{O} &= \left( \bar{a}_{17} + \frac{c_m}{c_a - c_m} (\delta^{17}\text{O}_m - \delta^{17}\text{O}_a) \right) - \lambda_{\text{RL}} \times \left( \bar{a}_{18} + \frac{c_m}{c_a - c_m} (\delta^{18}\text{O}_m - \delta^{18}\text{O}_a) \right) \quad (\text{S4.33}) \\
&= (\bar{a}_{17} - \lambda_{\text{RL}} \times \bar{a}_{18}) \\
&\quad + \left[ (\delta^{17}\text{O}_m - \lambda_{\text{RL}} \delta^{18}\text{O}_m) - (\delta^{17}\text{O}_a - \lambda_{\text{RL}} \delta^{18}\text{O}_a) \right] \frac{c_m}{c_a - c_m} \\
&= (\bar{a}_{17} - \lambda_{\text{RL}} \times \bar{a}_{18}) + \left[ \Delta^{17}\text{O}_m - \Delta^{17}\text{O}_a \right] \frac{c_m}{c_a - c_m}
\end{aligned}$$

Note that,  $\ln(\bar{a}_{18} + 1) \approx \bar{a}_{18}$  and  $(\bar{a}_{17} - \lambda_{\text{RL}} \times \bar{a}_{18}) = (\lambda_{\text{diffusion}} - \lambda_{\text{RL}}) \times \ln(\bar{a}_{18} + 1)$ .

#### 4.7.7. Calibration and characterization of the water vapor isotope analyzer (WVIA)

Based on the calibration using five water standards, a working standard was prepared to correct for short-term variability and to determine the non-linearity (dependency of  $\delta\text{D}$  and  $\delta^{18}\text{O}$  on the water vapor mole fraction). Each day the WVIA was calibrated with 3 standards that cover the isotopic composition of the samples measured ( $\delta^{18}\text{O}$  value of -24.777 ‰, -8.640 ‰ and 0.11 ‰, provided by IAEA (Wassenaar et al., 2018)), see Figure S4.2. Figure S4.3, shows the results of the non-linearity tests. All three isotope signatures of water vapor showed a different dependence on the mole fraction of water vapor measured. The  $\delta^{18}\text{O}$  is independent of the mole fraction above 11000 ppm but decreases at lower mole fraction until 4000 ppm, and then increases again.  $\delta^{17}\text{O}$  is relatively stable for mole fractions higher than 17000 ppm, but increases strongly and in a non-linear manner below. Similarly,  $\delta\text{D}$  is independent of the mole fraction of water vapor above 10000 ppm but increases non-linearly below.  $\delta^{18}\text{O}$ ,  $\delta^{17}\text{O}$  and  $\delta\text{D}$  values measured with the WVIA are dependent on the type of carrier gas used when measuring liquid samples as shown for pure  $\text{N}_2$  and zero air used as a carrier gas, Figure S4.3 (Johnson and Rella, 2017). To investigate how the precision of the isotope values depends on the averaging time, Allan deviation (square root of Allan variance) curves are shown in Figure S4.4. All three isotope signatures of water vapor show a similar pattern. The optimum precision is reached at averaging times of 16.7 minutes for  $\delta^{18}\text{O}$  and  $\delta\text{D}$  and 15 minutes for  $\delta^{17}\text{O}$  (Figure S4.4). Note that the  $\delta^{17}\text{O}$  measurements of water vapor are not calibrated to an international isotope scale for our experiments.

#### 4.7.8. Water extraction and analysis

The vial containing the leaf was frozen using a liquid nitrogen bath and connected to another empty vial by glass tubing. The system was then evacuated using a membrane pump (KNF Neuberger, Germany), (Figure S4.5). The pressure was monitored with a Dual pressure sensor (DualTrans transducer, MKS, USA). After the target vacuum was reached (1mbar or below) the extraction system was isolated from the pump. The vial containing the leaf was placed into a heater block (ORI BLOCK DB-1, Techne, England) while the empty vial was kept at liquid nitrogen temperature for 4 hr (Figure S4.5). The extracted leaf water, ~ 0.7 ml (determined based on weight by measuring the leaf weight before and after extraction), was collected in a

2 ml vial (Autosampler vials, National Scientific, the Netherlands) using a pipette and kept in the freezer at -20 °C before isotopic analysis.

$\Delta^{17}\text{O}$  of leaf water is measured using a fluorination method. The water was converted to  $\text{O}_2$  using  $\text{CoF}_3$  as fluorinating reagent and the  $\text{O}_2$  was collected in a sample tube immersed in liquid Helium (-270 °C). Finally,  $\delta^{17}\text{O}$  and  $\delta^{18}\text{O}$  of  $\text{O}_2$  were measured with an isotope ratio mass spectrometer (ThermoQuest MAT 253 Finnigan, Germany) in dual inlet mode. The measurement reproducibility for two replicates is 0.015 ‰, 0.010 ‰ and 0.005 ‰ for  $\delta^{17}\text{O}$ ,  $\delta^{18}\text{O}$  and  $\Delta^{17}\text{O}$ , respectively.

#### 4.7.9. Leaf cuvette model

In the simple leaf cuvette model, we partitioned the leaf into three different compartments: the intercellular air space, the mesophyll cell, and the chloroplast, as shown in Figure S4.7. For this model, we assumed an infinite boundary conductance. The conductance from the intercellular air space to the chloroplast, where assimilation takes place (mainly for the  $\text{C}_3$  plants), is represented by  $g_{m13}$ . The conductance from the intercellular air space to the mesophyll, where the  $\text{CO}_2$ - $\text{H}_2\text{O}$  exchange occurs is expressed as  $g_{m18}$ .

##### 4.7.9.1. $\text{CO}_2$ balance

First, we solve for the  $\text{CO}_2$  mole fractions in the atmosphere ( $c_a$ ), the intercellular air space ( $c_i$ ), the mesophyll cell ( $c_m$ ) and the chloroplast ( $c_c$ ). The main assumptions in the leaf cuvette model are:

- The system is in steady state ( $\frac{dc_i}{dt} = 0 = g_s c_a + g_{m18} c_m - g_i c_i - g_{m13} c_i$ )
- The mixing in the cuvette is perfect (i.e.  $c_a = c_o$ )
- Boundary layer resistance can be neglected
- The conductance between intercellular space and mesophyll is assumed to be 3 times higher than the conductance between intercellular space and chloroplast (i.e.  $g_{m18} = 3 \times g_{m13}$ ).

We modeled a 100 ppm drawdown of  $\text{CO}_2$  for each photosynthesis experiment. The mole fractions of  $\text{CO}_2$  entering and leaving the cuvette are 500 ppm and 400 ppm, respectively. The leaf area, flowrate and assimilation rate used in the model are  $30 \text{ cm}^2$ ,  $0.7 \text{ L min}^{-1}$  and  $20.0 \text{ mol m}^{-2}\text{s}^{-1}$ , respectively. The  $\text{CO}_2$  mole fractions in all leaf reservoirs are calculated for each given  $c_m/c_a$  ratio, by assuming  $g_{m18} = 0.3 \text{ mol m}^{-2}\text{s}^{-1}$ .

Next, we assume an initial value for the  $\text{C}^{18}\text{OO}$  mole fraction inside the cuvette ( $c_{a,\text{C}^{18}\text{OO}}$ ). From the mole fractions  $c_{a,\text{C}^{18}\text{OO}}$  and  $c_{m,\text{C}^{18}\text{OO}}$  and the conductance  $g_{s,\text{C}^{18}\text{OO}}$  and  $g_{m18,\text{C}^{18}\text{OO}}$  we can calculate the inflow of  $\text{C}^{18}\text{OO}$  into the intercellular air space. Since the system is in steady state, the inflow and outflow of  $\text{C}^{18}\text{OO}$  for the intercellular air space are equal and hence we can determine the mole fraction  $c_{i,\text{C}^{18}\text{OO}}$ . The ingoing  $\text{C}^{18}\text{OO}$  is known from the airflow rate and  $c_{e,\text{C}^{18}\text{OO}}$ , the outgoing  $\text{C}^{18}\text{OO}$  depends on the airflow rate and  $c_{a,\text{C}^{18}\text{OO}}$  and the plant uptake of  $\text{C}^{18}\text{OO}$  is  $A_{n,\text{C}^{18}\text{OO}} = g_{s,\text{C}^{18}\text{OO}} \times (c_{a,\text{C}^{18}\text{OO}} - c_{i,\text{C}^{18}\text{OO}})$ . By using an iterative procedure we can improve our estimate for  $c_{a,\text{C}^{18}\text{OO}}$ . Note that for each update in  $c_{a,\text{C}^{18}\text{OO}}$ , we also update the corresponding  $c_{i,\text{C}^{18}\text{OO}}$

#### 4.7.9.2. $^{13}\text{CO}_2$ balance

Next, we calculate the steady state  $^{13}\text{CO}_2$  mole fractions in the different model reservoirs and subsequently, we determine the discrimination  $\Delta^{13}\text{C}$ . The additional assumptions used are:

- For the fractionation factors we use  $a_{13s} = 4.4$ ,  $a_m = 1.8$  ‰ and  $b = 29$  ‰
- The uptake of  $\text{CO}_2$  scales linearly with the  $\text{CO}_2$  mole fraction in the chloroplast ( $A_n = k \times c_c$ ). Similarly, for  $^{13}\text{CO}_2$  we have:  $A_{n,13\text{CO}_2} = k \times (1 - b) \times C_{c,13\text{CO}_2}$

We solve the steady state  $^{13}\text{CO}_2$  balance by performing 2 nested iterations. We start with an initial guess for the atmospheric  $^{13}\text{CO}_2$  mole fraction ( $C_{a,13\text{CO}_2}$ ) and for the photosynthetic uptake of  $^{13}\text{CO}_2$  ( $A_{n,13\text{CO}_2}$ ). In the ‘inner’ iteration loop we use  $c_{a,13\text{CO}_2}$  and  $A_{n,13\text{CO}_2}$  to calculate the  $^{13}\text{CO}_2$  mole fractions in all leaf reservoirs. From the  $^{13}\text{CO}_2$  mole fraction in the chloroplast ( $c_{c,13\text{CO}_2}$ ) and the linear assimilation factor ( $k \times (1 - b)$ ) we can calculate the corresponding  $A_{n,13\text{CO}_2}$  and compare this to our initial guess. Using an iterative procedure, we can find the  $A_{n,13\text{CO}_2}$  that corresponds to the assumed  $c_{a,13\text{CO}_2}$ .

The ‘outer’ iteration loop is aimed at finding the steady state atmospheric  $^{13}\text{CO}_2$  mole fraction ( $c_{a,13\text{CO}_2}$ ) using a mass balance for  $^{13}\text{CO}_2$ . We know the  $^{13}\text{CO}_2$  mole fraction of the ingoing air ( $c_{in,13\text{CO}_2}$ ), we have assumed value for outgoing air ( $c_{a,13\text{CO}_2}$ ) and have calculated the corresponding photosynthetic uptake ( $A_{n,13\text{CO}_2}$ ). From the resulting imbalance, we can come up with a new guess for  $c_{a,13\text{CO}_2}$ . After each update of our estimate for  $c_{a,13\text{CO}_2}$ , we repeat the ‘inner’ iteration loop to update  $A_{n,13\text{CO}_2}$ .

#### 4.7.9.3. $\text{C}^{18}\text{OO}$ balance

The additional assumptions for solving the  $\text{C}^{18}\text{OO}$  balance are:

- For the fractionation of  $\text{C}^{18}\text{OO}$  for diffusion through stomata and diffusion into the mesophyll cell, we used  $a_{18s} = 8.8$  ‰ and  $a_{18w} = 0.8$  ‰, respectively
- The isotopic exchange between  $\text{CO}_2$  and water in the mesophyll is fast enough to reach complete equilibration, which is a function of temperature
- Isotopic equilibration between  $\text{CO}_2$  and water does not occur in the intercellular air space

We set the leaf water signature to  $\delta^{18}\text{O}_{\text{leaf}} = 10.467$  ‰ VSMOW and the leaf water temperature to  $T_{\text{leaf}} = 22^\circ\text{C}$ , from which we can calculate the  $\delta^{18}\text{O}$  signature and therefore (using  $c_m$  from above) the  $\text{C}^{18}\text{OO}$  mole fraction in the mesophyll ( $c_{m, \text{C}^{18}\text{OO}}$ ). Next, we assume a starting value for the  $\text{C}^{18}\text{OO}$  mole fraction inside the cuvette ( $c_{a, \text{C}^{18}\text{OO}}$ ). From the steady state mass balance, we can then determine the mole fraction  $c_{i, \text{C}^{18}\text{OO}}$  ( $c_i = \frac{g_s c_a + g_m c_m}{g_s + g_m}$ ). The ingoing  $\text{C}^{18}\text{OO}$  is known from the airflow rate and  $c_{e, \text{C}^{18}\text{OO}}$ , the outgoing  $\text{C}^{18}\text{OO}$  depends on the airflow rate and  $c_{a, \text{C}^{18}\text{OO}}$  and the plant uptake of  $\text{C}^{18}\text{OO}$  is  $A_{n, \text{C}^{18}\text{OO}} = g_{s, \text{C}^{18}\text{OO}} \times (c_{a, \text{C}^{18}\text{OO}} - c_{i, \text{C}^{18}\text{OO}})$ .

A similar mass balance is implemented for  $\text{C}^{17}\text{OO}$ , the fractionation of  $\text{C}^{17}\text{OO}$  for diffusion through stomata is  $a_{17s} = 4.4$  ‰ and for diffusion into the mesophyll cell we used and  $a_{18w} = 0.382$  ‰, respectively. We set the leaf water signature to  $\delta^{18}\text{O}_{\text{leaf}} = 5.39$  ‰ VSMOW.

#### 4.7.10. $^{13}\text{C}$ -photosynthetic discrimination

The isotope discrimination against  $^{13}\text{C}$  ( $\Delta_A^{13}\text{C}$ ) associated with photosynthesis for the three-plant species is shown in Figure S4.8 a) and b) as a function of  $c_c/c_a$  and  $c_i/c_a$  for  $\text{C}_3$  and  $\text{C}_4$  plants, respectively. Experiments at different light intensities are shown in different colors, blue for LL and yellow for HL. For ivy and sunflower,  $\Delta_A^{13}\text{C}$  and  $c_c/c_a$  are linearly correlated. As irradiance increases,  $c_c/c_a$  and  $\Delta_A^{13}\text{C}$  decrease.  $\Delta_A^{13}\text{C}$  for ivy increases from 13 ‰ to 16 ‰ when  $c_c/c_a$  increases from 0.34 to 0.55 while for sunflower  $\Delta_A^{13}\text{C}$  ranges from 13 ‰ to 25 ‰ for  $c_c/c_a$  ratios of 0.37 to 0.8. This is due to the lower assimilation rate and generally higher back-diffusion flux at a higher  $c_c/c_a$  ratio. When irradiance increases, the assimilation rate increases,  $c_c/c_a$  decreases, and less of the  $\text{CO}_2$  that has entered the stomata diffuses back to the atmosphere. As a result,  $\Delta_A^{13}\text{C}$  decreases with an increase in light intensity. For maize,  $\Delta_A^{13}\text{C}$  is much smaller than for the  $\text{C}_3$  plants, ranging from 2.4 ‰ to 3.5 ‰ for  $c_i/c_a$  ratios of 0.42 to 0.55, and we did not observe a strong correlation between  $\Delta_A^{13}\text{C}$  and  $c_i/c_a$ .  $\Delta_A^{13}\text{C}$  vs  $c_i/c_a$  is shown in Figure S4.9 of the for both  $\text{C}_3$  plants (sunflower and ivy) and a  $\text{C}_4$  plant (maize).

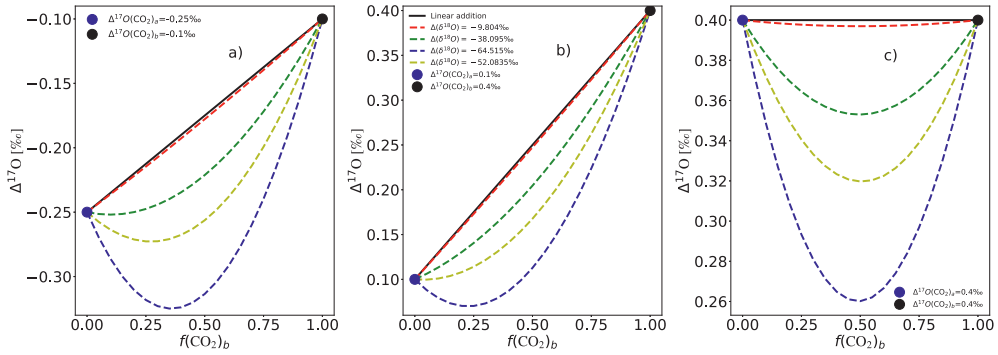


Figure S4.1 Illustration of the changes in  $\Delta^{17}\text{O}$  for mixing of two different gases when the  $\Delta^{17}\text{O}$  values are calculated in logarithmic form, as a function of the fraction of  $\text{CO}_2$  gas b. The blue and black circles show the  $\Delta^{17}\text{O}$  values of the mixing end members and the different colors show mixing lines for differences in  $\delta^{18}\text{O}$ .

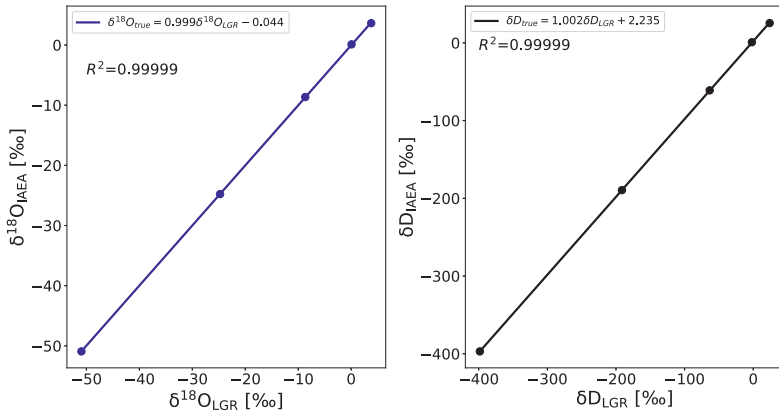


Figure S4.2 Calibration of the LGR water isotope analyser for the measurement of  $\delta^{18}\text{O}$  and  $\delta\text{D}$  of water vapor. a)  $\delta^{18}\text{O}_{\text{IAEA}}$  is the value assigned by IAEA while  $\delta^{18}\text{O}_{\text{LGR}}$  is the value reported by the LGR instrument. b)  $\delta\text{D}_{\text{IAEA}}$ , is the value assigned by IAEA while  $\delta\text{D}_{\text{LGR}}$  is the value reported by the LGR instrument.



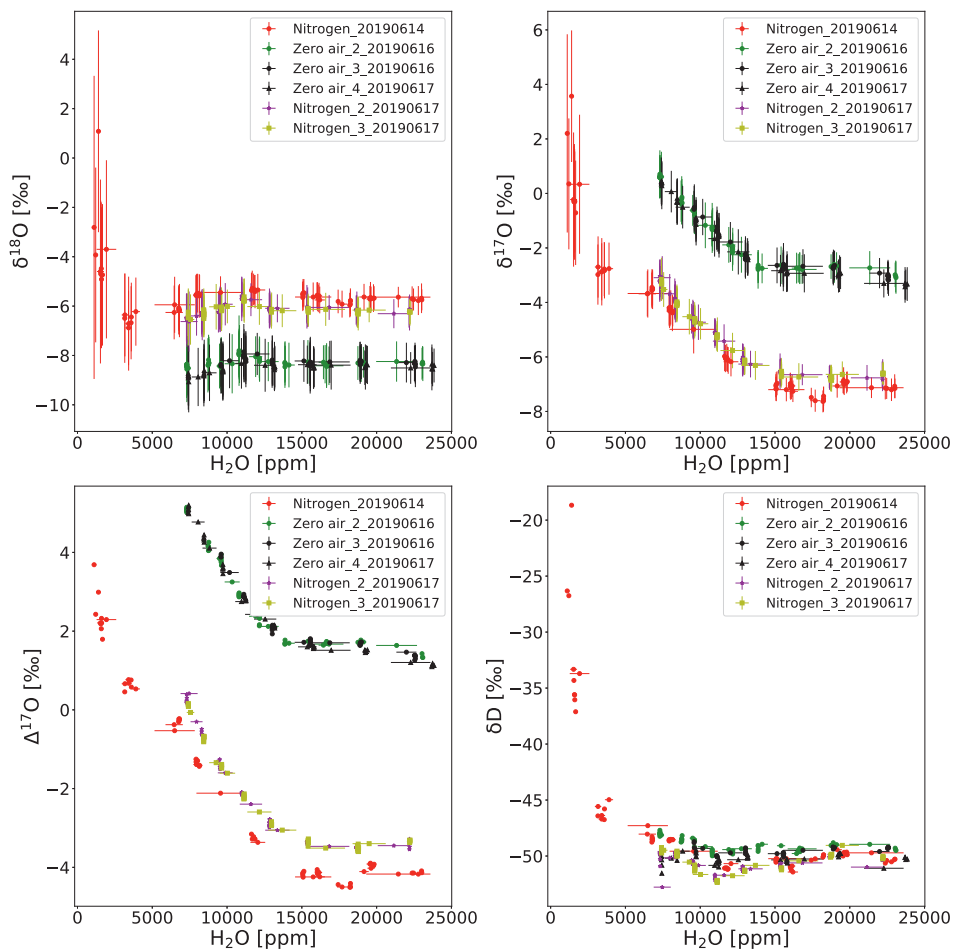


Figure S4.3 Dependency of isotope composition of water vapour on the water vapor concentration and the carrier gas used for the water vapor standard source for  $\delta^{18}\text{O}$ ,  $\delta^{17}\text{O}$ ,  $\Delta^{17}\text{O}$  and  $\delta\text{D}$ .

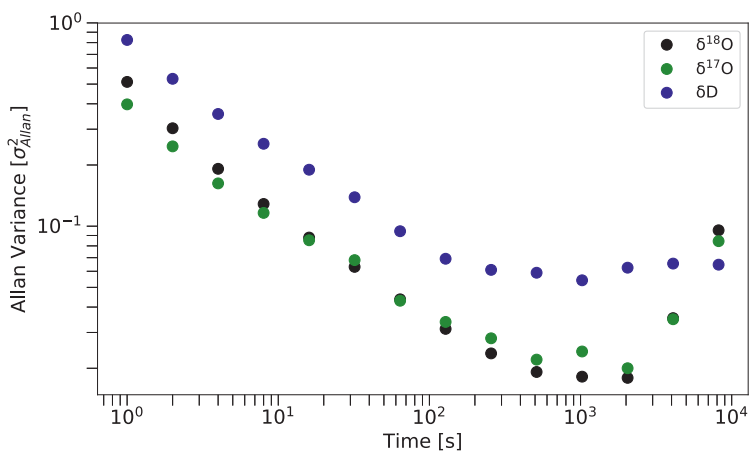


Figure S4.4 Allan variance curves of  $\delta D$ ,  $\delta^{17}O$  and  $\delta^{18}O$  for measurement at 20000 ppm water vapor concentration.

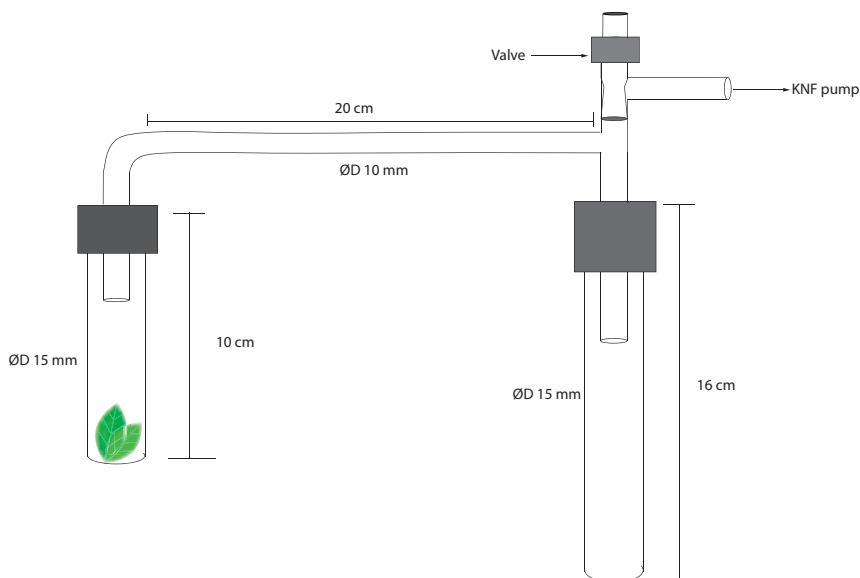


Figure S4.5 Schematic drawing of the setup used for the extraction of leaf water. The vial containing the leaf is heated to 60 °C while the other vial is immersed in the liquid nitrogen to collect the water vapor.

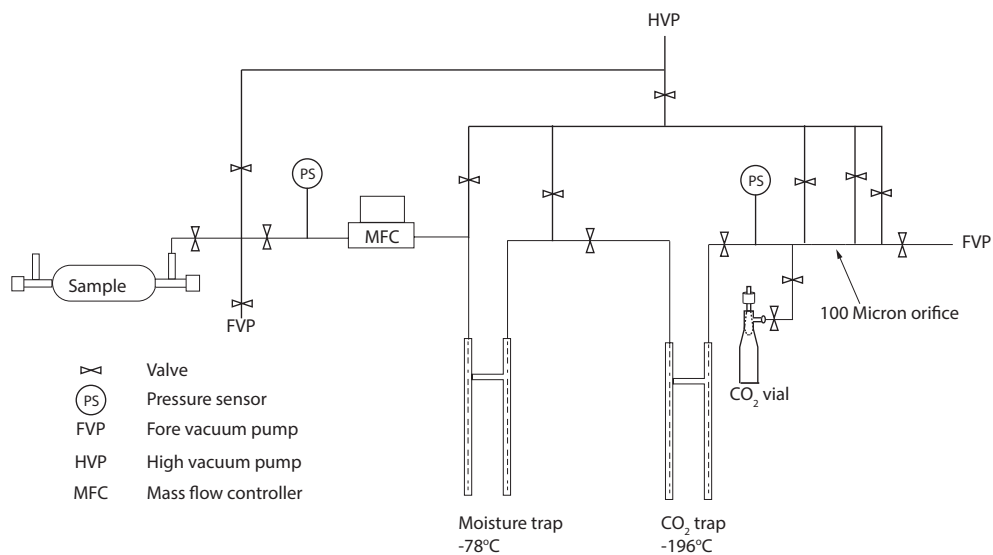


Figure S4.6 Schematic diagram of the system used for the extraction of carbon dioxide from air samples. The moisture trap is cooled by a dry ice-ethanol mixture while the  $\text{CO}_2$  trap is cooled by liquid nitrogen.

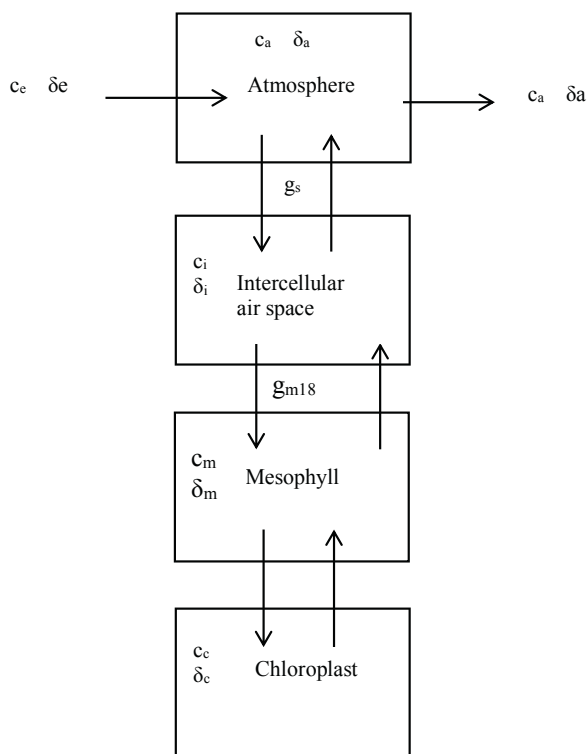


Figure S4.7 Schematic diagram of the conceptual leaf-cuvette model.  $\delta$  and  $c$  are the oxygen isotope composition and mixing ratio of  $\text{CO}_2$ . The subscripts  $e$ ,  $a$ ,  $i$ ,  $m$ ,  $c$  represents  $\text{CO}_2$  entering the cuvette, leaving the cuvette, in the intercellular air space, the mesophyll and the chloroplast, respectively.

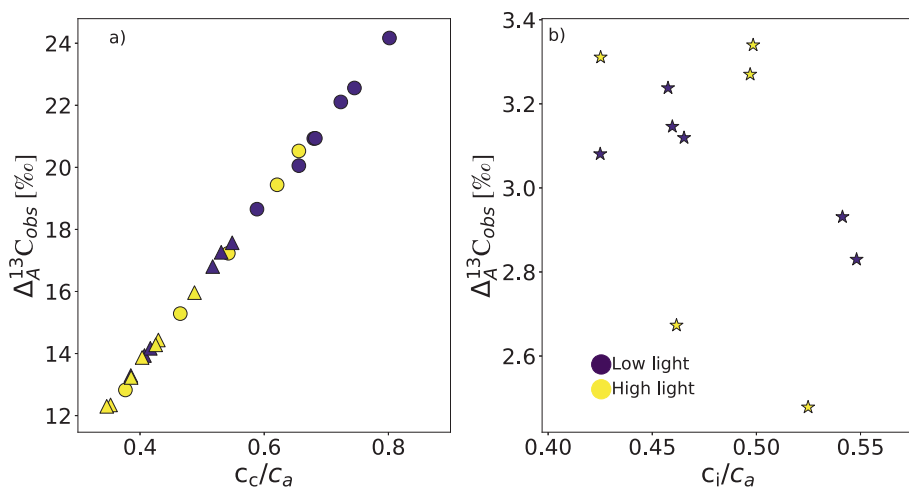


Figure S4.8.  $\Delta^{13}C$  of carbon dioxide during photosynthesis. a) The  $\Delta^{13}C$  of the two  $C_3$  plants sunflower (circles) and ivy (triangles) at two different irradiances. b) The  $\Delta^{13}C$  of maize at two different irradiances. The measurement error in  $\Delta^{13}C_{obs}$  is 0.15 ‰ (SD), calculated using error propagation.

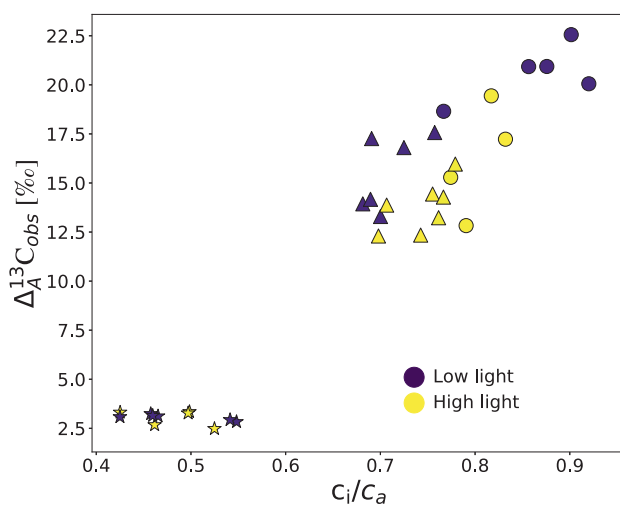


Figure S4.9.  $\Delta^{13}C$  of carbon dioxide during photosynthesis for the two  $C_3$  plants sunflower (circles) and ivy (triangles) and a  $C_4$  plant maize (stars).

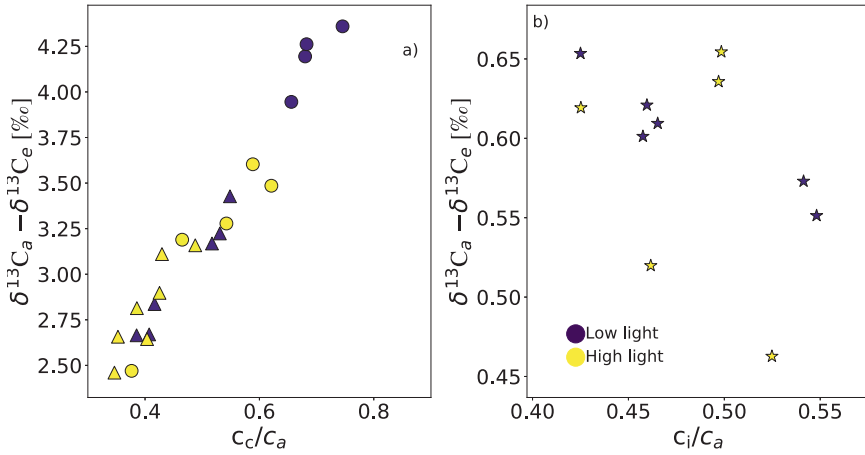


Figure S4.10. Relative difference in  $\delta^{13}\text{C}$  of  $\text{CO}_2$  leaving (index a) and entering (index e) the leaf cuvette during experiments with two  $\text{C}_3$  plants, sunflower (circles) and ivy (triangles) (panel a) as a function of the  $c_e/c_a$  ratio and a  $\text{C}_4$  plant maize (stars) (panel b) as a function of the  $c_i/c_a$  ratio. The experiments were performed under low light ( $300 \mu\text{mol m}^{-2}\text{s}^{-1}$ , purple) and high light ( $1200 \mu\text{mol m}^{-2}\text{s}^{-1}$ , yellow) conditions.

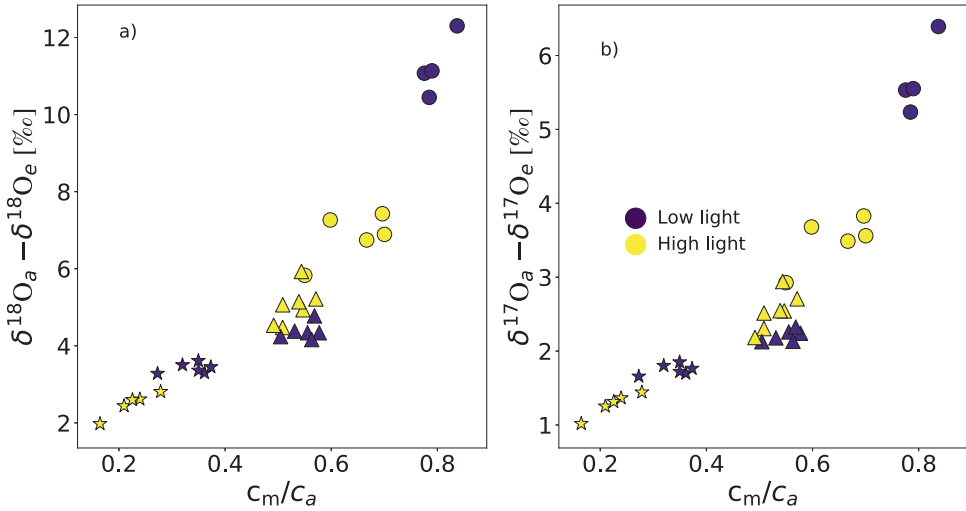


Figure S4.11 Relative difference in  $\delta^{17}\text{O}$  (a) and  $\delta^{18}\text{O}$  (b) of  $\text{CO}_2$  leaving (index a) and entering (index e) the leaf cuvette during experiments with two  $\text{C}_3$  plants, sunflower (circles) and ivy (triangles) and a  $\text{C}_4$  plant maize (stars) as a function of the  $c_m/c_a$  ratio. The experiments were performed under low light ( $300 \mu\text{mol m}^{-2}\text{s}^{-1}$ , purple) and high light ( $1200 \mu\text{mol m}^{-2}\text{s}^{-1}$ , yellow) conditions.

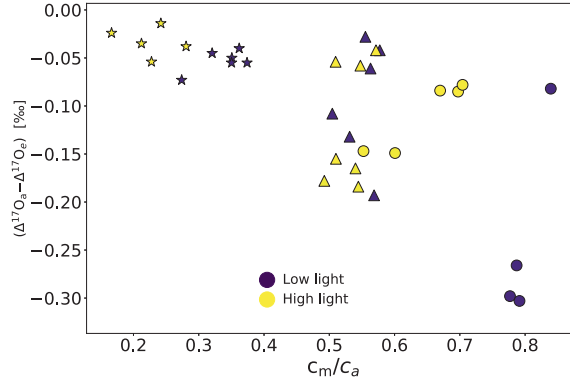


Figure S4.12 Difference in  $\Delta^{17}\text{O}$  of the  $\text{CO}_2$  leaving (index a) and entering (index e) the cuvette as a function of  $c_m/c_a$  for sunflower (circles), ivy (triangles) and maize (stars).

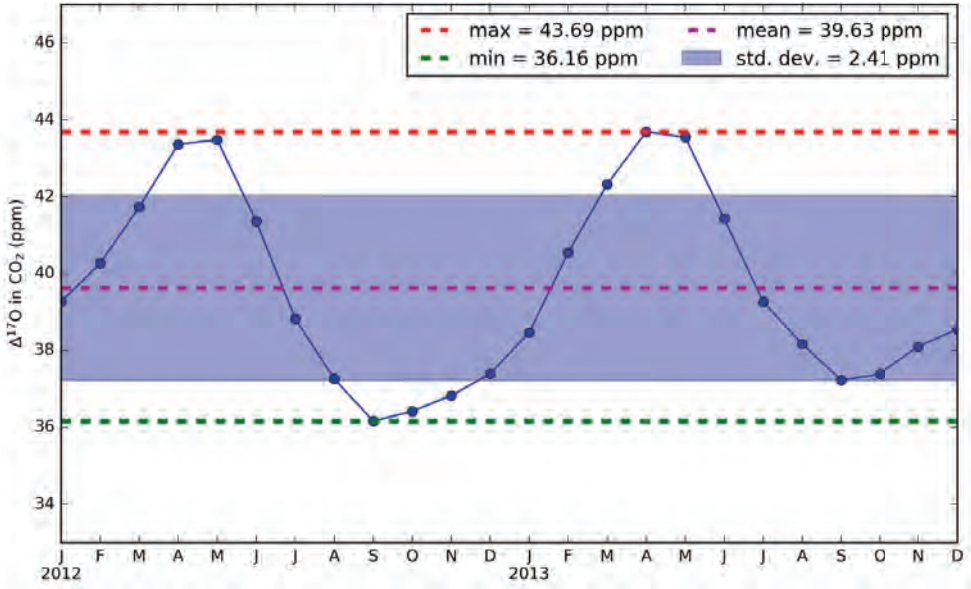


Figure S4.13. 3D model result for the global average seasonal cycle of  $\Delta^{17}\text{O}$  of atmospheric  $\text{CO}_2$  for the years 2012 and 2013 (Koren et al., 2019). Note that the  $\Delta^{17}\text{O}$  value was calculated in (Koren et al., 2019). with  $\lambda = 0.5229$ . To convert to the  $\lambda = 0.528$ , we use  $\Delta^{17}\text{O}(\text{CO}_2)_{\lambda=0.528} = \Delta^{17}\text{O}(\text{CO}_2)_{\lambda=0.5229} + (0.5229 - 0.528) \times \ln(\delta^{18}\text{O}(\text{CO}_2) + 1)$ . In the 3D global model,  $\delta^{18}\text{O}(\text{CO}_2)$  is 41.5 ‰.

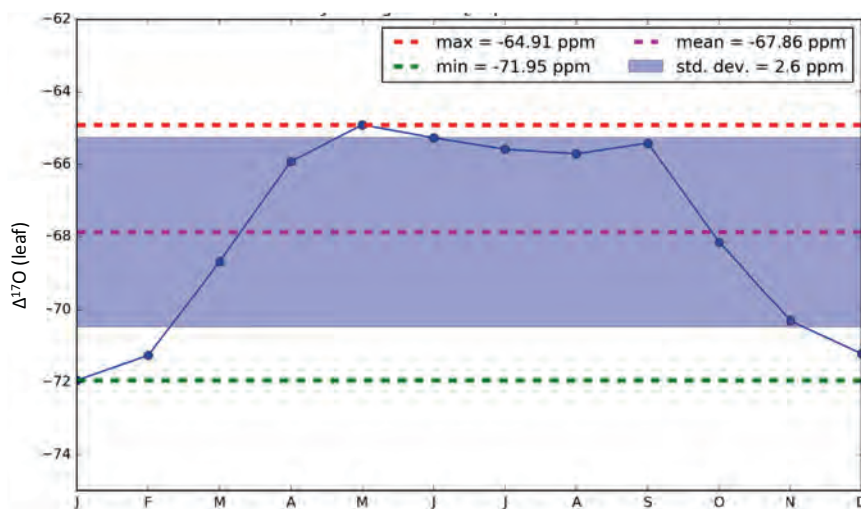


Figure S4.14. 3D model result for the seasonal cycle of the global average  $\Delta^{17}\text{O}$  value of leaf water for the year 2012 (Koren et al., 2019). Note that  $\Delta^{17}\text{O}$  value is reported here with  $\lambda = 0.5229$ . To convert to  $\lambda = 0.528$ , we use  $\Delta^{17}\text{O}(\text{leaf})_{\lambda=0.528} = \Delta^{17}\text{O}(\text{leaf})_{\lambda=0.5229} + (0.5229 - 0.528) \times \ln \alpha_{\text{trans}}$ .  $\alpha_{\text{trans}} = 1/0.9917$  (Koren et al., 2019; Hofmann et al., 2017).

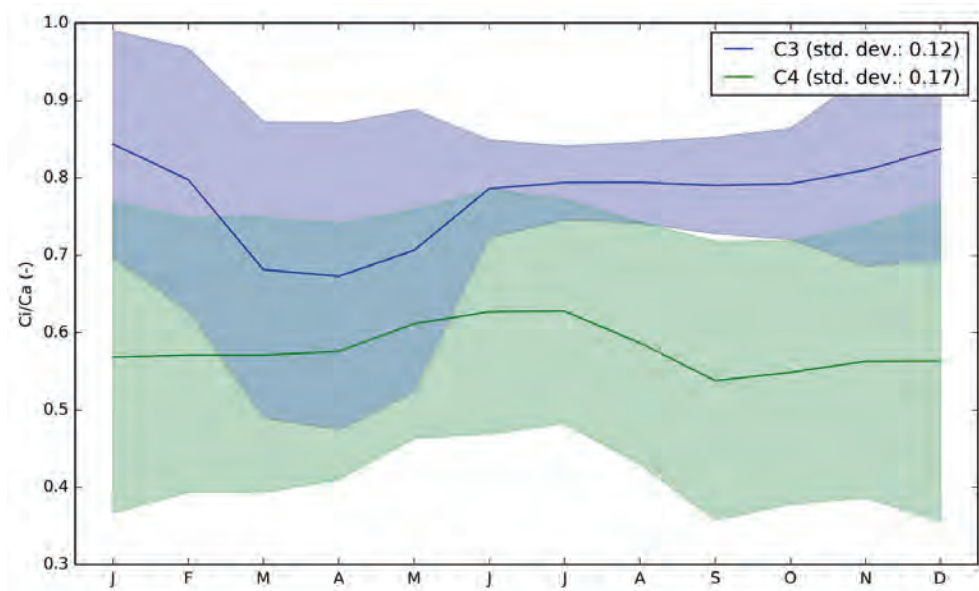


Figure S4.15 Annual variability of the  $c_i/c_a$  ratio for C<sub>4</sub> and C<sub>3</sub> plants from the SiBCASA model (Schaefer et al., 2008; Koren et al., 2019).

Table S4.1 Reproducibility of the extraction system and the CO<sub>2</sub>-O<sub>2</sub> exchange system. Extraction reproducibility experiments were performed using compressed air. To establish the reproducibility of the CO<sub>2</sub>-O<sub>2</sub> isotope exchange system we used pure CO<sub>2</sub> (SCOTT, Air Products, Germany). *SE* and *SD* stand for standard error and standard deviation. All the isotope values given in the table are in per mill [‰].

| Extraction system reproducibility                               |                             |                         |                              |                         |                              |                         |                         |
|---|-----------------------------|-------------------------|------------------------------|-------------------------|------------------------------|-------------------------|-------------------------|
| Extraction  | $\delta^{18}\text{O}$       |                         | SE                           |                         | $\delta^{13}\text{C}$        |                         | SE                      |
| 03/03/2019  | 41.411                      |                         | 0.005                        |                         | -8.636                       |                         | 0.004                   |
| 03/03/2019  | 41.352                      |                         | 0.006                        |                         | -8.642                       |                         | 0.003                   |
| 03/03/2019  | 41.355                      |                         | 0.020                        |                         | -8.636                       |                         | 0.005                   |
| 04/03/2019  | 41.314                      |                         | 0.008                        |                         | -8.647                       |                         | 0.007                   |
| 04/03/2019  | 41.359                      |                         | 0.007                        |                         | -8.651                       |                         | 0.004                   |
| 05/03/2019  | 41.297                      |                         | 0.006                        |                         | -8.648                       |                         | 0.004                   |
| 05/03/2019  | 41.330                      |                         | 0.008                        |                         | -8.652                       |                         | 0.004                   |
| 05/03/2019  | 41.387                      |                         | 0.005                        |                         | -8.648                       |                         | 0.004                   |
| 06/03/2019  | 41.368                      |                         | 0.010                        |                         | -8.660                       |                         | 0.004                   |
| 06/03/2019  | 41.369                      |                         | 0.007                        |                         | -8.653                       |                         | 0.004                   |
| 06/03/2019  | 41.329                      |                         | 0.008                        |                         | -8.652                       |                         | 0.003                   |
| 07/03/2019  | 41.373                      |                         | 0.007                        |                         | -8.646                       |                         | 0.004                   |
| 07/03/2019  | 41.324                      |                         | 0.007                        |                         | -8.646                       |                         | 0.004                   |
| 07/03/2019  | 41.352                      |                         | 0.007                        |                         | -8.643                       |                         | 0.002                   |
| Mean $\pm$ SD   | 41.351 $\pm$ 0.030          |                         |                              |                         | -8.647 $\pm$ 0.007           |                         |                         |
| CO <sub>2</sub> -O <sub>2</sub> exchange system reproducibility |                             |                         |                              |                         |                              |                         |                         |
| EXP   | Pre-exchange O <sub>2</sub> |                         | Post-exchange O <sub>2</sub> |                         | Pre-exchange CO <sub>2</sub> |                         |                         |
|   | $\delta^{17}\text{O}_i$     | $\delta^{18}\text{O}_i$ | $\delta^{17}\text{O}_f$      | $\delta^{18}\text{O}_f$ | $\delta^{18}\text{O}_i$      | $\delta^{17}\text{O}_i$ | $\Delta^{17}\text{O}_i$ |
| 1   | 9.254                       | 18.542                  | 10.949                       | 21.591                  | 25.803                       | 13.3967                 | -0.143                  |
| 2   | 9.254                       | 18.542                  | 10.986                       | 21.649                  | 25.803                       | 13.4066                 | -0.134                  |
| 3   | 9.254                       | 18.542                  | 10.972                       | 21.638                  | 25.803                       | 13.3907                 | -0.149                  |
| 4   | 9.254                       | 18.542                  | 10.967                       | 21.637                  | 25.803                       | 13.3823                 | -0.158                  |
| 5   | 9.254                       | 18.542                  | 10.934                       | 21.571                  | 25.803                       | 13.3894                 | -0.151                  |
| 6   | 9.254                       | 18.542                  | 10.942                       | 21.575                  | 25.803                       | 13.4006                 | -0.140                  |
| 7   | 9.254                       | 18.542                  | 11.080                       | 21.818                  | 25.803                       | 13.4061                 | -0.134                  |
| 8   | 9.254                       | 18.542                  | 11.038                       | 21.760                  | 25.803                       | 13.3868                 | -0.153                  |
| 9   | -20.85                      | -38.2                   | -4.373                       | -7.288                  | 25.803                       | 13.401                  | -0.139                  |
| 10  | -20.85                      | -38.2                   | -4.210                       | -6.9804                 | 25.803                       | 13.3978                 | -0.142                  |
| 11  | -20.85                      | -38.2                   | -4.497                       | -7.520                  | 25.803                       | 13.4003                 | -0.140                  |
| 12  | -20.85                      | -38.2                   | -3.987                       | -6.573                  | 25.803                       | 13.4103                 | -0.130                  |
| Mean $\pm$ SD   |                             |                         |                              |                         |                              | 13.398 $\pm$ 0.009      | -0.142 $\pm$ 0.008      |



Table S4.2 The ratio of stomatal conductance to mesophyll conductance and weighted mean fractionation of  $^{12}\text{C}^{18}\text{O}^{16}\text{O}$  as it diffuses from the  $\text{CO}_2\text{-H}_2\text{O}$  exchange site ( $\bar{a}_{18}$ ) for numerous species determined in previous investigations.

| gs/gm | $\bar{a}_{18}$ | Plant type                            | Reference                 |
|-------|----------------|---------------------------------------|---------------------------|
| 1.56  | 3.93           | <i>S. viridis</i> (C <sub>4</sub> )   | (Osborn et al., 2017)     |
| 1.26  | 4.33           | <i>S. viridis</i> (C <sub>4</sub> )   | (Osborn et al., 2017)     |
| 0.22  | 7.37           | Tobacco (C <sub>3</sub> )             | (Gillon and Yakir, 2000b) |
| 0.16  | 7.71           | Soya (C <sub>3</sub> )                | (Gillon and Yakir, 2000b) |
| 0.47  | 6.23           | Oak (C <sub>3</sub> )                 | (Gillon and Yakir, 2000b) |
| 0.17  | 7.76           | Tobacco (C <sub>3</sub> )             | (Barbour et al., 2016)    |
| 0.06  | 8.32           | Cotton (C <sub>3</sub> )              | (Barbour et al., 2016)    |
| 0.32  | 7.04           | Wheat (C <sub>3</sub> )               | (Barbour et al., 2016)    |
| 0.06  | 8.27           | Maize (C <sub>4</sub> )               | (Barbour et al., 2016)    |
| 0.24  | 7.29           | <i>S. Viridis</i> (C <sub>4</sub> )   | (Barbour et al., 2016)    |
| 0.29  | 7.21           | <i>F. bindensis</i> (C <sub>4</sub> ) | (Barbour et al., 2016)    |
| 0.88  | 5.05           | Sunflower (C <sub>3</sub> )           | This study                |
| 0.55  | 5.96           | Ivy (C <sub>3</sub> )                 | This study                |
| 0.27  | 7.12           | <i>S. viridis</i> (C <sub>4</sub> )   | This study                |
| 1.2   | 4.18           | <i>S. viridis</i> (C <sub>4</sub> )   | (Cousins et al., 2006)    |
| 2.1   | 3.74           | Tobacco (C <sub>3</sub> )             | (Cousins et al., 2006)    |
| 0.13  | 7.90           | <i>A. edulis</i> (C <sub>4</sub> )    | (Cousins et al., 2007)    |

# Chapter 5

## Discussion and outlook

In this chapter, an overview of the important findings reported in this thesis, and measurement challenges of  $\Delta^{17}\text{O}$  as a tracer for mesophyll conductance and GPP are presented and discussed. Finally, we provide an outlook based on the finding in this thesis and recommend future research in five concrete projects to follow up on the findings of this Ph.D. research.

### 5.1. Discussion

#### 5.1.1. Measuring $\Delta^{17}\text{O}$ of atmospheric $\text{CO}_2$

Measurements of  $\Delta^{17}\text{O}$  of atmospheric  $\text{CO}_2$  are limited in number compared to the conventional  $\delta^{13}\text{C}$  and  $\delta^{18}\text{O}$  measurements due to the measurement challenge. The challenge with measuring  $\Delta^{17}\text{O}$  (or  $\delta^{17}\text{O}$ ) using an isotope ratio mass spectrometer (IRMS) is the interference of  $^{13}\text{C}^{16}\text{O}^{16}\text{O}$  on the  $^{12}\text{C}^{17}\text{O}^{16}\text{O}$  isotopologue, in combination with the low abundance of  $^{12}\text{C}^{17}\text{O}^{16}\text{O}$  (15 times lower than  $^{13}\text{C}^{16}\text{O}^{16}\text{O}$ ). To separate these two isotopologues, a mass spectrometer with a resolving power ( $m/\Delta m$ ) of approximately  $> 56,000$  is required. The conventional IRMS have a far lower mass resolution, and therefore in the past  $\delta^{17}\text{O}$  measurement of  $\text{CO}_2$  using IRMS was realized only by conversion of  $\text{CO}_2$  to  $\text{O}_2$  (Thiemens et al., 1991) or isotope exchange with metal oxides or  $\text{O}_2$  (Hofmann and Pack, 2010; Barkan et al., 2015). In **Chapter 2** of this thesis, we developed a technique to measure the  $\delta^{17}\text{O}$  of  $\text{CO}_2$  without conversion/exchange, using ion fragments of  $\text{CO}_2$  that are formed by electron ionization in the ion source of a high-resolution IRMS. In addition, we established the previously developed  $\text{CO}_2$ - $\text{O}_2$  exchange method at Utrecht University.

Both  $\text{CO}_2$ - $\text{O}_2$  exchange and fragment techniques require pure  $\text{CO}_2$ , and interferences from other compounds (e.g. water) must be minimized. In the  $\text{CO}_2$ - $\text{O}_2$  exchange method, water will interfere with the isotope composition of the  $\text{CO}_2$ , since  $\text{CO}_2$  will also exchange isotopes with water and this will affect the isotope composition of the exchanged  $\text{O}_2$ . For the fragment method, the interference from adduct ions is well resolved with the high-resolution isotope ratio mass spectrometer (HR-IRMS), even at medium resolution setting. In addition, water interferes with the  $\Delta^{17}\text{O}$  measurement by contributing  $^{16}\text{O}^+$ ,  $^{17}\text{O}^+$ , and  $^{18}\text{O}^+$  fragment ions. The degree of interference of  $\text{H}_2\text{O}$  on  $\Delta^{17}\text{O}$  of  $\text{CO}_2$  depends on the proportion of  $[\text{H}_2\text{O}]/[\text{CO}_2]$  and the  $\Delta^{17}\text{O}$  of  $\text{H}_2\text{O}$ .

Another potential interference in the fragment method is from doubly ionized  $^{16}\text{O}^{18}\text{O}^{++}$  formed in the ion source, which cannot be resolved from  $^{17}\text{O}^+$  of  $\text{CO}_2$ . This means that the  $\Delta^{17}\text{O}$  value is slightly dependent on the relative difference in  $\delta^{18}\text{O}$  between the sample and working standard, and practice also on the source pressure since the relative abundance of double ionized  $\text{O}_2$  depends on source pressure. If the measurements are carried out using a working

gas with an isotope composition close to the sample and at higher source pressure, then the interference of  $^{16}\text{O}^{18}\text{O}^{++}$  on the  $\delta^{17}\text{O}$  is negligible.

The other challenge to measure  $\Delta^{17}\text{O}$  is scale contraction, a general phenomenon for isotope measurements using isotope ratio mass spectrometry. Scale contraction is different for different isotope ratio mass spectrometers, as observed for the two IRMS's in this study; the Ultra high-resolution isotope ratio mass spectrometer has a larger scale contraction compared to the Delta<sup>plus</sup>XL. The scale contraction depends on the emission current, equilibration time, source pressure, and the ion source conductance as discussed in (Verkouteren et al., 2003a; Verkouteren et al., 2003b) and these parameters were carefully evaluated for the 253 Ultra in chapter 2 of this thesis. Measuring a sample with low emission current, long equilibration time, higher source pressure, and open variable ion source conductance (VISC) window will give a lower scale contraction. However, lower emission current results in a lower ionization of the molecules, reducing the signal, and opening the VISC window also reduces the signal, in our machine by a factor 3 compared to the signal with the VISC closed. Increasing equilibration time reduces the measurement time of the sample, thus requiring long measurement times to get a required precision and sample loss. Using the  $\text{CO}_2$ - $\text{O}_2$  exchange method, we measured the  $\Delta^{17}\text{O}$  of  $\text{CO}_2$  samples with a precision better than 0.010 ‰. The fragment method does not require isotope exchange/conversion of the  $\text{CO}_2$ , but to reach a measurement precision of 0.01 ‰, it requires a measurement time of 24 hrs, which precludes widespread use and high sample throughput. Nevertheless, the fragment techniques provide a completely independent assessment of  $\Delta^{17}\text{O}$  of  $\text{CO}_2$  than other methods and may be valuable in the calibration of reference materials (see below).

During this study, we collaborated with the center for isotope research (CIO) of Groningen university to characterize a Quantum Cascade Dual-Laser Absorption Spectrometry (QCDLAS) instrument from Aerodyne (Aerodyne Research, Inc., Massachusetts, USA) to measure the  $^{17}\text{O}$ -excess of  $\text{CO}_2$ . QCDLAS does not require extraction of pure  $\text{CO}_2$  from air, allowing to measure the triple oxygen isotope composition of  $\text{CO}_2$  directly from air samples, unlike the IRMS techniques described in this study (McManus et al., 2015). QCDLAS requires a relatively smaller sample size and short measurement time compared to the IRMS technique and it is possible to perform a semi-continuous measurement in the field. The limitation of QCDLAS is its dependency on the mole fraction of  $\text{CO}_2$  that requires intensive calibration and decay in the sensitivity of the laser with time. The characterization of the QCDLAS instrument is in progress.

### 5.1.2. Mesophyll conductance for $\text{CO}_2$

As discussed in **Chapter 3** of this thesis, mesophyll conductance estimates using oxygen isotope composition strongly depend on the relative difference in the oxygen isotope composition between  $\text{CO}_2$  in the intercellular air space and at the  $\text{CO}_2$ - $\text{H}_2\text{O}$  exchange site. When the relative difference between the oxygen isotope composition between the  $\text{CO}_2$ - $\text{H}_2\text{O}$  exchange site and intercellular air space is close to zero,  $g_{m\Delta^{17}}$  or  $g_{m\Delta^{18}}$  estimates will have large errors. This can happen either when the oxygen isotope composition of  $\text{CO}_2$  entering the leaf is the same as the oxygen isotope composition of the  $\text{CO}_2$  equilibrated with leaf water or at higher mesophyll conductance. A larger difference in the oxygen isotope composition of  $\text{CO}_2$  between the intercellular air space and at the  $\text{CO}_2$ - $\text{H}_2\text{O}$  exchange site can be achieved using  $\text{CO}_2$  with a large difference in  $\Delta^{17}\text{O}$  and  $\delta^{18}\text{O}$  between the  $\text{CO}_2$  entering the leaf and the  $\text{CO}_2$

at the CO<sub>2</sub>-H<sub>2</sub>O exchange site. However, if the mesophyll conductance is very high, the oxygen isotope composition of CO<sub>2</sub> at the CO<sub>2</sub>-H<sub>2</sub>O exchange site ( $\Delta^{17}\text{O}_m$  and  $\delta^{18}\text{O}_m$ ) and in intercellular air space ( $\Delta^{17}\text{O}_i$  and  $\delta^{18}\text{O}_i$ ) will be similar regardless of the oxygen isotope composition of the CO<sub>2</sub> used.

The dependence on the difference between the CO<sub>2</sub>-H<sub>2</sub>O exchange site and intercellular air space might be one of the reasons for conflicting estimates of  $g_{m18}$  in the literature, but this is difficult to reconstruct because not always all the necessary values are reported. When reporting  $g_{m18}$  it is also important to report at what  $\delta^{18}\text{O}_i$ - $\delta^{18}\text{O}_m$  or  $\Delta^{17}\text{O}_i$  -  $\Delta^{17}\text{O}_m$  difference the measurement is carried out. The precision of the derived  $g_m$  estimate can be increased by using isotopically different CO<sub>2</sub> and water vapor entering the leaf compared to the CO<sub>2</sub> and water at the CO<sub>2</sub>-H<sub>2</sub>O exchange site. There is a strong variation in the oxygen isotope composition of water within a leaf and the CO<sub>2</sub>-H<sub>2</sub>O exchange site is unknown. Such variations result in a bias in  $g_{m18}$  estimates.  $\Delta^{17}\text{O}$  is less sensitive to mass-dependent isotope fractionation processes compared to  $\delta^{18}\text{O}$ , as a result, mesophyll conductance can be determined with better precision using slightly  $^{17}\text{O}$ -enriched CO<sub>2</sub>. We recommend exploring the  $g_{m\Delta 17}$  technique further. The experiment should be designed in a way to control the mixing ratio of oxygen entering the leaf cuvette to avoid artifacts due to photorespiration on  $g_{m13}$  and  $g_{m\Delta 17}$  estimates (Holloway-Phillips et al., 2019; Ubierna et al., 2019). The experiments should be performed with CO<sub>2</sub> having a  $\Delta^{17}\text{O}$  value higher than 10 ‰ without manipulating  $^{17}\text{O}$ -excess of the irrigation water and the water vapor entering the leaf cuvette.

### 5.1.3. Effect of photosynthesis on $\Delta^{17}\text{O}$ atmospheric CO<sub>2</sub>

To determine the effect of photosynthesis on the  $\Delta^{17}\text{O}$  of atmospheric CO<sub>2</sub> we carried out a leaf scale experiment under controlled conditions using a leaf cuvette as described in **Chapter 4** of this thesis. The relative difference in the  $\Delta^{17}\text{O}$  of the CO<sub>2</sub> entering the leaf and the CO<sub>2</sub> at the CO<sub>2</sub>-H<sub>2</sub>O exchange site, and type of plant have a large influence on the effect of photosynthesis on the  $\Delta^{17}\text{O}$  of atmospheric CO<sub>2</sub>. When the difference between the  $\Delta^{17}\text{O}$  of CO<sub>2</sub> entering the cuvette and at the CO<sub>2</sub>-H<sub>2</sub>O exchange site is small, the effect of photosynthesis on the  $\Delta^{17}\text{O}$  of the atmospheric CO<sub>2</sub> is small. When the  $\Delta^{17}\text{O}$  of CO<sub>2</sub> entering the leaf and at the CO<sub>2</sub>-H<sub>2</sub>O exchange site are different, the effect of photosynthesis on  $\Delta^{17}\text{O}$  of CO<sub>2</sub> is dominated by either diffusion or exchange depending on the  $c_m/c_a$  ratio. C<sub>3</sub> plants have a relatively higher mole fraction of CO<sub>2</sub> at the CO<sub>2</sub>-H<sub>2</sub>O exchange site ( $c_m$ ) to the leaf surrounding air ( $c_a$ ) compared to C<sub>4</sub> plants. The difference in the  $c_m/c_a$  ratio is due to the difference in the assimilation rate. For plants with a higher  $c_m/c_a$  ratio (C<sub>3</sub> plants), the discrimination in  $\Delta^{17}\text{O}$  of atmospheric CO<sub>2</sub> is dominated by the CO<sub>2</sub>-H<sub>2</sub>O exchange signal, whereas for plants with a lower  $c_m/c_a$  ratio (C<sub>4</sub> plants), the discrimination is dominated by diffusion.

The impact of land vegetation also depends on the proportional productivity of C<sub>4</sub> and C<sub>3</sub> plants. Currently, C<sub>4</sub> vegetation is responsible for 20-25 % of GPP (Still et al., 2003), but the proportion may change in the future due to an increase in the mole fraction of atmospheric CO<sub>2</sub> where C<sub>3</sub> plants are favored at higher atmospheric CO<sub>2</sub> mole fraction (Tippel and Pagani, 2007; Collatz et al., 1998; Ehleringer, 2005; Sage, 2004, 2005; Sage and Monson, 1998). Based on the leaf scale measurements, we estimated the discrimination in  $\Delta^{17}\text{O}$  for the global vegetation to be  $-0.57 \pm 0.14$  ‰. Extrapolation of the leaf level experiment to the global scale is difficult due to the limited information on  $c_m/c_a$  values under field conditions and their variation across the globe. This may improve in the future because new laser spectroscopic techniques (Nelson

et al., 2008; McManus et al., 2005; 2010; 2015) that can measure  $\Delta^{17}\text{O}$  of  $\text{CO}_2$  in the field semi-continuously may allow measurement of  $c_m/c_a$  ratios of different plant types in different environments.

## 5.2. Perspectives and recommendations

### 5.2.1. Consensus in the reference slope

The  $\Delta^{17}\text{O}$  of tropospheric  $\text{CO}_2$  variations represents an integral signal from anthropogenic and biochemical processes, therefore a single fractionation slope for the  $\ln(\delta^{18}\text{O}+1)-\ln(\delta^{17}\text{O}+1)$  space is not representative for all processes, and there is no a single best  $\lambda$  value (Miller et al., 2020). Choosing a single representative three isotope fractionation slope is a big dilemma in the triple oxygen isotope community. As a result, several different  $\lambda$  values are used in different studies (Hofmann et al., 2017).

The most commonly used  $\lambda_{ref}$  is 0.528, the value that is also used in this thesis (Sharp et al., 2018; Wostbrock et al., 2019; Passey et al., 2014; Landais et al., 2006; Meijer and Li, 1998; Barkan et al., 2019; Fosu et al., 2020; Schoenemann et al., 2013; Young et al., 2016a). This is the value that has been established for meteoric waters (Meijer and Li, 1998; Luz and Barkan, 2010), and the reason for using  $\lambda_{ref} = 0.528$  also for  $\text{CO}_2$  is that the carbon and hydrological cycle are connected via oxygen isotope exchange between water and  $\text{CO}_2$ . As a result, atmospheric  $\text{CO}_2$  will generally follow a similar three-isotope fractionation line as the meteoric waters (Meijer and Li, 1998; Luz and Barkan, 2010). This does not mean that all water bodies will have a  $\Delta^{17}\text{O}$  value of zero when using  $\lambda = 0.528$  since the formation of the precipitation is influenced by several isotope fractionation processes such as diffusion, evaporation and condensation, and the individual processes have a three isotope slope that deviate from  $\lambda = 0.528$  (Landais et al., 2008; Barkan and Luz, 2007; Luz and Barkan, 2010; Angert et al., 2004; Li et al., 2015; Miller, 2018; Sharp et al., 2018).

Other researchers have used different three isotope slopes, for example  $\lambda = 0.516$  (Laskar et al., 2020; Liang et al., 2017b; Boering et al., 2004; Hoag et al., 2005), close to the fractionation line for transpiration at a relative humidity of 75 % (Landais et al., 2006). Their main argument for the choice of  $\lambda_{ref} = 0.516$  is that it eliminates the effect of transpiration on the  $\Delta^{17}\text{O}$  of meteoric waters. The third commonly used reference slope is 0.5305, mainly in the solid rocks community (Pack et al., 2016; Pack, 2017) which is the high-temperature equilibrium fractionation. The fact that this value is related to a thermodynamic equilibrium is attractive since it would not depend on other factors, but it has not been adopted by the atmospheric community, possibly because it would be different from all the important slopes that act on the system. Some studies have used  $\lambda = 0.5229$  because this is the slope associated with  $\text{CO}_2\text{-H}_2\text{O}$  isotope exchange, the process that links atmospheric  $\text{CO}_2$  to leaf, soil, or ocean water (Hofmann et al., 2017; Koren et al., 2019).

Even though the choice of  $\lambda$  does not change the interpretation, similar to (Sharp et al., 2018), we recommended using  $\lambda = 0.528$ , because this takes into account variations in the isotopic composition of water in the natural environment and it is in line with the well-established hydrological reporting system (Luz and Barkan, 2010; Meijer and Li, 1998). In addition, the  $\lambda$

value of 0.528 is also recommended when applying the “ $^{17}\text{O}$  correction” for precise measurement of  $^{13}\text{C}$  in standard isotope ratio analysis of  $\text{CO}_2$  samples (Brand et al., 2010). Furthermore, using a  $\lambda$  value of 0.528 gives a better interlaboratory comparability for  $^{13}\text{C}^{16}\text{O}^{18}\text{O}$  isotope measurements than using the “Santrock correction” (Santrock et al., 1985) with a  $\lambda$  value of 0.516 (Schauer et al., 2016).

### 5.2.2. Interlaboratory comparison

In principle, international standards have assigned reference isotope ratios. For oxygen isotopes, reference materials are available in different physical forms (different types of material) e.g. waters, carbonates, and atmospheric  $\text{O}_2$ . When different laboratories measure the oxygen in these materials against each other, they report significantly different values, which shows that there are systematic discrepancies, see Table 5.1 for carbonate standards and atmospheric  $\text{O}_2$ . The standard deviation in the  $\Delta^{17}\text{O}$  of the atmospheric  $\text{O}_2$  assigned is different, with a standard deviation of 0.044 (1- $\sigma$ ,  $N=4$ ). This variation is much larger than the precision of the measurement techniques developed to measure  $\Delta^{17}\text{O}$  including this thesis. The variation might be due to the errors during the extraction of oxygen from the air, and/or scale issues in the isotopic ratio mass spectrometer or calibration. Scale distortions in  $\Delta^{17}\text{O}$  measurements can also originate from pressure baseline corrections (Yeung et al., 2018).

Oxygen isotope measurements are reported with a link to a single standard VSMOW (Vienna Standard Mean Ocean Water) or PDB (Pee Dee Belemnite) which only fixes the zero-point of the  $\delta$  scale. Vienna Standard Mean Ocean Water-Standard Light Antarctic Precipitation (SMOW-SLAP) normalizations are suggested as a better solution to reduce the scale issue of the isotope ratio mass spectrometer for inter-laboratory consistency since the  $\delta^{18}\text{O}$  value SLAP relative to SMOW is -55.5 ‰ (Gonfiantini, 1978). The normalization requires that the measured  $\delta^{18}\text{O}$  value of a sample relative to VSMOW be adjusted by a factor of  $(-55.5)/(\delta^{18}\text{O}_{\text{SLAP/VSMOW}})$ , where  $\delta^{18}\text{O}_{\text{SLAP/VSMOW}}$  is the measured value of SLAP relative to SMOW (Gonfiantini, 1978; Kaiser, 2008). However, not every research group has a facility to measure water and gas samples for  $\Delta^{17}\text{O}$  with a high precision. Furthermore, inconsistencies in the  $\Delta^{17}\text{O}$  value are also reported for the commonly used carbonate standards even though the values are VSMOW -SLAP normalized (Table 5.1).

For the carbonate standards, the variation is not only important for determining the absolute  $\Delta^{17}\text{O}$  value of the carbonate standards but also, maybe even more fundamentally, for the relative difference between the carbonate standards. Differences reported by different laboratories should agree, even if the absolute values may differ. However, the difference  $\Delta^{17}\text{O}(\text{NBS19}) - \Delta^{17}\text{O}(\text{NBS18})$  reported by (Wostbrock et al., 2019) and (Fosu et al., 2020) is  $\cong -0.050$  ‰, whereas (Passey et al., 2014) and (Barkan et al., 2019) reported smaller differences,  $-0.037$  ‰ and  $-0.019$  ‰, respectively. Part of the difference may be due to sample preparation. (Wostbrock et al., 2019) used a calcite fluorination method to extract  $\text{CO}_2$ , the other studies measured the  $\text{CO}_2$  extracted from carbonate using  $\text{H}_3\text{PO}_4$  acid digestion. The relative difference between  $\Delta^{17}\text{O}(\text{NBS18})$  and  $\Delta^{17}\text{O}(\text{IAEA603})$  (a replacement for NBS19) is reported as  $-0.042$  ‰ by Sha et al., (2020) and  $-0.010$  ‰ by (Barkan et al., 2019). The relative difference between the carbonate standards can be determined independently using the fragment technique developed in this PhD thesis (see below).

One of the possible causes for the differences in Table 5.1 is heterogeneity in the samples, resulting in sample-to-sample variability (Starkey et al., 2016). As far as the isotopic composition is concerned, tropospheric O<sub>2</sub> is distributed homogeneously, as a result, the variability between different measurements reported in the literature is very likely due to artifacts from the analytical techniques that are used to extract O<sub>2</sub> from the air and/or from IRMS scale distortions during measurement (calibration). These are the only limitations to using oxygen as reference material.

Table 5.1 Summary for the triple oxygen isotopic composition of carbonate standards (NBS18, NBS19, IAEA603) and atmospheric O<sub>2</sub> measured at different research groups. All the values are relative to VSMOW and they are in ‰.  $\Delta^{17}\text{O}$  values are calculated with a  $\lambda_{RL} = 0.528$ .

| Carbonate standards         |                       |                        |                          |                       |                       |
|-----------------------------|-----------------------|------------------------|--------------------------|-----------------------|-----------------------|
|                             |                       | (Passey et al., 2014)  | (Fosu et al., 2020)      | (Sha et al., 2020)    | (Barkan et al., 2019) |
| NBS19                       | $\delta^{17}\text{O}$ | 19.013                 | 20.334(0.008)            | -                     | 20.320(0.006)         |
|                             | $\delta^{18}\text{O}$ | 36.586(0.9)            | 39.194                   | -                     | 39.196                |
|                             | $\Delta^{17}\text{O}$ | -0.135(0.012)          | -0.169(0.005)            | -                     | -0.182(0.005)         |
| NBS18                       | $\delta^{17}\text{O}$ | 7.909                  | 9.095(0.006)             | 8.965(0.012)          | 9.049(0.005)          |
|                             | $\delta^{18}\text{O}$ | 15.225(0.6)            | 17.524                   | 17.481(0.019)         | 17.522                |
|                             | $\Delta^{17}\text{O}$ | -0.098(0.014)          | -0.119(0.005)            | -0.225(0.004)         | -0.163(0.005)         |
| IAEA 603                    | $\delta^{17}\text{O}$ | -                      | -                        | 20.182(0.015)         | 20.218(0.005)         |
|                             | $\delta^{18}\text{O}$ | -                      | -                        | 39.092(0.034)         | 39.019                |
|                             | $\Delta^{17}\text{O}$ |                        |                          | -0.267(0.006)         | -0.192(0.006)         |
| Tropospheric O <sub>2</sub> |                       |                        |                          |                       |                       |
|                             |                       | (Barkan and Luz, 2011) | (Wostbrock et al., 2019) | (Laskar et al., 2019) | (Pack, 2017)          |
| Air-O <sub>2</sub>          | $\delta^{17}\text{O}$ | 12.026(0.02)           | 12.178(0.066)            | 11.979(0.013)         | 12.27(0.02)           |
|                             | $\delta^{18}\text{O}$ | 23.881(0.02)           | 24.046(0.117)            | 23.732(0.006)         | 24.15(0.05)           |
|                             | $\Delta^{17}\text{O}$ | -0.507                 | -0.442                   | -0.476                | -0.404                |

Part of the variability in the reported  $\Delta^{17}\text{O}$  might also be due to the different definitions of  $\Delta^{17}\text{O}$  (equation 5.1).

$$\Delta^{17}\text{O} = \ln(\delta^{17}\text{O} + 1) - \lambda \times \ln(\delta^{18}\text{O} + 1) - \gamma \quad (5.1)$$

where  $\gamma$  is the intercept. In this study, we used equation 1 with  $\gamma=0$ . When equation 5.1 is used as a definition for  $\Delta^{17}\text{O}$ ,  $\lambda$  can be chosen as constant, independent of the oxygen isotope composition of the reference material used, but  $\gamma$  is dependent on the reference material used in the respective laboratory (Miller et al., 2020; Miller, 2002). As a result, the errors in the oxygen isotopic composition of the reference material will be translated to the sample oxygen isotopic composition.

The final possible cause for the variability in  $\Delta^{17}\text{O}$  might be an artifact in the CO<sub>2</sub> exchange/conversion step during sample preparation. The O-fragment technique developed in this thesis does not require chemical conversion/exchange and can be used as an independent method to investigate the inconsistency in the relative difference in  $\Delta^{17}\text{O}$  between different carbonate standards if the reported discrepancy by different research groups is due to the chemical conversion/exchange step. In addition, measuring atomic fragment ions of different compounds may be a useful tool to study fractionation processes in the ion source of an isotope ratio mass spectrometer. As discussed earlier above, the scale contractions for isotopic



measurements are different for the fragment ions and molecular ions of CO<sub>2</sub>. Examining these effects further may help to understand the chemistry and surface effects in the ion source of isotope ratio mass spectrometers by studying different fragments. The main challenge during fragment measurement is lower signal intensity of the fragment ions and interferences from adduct formation.

### 5.2.3. $\Delta^{17}\text{O}$ of atmospheric CO<sub>2</sub>

$\Delta^{17}\text{O}$  of CO<sub>2</sub> has been suggested to be a better tracer for GPP than  $\delta^{18}\text{O}$  (Hoag et al., 2005; Hofmann et al., 2017) since  $\Delta^{17}\text{O}$  probes directly the associated processes in the carbon and water cycle (Luz and Barkan, 2010; Luz et al., 1999; Barkan and Luz, 2007; Landais et al., 2006; Uemura et al., 2010). However, to use  $\Delta^{17}\text{O}$  of atmospheric CO<sub>2</sub> as a tracer for GPP requires the ability to distinguish the  $\Delta^{17}\text{O}$  of the different sources and sinks since variations of  $\Delta^{17}\text{O}$  in tropospheric CO<sub>2</sub>. This represents an integral signal from all the anthropogenic and biochemical processes. The  $\Delta^{17}\text{O}$  signature of stratospheric CO<sub>2</sub> is well-defined (Hofmann et al., 2017; Koren et al., 2019; Hoag et al., 2005), and sources of atmospheric CO<sub>2</sub> from photochemical oxidation processes in the atmosphere have a relatively smaller flux (Koren et al., 2019). Another important source is the exchange with ocean water, and for this, the triple oxygen isotopic composition is assumed to be close to zero (Affek and Yakir, 2014; Luz and Barkan, 2010; Koren et al., 2019; Liang et al., 2017b). This assumption is reasonable because it is expected that CO<sub>2</sub> will equilibrate with ocean water, but it has not been confirmed by a measurement. The other four unknown processes for the  $\Delta^{17}\text{O}$  atmospheric CO<sub>2</sub> are photosynthesis, respiration (foliage and soil respiration), soil invasion, and combustion. The  $\Delta^{17}\text{O}$  of CO<sub>2</sub> from fossil fuel and biomass combustion has a smaller effect on the global scale due to its smaller flux compared to photosynthesis and respiration (Hoag et al., 2005). However, in urban regions, both fossil fuel emission and biomass burning can be an important source for  $\Delta^{17}\text{O}$  of CO<sub>2</sub> (Pataki et al., 2007; Yanes and Yapp, 2010; Laskar et al., 2016).  $\Delta^{17}\text{O}$  of combustion depends on the material being combusted and CO<sub>2</sub> from fossil fuel combustion retains the  $\Delta^{17}\text{O}$  of air O<sub>2</sub> (Affek and Yakir, 2014; Laskar et al., 2016; Horváth et al., 2012; Liang et al., 2017b). When wood or straw from vegetation is burned, oxygen from other oxygenated compounds such as cellulose, hemicellulose [C<sub>6</sub>H<sub>10</sub>O<sub>5</sub>]<sub>n</sub>, and lignin(C<sub>10</sub>H<sub>12</sub>O) (Zhang et al., 2012) is added, which results in a different  $\Delta^{17}\text{O}$  signature of CO<sub>2</sub> compared to fossil fuel combustion (Horváth et al., 2012; Laskar et al., 2020).

The above argumentations underscore the necessity to precisely characterize the effect of different sources and sinks of the terrestrial carbon cycle on the  $\Delta^{17}\text{O}$  of tropospheric CO<sub>2</sub> as a prerequisite to use  $\Delta^{17}\text{O}$  of CO<sub>2</sub> to quantify the carbon cycle. In this thesis, the impact of photosynthesis on the  $\Delta^{17}\text{O}$  of tropospheric CO<sub>2</sub> has been quantified using three plant types representing two types of metabolism, C<sub>3</sub> and C<sub>4</sub>, and three biomes. To estimate the impact of photosynthesis on the  $\Delta^{17}\text{O}$  of tropospheric CO<sub>2</sub>, the measured  $\Delta^{17}\text{O}$  signature is weighted by the photosynthesis activity of plants and the  $c_m/c_a$  ratio. Weighting the effect of plants on the  $\Delta^{17}\text{O}$  of CO<sub>2</sub> based on the plant photosynthetic activity and  $c_m/c_a$  ratio might help in constraining climate change feedbacks in the future. For instance, if  $g_m$  would change in the future, the impact of photosynthesis on  $\Delta^{17}\text{O}$  of tropospheric CO<sub>2</sub> can be predicted based on the formalism obtained in this thesis. A similar approach can be used to further investigate/identify the impact of other sources of the terrestrial carbon cycle on the  $\Delta^{17}\text{O}$  of tropospheric CO<sub>2</sub>. An upscaled estimate of the effect of photosynthesis on the  $\Delta^{17}\text{O}$  of tropospheric CO<sub>2</sub> can be obtained by measuring  $c_m/c_a$  ratio of several plant types under different environmental



conditions. The estimated effect of C<sub>3</sub> and C<sub>4</sub> vegetation on the  $\Delta^{17}\text{O}$  of near-surface CO<sub>2</sub> in this thesis should be further extended by sampling air in areas dominated by C<sub>3</sub> vegetation (such as Amazonia) and C<sub>4</sub> vegetation (such as savanna grassland), respectively.

Nocturnal stomatal conductance and soil invasion are conceptually similar processes because in both cases the CO<sub>2</sub> that diffuses into the leaf and soils will diffuse back to the atmosphere after isotope exchange with either leaf water and soil water, respectively (Tans, 1998; Stern et al., 2001; Miller et al., 1999). Nocturnal stomatal conductance is not included in the global  $\Delta^{17}\text{O}$  budgets, reflecting the assumption that stomata will be fully closed during the night. However, recent studies suggest that this is not the case (Howard and Donovan, 2007; Caird et al., 2007; Kooijmans et al., 2019; Seibt et al., 2007; Seibt et al., 2006; Barbour et al., 2007; Zeppel et al., 2012). Howard and Donovan (2007) suggested that stomatal conductance may even reach values greater than 50 % of day time conductance depending on the plant type. To better constrain the atmosphere-biosphere interaction and flux, it is important to incorporate the effect of night-time stomatal conductance (Zeppel et al., 2012). Understanding the effects of nocturnal stomatal conductance and CO<sub>2</sub> from dark respiration on the triple isotope composition of CO<sub>2</sub> is important for interpreting  $\Delta^{17}\text{O}$  of atmospheric CO<sub>2</sub> at local, regional, and global scales since leaf dark respiration is an important component of carbon cycling between biosphere and atmosphere. Seibt and co-workers (Seibt et al., 2006) reported underestimation of daily canopy iso-fluxes (in  $\delta^{18}\text{O}$ ) of forest up to 30 % if nocturnal stomatal conductance is not included. The effects of nocturnal stomatal conductance and dark respiration can be quantified using a similar leaf cuvette experiment presented in chapter 4 of this thesis, under the dark conditions. The challenge is to establish a sufficient signal, and we recommend using a leaf with a large surface area to realize a relatively high mole fraction difference between the CO<sub>2</sub> entering the cuvette and the CO<sub>2</sub> leaving the cuvette because this will lead to better precision.

The effect of soil respiration and invasion on the  $\Delta^{17}\text{O}$  of atmospheric CO<sub>2</sub> is not quantified experimentally. Because of the unknown quantities of soil invasion flux estimates of GPP using  $\Delta^{17}\text{O}$  are not precise as primarily though (Liang et al., 2017b). The latest soil invasion estimate is carried out by (Wingate et al., 2009) using  $\delta^{18}\text{O}$  of CO<sub>2</sub> incorporating the effect of carbonic anhydrase for the first time. However, there is a strong vertical gradient at the soil surface because of soil evaporation (Miller et al., 1999; Wingate et al., 2009) which makes it complicated to use  $\delta^{18}\text{O}$  of CO<sub>2</sub> to estimate soil invasion flux.  $\Delta^{17}\text{O}$  of CO<sub>2</sub> is less affected by evaporation compared to  $\delta^{18}\text{O}$  of CO<sub>2</sub>, as a result,  $\Delta^{17}\text{O}$  of CO<sub>2</sub> might give a better estimate for invasion flux. The  $\Delta^{17}\text{O}$  (CO<sub>2</sub>) measurement technique developed in this thesis can be used to quantify the soil invasion flux with better precision based on chamber-based measurements.

### 5.3. Future Perspectives

In this thesis, we presented an automated system based on the CO<sub>2</sub>-O<sub>2</sub> exchange method suitable to perform routine measurements with a precision better than 0.01 ‰. Based on these measurement techniques, we recommend five research projects that would expand the spatial coverage of  $\Delta^{17}\text{O}$  measurements and address gaps in our understanding and quantification of the specific processes in the terrestrial carbon cycle.

- a) Quantification of  $\Delta^{17}\text{O}$  from soil invasion and constraining the soil invasion flux: The estimates of soil invasion fluxes reported in the literature vary from < 10 PgC yr<sup>-1</sup> (Stern

et al., 2001) to 450 PgCyr<sup>-1</sup> (Wingate et al., 2009) using  $\delta^{18}\text{O}$  of  $\text{CO}_2$ . There have been no follow-up studies in the past decade, since (Wingate et al., 2009). With the techniques presented in this thesis  $\Delta^{17}\text{O}$  measurements from the soil, chambers measurements are now possible and are a logical next step to better constrain the soil invasion flux.

- b) Quantifying the effect of nocturnal stomatal conductance and foliage respiration on the  $\Delta^{17}\text{O}$  of atmospheric  $\text{CO}_2$ : To partition respiration flux to foliage and soil respiration to requires understanding and quantifying nocturnal stomatal conductance and foliage respiration using leaf cuvette experiments described in this thesis during the dark.
- c) Determination of  $\Delta^{17}\text{O}$  emitted from the ocean: Quantifying the oceanic flux precisely requires a sampling campaign where there is no terrestrial vegetation interference, for example, the remote Pacific and southern hemisphere oceans.
- d) Determination of the seasonal variability  $\Delta^{17}\text{O}$  of tropospheric  $\text{CO}_2$  at different locations. Global 3D transport model calculations (Koren et al., 2019) predict large seasonal cycle amplitudes, e.g. 0.036 ‰ peak-to-peak at the Zotino Tall Tower Observatory (60.80°N, 89.35°E) (Heimann et al., 2014). The measurement precision developed in this thesis is precise enough to capture such seasonal variability and it would be interesting to measure a  $\Delta^{17}\text{O}$  time-series at Zotino to test the model predictions and understand the seasonal cycle of  $\Delta^{17}\text{O}$  in tropospheric  $\text{CO}_2$ . The study would give us an insight into both vegetation-atmosphere interaction and soil invasion flux.
- e) Partitioning fluxes between respiration, soil invasion, and photosynthesis in the field: Once the effect of the individual sources and sinks of the carbon cycle on  $\Delta^{17}\text{O}$  of  $\text{CO}_2$  are quantified,  $\Delta^{17}\text{O}$  measurements at the ecosystem level may be used to partition the fluxes. We have already carried out the first measurements at the Loobos ecosystem site (Koren, 2020).
- f) Linking the carbon and hydrological cycles: These cycles are closely coupled together via oxygen isotope exchange where a potential climate change feedback in one system will be expressed in the other system. This can be addressed by combined measurements of  $\Delta^{17}\text{O}$  in carbon dioxide and water vapor at the ecosystem level. Recent advancements in the measurement techniques of  $\Delta^{17}\text{O}$  of  $\text{CO}_2$  (Nelson et al., 2008; McManus et al., 2005; McManus et al., 2015; McManus et al., 2010) and water vapor (Galewsky et al., 2016; Steen-Larsen et al., 2013; Steig et al., 2014) may soon allow semi-continuous  $\Delta^{17}\text{O}$  measurements in the field to study the ecosystem and to explore the diurnal variability of  $\Delta^{17}\text{O}$  of atmospheric  $\text{CO}_2$  and water to deconvolve the different processes.



## SUMMARY

The abundance of greenhouse gases in the atmosphere has strongly increased since the industrial revolution due to human activity, and this increase is the primary cause of the ongoing climate change. To mitigate climate change, large reductions in greenhouse gas emissions are required, in particular strong reductions in CO<sub>2</sub> emissions from fossil fuel use, which is responsible for two-thirds of the radiative forcing caused by greenhouse gases. In addition to this initial forcing, the abundance of CO<sub>2</sub> is also determined by feedbacks from the exchange of CO<sub>2</sub> with the biosphere. Estimating this feedback requires an understanding of the gross fluxes between atmosphere and biosphere (and oceans) of CO<sub>2</sub> and their sensitivity to environmental perturbations. The work presented in this thesis is targeted at an improved understanding of these exchange fluxes, using innovative isotope tracers.

Photosynthesis, the process in which plants take up CO<sub>2</sub> to produce sugars for their growth, is a key process for life on earth. The total planetary photosynthetic flux is called gross primary productivity (GPP). It is the largest flux in the terrestrial carbon cycle, and the increase in GPP due to increasing levels of CO<sub>2</sub> in the atmosphere offsets one-quarter of anthropogenic carbon dioxide emissions. It is important to understand the variability of GPP in a changing climate to predict future climate and CO<sub>2</sub> levels in the atmosphere. However, it is not possible to measure GPP directly beyond the leaf scale. This is because the measurement of photosynthetic gas exchange is strongly influenced by terrestrial ecosystem respiration (TER). Most of the existing measurement techniques rely on inferring GPP from the net ecosystem exchange (NEE), the difference between GPP and terrestrial respiration (TER). However, this method is imprecise because it is hard to decipher small changes in the large GPP and TER fluxes from small differences of NEE.

GPP can also be determined using the isotope fractionation associated with photosynthesis. It was suggested that measuring  $\Delta^{17}\text{O}$  ( $\Delta^{17}\text{O} = \ln(\delta^{17} + 1) - 0.528 \times \ln(\delta^{18} + 1)$ ) of tropospheric CO<sub>2</sub> might be a better tracer for GPP than  $\delta^{18}\text{O}$  alone. This is because the  $\Delta^{17}\text{O}$  is less sensitive to isotope fractionation in the individual processes involved in the leaf-atmosphere exchange than  $\delta^{18}\text{O}$  since most of these processes follow mass-dependent isotope fractionation laws with a well defined three-isotope slope. One limitation is that the variability of  $\Delta^{17}\text{O}$  of tropospheric CO<sub>2</sub> is very small, typical seasonal signals may be of the order of 0.02 ‰. Therefore, it requires a measurement technique precise enough to capture small variations in  $\Delta^{17}\text{O}$  of tropospheric CO<sub>2</sub>. Furthermore, previous model studies used assumptions for different parameters that are not confirmed experimentally.

In this thesis, two measurement techniques were developed that are precise enough to capture the small variability in  $\Delta^{17}\text{O}$  of tropospheric CO<sub>2</sub>. One of these techniques was then used to quantify the effect of photosynthesis on the  $\Delta^{17}\text{O}$  of atmospheric CO<sub>2</sub> during gas exchange measurements under controlled conditions. This shows that theories that have been used to describe the effect of photosynthesis on  $\delta^{18}\text{O}$  can also be used for  $\Delta^{17}\text{O}$ . Also, the dependencies on key parameters that affect  $\Delta^{17}\text{O}$  during the photosynthetic gas exchange are determined. It is then investigated whether  $\Delta^{17}\text{O}$  can be used to estimate mesophyll conductance, the conductance of CO<sub>2</sub> from the intercellular air space to the site of CO<sub>2</sub>-H<sub>2</sub>O exchange in a leaf. Furthermore, the leaf scale measurements are used to quantify the impact of photosynthesis on  $\Delta^{17}\text{O}$  of atmospheric CO<sub>2</sub>.

As discussed in **Chapter 2** of this thesis, we set up two techniques to measure the  $\Delta^{17}\text{O}$  of  $\text{CO}_2$ . The  $\text{CO}_2$ - $\text{O}_2$  exchange technique was first developed by Mahata et al. (2013) and adopted in the work described here. Equal amounts of  $\text{CO}_2$  and  $\text{O}_2$  (with known oxygen isotope composition) are allowed to exchange isotopes at 750 °C for 2 hours in a quartz tube in the presence of a platinum sponge catalyst. The initial  $^{18}\text{O}$  isotope composition of the  $\text{CO}_2$  is measured. After the isotope exchange reaches a steady-state, the oxygen isotope composition of  $\text{O}_2$  is measured and the  $^{17}\text{O}$  isotopic composition of  $\text{CO}_2$  is calculated from the isotopic composition of  $\text{O}_2$  (initial and final) and the  $^{18}\text{O}$  isotopic composition of  $\text{CO}_2$  (initial).

In the fragment method, the  $\Delta^{17}\text{O}$  of the  $\text{CO}_2$  is obtained by measuring the  $^{17}\text{O}^+$  and  $^{18}\text{O}^+$  fragment ions that are formed in the ion source of a high-resolution isotope ratio mass spectrometer during electron ionization. Both methods require pure  $\text{CO}_2$ . The exchange method requires chemical manipulation of the  $\text{CO}_2$  by isotope exchange between  $\text{CO}_2$ - $\text{O}_2$  before measurement, which conceptually introduces a source of error, but it provides high precision information in a relatively short time. The fragment method does not require manipulation of the  $\text{CO}_2$  before measurement, but because of the low transmission of ions at the higher mass resolution, it requires long measurement times to get high precision in  $\Delta^{17}\text{O}$ . Conceptually, the fragment technique can also be used to measure  $^{13}\text{C}$  of carbon dioxide and other fragments of different molecules which suffer from isobaric mass interferences. The  $\text{CO}_2$ - $\text{O}_2$  exchange method was used for further experiments because it can be routinely operated at a precision better than 0.01 ‰ which is sufficient to detect  $\Delta^{17}\text{O}$  variabilities in tropospheric  $\text{CO}_2$ .

Photosynthesis is not only affected by the presence of photosynthetically active radiation and  $\text{CO}_2$  but also depends on the conductance of the  $\text{CO}_2$  from the air surrounding the leaf through the boundary layer and stomata to the intercellular air space, and from the intercellular airspace to the carboxylation site. Stomatal conductance ( $g_s$ ) can be calculated from the transpiration rate and mole fraction of water vapor in the intercellular air space, which is mainly controlled by guard cells. Mesophyll conductance,  $g_m$ , the conductance from the intercellular air space to the  $\text{CO}_2$ - $\text{H}_2\text{O}$  exchange site is a much more complex photosynthetic trait consisting of a complex of consecutive barriers with different phases (gas, water, and lipoproteins). Measurements of  $\delta^{18}\text{O}$  have been used previously to determine  $g_m$ , but this method is subject to significant uncertainties related to isotope fractionation processes in the plant. Isotope exchange between  $\text{CO}_2$  and  $\text{H}_2\text{O}$  can occur at many locations in the leaf depending on the availability of carbonic anhydrase. In  $\text{C}_3$  plants the exchange can occur between the mesophyll cell and chloroplast and for  $\text{C}_4$  plants it can occur anywhere in the mesophyll cell. This leads to an uncertainty in the oxygen isotope composition of leaf water at the  $\text{CO}_2$ - $\text{H}_2\text{O}$  exchange site where it is assumed to be the same as the isotope composition at the evaporation site. Besides, there is a strong variation in the oxygen isotope composition of water within a leaf due to evapotranspiration. The variation of  $\Delta^{17}\text{O}$  within the leaf is smaller since evaporation and diffusion are mass-dependent isotope fractionation processes.

In **Chapter 3** of this thesis, we explore the possibility to estimate mesophyll conductance using measurements of  $\Delta^{17}\text{O}$  of  $\text{CO}_2$  and leaf water. We adopt the existing theory for  $\delta^{18}\text{O}$  to  $\Delta^{17}\text{O}$  and compare mesophyll conductance estimates from  $\Delta^{17}\text{O}$  and  $\delta^{18}\text{O}$  measurements. Oxygen isotope measurements ( $\delta^{18}\text{O}$  and  $\Delta^{17}\text{O}$ ) allow us to estimate the mesophyll conductance for both  $\text{C}_3$  and  $\text{C}_4$  plants. A limitation of mesophyll conductance estimates using oxygen isotopes is that errors become large when the difference in  $\Delta^{17}\text{O}$  or  $\delta^{18}\text{O}$  between the  $\text{CO}_2$  in the intercellular air space and at the  $\text{CO}_2$ - $\text{H}_2\text{O}$  exchange site is small. This can happen either when the  $\Delta^{17}\text{O}$  or  $\delta^{18}\text{O}$  of the  $\text{CO}_2$  entering the leaf is similar to the  $\Delta^{17}\text{O}$  or  $\delta^{18}\text{O}$  of the  $\text{CO}_2$  at the  $\text{CO}_2$ - $\text{H}_2\text{O}$  exchange site, or when the mesophyll conductance is very high. The first limitation

can be compensated by using isotopically enriched CO<sub>2</sub> during the gas exchange experiment, but the second one is a conceptual limitation for  $g_m$  estimates using isotope measurements because high  $g_m$  means that there is a very small isotope gradient between the intercellular air space and CO<sub>2</sub>-H<sub>2</sub>O exchange site. Therefore, estimating mesophyll conductance using  $\Delta^{17}\text{O}$  measurements is prone to large errors for plants with higher mesophyll conductance relative to the plants with lower mesophyll conductance.

$\Delta^{17}\text{O}$  of CO<sub>2</sub> has been suggested as a tracer for gross primary production. However, tropospheric CO<sub>2</sub> is a mixture of several sources and sinks that contribute to the change in  $\Delta^{17}\text{O}$  of CO<sub>2</sub>. One of the largest sinks is photosynthesis where the CO<sub>2</sub> is taken up by plants and converted to sugar. Previous model studies made assumptions about the effect of photosynthesis on  $\Delta^{17}\text{O}$ , which were based on careful studies on the individual processes, but were not confirmed experimentally in a real gas exchange experiment. In **Chapter 4** of this thesis, we investigated the effect of photosynthesis on the  $\Delta^{17}\text{O}$  of CO<sub>2</sub> in the laboratory under controlled environmental conditions. We used two C<sub>3</sub> plants with contrasting stomatal conductance and assimilation rate ( $A_n$ ) and one C<sub>4</sub> plant. The two C<sub>3</sub> plants used in this study are sunflower (higher  $A_n$  and low  $g_s$ ) and ivy (low  $A_n$  and low  $g_s$ ) and C<sub>4</sub> plant maize (high  $A_n$  and low  $g_s$ ). Based on our leaf scale experiments, we demonstrate that theories developed for the interpretation of  $\delta^{18}\text{O}$  are conceptually applicable for  $\Delta^{17}\text{O}$  of CO<sub>2</sub>. The impact of photosynthesis on the  $\Delta^{17}\text{O}$  of atmospheric CO<sub>2</sub> depends on the relative difference in  $\Delta^{17}\text{O}$  between leaf water at the CO<sub>2</sub>-H<sub>2</sub>O exchange site and the CO<sub>2</sub> entering the leaf. Another important factor is the back-diffusion flux of CO<sub>2</sub> that has exchanged isotopes inside the plants that is not assimilated but diffuses back to the atmosphere. For plants with higher back-diffusion flux, the impact of photosynthesis on  $\Delta^{17}\text{O}$  of CO<sub>2</sub> is determined mainly by the relative difference between the CO<sub>2</sub> and leaf water at the CO<sub>2</sub>-H<sub>2</sub>O exchange site, while for plants with lower back-diffusion flux, the effect of photosynthesis on the  $\Delta^{17}\text{O}$  of CO<sub>2</sub> is dominated by diffusional fractionation. The back-diffusion flux can be quantified by the ratio of the mole fraction of CO<sub>2</sub> at the CO<sub>2</sub>-H<sub>2</sub>O exchange site ( $c_m$ ) and in the surrounding air ( $c_a$ ), the  $c_m/c_a$  ratio. Based on our leaf experiments, we estimate the effect of vegetation on the  $\Delta^{17}\text{O}$  of atmospheric CO<sub>2</sub> globally to be -0.65 ‰ and -0.3 ‰ for C<sub>3</sub> and C<sub>4</sub> plants, respectively. Using  $\Delta^{17}\text{O}$  estimates of leaf water and atmospheric CO<sub>2</sub> from a global model, we estimated the  $\Delta^{17}\text{O}$  isoflux due to photosynthesis to be  $-60 \pm 15 \text{ ‰PgCyr}^{-1}$  which is in good agreement with previous model studies.

This thesis presents methods to measure  $\Delta^{17}\text{O}$  of CO<sub>2</sub> with a precision of 0.01 ‰, precise enough to capture seasonal variabilities in the  $\Delta^{17}\text{O}$  tropospheric CO<sub>2</sub>. Precise measurement of  $\Delta^{17}\text{O}$  opens new opportunities for studying atmosphere-plant interaction at various scales. From a plant science perspective,  $\Delta^{17}\text{O}$  of CO<sub>2</sub>/H<sub>2</sub>O may be used as an additional tracer for mesophyll conductance, a parameter that limits photosynthesis strongly. The sensitivity of this measurement can be increased when relatively  $^{17}\text{O}$ -enriched CO<sub>2</sub> is used in the experiments. In general, our findings demonstrate that the established theory for  $\delta^{18}\text{O}$  can conceptually be used for  $\Delta^{17}\text{O}$ -CO<sub>2</sub> exchange, and the relevant theoretical equations are derived. From the atmospheric perspective,  $\Delta^{17}\text{O}$  can be used to quantify GPP. To this end, the effect of photosynthesis on  $\Delta^{17}\text{O}$  of atmospheric CO<sub>2</sub> is quantified experimentally for the first time in a real gas exchange experiment. The limiting factors for the effect of photosynthesis on the  $\Delta^{17}\text{O}$  of atmospheric CO<sub>2</sub> are investigated. We use the results to provide a bottom-up estimate for global  $\Delta^{17}\text{O}$ -photosynthetic discrimination based on the leaf scale experiments.

In **Chapter 5** we discuss the main findings and measurement challenges of  $\Delta^{17}\text{O}$  of CO<sub>2</sub>. Furthermore, we point out how the new techniques can be used to improve the interlaboratory

scale consistency of  $\Delta^{17}\text{O}$  measurements and to gain new insights into the carbon and hydrological cycle and photosynthesis mechanism in future studies.

## SAMENVATTING

De hoeveelheid aan broeikasgassen in de atmosfeer is sinds de industriële revolutie door menselijke activiteit sterk toegenomen en deze toename is de belangrijkste oorzaak van de huidige klimaatverandering. Om de klimaatverandering tegen te gaan, zijn grote reducties van de uitstoot van broeikasgassen nodig, met name een sterke reductie van de CO<sub>2</sub>-emissie door het gebruik van fossiele brandstoffen, die verantwoordelijk is voor tweederde van de stralingsforcering veroorzaakt door broeikasgassen. Naast deze initiële forcing wordt de hoeveelheid CO<sub>2</sub> ook bepaald door feedback van de uitwisseling van CO<sub>2</sub> met de biosfeer. Het schatten van deze feedback vereist inzicht in de bruto fluxen tussen atmosfeer en biosfeer (en oceanen) van CO<sub>2</sub> en hun gevoeligheid voor verstoringen. Het werk dat in dit proefschrift wordt gepresenteerd, is gericht op een beter begrip van deze uitwisselingsfluxen, met behulp van innovatieve isotop tracers.

Fotosynthese, het proces waarbij planten CO<sub>2</sub> opnemen om suikers te produceren voor hun groei, is een belangrijk proces voor het leven op aarde. De totale planetaire fotosynthetische flux wordt bruto primaire productiviteit (GPP) genoemd. Het is de grootste flux in de terrestrische koolstofcyclus en de toename van GPP als gevolg van toenemende CO<sub>2</sub>-niveaus in de atmosfeer compenseert een kwart van de antropogene koolstofdioxide-emissies. Het is belangrijk om de variabiliteit van GPP in een veranderend klimaat te begrijpen om toekomstig klimaat en CO<sub>2</sub>-niveaus in de atmosfeer te voorspellen. Het is echter niet mogelijk om GPP direct te meten op grotere schaal dan de bladschaal. Dit komt omdat de meting van fotosynthetische gasuitwisseling sterk wordt beïnvloed door terrestrische ecosysteem respiratie (TER). De meeste bestaande meettechnieken zijn gebaseerd op het afleiden van GPP uit de netto ecosysteemuitwisseling (NEE), het verschil tussen GPP en terrestrische respiratie (TER). Deze methode is echter onnauwkeurig omdat het moeilijk is om kleine veranderingen in de grote GPP- en TER-fluxen te ontcijferen uit kleine verschillen in NEE.

GPP kan ook worden bepaald met behulp van de isotopfractionering die is hoort bij fotosynthese. Er is gesuggereerd dat het meten van  $\Delta^{17}\text{O}$  ( $\Delta^{17}\text{O} = \ln(\delta^{17} + 1) - 0,528 \times \ln(\delta^{18} + 1)$ ) van troposferisch CO<sub>2</sub> een betere tracer kan zijn voor GPP dan alleen  $\delta^{18}\text{O}$ . Dit komt omdat de  $\Delta^{17}\text{O}$  minder gevoelig is voor fractionering van isotopen in de individuele processen die betrokken zijn bij de uitwisseling tussen blad en atmosfeer dan  $\delta^{18}\text{O}$ , aangezien de meeste van deze processen massa-afhankelijke wetten voor fractionering van isotopen volgen met een goed gedefinieerde drie isotopen-hellingshoek. Een beperking is dat de variabiliteit van  $\Delta^{17}\text{O}$  van troposferisch CO<sub>2</sub> erg klein is, typische seizoenssignalen zijn in de orde van 0,02 ‰. Daarom vereist het een meettechniek die nauwkeurig genoeg is om kleine variaties in  $\Delta^{17}\text{O}$  van troposferisch CO<sub>2</sub> te detecteren. Bovendien gebruikten eerdere modelstudies aannames voor verschillende parameters die niet experimenteel zijn bevestigd.

In dit proefschrift zijn twee meettechnieken ontwikkeld die nauwkeurig genoeg zijn om de kleine variaties in  $\Delta^{17}\text{O}$  van troposferisch CO<sub>2</sub> te detecteren. Een van deze technieken werd vervolgens gebruikt om het effect van fotosynthese op de  $\Delta^{17}\text{O}$  van atmosferisch CO<sub>2</sub> te kwantificeren tijdens metingen van gasuitwisseling onder gecontroleerde omstandigheden. Dit toont aan dat theorieën die zijn gebruikt om het effect van fotosynthese op  $^{18}\text{O}$  te beschrijven, ook kunnen worden gebruikt voor  $\Delta^{17}\text{O}$ . Ook zijn de afhankelijkheden van belangrijke parameters die  $\Delta^{17}\text{O}$  beïnvloeden tijdens de fotosynthetische gasuitwisseling bepaald. Vervolgens is onderzocht of  $\Delta^{17}\text{O}$  kan worden gebruikt om mesofylgeleiding, de geleiding van CO<sub>2</sub> van de intercellulaire ruimte naar de plaats van CO<sub>2</sub>-H<sub>2</sub>O-uitwisseling in een blad te



schatten. Verder worden de bladschaalmetingen gebruikt om de impact van fotosynthese op  $\Delta^{17}\text{O}$  van atmosferisch  $\text{CO}_2$  te kwantificeren.

Zoals besproken in hoofdstuk 2 van dit proefschrift, hebben we twee technieken gebruikt om de  $\Delta^{17}\text{O}$  van  $\text{CO}_2$  te meten. De  $\text{CO}_2$ - $\text{O}_2$ -uitwisselingstechniek werd voor het eerst ontwikkeld door Mahata et al. (2013) en overgenomen in het hier beschreven werk. Gelijke hoeveelheden  $\text{CO}_2$  en  $\text{O}_2$  (met bekende zuurstofisotopensamenstelling) wisselen isotopen uit gedurende 2 uur bij  $750^\circ\text{C}$  in een kwartsbuis in aanwezigheid van een platina sponskatalysator. De aanvankelijke  $^{18}\text{O}$ -isotopensamenstelling van de  $\text{CO}_2$  wordt gemeten. Nadat de isotoopuitwisseling een stationaire toestand heeft bereikt, wordt de zuurstofisotoopsamenstelling van  $\text{O}_2$  gemeten en wordt de  $^{17}\text{O}$ -isotopensamenstelling van  $\text{CO}_2$  berekend uit de isotopensamenstelling van  $\text{O}_2$  (aanvankelijk en uiteindelijk) en de  $^{18}\text{O}$ -isotopensamenstelling van  $\text{CO}_2$  (aanvankelijk).

In de fragmentmethode wordt de  $\Delta^{17}\text{O}$  van  $\text{CO}_2$  verkregen door het meten van de  $^{17}\text{O}^+$  en  $^{18}\text{O}^+$  fragmentionen die worden gevormd in de ionenbron van een hoge resolutie massaspectrometer tijdens elektronenionisatie. Beide methoden vereisen pure  $\text{CO}_2$ . De uitwisselingsmethode vereist chemische manipulatie van de  $\text{CO}_2$  door isotoopuitwisseling tussen  $\text{CO}_2$ - $\text{O}_2$  vóór meting, wat conceptueel een bron van fouten oplevert, maar het levert in relatief korte tijd zeer nauwkeurige informatie. De fragmentmethode vereist geen manipulatie van de  $\text{CO}_2$  voor de meting, maar vanwege de lage transmissie van ionen bij de hogere massa-resolutie, vereist het een lange meettijd om een hoge precisie te krijgen in  $\Delta^{17}\text{O}$ . Conceptueel kan de fragmenttechniek ook worden gebruikt om  $^{13}\text{C}$  van koolstofdioxide en andere fragmenten van verschillende moleculen te meten die te maken hebben met isobare massa-interferenties. De  $\text{CO}_2$ - $\text{O}_2$ -uitwisselingsmethode werd gebruikt voor verdere experimenten omdat deze routinematig kan worden gebruikt met een precisie die beter is dan  $0,01\text{‰}$ , wat voldoende is om  $\Delta^{17}\text{O}$ -variaties in troposferisch  $\text{CO}_2$  te detecteren.

Fotosynthese wordt niet alleen beïnvloed door de aanwezigheid van fotosynthetisch actieve straling en  $\text{CO}_2$ , maar hangt ook af van de geleiding van de  $\text{CO}_2$  van de lucht rond het blad door de grenslaag en huidmondjes naar de intercellulaire ruimte en van de intercellulaire ruimte naar de carboxylatieplaats. Stomatale geleiding ( $g_s$ ) kan worden berekend op basis van de transpiratiesnelheid en molfractie van waterdamp in de intercellulaire ruimte, die voornamelijk wordt gereguleerd door sluitcellen. Mesofylgeleiding,  $g_m$ , de geleiding van de intercellulaire ruimte naar de  $\text{CO}_2$ - $\text{H}_2\text{O}$ -uitwisselingsplaats, is een veel complexere fotosynthetische eigenschap die bestaat uit een complex van opeenvolgende barrières met verschillende fasen (gas, water en lipoproteïnen). Metingen van  $^{18}\text{O}$  zijn eerder gebruikt om  $g_m$  te bepalen, maar deze methode is onderhevig aan aanzienlijke onzekerheden met betrekking tot isotopenfractioneringsprocessen in de plant. Uitwisseling van isotopen tussen  $\text{CO}_2$  en  $\text{H}_2\text{O}$  kan op veel plaatsen in het blad plaatsvinden, afhankelijk van de beschikbaarheid van koolzuuranhydrase. In  $\text{C}_3$ -planten kan de uitwisseling plaatsvinden tussen mesofylcel en chloroplast en voor  $\text{C}_4$ -planten kan het overal in de mesofylcel plaatsvinden. Dit leidt tot een onzekerheid in de zuurstofisotopensamenstelling van bladwater op de  $\text{CO}_2$ - $\text{H}_2\text{O}$ -uitwisselingsplaats, waar wordt aangenomen dat deze gelijk is aan de isotopensamenstelling op de verdampingsplaats. Bovendien is er een sterke variabiliteit in de zuurstofisotoopsamenstelling van water in een blad als gevolg van verdamping. De variabiliteit van  $\Delta^{17}\text{O}$  in het blad is kleiner omdat verdamping en diffusie massa-afhankelijke isotopenfractioneringsprocessen zijn.

In hoofdstuk 3 van dit proefschrift onderzoeken we de mogelijkheid om mesofylgeleiding te schatten met metingen van  $\Delta^{17}\text{O}$  van  $\text{CO}_2$  en bladwater. We gebruiken de bestaande theorie van  $^{18}\text{O}$  voor  $\Delta^{17}\text{O}$  en vergelijken schattingen van mesofylgeleiding uit metingen van  $\Delta^{17}\text{O}$  en  $^{18}\text{O}$ . Zuurstofisotoopmetingen ( $\delta^{18}\text{O}$  en  $\Delta^{17}\text{O}$ ) stellen ons in staat de mesofylgeleiding voor zowel  $\text{C}_3$ - als  $\text{C}_4$ -planten te schatten. Een beperking van schattingen van de mesofylgeleiding met behulp van zuurstofisotopen is dat fouten groot worden wanneer het verschil in  $\Delta^{17}\text{O}$  of  $\delta^{18}\text{O}$  tussen het  $\text{CO}_2$  in de intercellulaire ruimte en op de  $\text{CO}_2$ - $\text{H}_2\text{O}$ -uitwisselingsplaats klein is. Dit kan gebeuren wanneer de  $\Delta^{17}\text{O}$  of  $\delta^{18}\text{O}$  van de  $\text{CO}_2$  die het blad binnenkomt vergelijkbaar is met de  $\Delta^{17}\text{O}$  of  $\delta^{18}\text{O}$  van de  $\text{CO}_2$  op de  $\text{CO}_2$ - $\text{H}_2\text{O}$ -uitwisselingsplaats, of wanneer de mesofylgeleiding erg hoog is. De eerste beperking kan worden gecompenseerd door isotopisch verrijkt  $\text{CO}_2$  te gebruiken tijdens het gasuitwisselingsexperiment, maar de tweede is een conceptuele beperking voor gm-schattingen met isotopenmetingen omdat hoge gm betekent dat er een zeer kleine isotopengradiënt is tussen de intercellulaire ruimte en  $\text{CO}_2$ - $\text{H}_2\text{O}$ -uitwisselingsplaats. Daarom is het schatten van mesofylgeleiding met behulp van  $\Delta^{17}\text{O}$ -metingen vatbaar voor grote fouten voor planten met een hogere mesofylgeleiding.

$\Delta^{17}\text{O}$  van  $\text{CO}_2$  is gesuggereerd als een tracer voor de bruto primaire productie. Troposferisch  $\text{CO}_2$  is echter een mengsel van verschillende bronnen en putten die bijdragen aan de verandering van  $\Delta^{17}\text{O}$  van  $\text{CO}_2$ . Een van de grootste putten is fotosynthese waarbij de  $\text{CO}_2$  door planten wordt opgenomen en omgezet in suiker. Eerdere modelstudies gebruikten aannames over het effect van fotosynthese op  $\Delta^{17}\text{O}$ , die gebaseerd waren op zorgvuldige studies van de individuele processen, maar niet experimenteel werden bevestigd in een echt gasuitwisselingsexperiment. In hoofdstuk 4 van dit proefschrift hebben we het effect van fotosynthese op de  $\Delta^{17}\text{O}$  van  $\text{CO}_2$  in het laboratorium onder gecontroleerde omstandigheden onderzocht. We gebruikten twee  $\text{C}_3$ -planten met een contrasterende stomatale geleiding en assimilatiesnelheid ( $A_n$ ) en één  $\text{C}_4$ -plant. De twee  $\text{C}_3$ -planten die in dit onderzoek zijn gebruikt, zijn zonnebloem (hogere  $A_n$  en lage  $g_s$ ) en klimop (lage  $A_n$  en lage  $g_s$ ) en de  $\text{C}_4$ -plant maïs (hoge  $A_n$  en lage  $g_s$ ). Op basis van onze bladschaalexperimenten tonen we aan dat theorieën die zijn ontwikkeld voor de interpretatie van  $^{18}\text{O}$  conceptueel toepasbaar zijn voor  $\Delta^{17}\text{O}$  van  $\text{CO}_2$ . De impact van fotosynthese op de  $\Delta^{17}\text{O}$  van atmosferisch  $\text{CO}_2$  hangt af van het relatieve verschil in  $\Delta^{17}\text{O}$  tussen bladwater op de  $\text{CO}_2$ - $\text{H}_2\text{O}$ -uitwisselingsplaats en de  $\text{CO}_2$  die het blad binnenkomt. Een andere belangrijke factor is de teruggediffusieflux van  $\text{CO}_2$  die isotopen in de planten heeft uitgewisseld, dat niet wordt geassimileerd, maar terug diffundeert naar de atmosfeer. Voor planten met een hogere teruggediffusieflux wordt de impact van fotosynthese op  $\Delta^{17}\text{O}$  van  $\text{CO}_2$  voornamelijk bepaald door het relatieve verschil tussen de  $\text{CO}_2$  en het bladwater op de  $\text{CO}_2$ - $\text{H}_2\text{O}$ -uitwisselingsplaats, terwijl voor planten met een lagere back-diffusieflux het effect van fotosynthese op de  $\Delta^{17}\text{O}$  van  $\text{CO}_2$  wordt gedomineerd door diffusie fractionering. De teruggediffusieflux kan worden gekwantificeerd door de verhouding van de molfractie  $\text{CO}_2$  op de  $\text{CO}_2$ - $\text{H}_2\text{O}$ -uitwisselingsplaats ( $c_m$ ) en in de omringende lucht ( $c_a$ ), de  $c_m/c_a$ -verhouding. Op basis van onze bladexperimenten schatten we het effect van vegetatie op de  $\Delta^{17}\text{O}$  van atmosferisch  $\text{CO}_2$  wereldwijd op  $-0,65\text{‰}$  en  $-0,3\text{‰}$  voor respectievelijk  $\text{C}_3$ - en  $\text{C}_4$ -planten. Met behulp van  $\Delta^{17}\text{O}$ -schattingen van bladwater en atmosferisch  $\text{CO}_2$  uit een globaal model, schatten we de  $\Delta^{17}\text{O}$ -isoflux als gevolg van fotosynthese op  $-60 \pm 15\text{‰ PgCyr}^{-1}$ , wat in goede overeenstemming is met eerdere modelstudies.

Dit proefschrift presenteert methoden om  $\Delta^{17}\text{O}$  van  $\text{CO}_2$  te meten met een precisie van  $0,01\text{‰}$ , precies genoeg om seizoensvariaties in de  $\Delta^{17}\text{O}$  van troposferisch  $\text{CO}_2$  te detecteren. Nauwkeurige meting van  $\Delta^{17}\text{O}$  biedt nieuwe mogelijkheden voor het bestuderen van de interactie tussen atmosfeer en plant op verschillende schalen. Vanuit een plantenwetenschappelijk perspectief kan  $\Delta^{17}\text{O}$  van  $\text{CO}_2/\text{H}_2\text{O}$  worden gebruikt als een extra

tracer voor de geleidbaarheid van het mesofyl, een parameter die de fotosynthese sterk beperkt. De gevoeligheid van deze meting kan worden verhoogd wanneer relatief  $^{17}\text{O}$ -verrijkt  $\text{CO}_2$  wordt gebruikt in de experimenten. In het algemeen tonen onze bevindingen aan dat de gevestigde theorie voor  $^{18}\text{O}$  conceptueel kan worden gebruikt voor  $\Delta^{17}\text{O}$ - $\text{CO}_2$ -uitwisseling, en de relevante theoretische vergelijkingen zijn afgeleid. Vanuit atmosferisch perspectief kan  $\Delta^{17}\text{O}$  worden gebruikt om GPP te kwantificeren. Daartoe is het effect van fotosynthese op  $\Delta^{17}\text{O}$  van atmosferisch  $\text{CO}_2$  voor het eerst experimenteel gekwantificeerd in een echt gasuitwisselingsexperiment. De beperkende factoren voor het effect van fotosynthese op de  $\Delta^{17}\text{O}$  van atmosferisch  $\text{CO}_2$  zijn onderzocht. We gebruiken de resultaten om een bottom-up schatting te geven voor wereldwijde  $\Delta^{17}\text{O}$ -fotosynthetische discriminatie op basis van de experimenten op bladschaal.

In hoofdstuk 5 bespreken we de belangrijkste bevindingen en meetuitdagingen van  $\Delta^{17}\text{O}$  van  $\text{CO}_2$ . Verder wijzen we erop hoe de nieuwe technieken gebruikt kunnen worden om de interlaboratoriumschaalconsistentie van  $\Delta^{17}\text{O}$ -metingen te verbeteren en om nieuwe inzichten te verkrijgen in de koolstof- en hydrologische cyclus en het fotosynthesemechanisme in toekomstige studies.

Translated by Gerbrand Koren

## References

- Adnew, G. A., Hofmann, M. E. G., Paul, D., Laskar, A., Surma, J., Albrecht, N., Pack, A., Schwieters, J., Koren, G., Peters, W., and Röckmann, T.: Determination of the triple oxygen and carbon isotopic composition of CO<sub>2</sub> from atomic ion fragments formed in the ion source of the 253 Ultra High-Resolution Isotope Ratio Mass Spectrometer, *Rapid Commun. Mass. Sp.*, 33, 17, 2019.
- Adnew, G. A., Pons, T. L., Koren, G., Peters, W., and Röckmann, T.: Leaf-scale quantification of the effect of photosynthetic gas exchange on  $\Delta^{17}\text{O}$  of atmospheric CO<sub>2</sub>, *Biogeosciences Discuss.*, 37, 2020.
- Affek, H. P., and Yakir, D.: The stable isotopic composition of atmospheric CO<sub>2</sub>, 2 ed., *Treasure on Geochemistry*, edited by: Karl, T., and Heinrich, H., Elsevier, 2014.
- Ainsworth, E. A., and Long, S. P.: What have we learned from 15 years of free-air CO<sub>2</sub> enrichment (FACE)? A meta-analytic review of the responses of photosynthesis, canopy properties and plant production to rising CO<sub>2</sub> *New phytologist*, 165, 21, 2005.
- Ainsworth, E. A., and Rogers, A.: The response of photosynthesis and stomatal conductance to rising [CO<sub>2</sub>]: mechanisms and environmental interactions, *Plant, cell & environment*, 30, 2007.
- Allison, C. E., Francey, R. J., and Meijer, H. A. J.: Reference and intercomparison materials for stable isotopes of light elements, IAEA-TECDOC-825, International Atomic Energy Agency, Vienna, 7, 1993.
- Allison, C. E., and Francey, R. J.: High precision stable isotope measurements of atmospheric trace gases. In *Reference and Intercomparison Materials for Stable Isotopes of Light Elements*, IAEA-TECDOC-825, 1995.
- Anav, A., Friedlingstein, P., Beer, C., Ciais, P., Harper, A., Jones, C., Murray-Tortarolo, G., Papale, D., Parazoo, N. C., and Peylin, P.: Spatiotemporal patterns of terrestrial gross primary production: A review, *Rev Geophys*, 53, 33, 2015.
- Angert, A., Cappa, C. D., and DePaolo, D. J.: Kinetic <sup>17</sup>O effects in the hydrologic cycle: Indirect evidence and implications, *Geochimica et Cosmochimica Acta*, 68, 8, 2004.
- Archer, D., Eby, M., Brovkin, V., Ridgwell, A., Cao, L., Mikolajewicz, U., Caldeira, K., Matsumoto, K., Munhoven, G., and Montenegro, A.: Atmospheric lifetime of fossil fuel carbon dioxide, *Annu. Rev. Earth Planet. Sci.*, 37, 17, 2009.
- Asaf, D., Rotenberg, E., Tatarinov, F., Dicken, U., Montzka, S. A., and Yakir, D.: Ecosystem photosynthesis inferred from measurements of carbonyl sulphide flux, *Nature Geoscience*, 6, 3, 2013.
- Assonov, S. S., and Brenninkmeijer, C. A.: A new method to determine the <sup>17</sup>O isotopic abundance in CO<sub>2</sub> using oxygen isotope exchange with a solid oxide, *Rapid Commun Mass Spectrom*, 15, 2426-2437, 10.1002/rm.529, 2001.
- Assonov, S. S., and Brenninkmeijer, C. A.: On the <sup>17</sup>O correction for CO<sub>2</sub> mass spectrometric isotopic analysis, *Rapid Commun Mass Spectrom*, 17, 1007-1016, 10.1002/rm.1012, 2003.
- Aubinet, M., Vesala, T., and Papale, D.: *Eddy covariance: a practical guide to measurement and data analysis* Springer Science & Business Media, 2012.
- Augustin, L., Barbante, C., Barnes, P. R. F., Barnola, J. M., Bigler, M., Castellano, E., Cattani, O., Chappellaz, J., Dahl-Jensen, D., and Delmonte, B.: Eight glacial cycles from an Antarctic ice core *Nature*, 429, 5, 2004.
- Badger, M. R., and Price, G. D.: The role of carbonic anhydrase in photosynthesis, *Annu. Rev. Plant Biol.*, 45, 23, 1994.
- Badgley, G., Anderegg, L. D. L., Berry, J. A., and Field, C. B.: Terrestrial gross primary production: using NIRV to scale from site to globe *Glob Change Biol*, 25, 9, 2019.
- Baldocchi, D., Ryu, Y., and Keenan, T.: Terrestrial carbon cycle variability, *F1000Research*, 5, 2016.

- Baldocchi, D. D.: Assessing the eddy covariance technique for evaluating carbon dioxide exchange rates of ecosystems: past, present and future, *Global change biology*, 9, 13, 2003.
- Ballantyne, A. P., Alden, C. B., Miller, J. B., Tans, P. P., and White, J. W. C.: Increase in observed net carbon dioxide uptake by land and oceans during the past 50 years, *Nature*, 488, 3, 2012.
- Bao, H., Cao, X., and Hayles, J. A.: Triple oxygen isotopes: fundamental relationships and applications, *Annu. Rev. Earth Planet. Sci.*, 44, 29, 2016.
- Barbour, M. M., Farquhar, G. D., Hanson, D. T., Bickford, C. P., Powers, H., and McDowell, N. G.: A new measurement technique reveals temporal variation in  $\delta^{18}\text{O}$  of leaf-respired  $\text{CO}_2$ , *Plant Cell Environ.*, 30, 12, 2007.
- Barbour, M. M., Evans, J. R., Simonin, K. A., and von Caemmerer, S.: Online  $\text{CO}_2$  and  $\text{H}_2\text{O}$  oxygen isotope fractionation allows estimation of mesophyll conductance in  $\text{C}_4$  plants, and reveals that mesophyll conductance decreases as leaves age in both  $\text{C}_4$  and  $\text{C}_3$  plants, *New Phytol.*, 14, 2016.
- Barkan, E., and Luz, B.: Conversion of  $\text{O}_2$  into  $\text{CO}_2$  for high-precision oxygen isotope measurements, *Anal. Chem.*, 68, 3, 1996.
- Barkan, E., and Luz, B.: Absolute ratios  $^{17}\text{O}/^{16}\text{O}$  and  $^{18}\text{O}/^{16}\text{O}$  in water standards and atmospheric  $\text{O}_2$ , IAEA, Vienna 2004.
- Barkan, E., and Luz, B.: High precision measurements of  $^{17}\text{O}/^{16}\text{O}$  and  $^{18}\text{O}/^{16}\text{O}$  ratios in  $\text{H}_2\text{O}$ , *Rapid Commun. Mass. Sp.*, 19, 3737-3742, 10.1002/rcm.2250, 2005.
- Barkan, E., and Luz, B.: Diffusivity fractionations of  $\text{H}_2^{16}\text{O}/\text{H}_2^{17}\text{O}$  and  $\text{H}_2^{16}\text{O}/\text{H}_2^{18}\text{O}$  in air and their implications for isotope hydrology, *Rapid Commun. Mass. Sp.*, 21, 6, 2007.
- Barkan, E., and Luz, B.: The relationships among the three stable isotopes of oxygen in air, seawater and marine photosynthesis, *Rapid Commun. Mass. Sp.*, 25, 2, 2011.
- Barkan, E., and Luz, B.: High-precision measurements of  $^{17}\text{O}/^{16}\text{O}$  and  $^{18}\text{O}/^{16}\text{O}$  ratios in  $\text{CO}_2$ , *Rapid Commun. Mass. Sp.*, 26, 2733-2738, 10.1002/rcm.6400, 2012.
- Barkan, E., Musan, I., and Luz, B.: High-precision measurements of  $\delta^{17}\text{O}$  and  $^{17}\text{O}$ -excess of NBS19 and NBS18, *Rapid Commun. Mass. Sp.*, 29, 2219-2224, 10.1002/rcm.7378, 2015.
- Barkan, E., Affek, H. P., Luz, B., Bergel, S. J., Voarintsoa, N. R. G., and Musan, I.: Calibration of  $\delta^{17}\text{O}$  and  $^{17}\text{O}$ -excess values of three international standards: IAEA-603, NBS19 and NBS18 *Rapid Commun Mass Sp*, 33, 2019.
- Beer, C., Reichstein, M., Tomelleri, E., Ciais, P., Jung, M., Carvalhais, N., Rodenbeck, C., Arain, M. A., Baldocchi, D., Bonan, G. B., Bondeau, A., Cescatti, A., Lasslop, G., Lindroth, A., Lomas, M., Luyssaert, S., Margolis, H., Oleson, K. W., Rouspard, O., Veenendaal, E., Viovy, N., Williams, C., Woodward, F. I., and Papale, D.: Terrestrial gross carbon dioxide uptake: global distribution and covariation with climate, *Science*, 329, 834-838, 10.1126/science.1184984, 2010.
- Bergamaschi, P., Brenninkmeijer, C. A. M., Hahn, M., Röckmann, T., Scharffe, D. H., Crutzen, P. J., Elansky, N. F., Belikov, I. B., Trivett, N. B. A., and Worthy, D. E. J.: Isotope analysis based source identification for atmospheric  $\text{CH}_4$  and  $\text{CO}$  sampled across Russia using the Trans-Siberian railroad *Journal of Geophysical Research* 103, 8, 1998.
- Berhanu, T. A., Savarino, J., Bhattacharya, S. K., and Vicars, W. C.:  $^{17}\text{O}$ -excess transfer during the  $\text{NO}_2 + \text{O}_3 \rightarrow \text{NO}_3 + \text{O}_2$  reaction, *The Journal of chemical physics*, 136, 044311, 2012.
- Berkelhammer, M., Asaf, D., Still, C., Montzka, S., Noone, D., Gupta, M., Provencal, R., Chen, H., and Yakir, D.: Constraining surface carbon fluxes using in situ measurements of carbonyl sulfide and carbon dioxide, *Global Biogeochemical Cycles*, 28, 18, 2014.
- Berner, R. A.: *The Phanerozoic carbon cycle:  $\text{CO}_2$  and  $\text{O}_2$* . Oxford University Press on Demand, 2004.
- Bigeleisen, J., and Mayer, M. G.: Calculation of equilibrium constants for isotopic exchange reactions *The Journal of Chemical Physics*, 15, 6, 1947.
- Blonquist, J., Mark, J., Montzka, S. A., Munger, J. W., Yakir, D., Desai, A. R., Dragoni, D., Griffis, T. J., Monson, R. K., Scott, R. L., and Bowling, D. R.: The potential of carbonyl sulfide as a

- proxy for gross primary production at flux tower sites, *Journal of Geophysical Research: Biogeosciences*, 116, 2011.
- Bloom, A. A., Exbrayat, J.-F., Velde, I. R. v. d., Feng, L., and Williams, M.: The decadal state of the terrestrial carbon cycle: Global retrievals of terrestrial carbon allocation, pools, and residence times *PNAS*, 113, 5, 2016.
- Boering, K. A., Jackson, T., Hoag, K. J., Cole, A. S., Perri, M. J., Thieme, M., and Atlas, E.: Observations of the anomalous oxygen isotopic composition of carbon dioxide in the lower stratosphere and the flux of the anomaly to the troposphere, *Geophys. Res. Lett.*, 31, 2004.
- Booth, B. B. B., Jones, C. D., Collins, M., Totterdell, I. J., Cox, P. M., Sitch, S., Huntingford, C., Betts, R. A., Harris, G. R., and Lloyd, J.: High sensitivity of future global warming to land carbon cycle processes, *Environmental Research Letters*, 7, 10.1088/1748-9326/7/2/024002, 2012.
- Bottinga, Y., and Craig, H.: Oxygen isotope fractionation between CO<sub>2</sub> and water, and the isotopic composition of marine atmospheric CO<sub>2</sub>, *Earth Planet Sc. Lett.*, 5, 10, 1968.
- Bowen, G. J., and Revenaugh, J.: Interpolating the isotopic composition of modern meteoric precipitation, *Water Resour. Res.*, 39, 2003.
- Brand, W. A., Assonov, S. S., and Coplen, T. B.: Correction for the <sup>17</sup>O interference in δ<sup>13</sup>C measurements when analyzing CO<sub>2</sub> with stable isotope mass spectrometry (IUPAC Technical Report), *Pure Appl. Chem.*, 82, 1719-1733, 10.1351/pac-rep-09-01-05, 2010.
- Brenninkmeijer, C. A. M., Kraft, P., and Mook, W. G.: Oxygen isotope fractionation between CO<sub>2</sub> and H<sub>2</sub>O, *Chem. Geol.*, 41, 8, 1983.
- Brenninkmeijer, C. A. M., and Rockmann, T.: A rapid method for the preparation of O<sub>2</sub> from CO<sub>2</sub> for mass spectrometric measurement of <sup>17</sup>O/<sup>16</sup>O ratios, *Rapid Commun. Mass Spectrom.*, 12, 1998.
- Brenninkmeijer, C. A. M., and Röckmann, T.: Mass spectrometry of the intramolecular nitrogen isotope distribution of environmental nitrous oxide using fragment ion analysis, *Rapid Commun. Mass Spectrom.*, 13, 5, 1999.
- Brenninkmeijer, C. A. M., Röckmann, T., Bräunlich, M., Jöckel, P., and Bergamaschi, P.: Review of progress in isotope studies of atmospheric carbon monoxide, *Chemosphere: Global Change Science*, 1, 19, 1999.
- Brenninkmeijer, C. A. M.: Applications of stable isotope analysis to atmospheric trace gas budgets, *Eur. Phys. J. Conferences*, 1, 11, 10.1140/epjconf/e2009-00915-x, 2009.
- von Caemmerer, S., and Farquhar, G. D.: Some relationships between the biochemistry of photosynthesis and the gas exchange of leaves, *Planta*, 153, 11, 1981.
- von Caemmerer, S., Ghannoum, O., Pengelly, J. J. L., and Cousins, A. B.: Carbon isotope discrimination as a tool to explore C<sub>4</sub> photosynthesis, *J. Exp. Bot.*, 65, 3459, 2014.
- Caird, M. A., Richards, J. H., and Donovan, L. A.: Nighttime stomatal conductance and transpiration in C<sub>3</sub> and C<sub>4</sub> plants, *Plant Physiol.*, 143, 4-10, 10.1104/pp.106.092940, 2007.
- Campbell, J. E., Carmichael, G. R., Chai, T., Mena-Carrasco, M., Tang, Y., Blake, D. R., Blake, N. J., Vay, S. A., Collatz, G. J., and Baker, I.: Photosynthetic control of atmospheric carbonyl sulfide during the growing season *Science* 322, 3, 2008.
- Campbell, J. E., Berry, J. A., Seibt, U., Smith, S. J., Montzka, S. A., Launois, T., Belviso, S., Bopp, L., and Laine, M.: Large historical growth in global terrestrial gross primary production, *Nature*, 544, 3, 2017.
- Canadell, J. G., Mooney, H. A., Baldocchi, D. D., Berry, J. A., Ehleringer, J. R., Field, C. B., Gower, S. T., Hollinger, D. Y., Hunt, J. E., and Jackson, R. B.: Commentary: Carbon metabolism of the terrestrial biosphere: A multitechnique approach for improved understanding *Ecosystems*, 3, 15, 2000.
- Canadell, J. G., Le Quéré, C., Raupach, M. R., Field, C. B., Buitenhuis, E. T., Ciais, P., Conway, T. J., Gillett, N. P., Houghton, R. A., and Marland, G.: Contributions to accelerating atmospheric CO<sub>2</sub> growth from economic activity, carbon intensity, and efficiency of natural sinks, *PNAS*, 104, 4, 2007.



- Cao, X., and Liu, Y.: Equilibrium mass-dependent fractionation relationships for triple oxygen isotopes, *Geochimica et Cosmochimica Acta*, 75, 7435-7445, 10.1016/j.gca.2011.09.048, 2011.
- Cassotta, S., Derkesen, C., Ekaykin, A., Hollowed, A., Kofinas, G., Mackintosh, A., Melbourne-Thomas, J., Muelbert, M. M. C., Ottersen, G., Pritchard, H., and Schuur, E. A. G.: Chapter 3: Polar regions. In IPCC Special Report on the Ocean and Cryosphere in a Changing Climate [H.-O. Pörtner, D.C. Roberts, V. Masson-Delmotte, P. Zhai, M. Tignor, E. Poloczanska, K. Mintenbeck, M. Nicolai, A. Okem, J. Petzold, B. Rama, N. Weyer (eds.)], , In press., 2019.
- Cernusak, L. A., Farquhar, G. D., Wong, S. C., and Stuart-Williams, H.: Measurement and interpretation of the oxygen isotope composition of carbon dioxide respired by leaves in the dark *Plant Physiology*, 136, 13, 2004.
- Cernusak, L. A., Barbour, M. M., Arndt, S. K., Cheesman, A. K., English, N. B., Feild, T. S., Helliker, B. R., Holloway-Phillips, M. M., Holtum, J. A., Kahmen, A., McNerney, F. A., Munksgaard, N. C., Simonin, K. A., Song, X., Stuart-Williams, H., West, J. B., and Farquhar, G. D.: Stable isotopes in leaf water of terrestrial plants, *Plant Cell Environ.*, 39, 1087-1102, 10.1111/pce.12703, 2016.
- Chollet, R., and Ogren, W. L.: Regulation of photorespiration in C<sub>3</sub> and C<sub>4</sub> species, *The Botanical Review*, 41, 42, 1975.
- Ciais, P., Tans, P. P., Trolier, M., White, J. W. C., and Francey, R. J.: A large northern hemisphere terrestrial CO<sub>2</sub> sink indicated by the <sup>13</sup>C/<sup>12</sup>C ratio of atmospheric CO<sub>2</sub> *Science*, 269, 4, 1995.
- Ciais, P., Denning, A. S., Tans, P. P., Berry, J. A., Randall, D. A., Collatz, G. J., Sellers, P. J., White, J. W. C., Trolier, M., Meijer, H. A. J., Francey, R. J., Monfray, P., and Heimann, M.: A three-dimensional synthesis study of δ<sup>18</sup>O in atmospheric CO<sub>2</sub>: 1. Surface fluxes, *J. Geophys. Res. Atmos.*, 102, 5857-5872, 10.1029/96jd02360, 1997a.
- Ciais, P., Tans, P. P., Denning, A. S., Francey, R. J., Trolier, M., Meijer, H. A. J., White, J. W. C., Berry, J. A., Randall, D. A., and Collatz, G. J.: A three-dimensional synthesis study of δ<sup>18</sup>O in atmospheric CO<sub>2</sub>: 2. Simulations with the TM2 transport model, *J. Geophys. Res. Atmos.*, 102, 10, 1997b.
- Clayton, R. N., Grossman, L., and Mayeda, T. K.: A component of primitive nuclear composition in carbonaceous meteorites, *Science*, 182, 3, 1973.
- Clayton, R. N., Onuma, N., and Mayeda, T. K.: A classification of meteorites based on oxygen isotopes, *Earth and Planetary Science Letters*, 30, 8, 1976.
- Clayton, R. N., and Mayeda, T. K.: Oxygen isotope studies of achondrites, *Geochimica et Cosmochimica Acta*, 60, 16, 10.1016/0016-7037(96)00074-9, 1996.
- Collatz, G. J., Berry, J. A., and Clark, J. S.: Effects of climate and atmospheric CO<sub>2</sub> partial pressure on the global distribution of C<sub>4</sub> grasses: present, past, and future, *Oecologia*, 114, 13, 1998.
- Cook, J., Nuccitelli, D., Green, S. A., Richardson, M., Winkler, B., Painting, R., Way, R., Jacobs, P., and Skuce, A.: Quantifying the consensus on anthropogenic global warming in the scientific literature *Environmental research letters*, 8, 2013.
- Cousins, A. B., Badger, M. R., and Caemmerer, S. v.: A transgenic approach to understanding the influence of carbonic anhydrase on C<sup>18</sup>OO discrimination during C<sub>4</sub> photosynthesis, *Plant Physiol.*, 142, 662-672, 10.1104/pp.106.085167, 2006.
- Cousins, A. B., Baroli, I., Badger, M. R., Ivakov, A., Lea, P. J., Leegood, R. C., and Caemmerer, S. v.: The role of phosphoenolpyruvate carboxylase during C<sub>4</sub> photosynthetic isotope exchange and stomatal conductance, *Plant Physiol.*, 145, 11, 2007.
- Cousins, A. B., Mullendore, D. L., and Sonawane, B. V.: Recent developments in mesophyll conductance in C<sub>3</sub>, C<sub>4</sub> and CAM plants *Plant J.*, 2020.
- Cox, P. M., Betts, R. A., Jones, C. D., Spall, S. A., and Totterdell, I. J.: Acceleration of global warming due to carbon-cycle feedbacks in a coupled climate model, *Nature*, 408, 3, 2000.

- Craig, H.: Isotopic standards for carbon and oxygen and correction factors for mass-spectrometric analysis of carbon dioxide, *Geochim Cosmochim Acta*, 12, 16, 10.1016/0016-7037(57)90024-8, 1957.
- Craig, H., and Gordon, L. I.: Deuterium and oxygen 18 variations in the ocean and the marine atmosphere, Consiglio nazionale delle ricerche, Laboratorio de geologia nucleare Pisa, 1965.
- Cuntz, M., Ciais, P., Hoffmann, G., Allison, C. E., Francey, R. J., Knorr, W., Tans, P. P., White, J. W. C., and Levin, I.: A comprehensive global three-dimensional model of  $\delta^{18}\text{O}$  in atmospheric  $\text{CO}_2$ : 2. Mapping the atmospheric signal *J. Geophys. Res. Atmos.*, 108, 2003a.
- Cuntz, M., Ciais, P., Hoffmann, G., and Knorr, W.: A comprehensive global three-dimensional model of  $\delta^{18}\text{O}$  in atmospheric  $\text{CO}_2$ : 1. Validation of surface processes, *J. Geophys. Res. Atmos.*, 108, 24, 2003b.
- Cuntz, M.: A dent in carbon's gold standard, *Nature*, 477, 547-548, 2011.
- Dauphas, N., and Schauble, E. A.: Mass fractionation laws, mass-independent effects, and isotopic anomalies, *Annu Rev Earth Pl Sc*, 44, 74, 2016.
- Degener, J. F.: Atmospheric  $\text{CO}_2$  fertilization effects on biomass yields of 10 crops in northern Germany, *Frontiers in Environmental Science*, 3, 2015.
- Dieleman, W. I. J., Vicca, S., Dijkstra, F. A., Hagedorn, F., Hovenden, M. J., Larsen, K. S., Morgan, J. A., Volder, A., Beier, C., and Dukes, J. S.: Simple additive effects are rare: a quantitative review of plant biomass and soil process responses to combined manipulations of  $\text{CO}_2$  and temperature, *Glob Change Biol*, 18, 12, 2012.
- DiMario, R. J., Quebedeaux, J. C., Longstreth, D. J., Dassanayake, M., Hartman, M. M., and Moroney, J. V.: The cytoplasmic carbonic anhydrases  $\beta\text{CA}_2$  and  $\beta\text{CA}_4$  are required for optimal plant growth at low  $\text{CO}_2$ , *Plant Physiol.*, 171, 13, 2016.
- Dlugokencky, E., and Tans, P.: Trends in atmospheric carbon dioxide, National Oceanic & Atmospheric Administration, Earth System Research Laboratory (NOAA/ESRL), [https://www.esrl.noaa.gov/gmd/ccgg/trends/gl\\_data.html](https://www.esrl.noaa.gov/gmd/ccgg/trends/gl_data.html), 16 Mar, 2020.
- Dongmann, G., Nürnberg, H. W., Förstel, H., and Wägenet, K.: On the enrichment of  $\text{H}_2^{18}\text{O}$  in the leaves of transpiring plants, *Radiation and environmental biophysics*, 11, 11, 1974.
- Drake, B. G., González-Meler, M. A., and Long, S. P.: More efficient plants: a consequence of rising atmospheric  $\text{CO}_2$ ?, *Annual review of plant biology*, 48, 30, 1997.
- Ehleringer, J. R., and Monson, R. K.: Evolutionary and ecological aspects of photosynthetic pathway variation, *Annu. Rev. Ecol. Syst.*, 24, 28, 1993.
- Ehleringer, J. R., and Cerling, T. E.:  $\text{C}_3$  and  $\text{C}_4$  photosynthesis, *Encyclopedia of Global Environmental Change*, 2, 4, 2002.
- Ehleringer, J. R.: The Influence of Atmospheric  $\text{CO}_2$ , Temperature, and Water on the Abundance of  $\text{C}_3/\text{C}_4$  Taxa, in: *A History of Atmospheric  $\text{CO}_2$  and Its Effects on Plants, Animals, and Ecosystems*, 1<sup>st</sup> ed., edited by: (eds), B. I. e. a., Ecological Studies (Analysis and Synthesis), Springer, New York, NY, 17, 2005.
- Eiler, J. M., Clog, M., Magyar, P., Piasecki, A., Sessions, A., Stolper, D., Deerberg, M., Schlueter, H.-J., and Schwieters, J.: A high-resolution gas-source isotope ratio mass spectrometer, *Int J. Mass Spect.*, 335, 45– 56, 2013.
- Evans, J. R., Sharkey, T. D., Berry, J. A., and Farquhar, G. D.: Carbon isotope discrimination measured concurrently with gas exchange to investigate  $\text{CO}_2$  diffusion in leaves of higher plants, *Funct. Plant. Biol.*, 13, 11, 1986.
- Evans, J. R., Kaldenhoff, R., Genty, B., and Terashima, I.: Resistances along the  $\text{CO}_2$  diffusion pathway inside leaves *J. Exp. Bot.*, 60, 13, 2009.
- Evans, J. R., and von Caemmerer, S.: Temperature response of carbon isotope discrimination and mesophyll conductance in tobacco, *Plant Cell Environ*, 36, 745-756, 10.1111/j.1365-3040.2012.02591.x, 2013.



- Fabre, N., Reiter, I. M., Becuwe-Linka, N., Genty, B., and Rumeau, D.: Characterization and expression analysis of genes encoding alpha and beta carbonic anhydrases in Arabidopsis, *Plant Cell Environ*, 30, 617-629, 10.1111/j.1365-3040.2007.01651.x, 2007.
- Farquhar, D. G., O'Leary, M. H., and J. A. Berry: On the relationship between carbon isotope discrimination and intercellular carbon dioxide concentration in leaves Australian Journal of Plant Physiology, 9, 16, 1982.
- Farquhar, G. D., von Caemmerer, S., and Berry, J. A.: A biochemical model of photosynthetic CO<sub>2</sub> assimilation in leaves of C<sub>3</sub> species *Planta*, 149, 12, 1980.
- Farquhar, G. D., and Richards, R. A.: Isotopic composition of plant carbon correlates with water-use efficiency of wheat genotypes, *Functional Plant Biology*, 11, 11, 1984.
- Farquhar, G. D., Ehleringer, J. R., and Hubick, K. T.: Carbon isotope discrimination and photosynthesis, *Annu. Rev. Plant Physiol. Plant Mol. Biol.*, 40, 34, 1989a.
- Farquhar, G. D., Hubick, K. T., Condon, A. G., and Richards, R. A.: Carbon isotope fractionation and plant water-use efficiency. In *Stable isotopes in ecological research*, edited by: Billings, W. D., Golley, F., Lange, O. L., Olson, J. S., and Remmert, H., Springer, New York, NY, 19 pp., 1989b.
- Farquhar, G. D., and Lloyd, J.: Carbon and oxygen isotope effects in the exchange of carbon dioxide between terrestrial plants and the atmosphere, *Stable isotopes and plant carbon-water relations*, edited by: Ehleringer, J. R., Hall, A. E., and Farquhar, G. D., Academic Press Inc, London, 33 pp., 1993.
- Farquhar, G. D., Lloyd, J., Taylor, J. A., Flanagan, L. B., Syvertsen, J. P., Hubick, K. T., Wong, S. C., and Ehleringer, J. R.: Vegetation effects on the isotope composition of oxygen in atmospheric CO<sub>2</sub>, *Nature*, 363, 4, 1993.
- Farquhar, G. D.: Carbon dioxide and vegetation, *Science*, 278, 1, 1997.
- Farquhar, G. D., and Gan, K. S.: On the progressive enrichment of the oxygen isotopic composition of water along a leaf, *Plant, Cell & Environment*, 26, 18, 2003.
- Farquhar, G. D., Cernusak, L. A., and Barnes, B.: Heavy water fractionation during transpiration, *Plant physiol.*, 143, 7, 2007.
- Farquhar, G. D., and Cernusak, L. A.: Ternary effects on the gas exchange of isotopologues of carbon dioxide, *Plant Cell Environ*, 35, 1221-1231, 10.1111/j.1365-3040.2012.02484.x, 2012.
- Flanagan, L. B., Comstock, J. P., and Ehleringer, J. R.: Comparison of modeled and observed environmental influences on the stable oxygen and hydrogen isotope composition of leaf water in *Phaseolus vulgaris* L, *Plant Physiology*, 96, 8, 1991.
- Flanagan, L. B.: Environmental and biological influences on the stable oxygen and hydrogen isotopic composition of leaf water, in: *Stable isotopes and plant carbon-water relations*, Elsevier, 1993.
- Flanagan, L. B., and Ehleringer, J. R.: Ecosystem-atmosphere CO<sub>2</sub> exchange: interpreting signals of change using stable isotope ratios, *Trends Ecol. Evol.*, 13, 4, 1998.
- Flexas, J., Diaz-Espejo, A., Galmes, J., Kaldenhoff, R., Medrano, H., and Ribas-Carbo, M.: Rapid variations of mesophyll conductance in response to changes in CO<sub>2</sub> concentration around leaves, *Plant, Cell & Environment*, 30, 14, 2007.
- Flexas, J., Ribas-Carbo, M., Diaz-Espejo, A., Galmes, J., and Medrano, H.: Mesophyll conductance to CO<sub>2</sub>: current knowledge and future prospects, *Plant Cell Environ.*, 31, 19, 2008.
- Flexas, J., Barbour, M. M., Brendel, O., Cabrera, H. M., Carriqui, M., Diaz-Espejo, A., Douthe, C., Dreyer, E., Ferrio, J. P., and Gago, J.: Mesophyll diffusion conductance to CO<sub>2</sub>: an unappreciated central player in photosynthesis *Plant Sci.*, 193, 14, 2012.
- Flexas, J., Niinemets, U., Gallé, A., Barbour, M. M., Centritto, M., Diaz-Espejo, A., Douthe, C., Galmes, J., Ribas-Carbo, M., and Rodriguez, P. L.: Diffusional conductances to CO<sub>2</sub> as a target for increasing photosynthesis and photosynthetic water-use efficiency, *Photosynth. Res.*, 117, 14, 2013.

- Forkel, M., Carvalhais, N., Rödenbeck, C., Keeling, R., Heimann, M., Thonicke, K., Zaehle, S., and Reichstein, M.: Enhanced seasonal CO<sub>2</sub> exchange caused by amplified plant productivity in northern ecosystems, *Science*, 351, 3, 2016.
- Fosu, B. J., Subba, R., Peethambaran, R., Bhattacharya, S. K., and Ghosh, P.: Developments and applications in triple oxygen isotope analysis of carbonates ACS Earth and Space Chemistry, 2020.
- Francey, R. J., and Tans, P. P.: Latitudinal variation in oxygen-18 of atmospheric CO<sub>2</sub>, *Nature*, 327, 2, 1987.
- Francey, R. J., Allison, C. E., Etheridge, D. M., Trudinger, C. M., Enting, I. G., Leuenberger, M., Langenfelds, R. L., Michel, E., and Steele, L. P.: A 1000-year high precision record of  $\delta^{13}\text{C}$  in atmospheric CO<sub>2</sub>, *Tellus B*, 51, 23, 1999.
- Frank, D., Reichstein, M., Bahn, M., Thonicke, K., Frank, D., Mahecha, M. D., Smith, P., Velde, M. V. d., Vicca, S., and Babst, F.: Effects of climate extremes on the terrestrial carbon cycle: concepts, processes and potential future impacts, *Global Change Biology*, 21, 19, 2015.
- Frank, D. C., Esper, J., Raible, C. C., Büntgen, U., Trouet, V., Stocker, B., and Joos, F.: Ensemble reconstruction constraints on the global carbon cycle sensitivity to climate, *Nature*, 463, 5, 2010.
- Fredeen, A. L., Gamon, J. A., and Field, C. B.: Responses of photosynthesis and carbohydrate-partitioning to limitations in nitrogen and water availability in field-grown sunflower *Plant Cell Environ.*, 14, 7, 1991.
- Friedli, H., Siegenthaler, U., Rauber, D., and Oeschger, H.: Measurements of concentration,  $^{13}\text{C}/^{12}\text{C}$  and  $^{18}\text{O}/^{16}\text{O}$  ratios of tropospheric carbon dioxide over Switzerland, *Tellus B*, 8, 1987.
- Friedlingstein, P., Cox, P., Betts, R., Bopp, L., Bloh, W. v., Brovkin, V., Cadule, P., Doney, S., Eby, M., Fung, I., Bala, G., John, J., Jones, C., Joos, F., Kato, T., Kawamiya, M., Knorr, W., Lindsay, K., Matthews, H. D., Raddatz, T., Rayner, P., Reick, C., Roeckner, E., Schnitzler, K.-G., Schnur, R., Strassmann, K., Weaver, A. J., Yoshikawa, C., and Zeng, N.: Climate-carbon cycle feedback analysis: results from the C4MIP model intercomparison, *Journal of climate*, 19, 16, 2006.
- Friedlingstein, P., Meinshausen, M., Arora, V. K., Jones, C. D., Anav, A., Liddicoat, S. K., and Knutti, R.: Uncertainties in CMIP5 climate projections due to carbon cycle feedbacks, *Journal of Climate*, 27, 15, 2014.
- Gaastra, P.: Photosynthesis of crop plants as influenced by light, carbon dioxide, temperature, and stomatal diffusion resistance, *Mededelingen van de Landbouwhogeschool te Wageningen. Nederland*, 59, 68, 1959.
- Galewsky, J., Steen-Larsen, H. C., Field, R. D., Worden, J., Risi, C., and Schneider, M.: Stable isotopes in atmospheric water vapor and applications to the hydrologic cycle *Reviews of Geophysics*, 54, 56, 2016.
- Gan, K. S., Wong, S. C., Yong, J. W. H., and Farquhar, G. D.:  $^{18}\text{O}$  spatial patterns of vein xylem water, leaf water, and dry matter in cotton leaves, *Plant Physiol.*, 130, 13, 2002.
- Gan, K. S., Wong, S. C., Yong, J. W. H., and Farquhar, G. D.: Evaluation of models of leaf water  $^{18}\text{O}$  enrichment using measurements of spatial patterns of vein xylem water, leaf water and dry matter in maize leaves, *Plant Cell Environ.*, 26, 16, 2003.
- Gatti, L. V., Gloor, M., Miller, J. B., Doughty, C. E., Malhi, Y., Domingues, L. G., Basso, L. S., Martinewski, A., Correia, C. S. C., and Borges, V. F.: Drought sensitivity of Amazonian carbon balance revealed by atmospheric measurements, *Nature*, 4, 2014.
- Gillon, J., and Yakir, D.: Influence of carbonic anhydrase activity in terrestrial vegetation on the  $^{18}\text{O}$  content of atmospheric CO<sub>2</sub>, *Science*, 291, 3, 2001.
- Gillon, J. S., and Yakir, D.: Naturally low carbonic anhydrase activity in C<sub>4</sub> and C<sub>3</sub> plants limits discrimination against C<sup>18</sup>OO during photosynthesis, *Plant Cell Environ.*, 23, 12, 2000a.

- Gillon, J. S., and Yakir, D.: Internal conductance to CO<sub>2</sub> diffusion and C<sup>18</sup>OO discrimination in C<sub>3</sub> leaves, *Plant Physiol.*, 123, 13, 2000b.
- Gonfiantini, R.: Standards for stable isotope measurements in natural compounds *Nature*, 271, 2, 1978.
- Graven, H. D., Keeling, R. F., Piper, S. C., Patra, P. K., Stephens, B. B., Wofsy, S. C., Welp, L. R., Sweeney, C., Tans, P. P., and Kelley, J. J.: Enhanced seasonal exchange of CO<sub>2</sub> by northern ecosystems since 1960 *Science* 341, 4, 2013.
- Harley, P. C., Loreto, F., Marco, G. D., and Sharkey, T. D.: Theoretical considerations when estimating the mesophyll conductance to CO<sub>2</sub> flux by analysis of the response of photosynthesis to CO<sub>2</sub> *Plant physiology*, 98, 7, 1992.
- Harwood, K. G., Gillon, J. S., Griffiths, H., and Broadmeadow, M. S. J.: Diurnal variation of  $\Delta^{13}\text{CO}_2$ ,  $\Delta\text{C}^{18}\text{O}^{16}\text{O}$  and evaporative site enrichment of  $\delta\text{H}_2^{18}\text{O}$  in *Piper aduncum* under field conditions in Trinidad *Plant Cell Environ.*, 21, 14, 1998.
- Hattori, S., Toyoda, A., Toyoda, S., Ishino, S., Ueno, Y., and Yoshida, N.: Determination of the sulfur isotope ratio in carbonyl sulfide using gas chromatography/isotope ratio mass spectrometry on fragment ions  $^{32}\text{S}^+$ ,  $^{33}\text{S}^+$ , and  $^{34}\text{S}^+$ , *Anal Chem*, 87, 477-484, 10.1021/ac502704d, 2015.
- Haverd, V., Smith, B., Canadell, J. G., Cuntz, M., Mikaloff-Fletcher, S., Farquhar, G. D., Woodgate, W., Briggs, P. R., and Trudinger, C. M.: Higher than expected CO<sub>2</sub> fertilization inferred from leaf to global observations, *Global Change Biology* 2020.
- Heidenreich, J. E., and Thiemens, M. H.: A non-mass-dependent isotope effect in the production of ozone from molecular oxygen *J. CHEM. Phys.*, 78, 3, 1983.
- Heidenreich, J. E., and Thiemens, M. H.: A non-mass-dependent oxygen isotope effect in the production of ozone from molecular oxygen: The role of molecular symmetry in isotope chemistry *J. Chem. Phys.*, 84, 5, 1986.
- Heimann, M., Schulze, E. D., Winderlich, J., Andreae, M. O., Chi, X., Gerbig, C., Kolle, O., Kübler, K., Lavric, J., and Mikhailov, E.: The zotino tall tower observatory (zotto): Quantifying large scale biogeochemical changes in central siberia, *Nova Acta Leopoldina NF*, 117, 13, 2014.
- Hoag, K. J., Still, C. J., Fung, I. Y., and Boering, K. A.: Triple oxygen isotope composition of tropospheric carbon dioxide as a tracer of terrestrial gross carbon fluxes, *Geophys. Res. Lett.*, 32, 10.1029/2004gl021011, 2005.
- Hofmann, M. E. G., and Pack, A.: Technique for high-precision analysis of triple oxygen isotope ratios in carbon dioxide *Analytical Chemistry*, 82, 4, 2010.
- Hofmann, M. E. G., Horváth, B., Schneider, L., Peters, W., Schützenmeister, K., and Pack, A.: Atmospheric measurements of  $\Delta^{17}\text{O}$  in CO<sub>2</sub> in Göttingen, Germany reveal a seasonal cycle driven by biospheric uptake, *Geochim. Cosmochim. Ac.*, 199, 143-163, 10.1016/j.gca.2016.11.019, 2017.
- Holloway-Phillips, M., Cernusak, L. A., Stuart-Williams, H., Ubierna, N., and Farquhar, G. D.: Two-source  $\delta^{18}\text{O}$  method to validate the CO<sup>18</sup>O-photosynthetic discrimination model: Implications for mesophyll conductance, *Plant Physiology*, 181, 15, 2019.
- Horváth, B., Hofmann, M. E. G., and Pack, A.: On the triple oxygen isotope composition of carbon dioxide from some combustion processes, *Geochimica et Cosmochimica Acta*, 95, 8, 2012.
- Howard, A. R., and Donovan, L. A.: *Helianthus* nighttime conductance and transpiration respond to soil water but not nutrient availability, *Plant Physiology*, 143, 5, 2007.
- Hu, B., Radke, J., Schluter, H. J., Heine, F. T., Zhou, L., and Bernasconi, S. M.: A modified procedure for gas-source isotope ratio mass spectrometry: the long-integration dual-inlet (LIDI) methodology and implications for clumped isotope measurements, *Rapid Commun Mass Spectrom*, 28, 1413-1425, 10.1002/rcm.6909, 2014.
- Hulston, J., and Thode, H.: Variations in the S<sup>33</sup>, S<sup>34</sup>, and S<sup>36</sup> contents of meteorites and their relation to chemical and nuclear effects, *Journal of Geophysical Research*, 70, 10, 1965.

- Jähne, B., Münnich, K. O., Bössinger, R., Dutzi, A., Huber, W., and Libner, P.: Jähne, Bernd, et al. "On the parameters influencing air-water gas exchange, *Journal of Geophysical Research, Oceans*, 92(C2), 12, 10.1029/JC092iC02p01937, 1987.
- James, H. B., and Stephen, A. M.: The NOAA annual greenhouse gas index (aggi), National Oceanic & Atmospheric Administration, Earth System Research Laboratory (NOAA/ESRL), <https://www.esrl.noaa.gov/gmd/aggi/aggi.html>, 05 May 2019.
- Johnson, J. E., and Rella, C. W.: Effects of variation in background mixing ratios of N<sub>2</sub>, O<sub>2</sub>, and Ar on the measurement of  $\delta^{18}\text{O}$ -H<sub>2</sub>O and  $\delta^2\text{H}$ -H<sub>2</sub>O values by cavity ring-down spectroscopy, *Atmos. Meas. Tech.*, 10, 18, 2017.
- Johnson, K. S.: Carbon dioxide hydration and dehydration kinetics in seawater 1, *Limnology and Oceanography*, 27, 6, 1982.
- Joiner, J., Yoshida, Y., Zhang, Y., Duveiller, G., Jung, M., Lyapustin, A., Wang, Y., and Tucker, C. J.: Estimation of terrestrial global gross primary production (GPP) with satellite data-driven models and eddy covariance flux data, *Remote Sensing*, 10, 38, 2018.
- Joos, F., and Spahni, R.: Rates of change in natural and anthropogenic radiative forcing over the past 20,000 years *Proceedings of the National Academy of Sciences*, 105, 5, 2008.
- Jouzel, J., Masson-Delmotte, V., Cattani, O., Dreyfus, G., Falourd, S., Hoffmann, G., Minster, B., Nouet, J., Barnola, J. M., Chappellaz, J., Fischer, H., Gallet, J. C., Johnsen, S., Leuenberger, M., Loulergue, L., Luethi, D., Oerter, H., Parrenin, F., Raisbeck, G., Raynaud, D., Schilt, A., Schwander, J., Selmo, E., Souchez, R., Spahni, R., Stauffer, B., Steffensen, J. P., Stenni, B., Stocker, T. F., Tison, J. L., Werner, M., and Wolff, E. W.: Orbital and Millennial Antarctic Climate Variability over the Past 800,000 Years, *Science*, 317, 4, 2007.
- Jung, M., Reichstein, M., and Bondeau, A.: Towards global empirical upscaling of FLUXNET eddy covariance observations: validation of a model tree ensemble approach using a biosphere model *Biogeosciences*, 6, 12, 2009.
- Jung, M., Reichstein, M., Margolis, H. A., Cescatti, A., Richardson, A. D., Arain, M. A., Arneth, A., Bernhofer, C., Bonal, D., and Chen, J.: Global patterns of land-atmosphere fluxes of carbon dioxide, latent heat, and sensible heat derived from eddy covariance, satellite, and meteorological observations, *Journal of Geophysical Research: Biogeosciences*, 116, 2011.
- Jung, M., Schwalm, C., Migliavacca, M., Walther, S., Camps-Valls, G., Koirala, S., Anthoni, P., Besnard, S., Bodesheim, P., and Carvalhais, N.: Scaling carbon fluxes from eddy covariance sites to globe: synthesis and evaluation of the FLUXCOM approach. In open review for *Biogeosciences*, *Biogeosciences*, 2019.
- Jung, M., Schwalm, C., Migliavacca, M., Walther, S., Camps-Valls, G., Koirala, S., Anthoni, P., Besnard, S., Bodesheim, P., and Carvalhais, N.: Scaling carbon fluxes from eddy covariance sites to globe: synthesis and evaluation of the FLUXCOM approach, *Biogeosciences*, 17, 22, 2020.
- Kaiser, J., Röckmann, T., and Brenninkmeijer, C. A. M.: Contribution of mass-dependent fractionation to the oxygen isotope anomaly of atmospheric nitrous oxide, *J. Geophys. Res.*, 109, D03305, 2004a.
- Kaiser, J.: Reformulated <sup>17</sup>O correction of mass spectrometric stable isotope measurements in carbon dioxide and a critical appraisal of historic 'absolute' carbon and oxygen isotope ratios, *Geochimica et Cosmochimica Acta*, 72, 22, 10.1016/j.gca.2007.12.011, 2008.
- Kammer, A., Tuzson, B., Emmenegger, L., Knohl, A., Mohn, J., and Hagedorn, F.: Application of a quantum cascade laser-based spectrometer in a closed chamber system for real-time  $\delta^{13}\text{C}$  and  $\delta^{18}\text{O}$  measurements of soil-respired CO<sub>2</sub>, *Agr. Forest. Meteorol.*, 151, 9, 2011.
- Katakis, D., and Taube, H.: Some photochemical reactions of O<sub>3</sub> in the gas phase, *The Journal of Chemical Physics*, 36, 8, 1962.

- Kawagucci, S., Tsunogai, U., Kudo, S., Nakagawa, F., Honda, H., Aoki, S., Nakazawa, T., and Gamo, T.: An analytical system for determining  $\delta^{17}\text{O}$  in  $\text{CO}_2$  using continuous flow-isotope ratio MS, *Anal. Chem.*, 77, 5, 2005.
- Kawagucci, S., Tsunogai, U., Kudo, S., Nakagawa, F., Honda, H., Aoki, S., Nakazawa, T., Tsutsumi, M., and Gamo, T.: Long-term observation of mass-independent oxygen isotope anomaly in stratospheric  $\text{CO}_2$ , *Atmos. Chem. Phys.*, 8, 8, 2008.
- Keeling, C. D.: The concentration and isotopic abundances of atmospheric carbon dioxide in rural areas, *Geochimica et cosmochimica acta*, 13, 12, 1958.
- Keeling, C. D.: The concentration and isotopic abundances of carbon dioxide in the atmosphere *Tellus* 12, 3, 1960.
- Keeling, C. D.: The concentration and isotopic abundances of carbon dioxide in rural and marine air, *Geochimica et Cosmochimica Acta*, 24, 21, 1961.
- Keeling, C. D., Mook, W. G., and Tans, P. P.: Recent trends in the  $^{13}\text{C}/^{12}\text{C}$  ratio of atmospheric carbon dioxide, *Nature* volume, 277, 3, 10.1038/277121a0, 1979.
- Keeling, C. D., Piper, S. C., Bacastow, R. B., Wahlen, M., Whorf, T. P., Heimann, M., and Meijer, H. A.: Exchanges of atmospheric  $\text{CO}_2$  and  $^{13}\text{CO}_2$  with the terrestrial biosphere and oceans from 1978 to 2000. I. Global aspects, 2001.
- Keeling, C. D., Piper, S. C., Bacastow, R. B., Wahlen, M., Whorf, T. P., Heimann, M., and Meijer, H. A.: Atmospheric  $\text{CO}_2$  and  $^{13}\text{CO}_2$  exchange with the terrestrial biosphere and oceans from 1978 to 2000: Observations and carbon cycle implications, *A history of atmospheric  $\text{CO}_2$  and its effects on plants, animals, and ecosystems*, 177, edited by: Ehleringer, J. R., Cerling, T. E., and Dearing, M. D., Springer, 2005.
- Kirschbaum, M. U. F., Miko, U. F., Zeng, G., Ximenes, F., Giltrap, D. L., and Zeldis, J. R.: Towards a more complete quantification of the global carbon cycle, *Biogeosciences*, 16, 2019.
- Knauer, J., Zaehle, S., Kauwe, M. G. D., Bahar, N. H., Evans, J. R., Medlyn, B. E., Reichstein, M., and Werner, C.: Effects of mesophyll conductance on vegetation responses to elevated  $\text{CO}_2$  concentrations in a land surface model, *Global change biology*, 25, 18, 2019a.
- Knauer, J., Zaehle, S., Kauwe, M. G. D., Haverd, V., Reichstein, M., and Sun, Y.: Mesophyll conductance in land surface models: Effects on photosynthesis and transpiration *The Plant Journal*, 2019b.
- Knorr, W.: Is the airborne fraction of anthropogenic  $\text{CO}_2$  emissions increasing?, *Geophys. Res. Lett.*, 36, L21710, 10.1029/2009GL040613, 2009.
- Kolbe, A. R., and Cousins, A. B.: Mesophyll conductance in *Zea mays* responds transiently to  $\text{CO}_2$  availability: implications for transpiration efficiency in  $\text{C}_4$  crops, *New Phytologist*, 217, 11, 2018.
- Kooijmans, L. M. J., Uitslag, N. A. M., Zahniser, M. S., Nelson, D. D., Montzka, S. A., and Chen, H. L.: Continuous and high-precision atmospheric concentration measurements of  $\text{COS}$ ,  $\text{CO}_2$ ,  $\text{CO}$  and  $\text{H}_2\text{O}$  using a quantum cascade laser spectrometer (QCLS), *Atmos. Meas. Tech.*, 9, 21, 2016.
- Kooijmans, L. M. J., Sun, W., Aalto, J., Erkkilä, K.-M., Maseyk, K., Seibt, U., Vesala, T., Mammarella, I., and Chen, H.: Influences of light and humidity on carbonyl sulfide-based estimates of photosynthesis *Proceedings of the National Academy of Sciences*, 116, 5, 2019.
- Koren G, Schneider L, van der Velde IR, van Schaik E, Gromov SS, Adnew GA, Mrozek DJ, Hofmann MED, Liang M.-C, Mahata S, Bergamaschi P, van der Laan-Luijkx IT, Krol MC, Röckmann T, Peters W ( 2019) Global 3-D simulations of the triple oxygen isotope signature  $\Delta^{17}\text{O}$  in Atmospheric  $\text{CO}_2$ . *J Geophys Res Atmos* 124:8808-8836.
- Koren, G.: Constraining the Amazon carbon balance with stable isotopes, remote sensing and inverse modeling, PhD. thesis 2020.
- Körner, C.: Biosphere responses to  $\text{CO}_2$  enrichment, *Ecological applications*, 10, 29, 2000.

- Lämmerzahl, P., Röckmann, T., and Brenninkmeijer, C. A. M.: Oxygen isotope composition of stratospheric carbon dioxide, *Geophys. Res. Lett.*, 29, 10.1029/2001gl014343, 2002.
- Landais, A., Barkan, E., Yakir, D., and Luz, B.: The triple isotopic composition of oxygen in leaf water, *Geochim. Cosmochim. Ac.*, 70, 4105-4115, 10.1016/j.gca.2006.06.1545, 2006.
- Landais, A., Barkan, E., and Luz, B.: Record of  $\delta^{18}\text{O}$  and  $^{17}\text{O}$ -excess in ice from Vostok Antarctica during the last 150,000 years, *Geophys. Res. Lett.*, 35, 10.1029/2007gl032096, 2008.
- Laskar, A. H., Mahata, S., and Liang, M.-C.: Identification of anthropogenic  $\text{CO}_2$  using triple oxygen and clumped isotopes, *Environ. Sci. Technol.*, 50, 18, 10.1021/acs.est.6b02989, 2016.
- Laskar, A. H., Peethambaran, R., Adnew, G. A., and Röckmann, T.: Measurement of  $^{18}\text{O}^{18}\text{O}$  and  $^{17}\text{O}^{18}\text{O}$  in atmospheric  $\text{O}_2$  using the 253 Ultra mass spectrometer and applications to stratospheric and tropospheric air samples *Rapid Communications in Mass Spectrometry*, 33, 13, 2019.
- Laskar, H. A., Abhayanand, S. M., Vishvendra, S., Bhola, R. G., and Liang, M.-C.: A new perspective of probing the level of pollution in the megacity Delhi affected by crop residue burning using the triple oxygen isotope technique in atmospheric  $\text{CO}_2$ , *Environmental Pollution*, 2020.
- Leakey, A. D. B.: Rising atmospheric carbon dioxide concentration and the future of  $\text{C}_4$  crops for food and fuel *Proceedings of the Royal Society B: Biological Sciences*, 276, 10, 2009.
- Lee, J. S.: Stomatal opening mechanism of CAM plants *Journal of Plant Biology*, 53, 4, 2010.
- Lenssen, N., Schmidt, G., Hansen, J., Menne, M., Persin, A., Ruedy, R., and Zyss, D.: Improvements in the GISTEMP uncertainty model, *J. Geophys. Res. Atmos.*, 124, 19, 2019.
- Lewis, S. L., Lloyd, J., Sitch, S., Mitchard, E. T. A., and Laurance, W. F.: Changing ecology of tropical forests: evidence and drivers, *Annual Review of Ecology, Evolution, and Systematics*, 40, 20, 2009.
- Li, S., Levin, N. E., and Chesson, L. A.: Continental scale variation in  $^{17}\text{O}$ -excess of meteoric waters in the United States, *Geochimica et Cosmochimica Acta*, 164, 16, 2015.
- Liang, M.-C., Blake, G. A., Lewis, B. R., and Yung, Y. L.: Oxygen isotopic composition of carbon dioxide in the middle atmosphere, *PNAS*, 104, 4, 2006.
- Liang, M.-C., and Mahata, S.: Oxygen anomaly in near surface carbon dioxide reveals deep stratospheric intrusion, *Sci. Rep.*, 5, 11352, 10.1038/srep11352, 2015.
- Liang, M.-C., Mahata, S., Laskar, A. H., and Bhattacharya, S. K.: Spatiotemporal variability of oxygen isotope anomaly in near surface air  $\text{CO}_2$  over urban, semi-urban and ocean areas in and around Taiwan, *Aerosol Air Qual. Res.*, 17, 24, 2017a.
- Liang, M.-C., Mahata, S., Laskar, A. H., Thieme, M. H., and Newman, S.: Oxygen isotope anomaly in tropospheric  $\text{CO}_2$  and implications for  $\text{CO}_2$  residence time in the atmosphere and gross primary productivity, *Sci Rep*, 7, 13180, 10.1038/s41598-017-12774-w, 2017b.
- Long, S. P., and Bernacchi, C. J.: Gas exchange measurements, what can they tell us about the underlying limitations to photosynthesis? Procedures and sources of error, *Journal of experimental botany*, 54, 8, 2003.
- Loreto, F., Harley, P. C., Marco, G. D., and Sharkey, T. D.: Estimation of mesophyll conductance to  $\text{CO}_2$  flux by three different methods, *Plant physiology*, 98, 6, 1992.
- Lowe, D. C., Brenninkmeijer, C. A. M., Tyler, S. C., and Dlugokencky, E. J.: Determination of the isotopic composition of atmospheric methane and its application in the Antarctic, *JGR Atmospheres*, 96, 12, 1991.
- Lüthi, D., Floch, M. L., Bereiter, B., Blunier, T., Barnola, J.-M., Siegenthaler, U., Raynaud, D., Jouzel, J., Fischer, H., Kawamura, K., and Stocker, T. F.: High-resolution carbon dioxide concentration record 650,000-800,000 years before present, *Nature*, 43, 3, 2008.
- Luz, B., Barkan, E., Bender, M. L., Thieme, M. K., and Boering, K. A.: Triple-isotope composition of atmospheric oxygen as a tracer of biosphere productivity *Nature*, 400, 3, 1999.



- Luz, B., and Barkan, E.: The isotopic ratios  $^{17}\text{O}/^{16}\text{O}$  and  $^{18}\text{O}/^{16}\text{O}$  in molecular oxygen and their significance in biogeochemistry, *Geochimica et Cosmochimica Acta*, 69, 1099-1110, 10.1016/j.gca.2004.09.001, 2005.
- Luz, B., and Barkan, E.: Variations of  $^{17}\text{O}/^{16}\text{O}$  and  $^{18}\text{O}/^{16}\text{O}$  in meteoric waters *Geochim. Cosmochim. Acta*, 74, 10, 2010.
- Lyons, J. R.: Transfer of mass-independent fractionation in ozone to other oxygen-containing radicals in the atmosphere, *Geophys. Res. Lett.*, 28, 3231-3234, 10.1029/2000gl012791, 2001.
- Ma, J., Yan, X., Dong, W., and Chou, J.: Gross primary production of global forest ecosystems has been overestimated *Scientific reports*, 5, 2015.
- Mahata, S., Bhattacharya, S. K., Wang, C. H., and Liang, M.-C.: An improved  $\text{CeO}_2$  method for high-precision measurements of  $^{17}\text{O}/^{16}\text{O}$  ratios for atmospheric carbon dioxide, *Rapid Commun Mass Sp*, 26, 22, 10.1002/rcm.6296, 2012.
- Mahata, S., Bhattacharya, S. K., Wang, C. H., and Liang, M.-C.: Oxygen isotope exchange between  $\text{O}_2$  and  $\text{CO}_2$  over hot platinum: an innovative technique for measuring  $\Delta^{17}\text{O}$  in  $\text{CO}_2$ , *Anal. Chem.*, 85, 6894-6901, 10.1021/ac4011777, 2013.
- Marco, G. D., Manes, F., Tricoli, D., and Vitale, E.: Fluorescence parameters measured concurrently with net photosynthesis to investigate chloroplastic  $\text{CO}_2$  concentration in leaves of *Quercus ilex* L., *Journal of Plant Physiology*, 136, 5, 1990.
- Mason, E. A., and Marrero, T. R.: The diffusion of atoms and molecules, *Advances in Atomic and Molecular Physics*, 6, 77, 10.1016/S0065-2199(08)60205-5, 1970.
- Matsuhisa, Y., Goldsmith, J. R., and Clayton, R. N.: Mechanisms of hydrothermal crystallization of quartz at 250°C and 15 kbar *Geochim. Cosmochim. Acta*, 42, 9, 1978a.
- McKinney, R. C., McCrea, M. J., Epstein, S., Allen, H. A., and Urey, H. C.: Improvements in mass spectrometers for the measurement of small differences in isotope abundance ratios *Review of Scientific Instruments*, 21, 6, 10.1063/1.1745698, 1950.
- McManus, J. B., Nelson, D. D., Shorter, J. H., Jimenez, R., Herndon, S., Saleska, S., and Zahniser, M.: A high precision pulsed quantum cascade laser spectrometer for measurements of stable isotopes of carbon dioxide, *J. Mod. Optic.*, 52, 12, 2005.
- McManus, J. B., Zahniser, M. S., Nelson, D. D., Shorter, J. H., Herndon, S. C., Wood, E. C., and Wehr, R.: Application of quantum cascade lasers to high-precision atmospheric trace gas measurements *Optical Engineering*, 49, 111124, 2010.
- McManus, J. B., Nelson, D. D., and Zahniser, M. S.: Design and performance of a dual-laser instrument for multiple isotopologues of carbon dioxide and water, *Opt Express*, 23, 6569-6586, 10.1364/OE.23.006569, 2015.
- Meijer, H., and Li, W.: The use of electrolysis for accurate  $^{17}\text{O}$  and  $^{18}\text{O}$  isotope measurements in water isotopes, *Isotopes Environ. Health Stud.*, 34, 20, 1998.
- Merlivat, L.: Molecular diffusivities of  $\text{H}_2^{16}\text{O}$ ,  $\text{HD}^{16}\text{O}$ , and  $\text{H}_2^{18}\text{O}$  in gases, *J. Chem. Phys.*, 69, 7, 1978.
- Meure, M. C., Etheridge, D., Trudinger, C., Steele, P., Langenfelds, R., Ommen, T. v., Smith, A., and Elkins, J.: The Law Dome  $\text{CO}_2$ ,  $\text{CH}_4$  and  $\text{N}_2\text{O}$  ice core records extended to 2000 years BP, *Geophysical Research Letters*, 33, L1480, 2006.
- Miller, J. B., Yakir, D., White, J. W. C., and Tans, P. P.: Measurement of  $^{18}\text{O}/^{16}\text{O}$  in the soil-atmosphere  $\text{CO}_2$  flux, *Global Biogeochem. Cy.*, 13, 13, 1999.
- Miller, M. F.: Isotopic fractionation and the quantification of  $^{17}\text{O}$  anomalies in the oxygen three-isotope system: an appraisal and geochemical significance, *Geochim. Cosmochim. Acta*, 66, 8, 2002.
- Miller, M. F., Röckmann, T., and Wright, I. P.: A general algorithm for the  $^{17}\text{O}$  abundance correction to  $^{13}\text{C}/^{12}\text{C}$  determinations from  $\text{CO}_2$  isotopologue measurements, including  $\text{CO}_2$  characterised by 'mass-independent' oxygen isotope distributions, *Geochim. Cosmochim. Acta*, 71, 3145-3161, 10.1016/j.gca.2007.03.007, 2007.

- Miller, M. F.: Precipitation regime influence on oxygen triple-isotope distributions in Antarctic precipitation and ice cores, *Earth Planet. Sc. Lett.*, 481, 11, 2018.
- Miller, M. F., Pack, A., Bindeman, I. N., and Greenwood, R. C.: Standardizing the reporting of  $\Delta^{17}\text{O}$  data from high precision oxygen triple-isotope ratio measurements of silicate rocks and minerals, *Chem. Geo.*, 532, 119332, 2020.
- Miller, R. F., Berkshire, D. C., Kelley, J. J., and Hood, D. W.: Method for determination of reaction rates of carbon dioxide with water and hydroxyl ion in seawater, *Environ. Sci. Tech.*, 5, 6, 1971.
- Mills, G. A., and Urey, H. C.: The kinetics of isotopic exchange between carbon dioxide, bicarbonate ion, carbonate ion and water, *J. AM. Chem. Soc.*, 62, 7, 1940.
- Mook, W. G., Koopmans, M., Carter, A. F., and Keeling, C. D.: Seasonal, latitudinal, and secular variations in the abundance and isotopic ratios of atmospheric carbon dioxide: 1. Results from land stations, *J. Geophys. Res.*, 88, 10.1029/JC088iC15p10915, 1983.
- Mrozek, D. J., van der Veen, C., Hofmann, M. E. G., Chen, H., Kivi, R., Heikkinen, P., and Röckmann, T.: Stratospheric Air Sub-sampler (SAS) and its application to analysis of  $\Delta^{17}\text{O}(\text{CO}_2)$  from small air samples collected with an AirCore, *Atmospheric Measurement Techniques*, 9, 5607-5620, 10.5194/amt-9-5607-2016, 2016.
- NASA/GISS: GISS Surface Temperature Analysis (GISTEMP), version 4. NASA Goddard Institute for Space Studies. Dataset accessed 2020-03-30 at <https://data.giss.nasa.gov/gistemp/>, 2020.
- Nelson, D. D., McManus, J. B., Herndon, S., Zahniser, M. S., Tuzson, B., and Emmenegger, L.: New method for isotopic ratio measurements of atmospheric carbon dioxide using a 4.3  $\mu\text{m}$  pulsed quantum cascade laser *Appl. Phys. B-Lasers. O.*, 90, 8, 2008.
- Mass spectrum (electron ionization)-the NIST webbook:  
<https://webbook.nist.gov/cgi/cbook.cgi?ID=C7732185&Mask=200>, access: December 17, 2018a.
- Carbon dioxide-the NIST webbook.:  
<https://webbook.nist.gov/cgi/cbook.cgi?ID=C124389&Mask=200>, access: December 17, 2018b.
- O'Leary, M. H.: Measurement of the isotope fractionation associated with diffusion of carbon dioxide in aqueous solution, *The Journal of Physical Chemistry*, 88, 4, 1984.
- Obermeier, W. A., Lehnert, L. W., Kammann, C. I., Müller, C., Grünhage, L., Luterbacher, J., Erbs, M., Moser, G., Seibert, R., and Yuan, N.: Reduced  $\text{CO}_2$  fertilization effect in temperate  $\text{C}_3$  grasslands under more extreme weather conditions *Nature Climate Change*, 7, 4, 2017.
- Ogée, J., Peylin, P., Cuntz, M., Bariac, T., Brunet, Y., Berbigier, P., Richard, P., and Ciais, P.: Partitioning net ecosystem carbon exchange into net assimilation and respiration with canopy-scale isotopic measurements: An error propagation analysis with  $^{13}\text{CO}_2$  and  $\text{CO}^{18}\text{O}$  data, *Global Biogeochemical Cycles*, 18, 2004.
- Orsenigo, M., Patrignani, G., and Rascio, N.: Ecophysiology of  $\text{C}_3$ ,  $\text{C}_4$  and CAM plants, *Handbook of photosynthesis*, edited by: M.Pessarakli, Marcel Dekker, United States of America, 1997.
- Osborn, H. L., Alonso-Cantabrana, H., Sharwood, R. E., Covshoff, S., Evans, J. R., Furbank, R. T., and Caemmerer, S. v.: Effects of reduced carbonic anhydrase activity on  $\text{CO}_2$  assimilation rates in *Setaria viridis*: a transgenic analysis, *J. Exp. Bot.*, 68, 11, 2017.
- Pack, A., and Herwartz, D.: The triple oxygen isotope composition of the Earth mantle and understanding  $\Delta^{17}\text{O}$  variations in terrestrial rocks and minerals *Earth. Planet. Sc. Lett.*, 390, 7, 2014.
- Pack, A., Tanaka, R., Hering, M., Sengupta, S., Peters, S., and Nakamura, E.: The oxygen isotope composition of San Carlos olivine on the VSMOW2-SLAP2 scale *Rapid Communications in Mass Spectrometry*, 30, 9, 2016.
- Pack, A. a. H., Andres and Hezel, Dominik C and Stefanak, Maren T and Beck, Anne-Katrin and Peters, Stefan TM and Sengupta, Sukanya and Herwartz, Daniel and Folco, Luigi: Tracing the oxygen isotope composition of the upper Earth's atmosphere using cosmic spherules, *Nature communications*, 8, 2017.



- Pack, M. E. G. H. a. A.: Technique for High-Precision Analysis of Triple oxygen isotope ratios in carbon dioxide, *Anal. Chem.*, 2010.
- Papale, D., Reichstein, M., Aubinet, M., Canfora, E., Bernhofer, C., Kutsch, W., Longdoz, B., Rambal, S., Valentini, R., Vesala, T., and Yakir, D.: Towards a standardized processing of net ecosystem exchange measured with eddy covariance technique: algorithms and uncertainty estimation, *Biogeosciences*, 3, 12, 2006.
- Passey, B. H., Hu, H., Ji, H., Montanari, S., Li, S., Henkes, G. A., and Levin, N. E.: Triple oxygen isotopes in biogenic and sedimentary carbonates, *Geochimica et Cosmochimica Acta*, 141, 1-25, 10.1016/j.gca.2014.06.006, 2014.
- Pataki, D. E., Xu, T., Luo, Y. Q., and Ehleringer, J. R.: Inferring biogenic and anthropogenic carbon dioxide sources across an urban to rural gradient, *Oecologia*, 152, 15, 2007.
- Pathirana, S. L., Veen, C. v. d., Popa, M. E., and Röckmann, T.: An analytical system for stable isotope analysis on carbon monoxide using continuous-flow isotope-ratio mass spectrometry, *Atmospheric Measurement Techniques*, 8, 9, 10.5194/amt-8-5315-2015, 2015.
- Peters, W., Velde, I. R. v. d., Schaik, E. V., Miller, J. B., Ciais, P., Duarte, H. F., Laan-Luijkx, I. T. v. d., Molen, M. K. v. d., Scholze, M., and Schaefer, K.: Increased water-use efficiency and reduced CO<sub>2</sub> uptake by plants during droughts at a continental scale, *Nat. Geosci.*, 11, 4, 2018.
- Peylin, P., Ciais, P., Denning, A. S., Tans, P. P., Berry, J. A., and White, J. W.: A 3-dimensional study of  $\delta^{18}\text{O}$  in atmospheric CO<sub>2</sub>: contribution of different land ecosystems, *Tellus B*, 51, 25, 1999.
- Piao, S., Sitch, S., Ciais, P., Friedlingstein, P., Peylin, P., Wang, X., Ahlström, A., Anav, A., Canadell, J. G., and Cong, N.: Evaluation of terrestrial carbon cycle models for their response to climate variability and to CO<sub>2</sub> trends *Global change biology*, 19, 25, 2013.
- Piasecki, A., Sessions, A., Lawson, M., Ferreira, A. A., Neto, E. V. S., and Eiler, J. M.: Analysis of the site-specific carbon isotope composition of propane by gas source isotope ratio mass spectrometer, *Geochimica et Cosmochimica Acta*, 188, 58-72, 10.1016/j.gca.2016.04.048, 2016.
- Pons, T. L., and Welschen, R. A. M.: Overestimation of respiration rates in commercially available clamp-on leaf chambers. Complications with measurement of net photosynthesis, *Plant, Cell and Environment*, 25, 5, 2002.
- Pons, T. L., Flexas, J., Caemmerer, S. v., Evans, J. R., Genty, B., Ribas-Carbo, M., and Brugnoli, E.: Estimating mesophyll conductance to CO<sub>2</sub>: methodology, potential errors, and recommendations *J. Exp. Bot.*, 60, 7, 2009.
- Prentice, I. C., Farquhar, G. D., Fasham, M. J. R., Goulden, M. L., Heimann, M., Jaramillo, V. J., Kheshgi, H. S., Le Quéré, C., Scholes, R. J., and Wallace, D. W. R.: The carbon cycle and atmospheric carbon dioxide, *IPCC*, 2007.
- Le Quéré, C., Andres, R. J., Boden, T., Conway, T., Houghton, R. A., House, J. I., Marland, G., Peters, G. P., Werf, G. R. V. D., and Ahlström, A.: The global carbon budget 1959–2011, *Earth Syst. Sci. Data*, 5, 20, 2013.
- Le Quéré, C., Moriarty, R., Andrew, R. M., Canadell, J. G., Sitch, S., Korsbakken, J. I., Friedlingstein, P., Peters, G. P., Andres, R. J., and Boden, T. A.: Global carbon budget 2015, *Earth System Science Data*, 7, 47, 2015.
- Le Quéré, C., Andrew, R. M., Friedlingstein, P., Sitch, S., Pongratz, J., Manning, A. C., Korsbakken, J. I., Peters, G. P., Canadell, J. G., and Jackson, R. B.: Global carbon budget 2017 *Earth System Science Data*, 10, 43, 2018.
- Raj, R., Hamm, N. A. S., Tol, C. v. d., and Stein, A.: Uncertainty analysis of gross primary production partitioned from net ecosystem exchange measurements, *Biogeosciences*, 13, 13, 2016.
- Raupach, M. R.: Pinning down the land carbon sink, *Nature Climate Change*, 1, 1, 2011.
- Reichstein, M., Falge, E., Baldocchi, D., Papale, D., Aubinet, M., Berbigier, P., Bernhofer, C., Buchmann, N., Gilmanov, T., and Granier, A.: On the separation of net ecosystem exchange

- into assimilation and ecosystem respiration: review and improved algorithm, *Global change biology*, 11, 15, 2005.
- Reichstein, M., Stoy, P. C., Desai, A. R., Lasslop, G., and Richardson, A. D.: Partitioning of net fluxes, in *Eddy Covariance: A Practical Guide to Measurement and Data Analysis*, edited by M. Aubinet, T. Vesala, and D. Papale, pp. 263–289, Springer, Netherlands., 2012.
- Reichstein, M., Bahn, M., Ciais, P., Frank, D., Mahecha, M. D., Seneviratne, S. I., Zscheischler, J., Beer, C., Buchmann, N., and Frank, D. C.: Climate extremes and the carbon cycle, *Nature* 500, 8, 2013.
- Röckmann, T., Kaiser, J., Crowley, J. N., Brenninkmeijer, C. A. M., and Crutzen, P. J.: The origin of the anomalous or “mass-independent” oxygen isotope fractionation in tropospheric N<sub>2</sub>O *Geophysical Research Letters*, 28, 3, 2001.
- Röckmann, T., Kaiser, J., and Brenninkmeijer, C. A. M.: The isotopic fingerprint of the pre-industrial and the anthropogenic N<sub>2</sub>O source, *Atmos. Chem. Phys.*, 3, 8, 2003.
- Rumble, D., Miller, M. F., Franchi, I. A., and Greenwood, R. C.: Oxygen three-isotope fractionation lines in terrestrial silicate minerals: An inter-laboratory comparison of hydrothermal quartz and eclogitic garnet, *Geochimica et Cosmochimica Acta*, 71, 8, 2007.
- Sage, R. F., and Monson, R. K.: *C<sub>4</sub> plant biology*, Elsevier, 1998.
- Sage, R. F.: The evolution of C<sub>4</sub> photosynthesis, *New phytologist*, 161, 29, 2004.
- Sage, R. F.: Atmospheric CO<sub>2</sub>, Environmental Stress, and the Evolution of C<sub>4</sub> Photosynthesis, in: *A History of Atmospheric CO<sub>2</sub> and Its Effects on Plants, Animals, and Ecosystems*, 1<sup>st</sup> ed., edited by: (eds), B. I. e. a., *Ecological Studies (Analysis and Synthesis)*, Springer, New York, NY, 22, 2005.
- Santrock, J., Studley, S. A., and Hayes, J. M.: Isotopic analyses based on the mass spectra of carbon dioxide, *Anal. Chem.*, 57, 4, 1985.
- Santrock J., S. S. S., and Hayes J. M: Isotopic analyses based on the mass spectrum of carbon dioxide., *Anal. Chem.*, 57, 4, 1985.
- Savarino, J., Lee, C. C. W., and Thiemens, M. H.: Laboratory oxygen isotopic study of sulfur (IV) oxidation: Origin of the mass-independent oxygen isotopic anomaly in atmospheric sulfates and sulfate mineral deposits on Earth, *Journal of Geophysical Research: Atmospheres*, 105, 9, 2000.
- Savarino, J., Bhattacharya, S. K., Morin, S., Baroni, M., and Doussin, J.-F.: The NO<sup>+</sup> O<sub>3</sub> reaction: A triple oxygen isotope perspective on the reaction dynamics and atmospheric implications for the transfer of the ozone isotope anomaly, *The Journal of chemical physics*, 128, 194303, 2008.
- Schaefer, K., Collatz, G. J., Tans, P., Denning, A. S., Baker, I., Berry, J., Prihodko, L., Suits, N., and Philpott, A.: Combined simple biosphere/Carnegie-Ames-Stanford approach terrestrial carbon cycle model, *J. Geophys. Res-Bioge.*, 113, 2008.
- Schauer, A. J., Kelson, J., Saenger, C., and Huntington, K. W.: Choice of <sup>17</sup>O correction affects clumped isotope (Δ<sub>47</sub>) values of CO<sub>2</sub> measured with mass spectrometry, *Rapid Communications in Mass Spectrometry*, 30, 9, 2016.
- Schimmel, D., Stephens, B. B., and Fisher, J. B.: Effect of increasing CO<sub>2</sub> on the terrestrial carbon cycle, *Proceedings of the National Academy of Sciences*, 112, 5, 2015.
- Schoenemann, S. W., Schauer, A. J., and Steig, E. J.: Measurement of SLAP2 and GISP δ<sup>17</sup>O and proposed VSMOW-SLAP normalization for δ<sup>17</sup>O and <sup>17</sup>O-excess, *Rapid Communications in Mass Spectrometry*, 27, 8, 2013.
- Seibt, U., Wingate, L., Berry, J., and Lloyd, J.: Non-steady state effects in diurnal 18O discrimination by Picea sitchensis branches in the field, *Plant, Cell & Environment*, 29, 11, 2006.
- Seibt, U., Wingate, L., and Berry, J.: Nocturnal stomatal conductance effects on the δ<sup>18</sup>O signatures of foliage gas exchange observed in two forest ecosystems *Tree Physiology*, 27, 10, 2007.

- Seibt, U., Kesselmeier, J., Sandoval-Soto, L., Kuhn, U., and Berry, J. A.: A kinetic analysis of leaf uptake of COS and its relation to transpiration, photosynthesis and carbon isotope fractionation, *Biogeosciences*, 7, 8, 2010.
- Sha, L., Mahata, S., Duan, P., Luz, B., Zhang, P., Baker, J., Zong, B., Ning, Y., Brahim, Y., and Zhang, H.: A novel application of triple oxygen isotope ratios of speleothems *Geochimica et Cosmochimica Acta*, 270, 18, 2020.
- Shaheen, R., Janssen, C., and Röckmann, T.: Investigations of the photochemical isotope equilibrium between O<sub>2</sub>, CO<sub>2</sub> and O<sub>3</sub>, *Atmos. Chem. Phys.*, 7, 495-509, 2007.
- Sharp, Z. D., Gibbons, J. A., Maltsev, O., Atudorei, V., Pack, A., Sengupta, S., Shock, E. L., and Knauth, L. P.: A calibration of the triple oxygen isotope fractionation in the SiO<sub>2</sub>–H<sub>2</sub>O system and applications to natural samples, *Geochim. Cosmochim. Acta*, 186, 14, 2016.
- Sharp, Z. D., Wostbrock, J. A. G., and Pack, A.: Mass-dependent triple oxygen isotope variations in terrestrial materials *Geochem. Persp. Lett.*, 7, 4, 2018.
- Shrestha, A., Song, X., and Barbour, M. M.: The temperature response of mesophyll conductance, and its component conductances, varies between species and genotypes, *Photosynth. Res.*, 18, 2019.
- Silverman, D. N.: Carbonic anhydrase: Oxygen-18 exchange catalyzed by an enzyme with rate-contributing Proton-transfer steps *Methods in enzymology*, Elsevier, 1982.
- Sitch, S., Friedlingstein, P., Gruber, N., Jones, S. D., Murray-Tortarolo, G., Ahlström, A., Doney, S. C., Graven, H., Heinze, C., and Huntingford, C.: Recent trends and drivers of regional sources and sinks of carbon dioxide, *Biogeosciences*, 12, 26, 2015.
- Sleen, P. V. D., Groenendijk, P., Vlam, M., Anten, N. P. R., Boom, A., Bongers, F., Pons, T. L., Terburg, G., and Zuidema, P. A.: No growth stimulation of tropical trees by 150 years of CO<sub>2</sub> fertilization but water-use efficiency increased, *Nature geoscience*, 8, 4, 2015.
- Song, X., Simonin, K. A., Loucos, K. E., and Barbour, M. M.: Modelling non-steady-state isotope enrichment of leaf water in a gas-exchange cuvette environment, *Plant Cell Environ.*, 38, 10, 2015.
- Starkey, N. A., Jackson, C. R. M., Greenwood, R. C., Parman, S., Franchi, I. A., Jackson, M., Fitton, J. G., Stuart, F. M., Kurz, M., and Larsen, L. M.: Triple oxygen isotopic composition of the high-<sup>3</sup>He/<sup>4</sup>He mantle, *Geochimica et Cosmochimica Acta*, 176, 11, 2016.
- Steele, P., Krummel, P., and Langenfelds, R.: CSIRO marine and atmospheric research gaslab flask CO<sub>2</sub> data, Australia, <https://www.csiro.au/en/Research/OandA/Areas/Assessing-our-climate/Latest-greenhouse-gas-data>, 19 Mar, 2020.
- Steen-Larsen, H. C., Johnsen, S. J., Masson-Delmotte, V., Stenni, B., Risi, C., Sodemann, H., Balslev-Clausen, D., Blunier, T., Dahl-Jensen, D., and Ellehøj, M. D.: Continuous monitoring of summer surface water vapor isotopic composition above the Greenland Ice Sheet, *Atmospheric Chemistry and Physics*, 13, 13, 2013.
- Steig, E. J., Gkinis, V., Schauer, A. J., Schoenemann, S. W., Samek, K., Hoffnagle, J., Dennis, K. J., and Tan, S. M.: Calibrated high-precision <sup>17</sup>O-excess measurements using cavity ring-down spectroscopy with laser-current-tuned cavity resonance *Atmos. Meas. Tech.*, 7, 14, 2014.
- Stern, L. A., Amundson, R., and Baisden, W. T.: Influence of soils on oxygen isotope ratio of atmospheric CO<sub>2</sub>, *Global Biogeochem. Cy.*, 15, 6, 2001.
- Still, C. J., Berry, J. A., Collatz, G. J., and DeFries, R. S.: Global distribution of C<sub>3</sub> and C<sub>4</sub> vegetation: Carbon cycle implications, *Global Biogeochem. Cy.*, 17, 6-16-14, 10.1029/2001gb001807, 2003.
- Still, C. J.: Trading water for carbon *Nature Geoscience*, 11, 2, 2018.
- Stimler, K., Montzka, S. A., Berry, J. A., Rudich, Y., and Yakir, D.: Relationships between carbonyl sulfide (COS) and CO<sub>2</sub> during leaf gas exchange, *New Phytologist*, 186, 9, 2010.
- Stocker, T. F., Qin, D., Plattner, G.-K., Tignor, M., Allen, S. K., Boschung, J., Nauels, A., Xia, Y., Bex, V., and Midgley, P. M.: Climate change 2013: The physical science basis Contribution of

- working group I to the fifth assessment report of the intergovernmental panel on climate change (IPCC), 2013.
- Stolper, D. A., Sessions, A. L., Ferreira, A. A., Neto, E. V. S., Schimmelmann, A., Shusta, S. S., Valentine, D. L., and Eiler, J. M.: Combined  $^{13}\text{C}$ -D and D-D clumping in methane: Methods and preliminary results, *Geochimica Et Cosmochimica Acta*, 126, 169-191, DOI 10.1016/j.gca.2013.10.045, 2014.
- Stoltmann, T., Casado, M., Daeron, M., Landais, A., and Kass, S.: Direct, precise measurements of isotopologue abundance ratios in  $\text{CO}_2$  using molecular absorption spectroscopy: Application to  $\Delta^{17}\text{O}$ , *Anal Chem*, 89, 10129-10132, 10.1021/acs.analchem.7b02853, 2017.
- Sun, Y., Gu, L., Dickinson, R. E., Norby, R. J., Pallardy, S. G., and Hoffman, F. M.: Impact of mesophyll diffusion on estimated global land  $\text{CO}_2$  fertilization, *Proceedings of the National Academy of Sciences*, 111, 5, 2014.
- Tans, P. P.: Oxygen isotopic equilibrium between carbon dioxide and water in soils, *Tellus B*, 50, 15, 1998.
- Thiemens, M. H., Jackson, T., Mauersberger, K., Schöler, B., and Morton, J.: Oxygen isotope fractionation in stratospheric  $\text{CO}_2$ , *Geophys. Res. Lett.*, 18, 669-672, 1991.
- Thiemens, M. H., Jackson, T., Zipf, E. C., Erdman, P. W., and Egmond, C. v.: Carbon dioxide and oxygen isotope anomalies in the mesosphere and stratosphere, *Science* 270, 3, 1995.
- Thiemens, M. H.: Mass-independent isotope effects in planetary atmospheres and the early solar system, *Science*, 283, 4, 1999.
- Thiemens, M. H.: History and Applications of Mass-Independent Isotope Effects, *Annu. Rev. Earth Planet. Sci.*, 34, 62, 10.1146/, 2006.
- Thiemens, M. H., Chakraborty, S., and Jackson, T. L.: Decadal  $\Delta^{17}\text{O}$  record of tropospheric  $\text{CO}_2$ : Verification of a stratospheric component in the troposphere, *J. Geophys. Res. Atmos.*, 119, 8, 10.1002/2013JD020317, 2013.
- Thiemens, M. H., and Shaheen, R.: Mass-independent isotopic composition of terrestrial and extraterrestrial materials, in: *Treatise on Geochemistry*, 2<sup>nd</sup> ed., edited by: Karl, T., and Heinrich, H., Elsevier Science, 151-177, 2014.
- Thiemens, M. H., and Heidenreich, J.E. III: Mass-independent fractionation of oxygen: a novel isotope effect and its possible cosmochemical implications, *Science* 10.1126/science.219.4588.1073, 1983.
- Thiemens, M. K., Savarino, J., Farquhar, J., and Bao, H.: Mass-independent isotopic compositions in terrestrial and extraterrestrial solids and their applications, *Accounts of chemical research*, 34, 7, 2001.
- Thiemens, M. K., Chakraborty, S., and Jackson, T. L.: Decadal  $\Delta^{17}\text{O}$  record of tropospheric  $\text{CO}_2$ : Verification of a stratospheric component in the troposphere, *J. Geophys. Res. Atmos.*, 119, 8, 2014.
- Thiemens, S. K. B. a. M. H.: New Evidence for Symmetry Dependent Isotope Effects OCO Reaction, 1989.
- Thomas, H.: The Arctic Ocean may not be a reliable carbon sink, *Eos*, 101, 10.1029/2020EO142366., 2020.
- Ting, I. P.: Crassulacean acid metabolism, *Annual review of plant physiology*, 36, 27, 1985.
- Tipple, B. J., and Pagani, M.: The early origins of terrestrial  $\text{C}_4$  photosynthesis, *Annu. Rev. Earth Planet. Sci.*, 35, 26, 2007.
- Tomás, M., Flexas, J., Copolovici, L., Galmés, J., Hallik, L., Medrano, H., Ribas-Carbó, M., Tosens, T., Vislap, V., and Niinemets, U.: Importance of leaf anatomy in determining mesophyll diffusion conductance to  $\text{CO}_2$  across species: quantitative limitations and scaling up by models, 2013, 64, 12, 2013.
- Toyoda, S., and Yoshida, N.: Determination of nitrogen isotopomers of nitrous oxide on a modified isotope ratio mass spectrometer, *Anal. Chem.*, 71, 7, 1999.

- Tuttas, D., Schwieters, J. B., Bouman, C., & Deerberg, M.: New compact discrete dynode multipliers integrated into the thermo scientific TRITON variable multicollector array, Thermo Fischer Scientific, 4, 2008.
- Tuzson, B., Mohn, J., Zeeman, M. J., Werner, R. A., Eugster, W., Zahniser, M. S., Nelson, D. D., McManus, J. B., and Emmenegger, L.: High precision and continuous field measurements of  $\delta^{13}\text{C}$  and  $\delta^{18}\text{O}$  in carbon dioxide with a cryogen-free QCLAS, Appl. Phys. B-Lasers O., 92, 7, 2008.
- Ubierna, N., Gandin, A., Boyd, R. A., and Cousins, A. B.: Temperature response of mesophyll conductance in three  $\text{C}_4$  species calculated with two methods:  $^{18}\text{O}$  discrimination and in vitro  $V_{\text{pmax}}$ , New Phytologist, 214, 14, 2007.
- Ubierna, N., Gandin, A., and Cousins, A. B.: The response of mesophyll conductance to short-term variation in  $\text{CO}_2$  in the  $\text{C}_4$  plants *Setaria viridis* and *Zea mays* Journal of experimental botany, 69, 11, 2018a.
- Ubierna, N., Holloway-Phillips, M.-M., and Farquhar, G. D.: Using stable carbon isotopes to study  $\text{C}_3$  and  $\text{C}_4$  photosynthesis: models and calculations Photosynthesis, 41 pp., 2018b.
- Ubierna, N., Cernusak, L. A., Holloway-Phillips, M., Busch, F. A., Cousins, A. B., and Farquhar, G. D.: Critical review: incorporating the arrangement of mitochondria and chloroplasts into models of photosynthesis and carbon isotope discrimination, Photosynth. Res., 141, 26, 2019.
- Uemura, R., Barkan, E., Abe, O., and Luz, B.: Triple isotope composition of oxygen in atmospheric water vapor, Geophys. Res. Lett., 37, L04402, 2010.
- Urey, H. C.: The thermodynamic properties of isotopic substances, Journal of the Chemical Society, 19, 1947.
- Verkouteren, R. M., Allison, C. E., Studley, S. A., and Leckrone, K. J.: Isotopic metrology of carbon dioxide. I. Interlaboratory comparison and empirical modeling of inlet equilibration time, inlet pressure, and ion source conductance, Rapid Commun Mass Spectrom, 17, 771-776, 10.1002/rcm.905, 2003a.
- Verkouteren, R. M., Assonov, S., Klinedinst, D. B., and Brand, W. A.: Isotopic metrology of carbon dioxide. II. Effects of ion source materials, conductance, emission, and accelerating voltage on dual-inlet cross contamination, Rapid Commun Mass Spectrom, 17, 777-782, 10.1002/rcm.906, 2003b.
- Vogel, J. C., Grootes, P. M., and Mook, W. G.: Isotopic fractionation between gaseous and dissolved carbon dioxide, Z. Physik, 230, 13, 1970.
- Wand, S. J. E., Midgley, G. F., Jones, M. H., and Curtis, P. S.: Responses of wild  $\text{C}_4$  and  $\text{C}_3$  grass (Poaceae) species to elevated atmospheric  $\text{CO}_2$  concentration: a meta-analytic test of current theories and perceptions, Global Change Biology, 5, 8, 1999.
- Wang, X.-F., and Yakir, D.: Using stable isotopes of water in evapotranspiration studies, Hydrol. Process., 14, 14, 2000.
- Wang, Y. P., Lu, X. J., Wright, I. J., Dai, Y. J., Rayner, P. J., and Reich, P. B.: Correlations among leaf traits provide a significant constraint on the estimate of global gross primary production, Geophys. Res. Lett., 39, L19405, 10.1029/2012GL053461, 2012.
- Warren, C.: Estimating the internal conductance to  $\text{CO}_2$  movement Functional Plant Biology, 33, 11, 2006.
- Wassenaar, L. I., Terzer-Wassmuth, S., Douence, C., Araguas-Araguas, L., Aggarwal, P. K., and Coplen, T. B.: Seeking excellence: An evaluation of 235 international laboratories conducting water isotope analyses by isotope-ratio and laser-absorption spectrometry, Rapid Commun Mass Spectrom, 32, 393-406, 10.1002/rcm.8052, 2018.
- Wehr, R., Munger, J. W., McManus, J. B., Nelson, D. D., Zahniser, M. S., Davidson, E. A., Wofsy, S. C., and Saleska, S. R.: Seasonality of temperate forest photosynthesis and daytime respiration, Nature, 534, 680-683, 2016.

- Weijde, T. v. d., Kamei, K. C. L. A., Torres, A. F., Vermerris, W., Dolstra, O., Visser, R. G. F., and Trindade, L. M.: The potential of C<sub>4</sub> grasses for cellulosic biofuel production, *Front. Plant. Sci.*, 4, 107, 2013.
- Welp, L. R., Keeling, R. F., Meijer, H. A. J., Bollenbacher, A. F., Piper, S. C., Yoshimura, K., Francey, R. J., Allison, C. A., and Wahlen, M.: Interannual variability in the oxygen isotopes of atmospheric CO<sub>2</sub> driven by El Niño, *Nature*, 477, 579-582, 10.1038/nature10421, 2011.
- West, A. G., Patrickson, S. J., and Ehleringer, J. R.: Water extraction times for plant and soil materials used in stable isotope analysis, *Rapid Commun Mass Spectrom*, 20, 1317-1321, 10.1002/rcm.2456, 2006.
- Westley, M. B., Popp, B. N., and Rust, T. M.: The calibration of the intramolecular nitrogen isotope distribution in nitrous oxide measured by isotope ratio mass spectrometry, *Rapid Commun Mass Spectrom*, 21, 391-405, 10.1002/rcm.2828, 2007.
- Weston, R. E.: Anomalous or mass-independent isotope effects, *Chemical Reviews*, 99, 2121, 1999.
- Whelan, M. E., Lennartz, S. T., Gimeno, T. E., Wehr, R., Wohlfahrt, G., Wang, Y., Kooijmans, L. M. J., Hilton, T. W., Belviso, S., Peylin, P., Commene, R., Sun, W., Chen, H., Kuai, L., Mammarella, I., Maseyk, K., Berkelhammer, M., Li, K.-F., Yakir, D., Zumkehr, A., Katayama, Y., Ogée, J., Spielmann, F. M., Kitz, F., Rastogi, B., Kesselmeier, J., Marshall, J., Erkkilä, K.-M., Wingate, L., Meredith, L. K., He, W., Bunk, R., Launois, T., Vesala, T., Schmidt, J. A., Fichot, C. G., Seibt, U., Saleska, S., Saltzman, E. S., Montzka, S. A., Berry, J. A., and Campbell, J. E.: Reviews and syntheses: Carbonyl sulfide as a multi-scale tracer for carbon and water cycles, *Biogeosciences*, 15, 12, 2018.
- White, J. W. C., Ferretti, D. F., Vaughn, B. H., Francey, R. J., & Allison, C. E: Stable isotope measurements of atmospheric CO<sub>2</sub>, Stable isotope measurement techniques for atmospheric greenhouse gases. International Atomic Agency, Vienna, IAEA-TECDOC-1268, 20, 2002.
- Wiegel, A. A., Cole, A. S., Hoag, K. J., Atlas, E. L., Schauffler, S. M., and Boering, K. A.: Unexpected variations in the triple oxygen isotope composition of stratospheric carbon dioxide, *PNAS*, 110, 17680-17685, 10.1073/pnas.1213082110, 2013.
- Windnagel, A., Brandt, M., Fetterer, F., and Meier, W.: Sea Ice Index Version 3 Analysis, NSIDC Special Report, 19, 2017.
- Wingate, L., Ogée, J., Cuntz, M., Genty, B., Reiter, I., Seibt, U., Yakir, D., Maseyk, K., Pendall, E. G., Barbour, M. M., Mortazavi, B., Burlett, R., Peylin, P., Miller, J., Mencuccini, M., Shim, J. H., Hunt, J., and Grace, J.: The impact of soil microorganisms on the global budget of  $\delta^{18}\text{O}$  in atmospheric CO<sub>2</sub>, *PNAS*, 106, 4, 2009.
- Wollnik, H.: Optics of charged particles, Elsevier Inc, 978-0-12-762130-2, Academic Press London, 1987.
- Wong, S. C., Cowan, I. R., and Farquhar, G. D.: Stomatal conductance correlates with photosynthetic capacity *Nature*, 282, 2, 1979.
- Woosley, R. J., and Millero, F. J.: Freshening of the western Arctic negates anthropogenic carbon uptake potential *Limnology and Oceanography*, 999, 12, 2020.
- Wostbrock, J. A. G., Cano, E., and Sharp, Z. D.: An internally consistent triple oxygen isotope calibration of standards for silicates, carbonates and air relative to VSMOW2 and SLAP2, *Chem. Geol.*, 2019.
- Yakir, D., and Wang, X.-F.: Fluxes of CO<sub>2</sub> and water between terrestrial vegetation and the atmosphere estimated from isotope measurements, *Nature*, 380, 2, 1996.
- Yakir, D.: Oxygen-18 of leaf water: a crossroad for plant-associated isotopic signals, *Stable isotopes: integration of biological, ecological and geochemical processes*, 21, 1998.
- Yakir, D., and Sternberg, L. S. L.: The use of stable isotopes to study ecosystem gas exchange, *Oecologia*, 123, 4, 2000.
- Yakir, D.: Global enzymes: sphere of influence, *Nature*, 416, 1, 2002.



- Yanes, Y., and Yapp, C. J.: Indoor and outdoor urban atmospheric CO<sub>2</sub>: Stable carbon isotope constraints on mixing and mass balance *Applied Geochemistry*, 25, 10, 2010.
- Yeung, L. Y., Hayles, J. A., Hu, H., Ash, J. L., and Sun, T.: Scale distortion from pressure baselines as a source of inaccuracy in triple-isotope measurements, *Rapid Communications in Mass Spectrometry*, 32, 10, 2018.
- Yoshida, N., and Toyoda, S.: Constraining the atmospheric N<sub>2</sub>O budget from intramolecular site preference in N<sub>2</sub>O isotopomers, *Nature*, 405, 3, 2000.
- Young, E. D., Galy, A., and Nagahara, H.: Kinetic and equilibrium mass-dependent isotope fractionation laws in nature and their geochemical and cosmochemical significance, *Geochim. Cosmochim. Ac.*, 66, 9, 2002.
- Young, E. D., Kohl, I. E., Warren, P. H., Rubie, D. C., Jacobson, S. A., and Morbidelli, A.: Oxygen isotopic evidence for vigorous mixing during the Moon-forming giant impact, *Science*, 351, 3, 2016a.
- Young, E. D., Rumble, D., Freedman, P., and Mills, M.: A large-radius high-mass-resolution multiple-collector isotope ratio mass spectrometer for analysis of rare isotopologues of O<sub>2</sub>, N<sub>2</sub>, CH<sub>4</sub> and other gases, *International Journal of Mass Spectrometry*, 401, 1-10, 10.1016/j.ijms.2016.01.006, 2016b.
- Yu, T., Sun, R., Xiao, Z., Zhang, Q., Liu, G., Cui, T., and Wang, J.: Estimation of global vegetation productivity from global land surface satellite data, *Remote sensing of Environment*, 10, 327, 2018.
- Yung, Y. L., DoMore, W. B., and Pinto, J. P.: Isotopic exchange between carbon dioxide and ozone via O (<sup>1</sup>D) in the stratosphere, *Geophys. Res. Lett.*, 18, 3, 1991.
- Yung, Y. L., Lee, A. Y. T., Irion, F. W., DeMore, W. B., and Wen, J.: Carbon dioxide in the atmosphere: Isotopic exchange with ozone and its use as a tracer in the middle atmosphere, *Journal of Geophysical Research: Atmospheres*, 102, 10857-10866, 10.1029/97jd00528, 1997.
- Zeebe, R. E., and Wolf-Gladrow, D.: CO<sub>2</sub> in seawater: equilibrium, kinetics, isotopes, Elsevier Oceanography series 65, edited by: David, H., Gulf Professional Publishing, 346 pp., 2001.
- Zeppel, M., Lewis, J. D., Chaszar, B., Smith, R. A., Medlyn, B. E., Huxman, T. E., and Tissue, D. T.: Nocturnal stomatal conductance responses to rising [CO<sub>2</sub>], temperature and drought, *New Phytologist*, 193, 9, 2012.
- Zhang, H., Pang, H., Shi, J., Fu, T., and Liao, B.: Investigation of liquefied wood residues based on cellulose, hemicellulose, and lignin *Journal of Applied Polymer Science*, 123, 850-856, 2012.
- Zhao, M., Heinsch, F. A., Nemani, R. R., and Running, S. W.: Improvements of the MODIS terrestrial gross and net primary production global data set, *Remote sensing of Environment*, 95, 12, 2005.
- Zhu, Z., Piao, S., Myneni, R. B., Huang, M., Zeng, Z., Canadell, J. G., Ciais, P., Sitch, S., Friedlingstein, P., and Arneeth, A.: Greening of the Earth and its drivers, *Nature climate change*, 6, 4, 2016.
- Zscheischler, J., Mahecha, M. D., Avitabile, V., Calle, L., Carvalhais, N., Ciais, P., Gans, F., Gruber, N., Hartmann, J., and Herold, M.: Reviews and syntheses: An empirical spatiotemporal description of the global surface-atmosphere carbon fluxes: opportunities and data limitations *Biogeosciences*, 14, 18, 2017.

## List of publications

- Adnew G.A., Pons T. L., Koren G., Peters W., and Röckmann T. Exploring the use of  $^{17}\text{O}$ -excess of  $\text{CO}_2$  for estimating mesophyll conductance of  $\text{C}_3$  and  $\text{C}_4$  plants, under review in Plant Physiology Journal, 2020.
- Vila-Guerau de Arellano, J., Ney, P., Hartogensis, O., de Boer, H., van Diepen, K., Emin, D., de Groot, G., Klosterhalfen, A., Langensiepen, M., Matveeva, M., Miranda, G., Moene, A., Rascher, U., Röckmann, T., Adnew, G.A., and Graf, A.: CloudRoots: Integration of advanced instrumental techniques and process modelling of sub-hourly and sub-kilometre land-atmosphere interactions, Biogeosciences, 17, 4375-4404,2020, DOI:10.5194/bg-17-4375-2020, 2020
- Adnew, G. A., Pons, T. L., Koren, G., Peters, W., and Röckmann, T.: Leaf-scale quantification of the effect of photosynthetic gas exchange on  $\Delta^{17}\text{O}$  of atmospheric  $\text{CO}_2$ , Biogeosciences, 17, 3903-3922,2020, DOI:10.5194/bg-17-3903-2020.
- Adnew, G. A., Hofmann, M. E. G., Paul, D., Laskar, A., Surma, J., Albrecht, N., Pack, A., Schwieters, J., Koren, G., Peters, W., and Röckmann, T.: Determination of the triple oxygen and carbon isotopic composition of  $\text{CO}_2$  from atomic ion fragments formed in the ion source of the 253 Ultra High-Resolution Isotope Ratio Mass Spectrometer, Rapid Commun Mass Spectrom., 33, 17, 2019, DOI:10.1002/rccm.8478.
- Laskar, A. H., Peethambaran, R., Adnew, G. A., and Röckmann, T.: Measurement of  $^{18}\text{O}^{18}\text{O}$  and  $^{17}\text{O}^{18}\text{O}$  in atmospheric  $\text{O}_2$  using the 253 Ultra mass spectrometer and applications to stratospheric and tropospheric air samples, Rapid Commun Mass Spectrom., 33, 13, 2019,DOI:10.1002/rccm.8434.
- Koren G, Schneider L, van der Velde IR, van Schaik E, Gromov SS, Adnew GA, Mrozek DJ, Hofmann MED, Liang M.-C, Mahata S, Bergamaschi P, van der Laan-Luijkx IT, Krol MC, Röckmann T, Peters W, Global 3-D simulations of the triple oxygen isotope signature  $\Delta^{17}\text{O}$  in Atmospheric  $\text{CO}_2$ . J Geophys Res Atmos 124:880-8836,2019,DOI:10.1029/2019jd030387.





## Acknowledgments

I would like to express my deepest gratitude to my supervisor Thomas Röckmann for his endless support, encouragement, and discussions about the isotope adventure. Thank you very much for believing in me and giving me a lot of freedom to do things in my own way which gave me extra motivation. Thomas, thank you very much for your patience with my speaking speed.

I would like to thank my second supervisor Wouter Peters for his regular meetings and suggestions through the course of the project. Thank you very much for organizing seminars within the ASICA project, which helped our collaboration a lot.

I would like to thank Gerbrand Koren: it was a pleasure working with you on the ASICA project, from sampling overnight in a forest, to attending conferences. Such great collaboration is rare to happen, and I call it “clumped” in isotopic terminology. Gerbrand, thank you very much for translating the summary of this thesis to Dutch. I also would like to thank Thijs Pons for introducing me to the gas exchange experiments and dealing with plants.

I would like to thank Elena, Magdalena, and Dipayan for helping me during the start of my project. Magdalena thanks for being my daily supervisor at the beginning of my PhD and teaching me about the isotope mass spectrometer. Elena, thank you very much for a lot of discussions about science and outside of science, for the nice bike trip, and for lending me your office couch.

I would like to thank the technicians Carina, Henk, Marcel: your support and help was endless and because of you, we managed to build my experimental setup. I am very surprised by how many things we build in the last four years. Building the experimental setup would not have been possible without the support from the glass workshop. I would like to thank Matthijs, Sander, Hans, Henkjan, and Peter for helping in building the experimental setup. Especially, thanks to Matthijs and Hans - you guys were very nice to me, you always received me with a smile and tried to help me a lot.

I would like to thank Jordi and Oscar for inviting me to join the Cloudroots project campaign. It was a very nice experience working with you, and I am looking forward to collaborating with you more.

I am thankful to the APCG group for the nice lunch and coffee breaks. I am very impressed by how international the group is. I am also delighted for constructive feedbacks during our group meetings to improve my presentation skills. Malika for being a running mate and also offering a nice bread, Juhi for the endless hugs whenever we meet, even though we have to stop it during corona times. Carina for being a nice office mate, and also for your advice to learn Dutch and driving (sorry I still did not learn either). Caroline, you were a very nice addition to the APCG group. Maarten, thank you very much for organizing Christmas dinners at your place. Rahul and Amzad, thank you very much for discussions about Ultra and isotopes in general. Stijn, thank you for your regular Friday visits at IMAU. Narcisa, Erik, Gerbrand, Elena, Maarten, Ingrid, Sudhanshu, Wouter, thanks a lot for the nice trip to Interlaken.

I am also thankful to the members of IMAU for making my stay pleasant with nice coffee moments and different activities. Special thanks to Abdel, Anne, Peter, Philippe, Erwin, Andre

for lunch runs. Peter, thank you for inviting me to sail with your beautiful boat, Philippe thank you very much for your patience with my questions about python. Claudia for your nice jokes and a nice dinner at your place. Tjebbe, thank you for the first sailing experience and for translating the Dutch documents. Julia for your contagious good humor. Sophie, Iris, Hossein, Marco, Bin, Bo, Wie, Michael, Mikael, Paul, David, Janneke, Sylvia, Jinyang thank you very much for making IMAU a nice working place. Grant and Evelyn, thank you very much for proofreading the introduction of my thesis. Sandra, Floor, and Clara thank you very much for your support.

I would like to thank my housemates Martina, Daniele, and Andre, it is a pleasure living with you. Daniele, from a coffee room meeting (Do you know that?) to living together. Andre, thank you very much for introducing me to a lot of sports even if I cannot keep up with you, and also inviting me to your parent's place for Christmas. Martina, you make the house so lively with a lot of plants. Living with you helps me to feel less homesick. Davide and Sylvia thank you very much for inviting us for Christmas dinner and lending me your phone.

This thesis would not have been possible without the support of my family and friends. I would like to thank Hannaye for advice and for being always supportive whenever I need help. Yared, thank you for inviting me to different events. My parents gave me a lot of support and encouragement in every step of my life. My mother, you are an amazing mom, if you were not there for me I would not have moved one step forward, you are an inspiration and role model for me. My father, Agmuas Adnew, thank you very much, you are such an example of a good father. My sisters, Hanna, Sewunet, Alemitu, Tirualeme, Betelehem, Mahilet, thank you very much for the regular phone calls. My brothers, Henok and Melsew, thank you very much for your support and encouragement.

Lastly, I would like to thank Mahi, you were there for me in every circumstance, encouraging and supporting me for the last three years of my PhD.

## Curriculum Vitae

Getachew Agumas Adnew was born on Nov 07, 1985, in Debre-Elias, Ethiopia. After finishing his primary school in there, he moved to Debre Markos, Ethiopia for his high school. He finished his Bachelor in applied chemistry at Arba-Minch University, Ethiopia. After this, he moved back to Debre Markos as a high school teacher for six months. In 2007, Getachew joined the University of Gondar, Ethiopia as an assistant lecturer. At the same university, he pursued a Master in organic chemistry and was employed at the chemistry department, as a lecturer for four years. As a young scholar growing up in a country affected by drought due to climate change, he was fascinated by the chemistry of the environment and climate in general. In 2013, he obtained a Danish government scholarship to study for a master's degree in environmental chemistry and health at the University of Copenhagen, Denmark. He completed his master project on air pollution treatment under the supervision of Prof. Dr. Matthew S. Johnson. After receiving his master's degree, he was employed as a research assistant for three months at the University of Copenhagen in the lab of Prof. Dr. Matthew S. Johnson. In 2016, he joined the atmospheric chemistry and physics group of IMAU to explore more about the chemistry that governs the atmosphere under the supervision of Prof. Dr. Thomas Röckmann and Prof. Dr. Wouter Peters. Currently, he is a postdoctoral researcher in the laboratory of Prof. Dr. Thomas Röckmann at IMAU.



CS4Δ

